Reports of the Department of Geodetic Science

Report No. 299

GEODETIC POSITIONING USING A GLOBAL POSITIONING SYSTEM OF SATELLITES

by

Patrick J. Fell

Prepared for

National Aeronautics and Space Administration
Goddard Space Flight Center
Greenbelt, Maryland 20770

Grant No. NSG 5265
OSURF Project No. 711055

and

Defense Mapping Agency
Washington, D.C. 20305
Under Contract to the Naval Surface
Weapons Center, Dahlgren, Virginia 22448

Reference No. DMA PE63701B/3201/240
SUBTASK KE

The Ohio State University
Research Foundation
Columbus, Ohio 43212

June, 1980

Reports of the Department of Geodetic Science

Report No. 299

GEODETIC POSITIONING USING A GLOBAL POSITIONING SYSTEM OF SATELLITES

by

Patrick J. Fell

Prepared for

National Aeronautics and Space Administration
Goddard Space Flight Center
Greenbelt, Maryland 20770

Grant No. NSG 5265
OSURF Project No. 711055

and

Defense Mapping Agency
Washington, D.C. 20305
Under Contract to the Naval Surface
Weapons Center, Dahlgren, Virginia 22448

Reference No. DMA PE63701B/3201/240
SUBTASK KE

The Ohio State University
Research Foundation
Columbus, Ohio 43212

June, 1980

PREFACE

This project is under the supervision of Professor Ivan I. Mueller, Department of Geodetic Science, The Ohio State University and Richard J. Anderle, Head, Astronautics and Geodesy Division, Naval Surface Weapons Center (NSWC), Dahlgren, Virginia. This work was supported, in part, through NASA Grant No. NSG 5265, The Ohio State University Research Foundation Project No. 711055 and through funding provided by the Defense Mapping Agency to NSWC under Reference No. DMA PE63701B/3201/240 SUBTASK KE. The NASA funding supporting this research was administered through the Goddard Space Flight Center, Greenbelt, Maryland with Dr. David E. Smith as Science Advisor and Mr. Edmond C. Holweck as Technical Officer.

Computer expenses were partially covered by the Instruction and Research Computer Center of The Ohio State University.

This report was submitted to the Graduate School of The Ohio State University as partial fulfillment of the requirements for the degree Doctor of Philosophy.

ABSTRACT

Geodetic positioning using range, integrated Doppler, and interferometric observations from a constellation of twenty-four Global Positioning System satellites is analyzed. A summary of the proposals for geodetic positioning and baseline determination is given which includes a description of measurement techniques and comments on rank deficiency and error sources. An analysis of variance comparison of range, Doppler, and interferometric time delay to determine their relative geometric strength for baseline determination is included. An analytic examination of the effect of a priori constraints on positioning using simultaneous observations from two stations is presented.

Dynamic point positioning and baseline determination using range and Doppler is examined in detail. Models for the error sources influencing dynamic positioning are developed. Included is a discussion of atomic clock stability, and range and Doppler observation error statistics based on random correlated atomic clock error are derived. Criteria for establishing observation schedules for optimum geometric strength for positioning solutions are examined. Results of geodetic positioning simulation studies are presented.

Satellite interferometry results based on the double differencing of simultaneous interferometric phase measurements from two satellites are given. The effects of ephemeris and refraction errors and the nonsimultaneity of observation are considered.

ACKNOWLEDGMENTS

First and foremost, I wish to express my gratitude to Professor Ivan I. Mueller for his support, guidance, and encouragement during this study and throughout my association with the Department of Geodetic Science. As my advisor, he was responsible for inspiring me to pursue high educational and personal goals.

My appreciation is also expressed to Richard J. Anderle for his support of my studies at The Ohio State University and of this work at the Naval Surface Weapons Center.

I thank Professors Urho A. Uotila and Clifford V. Heer as members of the reading committee for their valuable comments.

I would like to acknowledge Professors Ivan I. Mueller, Urho A. Uotila, and Richard H. Rapp for their efforts in developing and clarifying the concepts presented in the geodetic science program.

Financial support in the form of the Wild-Heerbrugg 1977 Geodetic Fellowship, The Ohio State University Graduate Research Assistantship, and NSWC Full Time Advanced Study are gratefully acknowledged.

I am grateful to my wife, Stefanie, for her constant support and understanding.

Finally, Irene Tesfai, Linda Wright, and Dorothy Burgess are to be thanked for their efforts and persistence in preparing this manuscript.

TABLE OF CONTENTS

TABLE OF CONTENTS (continued)

LIST OF TABLES

LIST OF FIGURES

1. INTRODUCTION

1.1 Background on a Global Positioning System

A Global Positioning System (GPS) is a passive all-weather navigation satellite system proposed for operation after 1985. The system uses the concept of passive satellite navigation based on highly accurate atomic frequency standards to enable the navigator to determine his three-dimensional position, velocity, and time instantaneously on a continuous worldwide basis. Range and range-rate measurements taken simultaneously from four satellites will be reduced to determine these parameters [Milliken, 1978]. A total of twenty-four satellites in three orbit planes will be available for navigation giving accuracies and availability far exceeding the current Navy Navigation Satellite System or Transit System [Stansell, 1978a] which GPS is designed to replace for navigation. With the number of satellites in view always exceeding the required number for navigation, the user may select a subset of four based on some criterion which optimizes the geometric strength of the navigation solution.

The GPS system consists of three major segments: Space System Segment, Control System Segment, and User System Segment. Each segment is developed over three separate phases, each being a logical extension of the previous phase in an integrated and cohesive manner.

Phase I encompasses the initial design and evaluation of system components including the development of user equipment satisfying the various navigation applications [Borel, 1978], testing of user equipment at a ground based simulation facility [Denaro, 1978], and the space based system as satellites become available. These satellites are prototypes of operational satellites which will validate a new ranging technique and the stability of atomic frequency standards in a space environment [Bartholomew, 1978]. This initial constellation will provide four-in-view geometry similar to the complete system for up to three hours each day over selected geographic areas. An initial ground tracking network will be developed and tested during Phase I as a prototype of the operational ground system [Russell, 1978]. Certain limited demonstrations of operational scenarios are to be conducted.

Phase II consists of the initial production of low cost user equipment and development of operational satellites. During this phase additional satellites will augment the Phase I constellation. This will result in a constellation of four satellites in each of three orbit planes providing eight hours of continuous four-in-view geometry each day. These satellites will later be maneuvered to provide continuous worldwide two-dimensional navigation.

Phase III builds upon this two-dimensional capability augmenting the constellation until a total system of twenty-four satellites in three orbit planes exists. Orbital periods are twelve hours. The ground tracking stations will become operational and modified as necessary to accommodate full system operation.

Summarizing, Phase I is the concept validation period, Phase II is the system validation period, and Phase III consists of production and operation. Initial worldwide operational capability should become a reality after 1985. Phase I has been completed.

The final Space System Segment will consist of twenty-four satellites deployed in three orbit planes separated in right ascension by sixty degrees. Eight satellites are equally spaced within each plane. Integrated into each satellite will be at least two atomic frequency standards to maintain stable time and frequency required for precise ranging.

The Control System Segment is composed of a master control station, an upload station, and three monitor stations [Russell, 1978]. The master control station and the upload station are currently located at Vandenberg Air Force Base in California and three monitor stations are located on Guam and in Alaska and Hawaii. These monitor stations measure the range and range-rate of the satellites, collect meteorological data and forward this information to the master control station. Every monitor station is equipped with a cesium frequency standard. The master control station processes the data collected at the monitor stations and its own tracking data to obtain best estimates of satellite ephemerides and time synchronization offsets for the system. Predicted ephemerides and clock corrections are forwarded to the upload station for transmission to the satellite.

The User Control Segment consists of the development and testing of electronic receivers and associated equipment required to perform navigation. The function of this equipment is to detect and to acquire

the GPS satellite navigation signals, to extract range and range-rate information, to perform corrections for ionospheric refraction, and to compute three-dimensional position and velocity and time. The expected positional accuracies of the system are nine meters in each horizontal component of position and ten meters in the vertical component ninety percent of the time. These estimates of accuracy are based on a single determination of position using four satellites based on the expected error budget and optimum satellite geometry [Milliken, 1978].

An eventual replacement of the Transit System by GPS would possibly curtail geodetic positioning currently available with the former system using integrated Doppler observations and precise satellite ephemerides [Sims, 1972]. At the present time Doppler positioning is playing an increasingly important role in many countries for network densification and control as detailed in the Proceedings of the First and Second International Geodetic Symposiums on Satellite Doppler Positioning [1976, 1979]. The curtailment of this program could have significant implications within the geodetic community.

1.2 Review of Previous Studies

A Global Positioning System, although designed for navigation, can offer the means for continued geodetic positioning using Doppler or range observations. Anderle and Tanenbaum [1974] point out that a GPS system is orders of magnitude better in oscillator stability and suppression of ionospheric refraction and is effected less by uncertainties in the gravity field. These factors imply that the typical errors present in current Transit positioning would be reduced using GPS.

In addition the presence of six to nine satellites in view at all times means that continuous data acquisition will be possible as opposed to intermittent data obtained from Transit.

However the extreme altitude of these satellites, having an orbital semi-major axis of over 25,000 kilometers, means that the relative velocity or Doppler shift between a satellite and an electronic receiver on the earth would be smaller limiting the amount of positioning information available from each integrated Doppler observation. A comparison of simulated range difference data from GPS and Transit demonstrates this geometric dilution of information. GPS range difference data which have a maximum value of around 17 kilometers for a thirty-second integration period are approximately an order of magnitude smaller than typical Transit observations which can have a maximum range difference of 150 kilometers over the same integration interval. Figures 1.2.1 and 1.2.2 illustrate thirty-second integrated Doppler range differences for a typical Transit pass and for a high elevation GPS satellite pass respectively. The elevation angle of the satellite is given at the endpoints of the curve and at the time of closest approach (TCA). In addition the maximum length of a GPS satellite pass is about six hours whereas a Transit satellite pass lasts about twenty minutes. Thus GPS range differences are smaller in magnitude than currently obtainable Transit observations and, due to the length of a pass, range differences from consecutive integration periods will vary less. This implies that continuous tracking of GPS satellites over a complete pass may not represent an optimum data acquisition procedure. A sequential tracking approach in which a number of satellites are tracked over

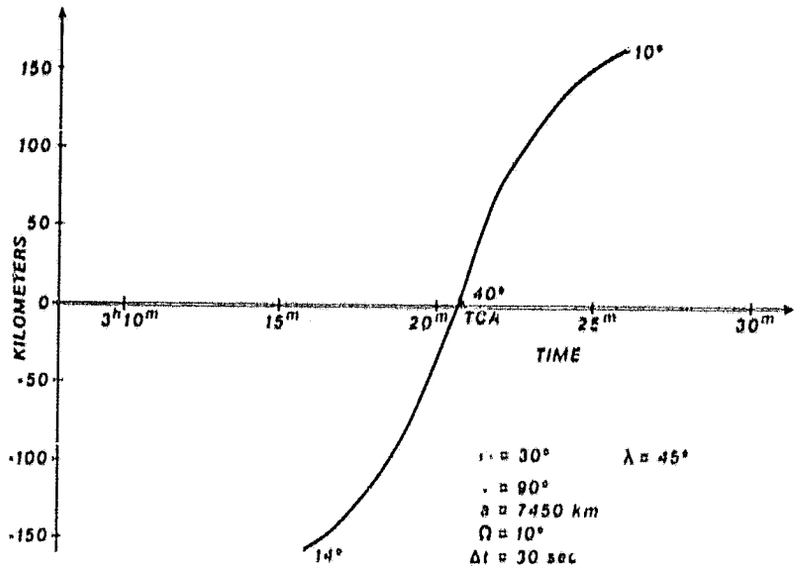

Figure 1.2.1. NAVSAT Range Differences

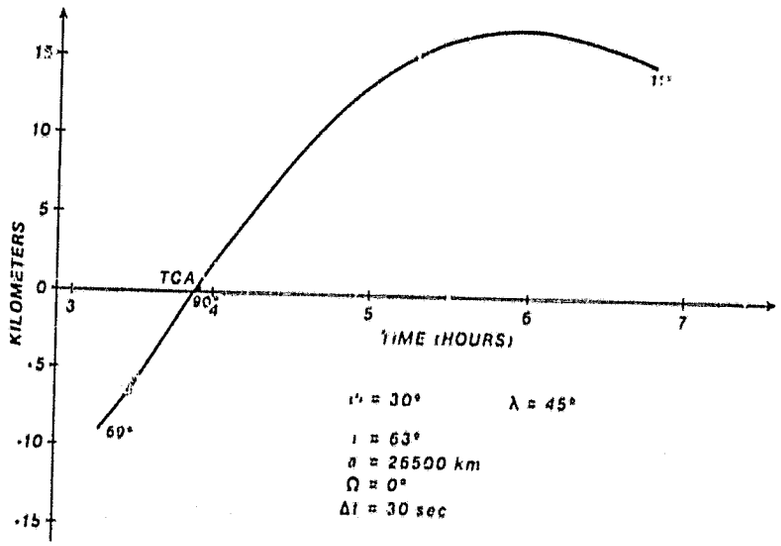

Figure 1.2.2. GPS Range Differences

segments of a pass may give a more geometrically significant collection of observations.

Thus it is evident that GPS integrated Doppler observations offer certain real advantages over Transit observations but lack in geometric strength of observation. However the GPS system offers additional observational approaches, namely, ranging and, as will be discussed below, the potential for interferometric observation.

The majority of the investigations made to date have centered on the navigational capabilities of the GPS system. These studies consist of both simulations and analysis of actual observations to determine the accuracies achievable in numerous navigational applications. Denaro [1978] describes the initial testing of aircraft and land-based navigation receivers using the Inverted Test Range at Yuma, Arizona. These tests involved the use of ground-based transmitters simulating the satellite system. Stansell [1978b] considers the civil marine applications of GPS and Cox [1978] describes the augmentation of an inertial navigation system with GPS observations. Miller [1977] gives results of an analysis of ocean navigation using GPS range observations, and Kruczynski [1978] considers aircraft navigation using a limited operational phase of the GPS system.

Numerous additional studies have centered on the theme of navigation using the GPS system. However only relatively few studies have examined the possible geodetic or geophysical potential of this system. One of the earliest papers, given by Anderle [1978a], discusses the major error sources effecting GPS range and Doppler observations and arrives at anticipated accuracies for geodetic positioning and baseline

components by extrapolating results of a limited analysis based on single pass solutions for two components of position. Anderle [1978b] again gives estimates of precision of relative station positioning based on GPS range observations. The results were again based on the projection of limited results. Fell [1979] gives an indication of the effect of atomic clock stability errors on positioning based on the use of range and Doppler observations obtained from one or two GPS satellite passes. These limited studies comprise the present results indicating the potential of GPS range and Doppler observations for geodetic positioning derived using a dynamic point positioning approach.

In addition to dynamic positioning, interferometric approaches have been proposed which utilize radio signals broadcast by GPS satellites to determine baseline components by measuring the time difference of arrival or phase of these signals at two stations. Counselman [1978] proposes to utilize interferometric observations derived from a series of continuous wave signals transmitted by equipment which would augment the GPS system satellites. Using this approach baselines ranging up to a few hundred kilometers would be measured. Counselman presents baseline uncertainty estimates for this system based on the geometry of the satellite passes. These results are then adjusted to reflect the effect of unmodeled tropospheric refraction. Applications of the system are discussed.

MacDoran [1979] proposes to derive interferometric observations from broadcast GPS satellite radio signals in a manner similar to that used in very long baseline interferometry [Dermanis, 1977] or in the portable ARIES system [MacDoran et al., 1978] both using

quasar sources. MacDoran gives a summary of the proposed SERIES system and estimates of the effects of random and systematic error sources. A graph of estimated baseline accuracy derived from SERIES is given.

Finally, Bender [Letter to I. I. Mueller, 1979] proposes an interferometric approach in which the phases of the reconstructed GPS carrier frequencies with respect to a local oscillator are measured at two stations in order to monitor crustal movements. As with the previous two interferometric proposals this approach remains in an early stage of development and the exact magnitudes of the error sources can only be conjectured at present. A more detailed examination of all proposed systems of usage is presented in Chapter 2.

1.3 Description of Present Study

The major objective of this study is to present an analysis of geodetic positioning obtained from both dynamic point positioning using GPS range and integrated Doppler observations and from interferometric satellite observations. One of the basic aims of geodesy is the precise and consistent determination of the coordinates of points of interest in an adopted earth-fixed frame of reference. How well this can be accomplished using GPS satellite observations will depend on many factors which must be examined in detail.

The first step in this study, described in Chapter 2, is to examine the proposed methods for the geodetic implementation of Global Positioning System observations. These proposals are divided into two basic classes, dynamic positioning with range and Doppler observations based on the use of satellite ephemerides and satellite interferometry.

A discussion of these techniques is presented giving the mathematical description of the observing technique. A brief discussion of rank deficiency is presented for each system along with a discussion of the error sources effecting each.

The second phase of the study is a comparison of range, Doppler and interferometric observations to determine their relative geometric strength for baseline component and chord length determinations. Ranging observations are treated in three distinct modes, as range, correlated range difference and as interferometric observations. A description of the adjustment procedure is given and an examination of the effect of a priori constraints on positioning using simultaneous observations from two stations is given for each approach. This analysis is presented in Chapter 3.

Dynamic positioning using range and Doppler observations is addressed in Chapter 4. A detailed description of the error sources influencing dynamic positioning is presented and error models for these sources are developed. Included are a discussion of atomic clock error modeling and the development of the statistics for range and Doppler observation errors due to random atomic clock error. Ephemeris, atmospheric refraction and instrumental error sources are considered. Simulation of GPS range and Doppler observations is discussed along with criteria for the selection of satellites to be tracked which yield optimum geometric strength of solution. A sequential algorithm is derived for the estimation of geodetic station coordinates from range and Doppler observations with fully correlated weighting. Results of geodetic positioning simulation studies are presented.

Satellite interferometry results are presented in Chapter 5 based on the double differencing of interferometric phase measurements from two satellites observed simultaneously at two locations. This observation procedure is designed to eliminate the effect of timing errors on the determination of baseline components. The effects of ephemeris and tropospheric refraction errors and the nonsimultaneity of observation are considered.

A final summary and recommendations for additional analysis are presented in Chapter 6.

2. SUMMARY AND CONSOLIDATION OF PROPOSED SYSTEMS OF USAGE

2.1 Introductory Remarks

All currently proposed methods for the geodetic implementation of a Global Positioning System of navigation satellites have centered on the use of three basic types of measurement. These observations are range, integrated Doppler or range difference, and the interferometric delay in time of reception or difference in phase of electromagnetic signals at two sites. Ranging and Doppler techniques discussed by Anderle [1978a] are suitable for dynamic point positioning applications in which the coordinates of the tracking receiver are determined in an adopted earth-fixed frame of reference. Coordinate differences, or baseline components, may also be obtained from such observations acquired at two or more stations. The interferometric approaches advanced by MacDoran [1979], Counselman and Shapiro [1979], and Bender [Letter to I. I. Mueller, 1979], although differing greatly in methodology, are proposals for using the measured time delay or phase difference at two stations to determine baseline components in order to densify existing geodetic control and to monitor crustal movements.

In this chapter a discussion of these techniques is presented which summarizes each observational procedure and gives a mathematical description of the observation equations. A brief discussion of rank

deficiency is presented for each system and the error sources effecting each are addressed.

2.2 Dynamic Positioning Using Range and Doppler Observations

The concept of dynamic point positioning using satellite observations is nearly two decades old. At present geodetic point positioning using integrated Doppler observations from Navy Navigation Satellites forming the Transit System is performed on a worldwide basis primarily for network densification and control. Stansell [1978a] and Laurila [1975] give overviews of this system and its applications in geodesy and navigation. Although differing philosophies exist for the exact implementation of Doppler observations for geodetic positioning, as seen in the discussions of Brown [1976], Anderle [1974, 1976], and Colquitt [1979], where differences in methodology exist in such areas as parameter definition and procedures for treating Doppler observations either as uncorrelated range differences or as biased range, this system has made a great impact on geodesy.

With a Global Positioning System of navigation satellites both range and Doppler observations are available for point positioning, although the electronic technology required to acquire these observations differs greatly from current Doppler measurement methods.

2.2.1 Measurement of Range and Doppler

2.2.1.1 Range Measurement Procedure

Each GPS satellite broadcasts on two L band frequencies, 1575.4 MHz and 1227.6 MHz, called L_1 and L_2 respectively, to allow for

precise first order ionospheric compensation. Modulated on the L_1 carrier are two pseudo random noise (PRN) code sequences known as the precision (P) code and the course acquisition (C/A) code. The P code is a binary random sequence generated at a rate of 10.23 megabits each second and may be considered as a square wave whose frequency is 10.23 Mlz and whose amplitude is randomly taken as plus or minus one every cycle depending on the code sequence. The C/A code is generated at a rate of 1.023 megabits each second and may be considered as a square wave similar to the P code but having lower frequency. The C/A code repeats itself approximately every millisecond; whereas the P code has a repetition rate of approximately 38 weeks, although in practice the sequence will be reset every week.

Lindsey [1973] discusses the general properties of digital sequences known as pseudo random noise sequences for use in ranging applications. The desired properties of these sequences are:

(i) the complete code cycle length must be long enough to avoid ambiguities in range measurements;

(ii) the code symbol repetition rate must be high enough to obtain the required resolution of the range measurement;

(iii) the autocorrelation function of the code should be similar to that of band limited white noise having two distinct levels;

(iv) to improve efficiency in radio frequency (RF) transmission the code should have a balanced number of ones and zeros over a complete period of the sequence so that the power of the modulated signal is more evenly distributed about the carrier frequency.

The significance of these properties will be apparent shortly.

The L_1 signal transmitted by satellite i has the following form as given by Spilker [1978] due to the biphase modulation of the PRN codes and phase quadrature

$$S_{L_1}^{i}(t) = A_p P_i'(t) D_i(t) \cos(\omega_1 t+\phi) + A_c C_i'(t) D_i(t) \sin(\omega_1 t+\phi) \qquad (2.2.1)$$

where the L_1 carrier has the form

$$L_1(t) = \cos(\omega_1 t+\phi) \ . \qquad (2.2.2)$$

In equation (2.2.1) $P_i'(t)$ is a ± 1 pseudo random noise sequence. Thus whenever the P code changes sign the phase of the cosine component is reversed by 180 degrees or biphase modulated. These phase shifts occur at the positive zero crossings of the L_1 carrier. The factor $C_i'(t)$ has an amplitude of plus or minus one and has the property that when the C/A code is minus one, the phase of the second term in equation (2.2.1) is reversed by 180 degrees. Thus the first and second term in that equation will remain out of phase by 90 degrees or retain phase quadrature regardless of the code values. The factors A_p and A_c represent the amplitude of each signal when transmitted. The factor $D_i(t)$ is an additional data code of amplitude ± 1, modulated on the carrier at a rate of 50 bits per second, which gives the navigation message along with the information required to determine the time shift between the epoch of the received C/A code and the epoch of the received P code. Figure 2.2.1 taken from [Butler, 1978] displays the biphase modulation of a

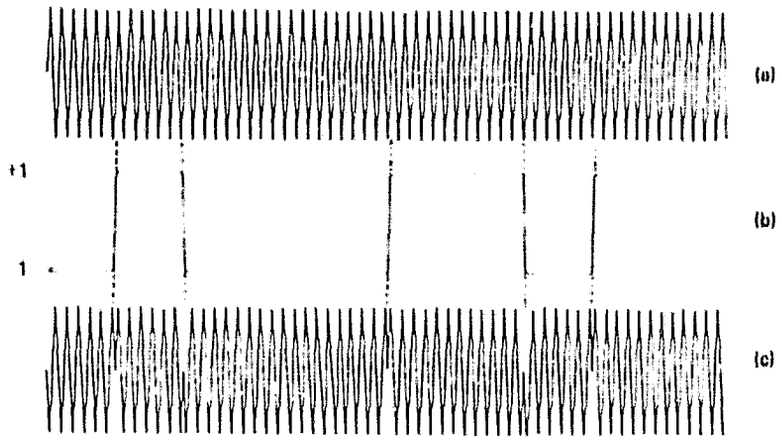

Figure 2.2.1. Time Domain Waveforms: (a) Unmodulated Carrier, (b) PRN Code Sequence, (c) Biphase Code-Modulated Carrier

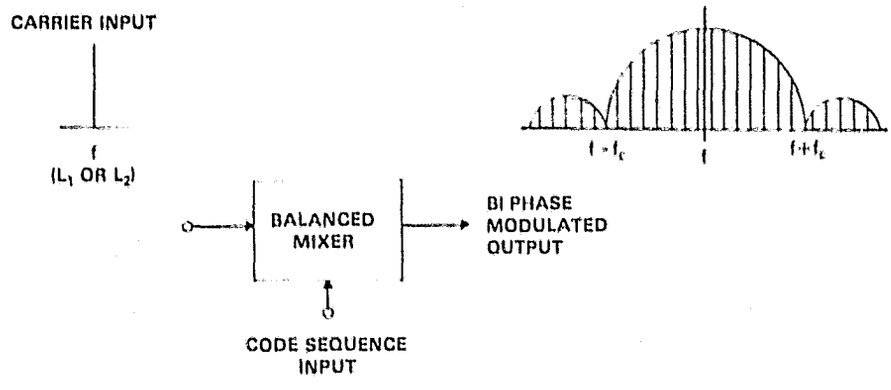

Figure 2.2.2. Effect of PRN Code Modulation on the RF Spectrum

carrier with a PRN code. The resulting RF signal and its power are spread into a frequency interval centered on the carrier whose distribution depends on both the bit rate of the code and on the code itself. Figure 2.2.2 also taken from [Butler, 1978] demonstrates this spread spectrum effect where f_c is the frequency of the code.

The L_2 signal is biphase modulated by either the P code or the C/A code. Assuming the former the L_2 signal has the form

$$S_{L_2}^{i}(t) = B_p P_i'(t) D_i(t) \cos(\omega_2 t + \phi) \qquad (2.2.3)$$

where

$$L_2(t) = \cos(\omega_2 t + \phi) \ . \qquad (2.2.4)$$

Both the L_1 and L_2 signals and all codes are in synchronization with one another when generated.

To measure range a ground receiver must generate the same PRN codes that are broadcast by the tracked satellite. This requires a priori knowledge of the codes selected for broadcast by each satellite during the current week. With the receiver generating the appropriate P and C/A codes the range measurement is obtained by first shifting the C/A code in time, compensating electronically for the Doppler shift, until a maximum correlation with the received signal is obtained. Thus the C/A code is shifted in time by t' and biphase modulated with the received signal giving

$$\begin{aligned} C_i'(t-t')S_{L_1}^{i}(t) = {} & A_p C_i'(t-t') P_i'(t) D_i(t) \cos(\omega_1 t + \phi) \\ & + A_c C_i'(t-t') C_i'(t) D_i(t) \sin(\omega_1 t + \phi) \ . \end{aligned} \qquad (2.2.5)$$

When a maximum correlation of the C/A codes is reached the second term on the right side of equation (2.2.5) will have its power compressed into a much narrower band about the carrier frequency since the product $C_i'(t-t')C_i'(t)$ is one, demodulating the signal. Since $C_i'(t-t')$ and $P_i'(t)$ do not correlate the power of the first term is spread into an even wider band. Since the code correlation functions $\Phi(P,C/A)$ and $\Phi(C/A,C/A)$ are essentially two valued with a distinct maximum as discussed above, a value t' can be determined where maximum C/A code correlation occurs.

Since the C/A code has a short period, t' may be multivalued, but a maximum correlation can be obtained readily. The data code $D_i(t)$ then provides the receiver with information relating the epoch of the broadcast C/A code to the epoch of the P code. Thus the approximate time required to shift the receiver generated P code to correlate with the broadcast P code modulated signal can be determined based on t' and the data message. The P code correlation processes is performed until a maximum correlation occurs as in the C/A code correlation process. The unique time τ for which $P(t-\tau)$ correlates with the signal is the measured quantity. By performing a second correlation on $S_{L_2}^{i}(t)$ an estimate of the first order ionospheric refraction may be obtained and applied to correct τ as described in Section 4.1.3 and in [Spilker, 1978]. The corrected value of τ multiplied by the speed of light c is known as the pseudo range measurement. It represents the geometric range between the receiver and the transmitter plus the effect of the synchronization error between the receiver and satellite clocks. In addition the measurement is subject to other error sources

discussed below. For the moment, ignoring these error sources, the observation equation for pseudo range is

$$\begin{aligned} R = c\tau &= |\overline{\rho}_s - \overline{\rho}| + c\Delta\tau \\ &= [(u_s - u)^2 + (v_s - v)^2 + (w_s - w)^2]^{1/2} + c\Delta\tau \end{aligned} \tag{2.2.6}$$

where u_s, v_s, w_s are the coordinates of the satellite in an adopted earth-fixed reference frame. The quantities u, v, w represent the receiver coordinates in the same frame and $\Delta\tau$ represents the synchronization error between the satellite and receiver clocks.

2.2.1.2 Doppler Measurement Procedure

In the range measurement process both carriers are reconstructed since the C/A and P codes are correlated and biphase modulated with the received signal. In addition the data code is deciphered by the receiver and removed from the carrier. The result is a continuous wave carrier subject to Doppler shift.

Two approaches may be taken to measure the accumulated Doppler shift over an interval of time. First, in forming the range measurement the P code must be correlated with the received signal. Because of the relative motion of the satellite with respect to the receiver the signal is subject to a varying Doppler shift and the electronic correlation process must time shift the receiver code at rates proportional to the range rate to maintain correlation. Thus a Doppler measurement can be obtained by monitoring the code sequence shift rates over an interval. The second procedure is to difference the reconstructed carrier f_s with a frequency generated by the receiver f_0 and count the zero crossings

of the resulting signal over a time interval. This second procedure is the standard Doppler technique in use currently. GPS Doppler receivers however could theoretically use either approach.

In either case the observation equation for integrated Doppler can be expressed as the range difference over the integration interval $[t_i, t_j]$. The equation is

$$\begin{aligned} \Delta R &= |\overline{\rho}_s(t_j) - \overline{\rho}| - |\overline{\rho}_s(t_i) - \overline{\rho}| \\ &= \frac{c}{f_0} [N_{ji} - (f_0 - f_s)(t_j - t_i)] \end{aligned} \tag{2.2.7}$$

where N_{ji} is the accumulated Doppler count over the interval. The measurement is subject to errors due to oscillator frequency variations and atmospheric refraction. As with range this measurement is made on two frequencies to allow for ionospheric refraction correction.

2.2.2 Comments on Rank Deficiency of Range and Doppler Approaches

Dynamic point positioning solutions are obtained from range and Doppler observations by linearizing equations (2.2.6) and (2.2.7) about an initial estimate of station and satellite position

$$V = AX + L \tag{2.2.8}$$

and minimizing $V^T PV$ with respect to the unknown parameters X. This minimization leads [Uotila, 1967] to the least squares normal equations

$$NX + U = 0 \tag{2.2.9}$$

where

$$N = A^T PA \tag{2.2.10}$$

and

$$U = A^{T}PL \ . \qquad (2.2.11)$$

Because of a lack of coordinate system definition a unique solution to equation (2.2.9) is not possible since N is a singular matrix with rank less than the number of parameters. Despite the dynamical constraints imposed on satellite motion a unique solution to equation (2.2.9) can only be achieved if origin and orientation constraints are imposed on the solution. In dynamic point positioning solutions these necessary constraints are usually imposed through the use of previously estimated satellite ephemerides. The satellite positions appearing in equation (2.2.6) and (2.2.7) are included in the normal equations (2.2.9) with weighted constraints based on the accuracy estimates of the satellite ephemerides utilized. If range or Doppler observations are made at two sites the station position solutions may be transformed into estimates of the parameters of the baseline connecting the sites.

Arur [1977] performed a rank analysis of Doppler observations and found that the vector of coordinate differences between the observing station and the mid-arc state vector of the satellite pass, the velocity components of this vector, and the frequency offset (f_0-f_s) are estimable. The components of station position only become estimable if constraints are imposed on the ephemeris. For coobserving stations the interstation coordinate differences are estimable quantities. A theoretical rank analysis carried out for ranging [Van Gelder, 1978] showed that the rank deficiency for the short arc mode is two. Thus without the use of sufficient constraints unique solutions to equation

(2.2.9) are not possible. Pavlis [1979] discusses the general problem of rank deficiency and procedures for obtaining solutions.

For positioning applications of the GPS system, satellite ephemerides will be estimated based on ranging observations from four stations. The projected accuracy of these ephemerides is discussed in Section 4.1.2. Range and Doppler positioning studies described in Chapter 4 will incorporate weight constraints based on assumed ephemeris accuracy.

2.2.3 Range and Doppler Error Sources

The accuracy of satellite ephemerides and tropospheric refraction modeling and the stability of satellite and receiver atomic clocks will have important consequences in the application of range and Doppler observations to geodetic positioning. An additional factor will be the precision of the electronic receiver. These sources of error are discussed in detail in Section 4.1. Their effect on geodetic positioning are discussed in Section 4.5.

2.3 Satellite Interferometry

Radio signals transmitted by GPS satellites have been proposed as a new resource for the application of interferometric techniques to baseline determination. The interferometry technique is based on observing the time (phase) difference of arrival of radio signals from a single source at two or more coobserving sites. Three different satellite interferometry proposals have been advanced. MacDoran [1979] proposes to utilize the broadcast GPS spread spectrum signals by

cross-correlating the recorded signals at two sites as in very long baseline interferometry. The observed quantity is the time difference of arrival of the signal at the two sites subject to a time synchronization error. A second proposal [Counselman, 1979] would derive interferometric phase observations from a series of continuous wave signals transmitted by equipment which would augment the GPS satellites. Observations would be made from at least four satellites simultaneously at each site to recover the components of the baseline in near real time. This technique relies on measuring the phase of up to ten continuous coherent signals broadcast from each satellite to eliminate the 2π phase ambiguity which occurs when a continuous wave is used. The phase measurements are differenced at both observing sites to form the interferometric phase difference. Bender [Letter to I. I. Mueller, 1979] proposes an alternative approach based on measurement of the phase of the reconstructed GPS carrier frequencies at two sites. The phase of the reconstructed carrier is measured with respect to a signal based on the receivers local frequency standard. Bender proposes making such measurements from three or more satellites simultaneously or within a relatively short time interval so that the local frequency standard stability is not a serious limitation. The use of a water vapor radiometer is proposed as in the MacDoran approach to virtually eliminate tropospheric refraction effects. This approach is also subject to the 2π phase ambiguity which must be resolved.

Thus three separate proposals have been advanced for an interferometric determination of baselines. The first is based on observing

the time difference of arrival of random signals at two sites. The other two proposals are based on the measurement of phase of continuous wave signals.

2.3.1 Measurement of Interferometric Time Delay and Phase

The interferometric time delay is the difference in the time of arrival of radio signals from a common source at two sites. In very long baseline interferometry the sources are the extremely distant quasars. For the proposals described above the sources are radio signals emitted from GPS satellites. Using the notation of equation (2.2.6) the time difference of arrival at sites i and ℓ is given by

$$\delta\tau = (R_i - R_\ell)/c = (|\overline{\rho}_s - \overline{\rho}_i| - |\overline{\rho}_s - \overline{\rho}_\ell|)/c + (\Delta\tau_i - \Delta\tau_\ell) \ . \quad (2.2.12)$$

In equation (2.2.12) the earth-fixed coordinates of the satellite appear since the radio signals received at each site are not incoming along parallel paths as with quasar sources. The last term in equation (2.2.12) is the clock synchronization error of the two observing sites.

If the observation is interferometric phase based on continuous wave radio signals, either broadcast or reconstructed, the observation equation has the form

$$\theta_i = \frac{2\pi}{\lambda}[|\overline{\rho}_s - \overline{\rho}_i| - m_i\lambda + c\Delta\tau_i] \quad (2.2.13)$$

where λ is the wavelength of the signal, m_i is the integer number of wavelengths comprising the geometric range and $\Delta\tau_i$ is the

synchronization error of equation (2.2.6). The wavelength λ is a function of time due to the Doppler shift. The difference in phase at two sites is given by

$$\Delta\theta = \theta_1 - \theta_2 = \frac{2\pi}{\lambda}\left[\left|\vec{\rho}_s - \vec{\rho}_1\right| - \left|\vec{\rho}_s - \vec{\rho}_2\right| - (m_1 - m_2)\lambda + c(\Delta\tau_1 - \Delta\tau_2)\right] . \quad (2.2.14)$$

Since the Doppler shift in frequency will not be identical at both observing sites equation (2.2.14) is an approximation to the order of accuracy that the Doppler shift is known a priori. The third term in equation (2.2.14) is the 2π ambiguity mentioned previously. Its a priori uncertainty will be a function of the initial accuracy of the observing station's coordinates.

Finally an examination of equations (2.2.12) and (2.2.14) shows that the time delay and the difference in interferometric phase are related by

$$\delta\tau = \frac{\lambda}{c}\left[\frac{\Delta\theta}{2\pi} + m_1 - m_2\right] \quad (2.2.15)$$

2.3.2 Comments on Rank Deficiency of Satellite Interferometry

Equation (2.2.12) and (2.2.14) reveal that satellite interferometry observations are a function of satellite position unlike quasar observations and are related to the difference in range between the satellite and the two observing sites. If normal equations for station position are formed from such observations the normal matrix N will not have full rank. Unless sufficient information is available on satellite position, a unique solution for earth-fixed station

coordinates is not possible. Even with such constraints the normal equations can still tend to become singular as the baseline distance decreases. This is demonstrated in Chapter 3.

The following approximation [Counselman, 1978] can be used in equations (2.2.12) and (2.2.14) to recast these equations in terms of baseline components

$$|\vec{\rho}_s - \vec{\rho}_1| - |\vec{\rho}_s - \vec{\rho}_2| \approx (\vec{\rho}_1 - \vec{\rho}_2) \cdot \hat{\rho}_s + \frac{1}{4\rho_s} [2(\rho_1^2 - \rho_2^2) - (\vec{\rho}_1 \cdot \hat{\rho}_s)^2 + (\vec{\rho}_2 \cdot \hat{\rho}_s)^2] \tag{2.2.16}$$

where $\hat{\rho}_s$ is the unit vector in the direction of the satellite. For short baselines defined as having

$$|\vec{\rho}_1 - \vec{\rho}_2| \ll \rho_s \tag{2.2.17}$$

the second term in equation (2.2.16) may be deleted. Then equations (2.2.12) and (2.2.14) become

$$\delta\tau = (\vec{\rho}_1 - \vec{\rho}_2) \cdot \hat{\rho}_s / c + (\Delta\tau_1 - \Delta\tau_2) \tag{2.2.18}$$

and

$$\Delta\theta = \frac{2\pi}{\lambda} [(\vec{\rho}_1 - \vec{\rho}_2) \cdot \hat{\rho}_s - (m_1 - m_2)\lambda + c(\Delta\tau_1 - \Delta\tau_2)] \ . \tag{2.2.19}$$

An examination of the derivatives of equation (2.2.18) with respect to baseline components and the time synchronization error reveals that these parameters are estimable if four satellites are observed which do not lie on the same circle in the sky [Counselman, 1978].

Equation (2.2.19) has the same form as equation (2.2.18) except for the $2n$ ambiguity term which cannot be separated from the synchronization error unless special procedures are implemented [Counselman, 1979]. The double differencing approach examined in Chapter 5 is another technique for handling this problem.

2.3.3 Interferometric Error Sources

MacDoran [1979] and Counselman [1979] outline the systematic and random error sources effecting their proposals. Included are the frequency stability of the receiver clocks, transmission media errors consisting of tropospheric and ionospheric refraction, GPS satellite positional accuracy and the precision of the instrumentation.

3. PRECISION COMPARISON OF RANGE, DOPPLER, AND INTERFEROMETRIC APPROACHES FOR BASELINE DETERMINATION

A complete comparison of the positioning accuracies obtainable from range, Doppler, and interferometric satellite observations would be difficult to perform since proposals based on the latter approach remain in an early stage of development. For instance, the exact nature of the instrumental error sources associated with satellite interferometry can only be conjectured at present. However range and Doppler geodetic receivers are currently being tested and estimates of measurement error are available. Therefore, for the range and Doppler proposals a detailed error analysis is presented in Chapter 4. Then in Chapter 5 an interferometric observation technique for baseline determination is considered which has a distinct advantage over the range and Doppler approaches.

In this chapter a comparison of the geometric strength of the three approaches is given based on the processing of range observations as range, correlated range difference and as interferometry or differenced ranges from two stations. This analysis will give an indication of the relative geometric strength of each approach for the determination of coordinate differences and baseline distances using observations from a constellation of high altitude satellites.

3.1 Mathematical Model and Adjustment Procedure

3.1.1 Mathematical Model

Let R_{ij} be the topocentric range from any ground station $P_i(u_i,v_i,w_i)$ to any satellite position $Q_j(u_j,v_j,w_j)$ as shown in Figure 3.1.1, where the earth-fixed coordinate system (u,v,w), is oriented towards the Greenwich mean astronomical meridian (u-axis) and the Conventional International Origin (w-axis) with the v-axis forming a right-handed coordinate system with u and w, this coordinate system being defined by the Bureau International de l'Heure (BIH). From Figure 3.1.1, the following equation can be written for the topocentric range

$$R_{ij} = [(u_j - u_i)^2 + (v_j - v_i)^2 + (w_j - w_i)^2]^{1/2} \quad . \qquad (3.1.1)$$

From two consecutive topocentric ranges, R_{ij} and R_{ik}, the range difference is defined as

$$\Delta R_{ijk} = R_{ik} - R_{ij} \qquad (3.1.2)$$

and from simultaneous range observations, R_{ij} and $R_{\ell j}$, taken at two stations $P_i(u_i,v_i,w_i)$ and $P_\ell(u_\ell,v_\ell,w_\ell)$, the interferometric observation is defined as

$$\delta R_{i\ell j} = R_{ij} - R_{\ell j} \quad . \qquad (3.1.3)$$

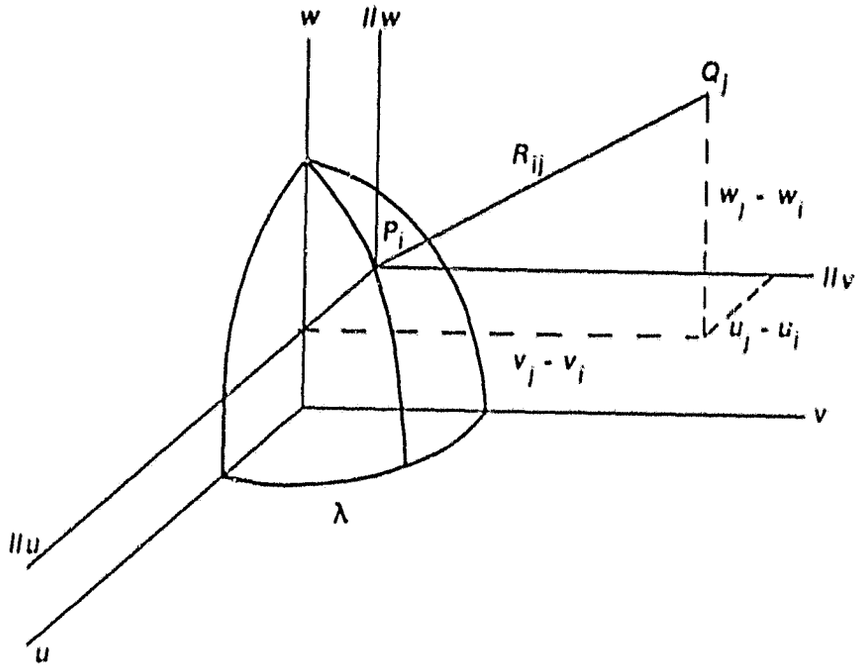

Figure 3.1.1. Geometry of Topocentric Range

3.1.2 Adjustment Procedure

The mathematical models (3.1.1) through (3.1.3) of the general form

$$L_a = F(X_a) \tag{3.1.4}$$

may be linearized by a Taylor series expansion about preliminary values for station and satellite coordinates X_o to obtain the observation equations [Uotila, 1967]

$$V = AX + L \tag{3.1.5}$$

where V is the vector of observation residuals defined by

$$V = L_a - L_b \ . \tag{3.1.6}$$

The elements of L are the differences between the function F evaluated at the preliminary values for the coordinates and the observed quantities L_b and A is a matrix of partial derivatives of F with respect to the coordinates. The vector X, representing corrections to the preliminary coordinate values, will be estimated from the observations L_b giving

$$X_a = X_o + X \tag{3.1.7}$$

using least squares minimum variance estimation.

For range observations R_{ij} and $R_{\ell j}$ made simultaneously at two stations the rows of the design matrix have the form

$$\begin{aligned} A_{ij} &= \frac{\partial R_{ij}}{\partial u_i, \partial u_\ell, \partial u_j} \\ &= [\, a_{ij} \mid 0 \mid -a_{ij} \,] \end{aligned} \tag{3.1.8}$$

and

$$\begin{aligned} A_{\ell j} &= \frac{\partial R_{\ell j}}{\partial u_i, \partial u_\ell, \partial u_j} \\ &= [\, 0 \mid a_{\ell j} \mid -a_{\ell j} \,] \end{aligned} \tag{3.1.9}$$

where

$$a_{ij} = \left[\frac{u_i - u_j}{R_{ij}} , \frac{v_i - v_j}{R_{ij}} , \frac{w_i - w_j}{R_{ij}} \right] \tag{3.1.10}$$

and

$$X^T = [du_i, dv_i, dw_i, du_\ell, dv_\ell, dw_\ell, du_j, dv_j, dw_j] \, . \tag{3.1.11}$$

The index j ranges over the number of satellite positions where range

observations are acquired. For single station tracking the parameters du_ℓ, dv_ℓ, and dw_ℓ are naturally omitted.

For range difference observations ΔR_{ijk} the contribution to the design matrix takes the form

$$\begin{aligned} A_{ijk} &= \frac{\partial \Delta R_{ijk}}{\partial u_i, \partial u_k, \partial u_j} \\ &= [a_{ik} - a_{ij} \mid - a_{ik} \mid a_{ij}] \end{aligned} \tag{3.1.12}$$

where

$$X^T = [du_i, dv_i, dw_i, du_k, dv_k, dw_k, du_j, dv_j, dw_j] \ . \tag{3.1.13}$$

And finally for interferometric observations $\delta R_{i\ell j}$ from two stations the contribution to the design matrix for each observation is

$$\begin{aligned} A_{i\ell j} &= \frac{\partial \delta R_{i\ell j}}{\partial u_i, \partial u_\ell, \partial u_j} \\ &= [a_{ij} \mid - a_{\ell j} \mid - a_{ij} + a_{\ell j}] \end{aligned} \tag{3.1.14}$$

with

$$X^T = [du_i, dv_i, dw_i, du_\ell, dv_\ell, dw_\ell, du_j, dv_j, dw_j] \ . \tag{3.1.15}$$

In the analysis presented in this chapter, which is intended to compare the geometric strength of these three observational approaches, the satellite ephemeris will be assumed known and excluded from the normal equations.

The least squares minimum variance estimate of X based on a set of observations is obtained by minimizing the function

$$\phi = V^T P V - 2K^T(AX + L - V) \tag{3.1.16}$$

with respect to the unknowns V, K, and X. P is the weight matrix for the observation set. After minimizing ϕ and eliminating the unknowns K and V, the least squares estimate for X is given by the solution of the normal equations

$$NX + U = 0 \tag{3.1.17}$$

where

$$N = A^T PA \tag{3.1.18}$$

and

$$U = A^T PL \ . \tag{3.1.19}$$

Solving equation (3.1.17) gives

$$X = N^{-1}U \ . \tag{3.1.20}$$

The covariance of the parameter estimates is given by the inverse of the normal matrix provided P is the inverse of the observation covariance matrix,

$$\Sigma_x = N^{-1} \ . \tag{3.1.21}$$

For observations from two stations the uncertainties in the baseline components are obtained by the linear transformation

$$\Sigma_{\Delta X} = G\Sigma_x G^T \tag{3.1.22}$$

where

$$G = [-I \quad I] \tag{3.1.23}$$

and

$$\Delta X^T = [du_\ell - du_i, \ dv_\ell - dv_i, \ dw_\ell - dw_i] = [\Delta u, \Delta v, \Delta w] \ . \tag{3.1.24}$$

The uncertainty in the chord length d is given by the transformation

$$\sigma_d^2 = H\Sigma_{\Delta x}H^T = HG\Sigma_x G^T H^T \qquad (3.1.25)$$

where

$$H = \left[\frac{u_\ell - u_i}{d} , \frac{v_\ell - v_i}{d} , \frac{w_\ell - w_i}{d} \right] . \qquad (3.1.26)$$

3.1.3 Weight Matrix

In minimum variance least squares estimation the weight matrix is taken to be the inverse of the covariance matrix of the observational errors

$$P = \Sigma_{L_b}^{-1} . \qquad (3.1.27)$$

For statistically independent range observations with constant variance the covariance matrix is given by

$$\Sigma_R = \sigma^2 I . \qquad (3.1.28)$$

The dimension of this matrix is equal to the number of observations acquired.

For N independent range observations taken from a single station, whose statistics are given by equation (3.1.28), the least squares normal equations for station coordinate improvement are

$$(A_R^T P_R A_R)X + A_R^T P_R L_R = 0 \qquad (3.1.29)$$

where

$$X^T = [du, dv, dw] . \qquad (3.1.30)$$

For (N-1) correlated range difference observations, defined as the difference between successive ranges, the least squares normal

equations can be directly obtained from the matrix components in equation (3.1.29) by the transformations

$$A_{\Delta R} = BA_R \tag{3.1.31}$$

$$L_{\Delta R} = BL_R \tag{3.1.32}$$

$$\Sigma_{\Delta R} = B\Sigma_R B^T \tag{3.1.33}$$

where the matrix B is defined by

$$B = \begin{bmatrix} -1 & 1 & 0 & \cdots & 0 \\ 0 & -1 & 1 & \cdots & 0 \\ & & \vdots & & \\ 0 & 0 & 0 & -1 & 1 \end{bmatrix}_{(N-1 \times N)} \tag{3.1.34}$$

with the range observation covariance matrix given by equation (3.1.28). The weight matrix for correlated range difference observations is given by

$$P_{\Delta R} = \Sigma_{\Delta R}^{-1} = (B\Sigma_R B^T)^{-1} = \frac{1}{\sigma^2}(BB^T)^{-1} . \tag{3.1.35}$$

For unit variance equation (3.1.35) becomes

$$P_{\Delta R} = (BB^T)^{-1} = \begin{bmatrix} 2 & -1 & 0 & \cdots & 0 \\ -1 & 2 & -1 & \cdots & 0 \\ 0 & -1 & 2 & \cdots & 0 \\ & & & \vdots & \\ 0 & \cdots & & 2 & -1 \\ 0 & \cdots & & -1 & 2 \end{bmatrix}^{-1}_{(N-1 \times N-1)} . \tag{3.1.36}$$

The normal equations for (N-1) correlated range difference observations, according to equation (3.1.17), may be written as

$$(A_{\Delta R}^T P_{\Delta R} A_{\Delta R})X + A_{\Delta R}^T P_{\Delta R} L_{\Delta R} = 0 \qquad (3.1.37)$$

or, using equations (3.1.31) through (3.1.36), equation (3.1.37) becomes

$$(A_R^T B^T (BB^T)^{-1} B A_R)X + A_R^T B^T (BB^T)^{-1} B L_R = 0 \ . \qquad (3.1.38)$$

Consider now N independent range observations taken simultaneously at two stations at times $t_1, t_2, \ldots, t_N$

$$R^T = [R_1^i, \ldots, R_N^i, R_1^\ell, \ldots, R_N^\ell] \ . \qquad (3.1.39)$$

The least squares normal equations for the parameter set

$$X^T = [du_i, dv_i, dw_i, du_\ell, dv_\ell, dw_\ell] \qquad (3.1.40)$$

are given by equation (3.1.29) with modifications to allow for the additional set of parameters. Defining N independent satellite interferometry observations as the difference between simultaneous ranges, the least squares normal equations for interferometry can similarly be developed from the matrix components of equation (3.1.29) by the transformations

$$A_{\delta R} = M A_R \qquad (3.1.41)$$

$$L_{\delta R} = M L_R \qquad (3.1.42)$$

$$\Sigma_{\delta R} = M \Sigma_R M^T \qquad (3.1.43)$$

where

$$M = [-I\ I]_{(N \times 2N)} \ . \tag{3.1.44}$$

The weight matrix for the statistically independent interferometric observations is given by

$$\begin{aligned} P_{\delta R} &= \Sigma_{\delta R}^{-1} = (M\Sigma_R M^T)^{-1} = (2\sigma^2 I)^{-1} \\ &= (2I)^{-1} \end{aligned} \tag{3.1.45}$$

for unit variance. The normal equations for interferometry are

$$(A_{\delta R}^T P_{\delta R} A_{\delta R})X + A_{\delta R}^T P_{\delta R} L_{\delta R} = 0 \tag{3.1.46}$$

or, using equations (3.1.41) through (3.1.45), are equivalent to

$$(A_R^T M^T (MM^T)^{-1} M A_R)X + A_R^T M^T (MM^T)^{-1} M L_R = 0 \ . \tag{3.1.47}$$

Thus the weight matrices for range difference and interferometric observations are obtained using the same linear transformation matrices which convert the range observations to the alternative data form. The range difference observations are correlated since each successive range difference observation is formed using a common range. This is reflected by the off-diagonal elements in matrix equation (3.1.36). Finally, it was shown that the range difference and interferometric normal equations are directly obtained from the range normal equations if the weight matrix is also modified accordingly. In equation (3.1.38) the modified weight matrix becomes $B^T(BB^T)^{-1}B$ and in equation (3.1.47) it is $M^T(MM^T)^{-1}M$.

3.1.4 Effect of A Priori Constraints on Positioning Based on Simultaneous Observation

In general, for simultaneous observations from two stations, the normal equations are developed for two sets of parameters, station coordinates and ephemeris variables. Although the analysis in this chapter assumes the latter to be known, it is of interest to examine the more general form of the normal equations to arrive at an understanding of what effect a priori information on either the ephemeris variables or the coordinates of one station has on the variance of the coordinates of the second station and baseline components. This situation would naturally arise in network densification using any of the observation types considered herein.

3.1.4.1 Range and Doppler

For simultaneous range and integrated Doppler observations from two stations, the least squares normal equations for station coordinates and ephemeris parameters have the following form for measurements that are either uncorrelated or are correlated by errors at individual tracking stations

$$\begin{bmatrix} N_{11} & 0 & N_{1S} \\ 0 & N_{22} & N_{2S} \\ N_{S1} & N_{S2} & N_{SS} \end{bmatrix} \begin{bmatrix} X_1 \\ X_2 \\ X_S \end{bmatrix} + \begin{bmatrix} U_1 \\ U_2 \\ U_S \end{bmatrix} = 0 \ . \qquad (3.1.48)$$

The covariance matrix for station coordinates based on the observations and on a priori knowledge of the first station's coordinates and the ephemeris parameters is

$$\Sigma_X = \begin{bmatrix} N_{11} + P_1 - N_{1S}(N_{SS} + P_S)^{-1}N_{S1} & -N_{1S}(N_{SS} + P_S)^{-1}N_{S2} \\ -N_{2S}(N_{SS} + P_S)^{-1}N_{S1} & N_{22} - N_{2S}(N_{SS} + P_S)^{-1}N_{S2} \end{bmatrix}^{-1} \tag{3.1.49}$$

$$= \begin{bmatrix} B_{11} & B_{12} \\ B_{21} & B_{22} \end{bmatrix}^{-1} = \begin{bmatrix} Q_{11} & Q_{12} \\ Q_{21} & Q_{22} \end{bmatrix}$$

where the parameter set X is defined by

$$X^T = [du_1, dv_1, dw_1, du_2, dv_2, dw_2] \ .$$

The covariance matrix elements are given by

$$\begin{aligned} Q_{11} &= [B_{11} - B_{12}B_{22}^{-1}B_{21}]^{-1} \\ &= [N_{11} + P_1 - N_{1S}(N_{SS} + P_S)^{-1}N_{S1} - N_{1S}(N_{SS} + P_S)^{-1}N_{S2} \\ &\quad (N_{22} - N_{2S}(N_{SS} + P_S)^{-1}N_{S2})^{-1}N_{2S}(N_{SS} + P_S)^{-1}N_{S1}]^{-1} \end{aligned} \tag{3.1.50}$$

$$\begin{aligned} Q_{22} &= B_{22}^{-1} + B_{22}^{-1}B_{21}Q_{11}B_{12}B_{22}^{-1} \\ &= [N_{22} - N_{2S}(N_{SS} + P_S)^{-1}N_{S2} - N_{2S}(N_{SS} + P_S)^{-1}N_{S1} \\ &\quad (N_{11} + P_1 - N_{1S}(N_{SS} + P_S)^{-1}N_{S1})^{-1}N_{1S}N_{SS}^{-1}N_{S2}]^{-1} \end{aligned} \tag{3.1.51}$$

$$\begin{aligned} Q_{12} &= -Q_{11}B_{12}B_{22}^{-1} \\ &= Q_{11}N_{1S}(N_{SS} + P_S)^{-1}N_{S2}[N_{22} - N_{2S}(N_{SS} + P_S)^{-1}N_{S2}]^{-1} \end{aligned} \tag{3.1.52}$$

$$Q_{21} = Q_{12}^T \ . \tag{3.1.53}$$

The matrix Q_{11} is the covariance matrix for the first station's

coordinates Σ_{X_1}, and Q_{22} is the covariance matrix for the second station's coordinates Σ_{X_2}.

The covariance matrix for coordinate differences, or baseline components, is obtained from equation (3.1.49) by the linear transformation

$$\begin{aligned}\Sigma_{\Delta X} &= [-I\ I]\begin{bmatrix} Q_{11} & Q_{12} \\ Q_{21} & Q_{22} \end{bmatrix}\begin{bmatrix} -I \\ I \end{bmatrix} \\ &= Q_{11} + Q_{22} - Q_{12} - Q_{21} \ .\end{aligned} \tag{3.1.54}$$

In terms of equations (3.1.50) through (3.1.53), equation (3.1.54) becomes

$$\begin{aligned}\Sigma_{\Delta X} &= Q_{11} + B_{22}^{-1} + B_{22}^{-1}B_{21}Q_{11}B_{12}B_{22}^{-1} + Q_{11}B_{12}B_{22}^{-1} \\ &\quad + B_{22}^{-1}B_{21}Q_{11} \\ &= B_{22}^{-1} + [B_{22}^{-1}B_{21} + I]Q_{11}[B_{22}^{-1}B_{21} + I]^T \ .\end{aligned} \tag{3.1.55}$$

This equation may also be written in the form

$$\Sigma_{\Delta X} = \Sigma_{X_1} + \Sigma_{X_2} + \Sigma_{X_1}B_{12}B_{22}^{-1} + B_{22}^{-1}B_{21}\Sigma_{X_1} \ . \tag{3.1.56}$$

Consider now the effect of a priori information on the covariance matrices given by equations (3.1.50), (3.1.51), and (3.1.56). The following cases are considered:

Case (i). Ephemeris parameters constrained and no knowledge of station 1 coordinates ($P_S = \infty$, $P_1 = 0$). Under these assumptions equations (3.1.49) through (3.1.56) reduce to the results

$$\Sigma_{X_1} = N_{11}^{-1} \tag{3.1.57}$$

$$\Sigma_{X_2} = N_{22}^{-1} \tag{3.1.58}$$

$$\Sigma_{\Delta X} = N_{11}^{-1} + N_{22}^{-1} \ . \tag{3.1.59}$$

Case (ii). Ephemeris parameters partially known and station 1 coordinates constrained ($0 < P_S < \infty$, $P_1 = \infty$).

$$\Sigma_{X_1} = 0 \tag{3.1.60}$$

$$\Sigma_{X_2} = [N_{22} - N_{2S}(N_{SS} + P_S)^{-1}N_{S2}]^{-1} \tag{3.1.61}$$

$$\Sigma_{\Delta X} = [N_{22} - N_{2S}(N_{SS} + P_S)^{-1}N_{S2}]^{-1} \ . \tag{3.1.62}$$

Case (iii). Ephemeris parameters constrained and station 1 coordinates constrained ($P_S = \infty$, $P_1 = \infty$).

$$\Sigma_{X_1} = 0 \tag{3.1.63}$$

$$\Sigma_{X_2} = N_{22}^{-1} \tag{3.1.64}$$

$$\Sigma_{\Delta X} = N_{22}^{-1} \ . \tag{3.1.65}$$

Case (iv). Ephemeris parameters and station 1 coordinates are partially known ($0 < P_S < \infty$, $0 < P_1 < \infty$).

$$\begin{aligned}\Sigma_{X_1} = [&N_{11} + P_1 - N_{1S}(N_{SS} + P_S)^{-1}N_{S1} - N_{1S}(N_{SS}+P_S)^{-1}N_{S2} \\ &(N_{22} - N_{2S}(N_{SS} + P_S)^{-1}N_{S2})^{-1}N_{2S}(N_{SS} + P_S)^{-1}N_{S1}]^{-1}\end{aligned} \tag{3.1.66}$$

$$\Sigma_{X_2} = [N_{22} - N_{2S}(N_{SS} + P_S)^{-1}N_{S2}]^{-1}$$
$$+ [N_{22} - N_{2S}(N_{SS} + P_S)^{-1}N_{S2}]^{-1}N_{2S}(N_{SS} + P_S)^{-1}N_{S1}\Sigma_{X_1} \qquad (3.1.67)$$
$$N_{1S}(N_{SS} + P_S)^{-1}N_{S2}[N_{22} - N_{2S}(N_{SS} + P_S)^{-1}N_{S2}]^{-1}$$

$$\Sigma_{\Delta X} = \Sigma_{X_1} + \Sigma_{X_2} + \Sigma_{X_1}B_{12}B_{22}^{-1} + B_{22}^{-1}B_{21}\Sigma_{X_1} \ . \qquad (3.1.68)$$

A comparison of these results indicates that the uncertainties in the coordinates u_2, v_2, w_2 are equivalent in cases (i) and (iii) where the ephemeris was assumed known and that this uncertainty can be expected to increase as the orbit uncertainty increases as in case (ii) and increase further as the uncertainty in station 1 also increases. In terms of eigenvalues of the covariance matrix, or parameter uncertainties, the following relationship can be established among the cases

$$\lambda_{X_2}^{(iii)} = \lambda_{X_2}^{(i)} < \lambda_{X_2}^{(ii)} < \lambda_{X_2}^{(iv)} \ . \qquad (3.1.69)$$

The uncertainties in the coordinate differences $u_2 - u_1$, $v_2 - v_1$, $w_2 - w_1$ are likewise a function of the assumed a priori information. Comparison of the results indicates first that if the coordinates of one of the observing stations are known, increasing the ephemeris uncertainty increases the uncertainty of the baseline components; and second, that if the ephemeris is known, increasing the uncertainty of the first station's coordinates also increases the baseline component uncertainty. The relationships among the baseline component covariance matrices are established to be

$$\lambda_{\Delta X}^{(iii)} < \lambda_{\Delta X}^{(ii)} \qquad (3.1.70)$$

and

$$\lambda_{\Delta X}^{(iii)} < \lambda_{\Delta X}^{(i)} \quad . \tag{3.1.71}$$

The most important result however is obtained by noting that for relatively close stations the submatrices N_{1S} and N_{2S} in equation (3.1.48) are approximately equal. Thus the last term in equation (3.1.68) of case (iv) will be negative definite insuring that the covariance for coordinate differences will be smaller than the sum of the coordinate covariance matrices, as opposed to case (i) when the ephemeris is constrained. Thus in general

$$\lambda_{\Delta X}^{(iv)} < \lambda_{X_1}^{(iv)} + \lambda_{X_2}^{(iv)} \quad . \tag{3.1.72}$$

This demonstrates how baseline component determinations may be obtained successfully in the presence of ephemeris errors which cause larger uncertainty in the coordinates themselves.

3.1.4.2 Interferometry

For satellite interferometry observations from two stations the least squares normal equations for station coordinates and ephemeris parameters have the form

$$\begin{bmatrix} N_{11} & N_{12} & N_{1S} \\ N_{21} & N_{22} & N_{2S} \\ N_{S1} & N_{S2} & N_{SS} \end{bmatrix} \begin{bmatrix} X_1 \\ X_2 \\ X_S \end{bmatrix} + \begin{bmatrix} U_1 \\ U_2 \\ U_S \end{bmatrix} = 0 \quad . \tag{3.1.73}$$

After algebraic elimination of the ephemeris parameters the covariance matrix for station coordinates including a priori information is

$$\Sigma_X = \begin{bmatrix} N_{11} + P_1 - N_{1S}(N_{SS} + P_S)^{-1}N_{S1} & N_{12} - N_{1S}(N_{SS} + P_S)^{-1}N_{S2} \\ N_{21} - N_{2S}(N_{SS} + P_S)^{-1}N_{S1} & N_{22} - N_{2S}(N_{SS} + P_S)^{-1}N_{S2} \end{bmatrix}^{-1} \tag{3.1.74}$$

$$= \begin{bmatrix} B_{11} & B_{12} \\ B_{21} & B_{22} \end{bmatrix}^{-1} = \begin{bmatrix} Q_{11} & Q_{12} \\ Q_{21} & Q_{22} \end{bmatrix}$$

where the covariance matrix elements are given by

$$Q_{11} = [B_{11} - B_{12}B_{22}^{-1}B_{21}]^{-1}$$

$$= [N_{11} + P_1 - N_{1S}(N_{SS} + P_S)^{-1}N_{S1} - (N_{12} - N_{1S}(N_{SS} + P_S)^{-1}N_{S2}) \tag{3.1.75}$$

$$(N_{22} - N_{2S}(N_{SS} + P_S)^{-1}N_{S2})^{-1}(N_{12} - N_{1S}(N_{SS} + P_S)^{-1}N_{S2})^T]^{-1}$$

$$Q_{22} = B_{22}^{-1} + B_{22}^{-1}B_{21}Q_{11}B_{12}B_{22}^{-1}$$

$$= [N_{22} - N_{2S}(N_{SS} + P_S)^{-1}N_{S2} - (N_{21} - N_{2S}(N_{SS} + P_S)^{-1}N_{S1}) \tag{3.1.76}$$

$$(N_{11} + P_1 - N_{1S}(N_{SS} + P_S)^{-1}N_{S1})^{-1}(N_{21} - N_{2S}(N_{SS} + P_S)^{-1}N_{S1})^T]^{-1}$$

$$Q_{21} = -Q_{11}B_{12}B_{22}^{-1}$$

$$= -Q_{11}(N_{12} - N_{1S}(N_{SS} + P_S)^{-1}N_{S2})(N_{22} - N_{2S}(N_{SS} + P_S)^{-1}N_{S2})^{-1} \tag{3.1.77}$$

$$Q_{21} = Q_{12}^T \ . \tag{3.1.78}$$

Again Q_{11} and Q_{22} are the covariance matrices for the station coordinates.

The covariance matrix for the baseline components is obtained using the transformation equation (3.1.54) and has the same form as equation (3.1.56):

$$\begin{aligned}\Sigma_{\Delta X} &= Q_{11} + Q_{22} - Q_{12} - Q_{21} \\ &= \Sigma_{X_1} + \Sigma_{X_2} + \Sigma_{X_1} B_{12} B_{22}^{-1} + B_{22}^{-1} B_{21} \Sigma_{X_1} \ .\end{aligned} \tag{3.1.79}$$

For the cases considered previously, equations (3.1.75) through (3.1.79) reduce to the following

Case (i). Ephemeris parameters constrained and no knowledge of station 1 coordinates ($P_S = \infty$, $P_1 = 0$).

$$\Sigma_{X_1} = [N_{11} - N_{12} N_{22}^{-1} N_{21}]^{-1} \tag{3.1.80}$$

$$\Sigma_{X_2} = [N_{22} - N_{21} N_{11}^{-1} N_{12}]^{-1} \tag{3.1.81}$$

$$\Sigma_{\Delta X} = \Sigma_{X_1} + \Sigma_{X_2} + \Sigma_{X_1} N_{12} N_{22}^{-1} + N_{22}^{-1} N_{21} \Sigma_{X_1} \ . \tag{3.1.82}$$

Case (ii). Ephemeris parameters partially known and station 1 coordinates constrained ($0 < P_S < \infty$, $P_1 = \infty$).

$$\Sigma_{X_1} = 0 \tag{3.1.83}$$

$$\Sigma_{X_2} = [N_{22} - N_{2S}(N_{SS} + P_S)^{-1} N_{S2}]^{-1} \tag{3.1.84}$$

$$\Sigma_{\Delta X} = [N_{22} - N_{2S}(N_{SS} + P_S)^{-1} N_{S2}]^{-1} \ . \tag{3.1.85}$$

Case (iii). Ephemeris parameters constrained and station 1 coordinates constrained ($P_S = \infty$, $P_1 = \infty$).

$$\Sigma_{X_1} = 0 \tag{3.1.86}$$

$$\Sigma_{X_2} = N_{22}^{-1} \tag{3.1.87}$$

$$\Sigma_{\Delta X} = N_{22}^{-1} \, . \tag{3.1.88}$$

Case (iv). Ephemeris parameters and station 1 coordinates are partially known ($0 < P_S < \infty$, $0 < P_1 < \infty$).

$$\Sigma_{X_1} = \text{(see equation (3.1.75))}$$

$$\Sigma_{X_2} = \text{(see equation (3.1.76))}$$

$$\Sigma_{\Delta X} = \Sigma_{X_1} + \Sigma_{X_2} + \Sigma_{X_1} B_{12} B_{22}^{-1} + B_{22}^{-1} B_{21} \Sigma_{X_1} \, . \tag{3.1.89}$$

An examination of these cases reveals the following relationships in terms of the eigenvalues of the station covariance matrices

$$\lambda_{X_2}^{(iii)} < \lambda_{X_2}^{(ii)} < \lambda_{X_2}^{(iv)} \tag{3.1.90}$$

and

$$\lambda_{X_2}^{(iii)} < \lambda_{X_2}^{(i)} \, . \tag{3.1.91}$$

For baseline component determinations

$$\lambda_{\Delta X}^{(iii)} < \lambda_{\Delta X}^{(ii)} \tag{3.1.92}$$

In cases (i) and (iv), however, the equations reveal how interferometry is suited for the determination of baseline components for close stations. Under those circumstances

$$N_{12} \cong -N_{22} \tag{3.1.93}$$

$$B_{12} \cong -B_{22} \cdot \tag{3.1.94}$$

Thus, the last two terms in equations (3.1.82) and (3.1.89) are nearly the additive inverse of the sum of the first two terms yielding an acceptable baseline component covariance even in the presence of large ephemeris error.

Interesting also, under conditions where approximations (3.1.93) and (3.1.94) are valid, are the results obtained in cases (i) and (iv) for the coordinate covariances, equations (3.1.80), (3.1.81), (3.1.75), and (3.1.76). In these cases, even when the satellite ephemeris is known, the covariance matrix tends to be singular as the baseline distance decreases. For interferometry, station coordinates are not estimable under these conditions; however, baseline components are.

3.2 Comparison of Range, Doppler, and Satellite Interferometry

In this section, a comparison of range, integrated Doppler, and satellite interferometry techniques for the determination of baseline components and chord distances is described. The basic intent of this analysis is to compare the relative geometric strength of each technique and obtain a measure of how the results themselves vary under differing circumstances of usage. The analysis is based on statistically independent range observations of unit variance taken simultaneously from two sites using a single-channel receiver as shown in Figure 3.2.1.

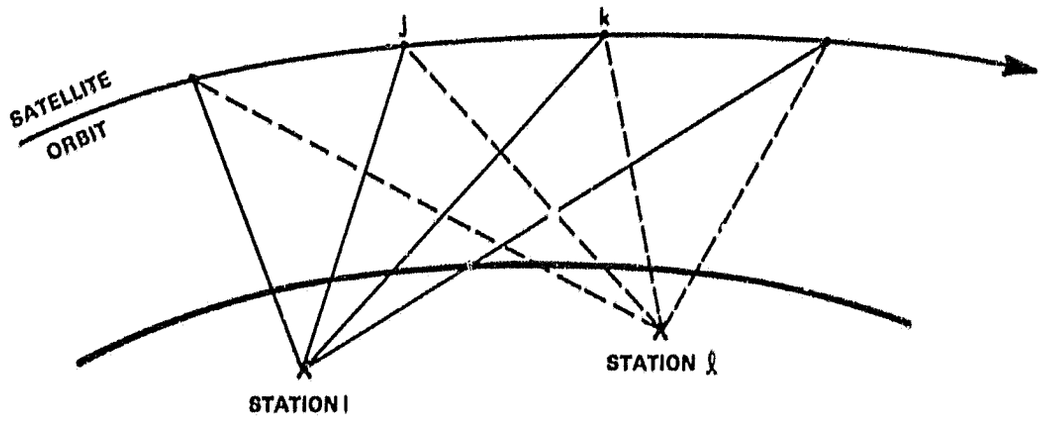

Figure 3.2.1. Simultaneous Range Measurements From Two Ground Stations

These observations are treated as range, correlated range difference, and as interferometric observations. Observations are included in the analysis if the satellite elevation exceeds 10 degrees. An analysis of variance is performed using least squares minimum variance estimation incorporating the weight matrices of Section 3.1.3. The parameters are the corrections to the baseline components

$$\begin{aligned} \Delta u &= du_\ell - du_i \\ \Delta v &= dv_\ell - dv_i \\ \Delta w &= dw_\ell - dw_i \end{aligned} \tag{3.2.1}$$

and the chord distance d, defined as

$$d = [(u_\ell - u_i)^2 + (v_\ell - v_i)^2 + (w_\ell - w_i)^2]^{1/2} . \tag{3.2.2}$$

No time synchronization parameters are included.

The orbital elements used in this study are given in Table 3.2.1. With a 24-satellite constellation five to nine satellites are

in view of a station at all times. For simultaneous observations from two stations, the number in view decreases with an increase in the separation distance. Simultaneous three-station tracking was not considered since each baseline would not be determined as well, especially for stations of great separation where the number of satellites in common view is less.

TABLE 3.2.1. GLOBAL POSITIONING SYSTEM ORBITAL ELEMENTS

EPOCH: 1975 DAY 116.0 $a = 26560$ km $e = 0.0$ $i = 63°$ $\omega = 0°$

SATELLITE	M	Ω
1	0°	0°
2	45	0
3	90	0
4	135	0
5	180	0
6	225	0
7	270	0
8	315	0
9	345	120°
10	30	120
11	75	120
12	120	120
13	165	120
14	210	120
15	255	120
16	300	120
17	15	240°
18	60	240
19	105	240
20	150	240
21	195	240
22	240	240
23	285	240
24	330	240

Two station groups are considered. The first is a mid-latitude group of three stations whose geodetic coordinates are given in Table 3.2.2. The chord distances separating the station pairs 1001-1002 and 1001-1003 are approximately 100 kilometers. The second group of stations is the so-called "Iron Triangle" very long baseline

interferometry (VLBI) stations whose geodetic coordinates are given in Table 3.2.3 and whose chord distances are found in Table 3.2.4. The maximum baseline distance for this group is nearly 4000 kilometers, and the minimum is 1500 kilometers.

Since variations in the tracking scenario are possible with multiple satellites in view, a criterion for satellite selection is adopted. Given the normal matrix N based on all prior observational data, the next satellite to be selected for observation will be the one whose observations, when included with prior data, minimize the trace of the parameter covariance matrix. For baseline components this trace is the sum of the baseline parameter variances

$$\mathrm{Tr}(\Sigma_{\Delta X}) = \sigma^2_{\Delta u} + \sigma^2_{\Delta v} + \sigma^2_{\Delta w} \ . \qquad (3.2.3)$$

For the chord the trace is the variance of the estimated chord length. For each type of observation these criteria are virtually independent since minimizing the trace of the baseline component covariance matrix does not guarantee that the chord length variance is a minimum. That will depend on the correlations between the baseline components.

3.2.1 Short Baseline Comparison

An analysis of variance study was made for the mid-latitude stations with parameter sets consisting of the baseline components and chord length. The observation schedules for the two baselines considered, the north-south baseline 1001-1002 and the east-west baseline 1001-1003, were based on ranging measurements taken every five minutes. Range observations were processed as range, correlated range difference

TABLE 3.2.2. GEODETIC COORDINATES OF MID-LATITUDE STATIONS

STATION NO.	GEODETIC COORDINATES						
	LATITUDE			LONGITUDE			HEIGHT (m)
1001	30°	0′	0.00″	45°	0′	0.00″	0.0
1002	30	54	7.56	45	0	0.00	0.0
1003	30	0	0.00	43	57	48.96	0.0

TABLE 3.2.3. IRON TRIANGLE STATION COORDINATES

STATION	GEODETIC COORDINATES						
	LATITUDE			LONGITUDE			HEIGHT (m)
WESTFORD (WS)	42°	36′	46.518″	288°	30′	22.720″	67.4
OWENS VALLEY (OV)	37	13	53.287	241	43	2.441	1172.9
FORT DAVIS (FD)	30	38	44.924	256	3	0.0	1580.0

TABLE 3.2.4. BASELINE DISTANCES (km)

WS	–		
OV	*3929*	–	
FD	*3135*	*1508*	–
	WS	*OV*	*FD*

and as interferometry. The results are based on an equivalent number of observations of each type. The satellites selected for tracking were chosen using the criteria defined above which are a function of the observation type and the parameter set definition. Several observation schedules were considered where the time allotted for simultaneously tracking each satellite was fixed at one, two, or three hours. One typical observation schedule is given in Figure 3.2.2 where the satellite tracking interval is three hours. The analysis of variance results for the mid-latitude station group are given in Tables 3.2.5 through 3.2.7. The results are based on 24 hours of continuous observation with intermediate results given at either 8 or 9 hours. No a priori knowledge of the station coordinates was assumed in these results. The range observations were taken as statistically independent having unit variance or a one meter standard error. To obtain an estimate of the ultimate precision obtainable for a particular observation type the results found in the tables must be scaled by the ratio of the assumed standard error in centimeters of that observation type, converted to the uncertainty of an equivalent range observation, to the 100 centimeter standard error used to obtain the results. For instance, if it were assumed that correlated range differences may be measured with a standard error of 10 centimeters then, noting the defining equation (3.1.3) for range differences and equation (3.1.35), the standard error of an equivalent range measurement would be 10 centimeters divided by the square root of two. The standard error of an equivalent range measurement is defined as that value which when utilized in equation

(3.1.35) or (3.1.45) would yield the assumed standard error for range difference or interferometric observations respectively.

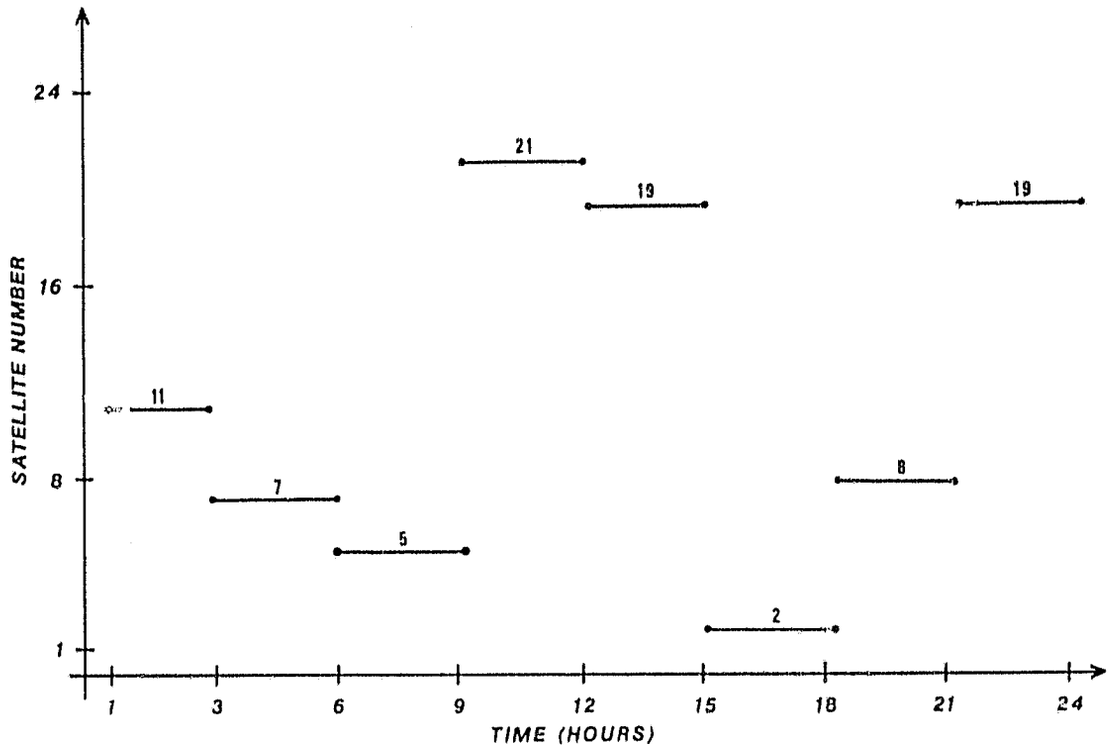

Figure 3.2.2. Typical Observation Schedule for a Three-Hour Satellite Tracking Interval (Stations 1001 and 1002, Range Observations)

Using 24 hours of range observations the baseline components are determined with an uncertainty of approximately 15 centimeters with slight variation as a function of the time interval each satellite is tracked. The chord distance has a standard error of approximately 11.5 centimeters and increases, but not more than 10 percent, as the tracking interval increases to three hours. This increase is due to an increase in the correlations between baseline parameters. There are no discernible trends due to the orientation of the baseline.

For correlated Doppler observations based on one-hour tracking intervals there is a six-fold increase in the baseline component uncertainty compared to the range results as seen from Table 3.2.5. However as the satellite tracking interval is increased to three hours this standard error decreases dramatically. The same is true of the uncertainty in chord length. No variation in the Doppler results is seen on the basis of orientation except with chord length where the uncertainty in the length of the east-west chord remains significantly larger in all cases, ranging from a difference of 2 parts to 0.9 parts per million (ppm). A comparison of the best Doppler results from Table 3.2.7 with the corresponding range results from Tables 3.2.5 through 3.2.7 indicates that results obtained from range observations with a one meter standard error can be equivalently obtained using correlated range differences if the standard error of the latter observation type is approximately 49 centimeters. This result is obtained by determining the uncertainty of an equivalent range observation (35 centimeters) which when used in the range difference weighting equation (3.1.35) will scale the Doppler results of Table 3.2.7 to be equivalent to those of Table 3.2.5 obtained using range observations with a one meter standard error. To obtain an equivalent uncertainty in estimated chord length, correlated range difference would require a standard error of 54 centimeters.

Also of importance is the ratio of the uncertainty of the estimated parameters to the observation uncertainty. This ratio is obtained by dividing the parameter uncertainties found in Tables 3.2.5 through 3.2.7 by the standard error of the appropriate measurement type.

The standard errors for range, range difference, and interferometry observations are 100, 141, and 141 centimeters respectively which may be verified using equations (3.1.33) and (3.1.43) assuming the one meter standard error for range. Based on 24 hours of observation this ratio is approximately 0.15 for range and 0.28 for correlated range difference considering the best results for the latter. For the chord length the ratios for range and range difference are 0.12 and 0.14 to 0.21, respectively. The last two ratios for range difference reflect the variation in the results in Table 3.2.7 for the two orientations. These ratios are of importance as scale factors which can be applied to assumed observational uncertainties to obtain estimates for parameter uncertainties. For instance, if correlated range differences had a measurement uncertainty of X centimeters, the uncertainty in the derived baseline components would be approximately 0.28X centimeters instead of the approximately 40 centimeters as given in Table 3.2.7.

With interferometric observations the resulting uncertainties of the baseline components are approximately twice as large as the range observation results after 24 hours. The uncertainty increases about 25 percent as the tracking interval increases from one to three hours. The uncertainty in the chord length is about 2.5 times greater than the range-derived chord. The trace of the covariance matrix from interferometry shows little variation with orientation but variation in the distribution of the uncertainty among the parameters exists. The chord length uncertainty is nearly equivalent for the two orientations. To produce baseline component uncertainties equivalent to the range results, the standard error of interferometric observations would be

required to be 71 centimeters. Again this result is obtained by determining the uncertainty of an equivalent range measurement (51 centimeters) which when used in the interferometry weighting equation (3.1.45) will scale the interferometry results of Table 3.2.5 to be equivalent with the range results of Table 3.2.5 based on a one meter standard error of observation. For comparable chord results with interferometry a standard error of 54 centimeters or an equivalent range uncertainty of 38 centimeters would be necessary. The ratio of parameter uncertainty to measurement uncertainty is approximately 0.21 for baseline components and 0.38 for the chord length.

The covariance computations for the one-hour tracking interval were repeated to obtain a measure of how knowledge of one station's coordinates could improve the results. The expected change in the baseline component covariance is given by a comparison of equations (3.1.59) and (3.1.65), which predict a square root of two decrease in the coordinate difference uncertainty for range and Doppler observations and by a comparison of equations (3.1.82) and (3.1.88) for interferometric observations. In the latter comparison the exact decrease in the uncertainty to be expected is not as obvious. An examination of Tables 3.2.5 and 3.2.8 show in fact that the uncertainty of the coordinate differences and also of the chord length decrease by the square root of two for range and Doppler. For interferometry the baseline component uncertainties decrease by approximately the square root of three and the chord uncertainty by approximately the square root of seven. Notice that the uncertainty in the chord based on interferometry with one station held fixed is equal, to the number of digits given, to the chord uncertainty

TABLE 3.2.5. STANDARD ERROR OF BASELINE PARAMETERS FOR MID-LATITUDE STATIONS BASED ON RANGE, INTEGRATED DOPPLER AND INTERFEROMETRIC TIME DELAY (ONE-HOUR TRACKING INTERVAL)

TOTAL OBSERVATION TIME		8 HOURS						24 HOURS					
BASELINE CONFIGURATION		1001 - 1002			1001 - 1003			1001 - 1002			1001 - 1003		
OBSERVATION TYPE		R	D	I	R	D	I	R	D	I	R	D	I
BASELINE PARAMETERS (cm)	Δu	25.1	136.2	47.4	25.1	166.4	53.2	14.8	95.3	25.2	14.2	95.4	29.4
	Δv	23.0	143.6	52.8	23.0	143.7	54.2	14.4	92.2	25.6	14.2	92.3	30.8
	Δw	24.6	148.5	62.3	24.6	148.5	43.1	14.4	84.1	34.4	15.1	84.1	23.5
	$\sqrt{\text{TRACE}}$	42.0	265.2	94.4	42.0	265.3	87.3	25.1	157.0	49.7	25.1	157.2	48.7
BASELINE DISTANCES (cm)	d	23.3	93.9	32.3	21.8	125.1	56.9	11.7	52.4	30.5	11.2	71.9	29.2
		(2.3)	(9.4)	(3.2)	(2.2)	(12.5)	(5.7)	(1.2)	(5.2)	(3.1)	(1.1)	(7.2)	(2.9)

COMMENTS: NUMBERS IN PARENTHESIS INDICATE RELATIVE PRECISION IN PARTS PER 10^6. RESULTS ARE BASED ON SIMULTANEOUS OBSERVATIONS EVERY 5 MINUTES WITH MEASUREMENT UNCERTAINTIES OF 100, 141, AND 141 CENTIMETERS FOR RANGE, RANGE DIFFERENCE, AND INTERFEROMETRY RESPECTIVELY. TO OBTAIN AN ESTIMATE OF THE PRECISION OBTAINABLE USING AN OBSERVATION TYPE WITH DIFFERENT MEASUREMENT UNCERTAINTY MULTIPLY TABLE VALUE BY THE RATIO OF THAT UNCERTAINTY TO THE CORRESPONDING UNCERTAINTY ABOVE.

TABLE 3.2.6. STANDARD ERROR OF BASELINE PARAMETERS FOR MID-LATITUDE STATIONS BASED ON RANGE, INTEGRATED DOPPLER AND INTERFEROMETRIC TIME DELAY (TWO-HOUR TRACKING INTERVAL)

TOTAL OBSERVATION TIME		8 HOURS						24 HOURS					
BASELINE CONFIGURATION		1001-1002			1001-1003			1001-1002			1001-1003		
OBSERVATION TYPE		R	D	I	R	D	I	R	D	I	R	D	I
BASELINE PARAMETERS (cm)	Δu	29.2	108.7	61.4	29.2	108.9	56.1	14.8	49.1	26.6	14.8	49.2	36.3
	Δv	26.0	85.3	67.8	26.0	85.4	85.5	14.1	51.9	28.0	14.1	51.9	39.0
	Δw	22.7	86.3	67.3	22.7	86.5	40.1	14.5	43.2	38.7	14.5	43.2	26.?
	$\sqrt{\text{TRACE}}$	45.2	162.9	113.6	45.2	163.2	109.8	25.1	83.5	54.7	25.1	83.5	59.4
BASELINE DISTANCES (cm)	d	26.0	55.7	61.7	25.5	71.7	56.9	12.4	28.4	31.6	13.3	37.6	29.9
		(2.6)	(5.6)	(6.2)	(2.6)	(7.2)	(5.7)	(1.2)	(2.8)	(3.2)	(1.3)	(3.8)	(3.0)

COMMENTS: NUMBERS IN PARENTHESIS INDICATE RELATIVE PRECISION IN PARTS PER 10^6. RESULTS ARE BASED ON SIMULTANEOUS OBSERVATIONS EVERY 5 MINUTES WITH MEASUREMENT UNCERTAINTIES OF 100, 141, AND 141 CENTIMETERS FOR RANGE, RANGE DIFFERENCE, AND INTERFEROMETRY RESPECTIVELY. TO OBTAIN AN ESTIMATE OF THE PRECISION OBTAINABLE USING AN OBSERVATION TYPE WITH DIFFERENT MEASUREMENT UNCERTAINTY MULTIPLY TABLE VALUE BY THE RATIO OF THAT UNCERTAINTY TO THE CORRESPONDING UNCERTAINTY ABOVE.

TABLE 3.2.7. STANDARD ERROR OF BASELINE PARAMETERS FOR MID-LATITUDE STATIONS BASED ON RANGE, INTEGRATED DOPPLER AND INTERFEROMETRIC TIME DELAY (THREE-HOUR TRACKING INTERVAL)

TOTAL OBSERVATION TIME		9 HOURS						[illegible] HOURS					
BASELINE CONFIGURATION		1001-1002			1001-1003			1001-[illegible]			1001-1003		
OBSERVATION TYPE		R	D	I	R	D	I	R	D	I	R	D	I
BASELINE PARAMETERS (cm)	Δu	30.3	88.1	62.9	30.4	88.2	91.9	15.3	43.0	27.5	15.3	35.1	33.6
	Δv	26.3	61.6	72.7	26.3	61.7	82.4	14.4	38.0	33.1	14.4	42.9	43.7
	Δw	24.4	49 7	90.5	24.4	49.8	92.4	14.3	32.1	41.5	14.2	31.5	26.2
	$\sqrt{\text{TRACE}}$	47.0	118.5	132.0	47.0	118.6	154.1	25.4	65.8	59.8	25.4	63.7	61.1
BASELINE DISTANCES (cm)	d	21.9	34.5	84.3	24.8	64.9	74.2	13.6	19.6	34.3	13.0	28.8	36.3
		(2.2)	(3.5)	(8.4)	(2.5)	(6.5)	(7.4)	(1.4)	(2.0)	(3.4)	(1.3)	(2.9)	(3.6)

COMMENTS: NUMBERS IN PARENTHESIS INDICATE RELATIVE PRECISION IN PARTS PER 10^6. RESULTS ARE BASED ON SIMULTANEOUS OBSERVATIONS EVERY 5 MINUTES WITH MEASUREMENT UNCERTAINTIES OF 100, 141, AND 141 CENTIMETERS FOR RANGE, RANGE DIFFERENCE, AND INTERFEROMETRY RESPECTIVELY. TO OBTAIN AN ESTIMATE OF THE PRECISION OBTAINABLE USING AN OBSERVATION TYPE WITH DIFFERENT MEASUREMENT UNCERTAINTY MULTIPLY TABLE VALUE BY THE RATIO OF THAT UNCERTAINTY TO THE CORRESPONDING UNCERTAINTY ABOVE.

TABLE 3.2.8. EFFECT OF A PRIORI CONSTRAINT ON STANDARD ERROR OF BASELINE PARAMETERS FOR MID-LATITUDE STATIONS BASED ON RANGE, INTEGRATED DOPPLER AND INTERFEROMETRIC TIME DELAY (ONE-HOUR TRACKING INTERVAL)*

TOTAL OBSERVATION TIME		8 HOURS						24 HOURS					
BASELINE CONFIGURATION		1001 - 1002			1001 - 1003			1001 - 1002			1001 - 1003		
OBSERVATION TYPE		R	D	I	R	D	I	R	D	I	R	D	I
BASELINE PARAMETERS (cm)	Δu	17.7	117.6	27.7	17.7	117.6	33.5	10.4	67.3	16.5	10.0	67.5	14.8
	Δv	16.3	101.6	34.3	16.3	101.6	25.5	10.2	65.1	18.0	10.0	65.2	14.7
	Δw	17.4	105.1	24.1	17.4	105.1	24.8	10.2	59.5	12.7	10.7	59.5	18.6
	$\sqrt{\text{TRACE}}$	29.7	187.6	50.3	29.7	187.6	48.9	17.8	111.0	27.5	17.8	111.1	27.9
BASELINE DISTANCE (cm)	d	16.5	66.4	23.4	15.4	88.5	21.7	8.3	37.0	11.7	7.9	50.9	11.2
		(1.7)	(6.6)	(2.3)	(1.5)	(8.8)	(2.2)	(0.8)	(3.7)	(1.2)	(0.8)	(5.1)	(1.1)

COMMENTS: NUMBERS IN PARENTHESIS INDICATE RELATIVE PRECISION IN PARTS PER 10^6. RESULTS ARE BASED ON SIMULTANEOUS OBSERVATIONS EVERY 5 MINUTES WITH MEASUREMENT UNCERTAINTIES OF 100, 141, AND 141 CENTIMETERS FOR RANGE, RANGE DIFFERENCE, AND INTERFEROMETRY RESPECTIVELY. TO OBTAIN AN ESTIMATE OF THE PRECISION OBTAINABLE USING AN OBSERVATION TYPE WITH DIFFERENT MEASUREMENT UNCERTAINTY MULTIPLY TABLE VALUE BY THE RATIO OF THAT UNCERTAINTY TO THE CORRESPONDING UNCERTAINTY ABOVE.

* STATION 1001 FIXED IN ADJUSTMENT

based on range with no a priori constraints. For shorter baselines these results will be nearly equal, and this can be shown mathematically using equations (3.1.43), (3.1.54), (3.1.59), and (3.1.88) keeping in mind the partial derivative equations (3.1.10) and (3.1.14). It can be concluded for network densification that a priori knowledge of the coordinates of the existing control point has a greater impact on interferometry than on range and Doppler.

3.2.2 Long Baseline Comparison

For the long baselines of the Iron Triangle (Table 3.2.3) a similar analysis was performed to determine the relative geometric strength of each observation type for determining baseline components and chord length. The results are based on an observation schedule of simultaneous observations taken from two stations every five minutes for a full day. Here, one- and two-hour satellite tracking intervals are examined. Parameters corresponding to each side of the triangle are determined using only observations from the two stations forming that side. This allows the greatest flexibility in satellite geometry. The results are given in Tables 3.2.9 and 3.2.10.

Based on 24 hours of range observations with one-hour tracking intervals, the uncertainties of the baseline components range from 13.5 to 17.0 centimeters showing minor variation with triangle side despite the different orientations and lengths. Increasing the satellite tracking interval to two hours produces a marginal increase in these uncertainties. The chord length uncertainty also increases slightly with side length but in terms of ppm decreases significantly.

TABLE 3.2.9. STANDARD ERROR OF BASELINE PARAMETERS FOR IRON TRIANGLE BASED ON RANGE, INTEGRATED DOPPLER, AND INTERFEROMETRIC TIME DELAY (ONE-HOUR TRACKING INTERVAL)

TOTAL OBSERVATION TIME		8 HOURS									24 HOURS								
BASELINE CONFIGURATION		W-OV			W-FD			OV-FD			W-OV			W-FD			OV-FD		
OBSERVATION TYPE		R	D	I	R	D	I	R	D	I	R	D	I	R	D	I	R	D	I
BASELINE PARAMETERS (cm)	Δu	31.8	148.1	178.2	30.7	151.3	179.1	24.0	153.3	67.5	17.0	87.9	71.1	16.4	88.0	54.5	14.6	90.2	33.5
	Δv	25.6	162.4	87.1	25.0	167.0	84.9	23.6	167.3	135.8	14.7	100.2	41.6	14.4	96.3	40.6	25.0	99.4	37.6
	Δw	22.8	151.3	93.8	23.9	138.5	74.9	25.1	149.1	48.6	13.5	88.1	35.0	14.5	91.0	32.4	14.4	88.4	32.0
	$\sqrt{\text{TRACE}}$	46.7	260.8	219.4	46.3	272.9	154.7	41.9	272.5	134.6	26.3	159.8	89.5	26.2	159.1	75.3	26.4	159.7	69.1
BASELINE DISTANCE (cm)	d	27.9	130.5	142.9	24.4	140.2	120.5	2.6	1.6	64.0	13.5	81.7	68.2	13.1	71.4	53.6	1.4	69.4	33.3
		(0.7)	(3.3)	(3.6)	(0.8)	(4.7)	(3.8)	(1.5)	(8.4)	(5.6)	(0.4)	(1.8)	(1.7)	(0.4)	(2.3)	(1.7)	(1.8)	(4.6)	(2.6)

COMMENTS: NUMBERS IN PARENTHESIS INDICATE RELATIVE PRECISION IN PARTS PER 10^7. RESULTS ARE BASED ON SIMULTANEOUS OBSERVATIONS EVERY 5 MINUTES WITH MEASUREMENT UNCERTAINTIES OF 100, 141, AND 141 CENTIMETERS FOR RANGE, RANGE DIFFERENCE, AND INTERFEROMETRY RESPECTIVELY. TO OBTAIN AN ESTIMATE OF THE PRECISION OBTAINABLE USING AN OBSERVATION TYPE WITH DIFFERENT MEASUREMENT UNCERTAINTY MULTIPLY TABLE VALUE BY THE RATIO OF THAT UNCERTAINTY TO THE CORRESPONDING UNCERTAINTY ABOVE.

TABLE 3.2.10. STANDARD ERROR OF BASELINE PARAMETERS FOR IRON TRIANGLE BASED ON RANGE, INTEGRATED DOPPLER, AND INTERFEROMETRIC TIME DELAY (TWO-HOUR TRACKING INTERVAL)

TOTAL OBSERVATION TIME		6 HOURS									24 HOURS								
BASELINE CONFIGURATION		W-OV			W-FD			OV-FD			W-OV			W-FD			OV-FD		
OBSERVATION TYPE		R	D	I	R	D	I	R	D	I	R	D	I	R	D	I	R	D	I
BASELINE PARAMETERS (cm)	Δu	27.9	104.1	135.7	31.0	101.6	103.9	24.6	80.5	71.8	17.1	48.8	83.0	17.4	48.9	57.2	15.6	46.7	36.4
	Δv	49.9	123.8	109.3	25.6	121.[illegible]	85.9	24.1	132.3	79.5	15.7	61.8	46.9	14.3	57.7	51.7	15.3	54.4	42.0
	Δw	33.0	85.5	81.0	28.9	85.7	69.7	25.3	70.2	78.1	15.6	46.3	39.7	15.8	46.1	37.4	15.4	46.8	31.7
	$\sqrt{\text{TRACE}}$	59.5	183.0	192.2	49.5	139.8	161.8	42.7	170.1	129.7	27.6	91.4	103.3	27.5	88.8	85.8	26.7	85.2	64.0
BASELINE DISTANCE (cm)	d	21.9	78.9	135.1	24.9	82.5	121.9	32.3	80.1	120.7	14.4	47.9	67.5	14.[illegible]	39.1	61.1	13.2	47.1	42.9
		(0.7)	(1.6)	(3.4)	(0.8)	(2.[illegible])	(3.9)	(2.1)	(5.3)	(8.7)	(0.4)	(1.[illegible])	(1.7)	(0.5)	(1.2)	(2.[illegible])	(0.9)	(2.7)	(4.9)

COMMENTS: NUMBERS IN PARENTHESIS INDICATE RELATIVE PRECISION IN PARTS PER 10^7. RESULTS ARE BASED ON SIMULTANEOUS OBSERVATIONS EVERY 5 MINUTES WITH MEASUREMENT UNCERTAINTIES OF 100, 141, AND 141 CENTIMETERS FOR RANGE, RANGE DIFFERENCE, AND INTERFEROMETRY RESPECTIVELY. TO OBTAIN AN ESTIMATE OF THE PRECISION OBTAINABLE USING AN OBSERVATION TYPE WITH DIFFERENT MEASUREMENT UNCERTAINTY MULTIPLY TABLE VALUE BY THE RATIO OF THAT UNCERTAINTY TO THE CORRESPONDING UNCERTAINTY ABOVE.

Increasing the tracking interval to two hours produces a small increase in the standard error of the chord.

For correlated range differences the uncertainties are again much larger than the range results after one day of observation. The results improve relative to the range results as the tracking interval increases. The trace of the baseline covariance matrix shows more variation with baseline length than range, and the chord uncertainty is about three times larger than the range case, comparing best results.

Interferometry observations give baseline component results which are better than correlated range difference results; however, the uncertainty in the chord length can be determined better from range differences from longer satellite tracking intervals. The uncertainties of the parameters tend to increase as the tracking interval is increased and a pronounced increase in parameter uncertainty is noticed as the baseline length increases.

For range difference observations to yield equivalent baseline component uncertainties to range observations after 24 hours the standard error of range difference observations would need to be reduced to approximately 41 centimeters. In that case the range difference results given in Table 3.2.10 would be reduced to approximately the level of uncertainty given in Table 3.2.9 for range observations with a one meter standard error. For chord length a range difference uncertainty of 46 centimeters would be necessary to achieve equivalent results with range.

For interferometry, a statement of the required observational uncertainty necessary to produce range equivalent results is more complicated since the results based on interferometry are more variable as a function of station separation. All 24-hour interferometry results in Table 3.2.9 would be at least as good as the range results in that table if the Westford-Owens Valley results were equivalent. The parameter uncertainties are greatest for this baseline. For this to occur a measurement uncertainty of 41 centimeters would be required for equivalent baseline component results and 30 centimeters for chord length.

Ratios of parameter uncertainty to observational uncertainty may likewise be developed from Tables 3.2.9 and 3.2.10.

3.2.3 Summary

Some general conclusions can be drawn from an examination of the results. For the observation types considered it is evident that ranging measurements provide the best geometric strength of solution. The two other derived observation types, correlated range difference and interferometry, are geometrically weaker although the results obtained from these latter procedures can be improved upon by increased observational precision. Correlated range difference observations give the best geometric strength of solution if observed satellites are tracked over longer time intervals. With this type of tracking procedure both the baseline component and chord length uncertainties are minimized. For range and interferometric observations shorter satellite tracking intervals produce the least uncertainty in the baseline parameters. Lengthening the tracking interval for these observation types increases the resulting parameter uncertainties. However the

rate of increase is smaller than the variation in Doppler results produced by decreasing the tracking interval. And finally the interferometry approach becomes geometrically weaker as the baseline length increases to become a more significant percentage of the distance to the satellite, although the relative error in parts per million decreases for the baselines considered.

The analysis presented above considered the relative geometric strength of three observation types, two derived from basic ranging. The results were based on the assumptions that satellite positions in space were known and that the basic ranging measurements were subject to uncorrelated stationary random noise. Some additional comments concerning these assumptions are appropriate. If the ranging measurements are in addition subject to a receiver timing bias, then timing parameters would be required to augment the current parameter set, at least one for each observing station. Under these conditions the range and correlated range difference results would be approximately equivalent depending on the satellite geometries sampled, tracking interval adopted, and the a priori uncertainty of the timing parameters. The interferometry normal equations will also have to include these parameters and the baseline parameter uncertainty will be increased. For close stations the effective error introduced into interferometry observations would be the difference in the timing error at each station. The effect of timing error on interferometry can be greatly reduced by tracking additional satellites simultaneously as considered in Chapter 2. If the first assumption concerning the accuracy of satellite positions is violated, the resulting baseline parameter uncertainty will increase.

This was shown analytically. For short baselines the effect of the ephemeris error will be minor for all three approaches.

Finally a comment concerning Doppler observations is necessary. In the precision comparison study the derived range difference observations were correlated since successive range differences were formed using a common range. If Doppler results were obtained from independent Doppler counts over the same time intervals the correlations in the weight matrix would vanish and the resulting parameter uncertainties can be expected to increase.

4. DYNAMIC POSITIONING USING RANGE AND DOPPLER OBSERVATIONS

In this chapter a study is presented which attempts to determine the accuracy of dynamic point positioning using range and Doppler observations from a constellation of twenty-four Global Positioning System satellites. Two positioning problems have been addressed. These are the determination of the geodetic coordinates of a station and the determination of baseline components for stations which lie 100 to 2000 kilometers apart. An error analysis is performed to determine what effect various systematic and random modeling errors have on tracking station positions determined by a least squares adjustment using simulated observations. All results are based on the use of a single channel, dual frequency, sequential receiver whereby only one satellite is tracked at a time on two frequencies to virtually eliminate ionospheric refraction.

The observations analyzed consisted of range and integrated Doppler measurements. For both data types the assumption is made that the observations are subject to two random noise processes, namely uncorrelated white noise with a normal distribution and correlated error due to integrated fractional frequency errors in both satellite and receiver atomic oscillators.

In order to perform rigorous simulations of dynamic point positioning a complete adjustment model must be adopted. Model parameters included in this study are receiver coordinates, polynomial clock error models for station clocks, satellite state vector components, and a polynomial satellite clock model for each pass. A priori weighting consistent with the model error levels introduced is included for satellite ephemeris and clock parameters allowing station coordinates to be estimated. Since two sources of random error are present in the observations weight matrices used in the adjustment account for each random process, the complex one being correlated atomic clock error. An analytical method is developed to give the statistics of this random process. The procedure starts with either actual or models of the Allan variance for a particular oscillator or class of oscillators and develops the statistics of range and integrated Doppler observations based on the two oscillators used in deriving the measurements. Statistics for residuals to polynomial clock models are then obtained by a transformation. These residual statistics are incorporated into the adjustment weighting.

To further define the adjustment procedure, several studies were performed and are described in this chapter. A study was made to determine if it is possible to perform a sequential adjustment of the continuously observed measurements. Since all observations based on the receiver clock are correlated through random atomic clock error, must all data be processed simultaneously using a fully correlated weight matrix or can the measurements be divided into fully correlated blocks each with independent clock models requiring adjustment? Secondly, a

study was made to determine the time span over which a given polynomial clock model might be adopted. Further, tests were conducted for range and Doppler tracking to determine the optimal selection of satellites which produce the least uncertainty in derived station coordinates, a selection which produces the best geometric strength. And finally, the use of two-body analytic partial derivatives for orbit improvement rather than rigorous numerically integrated partials based on a spherical harmonic gravity field complete through degree and order eight was examined.

Results from numerous computer simulations of station positioning are included to demonstrate the effect of the error sources and evaluate the full weight matrix concept. In general the results were computed for cases where observations are six second ranges smoothed over 300 second intervals and 60 second integrated Doppler observations aggregated over 300 seconds.

4.1 Error Sources Influencing Dynamic Positioning

In this section the dominant systematic and random error sources influencing dynamic point positioning using GPS range and Doppler observations are described in detail and error models for these sources are developed. Also included is background information on atomic clock frequency error characterization required for an understanding of the discussion in Section 4.4.

The error sources considered here are believed to be the dominate ones effecting dynamic positioning. They include:

(i) systematic errors in the computed ephemerides of GPS satellites represented by periodic radial, along-track, and out-of-plane errors and in addition by a quadratic along-track error. Models for these errors were chosen to produce satellite position errors having the same signature as errors produced in simultations of ephemeris accuracy by investigators currently involved in computing GPS navigational and post-fit ephemerides. The simulations performed by these investigators were done to establish probable error levels in future estimated orbits;

(ii) residual systematic bias and drift in GPS satellite clocks after ephemeris and clock error estimates are obtained in the orbit determination problem. The levels of these errors were extracted from the same references as in (i);

(iii) correlated random satellite clock errors due to the inadequacy of polynomial satellite clock models. These errors are based on Allan variance frequency stability models for the rubidium oscillators on GPS satellites;

(iv) uncorrelated random noise from the tracking receiver. Nominal range measurement uncertainty is one meter for a six-second measurement and three centimeters for 60-second integrated Doppler;

(v) systematic bias and drift of the receiver's cesium atomic clock;

(vi) correlated random receiver clock error based on an Allan variance model for the receiver cesium frequency standard;

(vii) systematic tropospheric refraction error equivalent to five percent of the tropospheric model predictions.

Residual second-order ionospheric refraction errors were not included since this error is shown to be only a few millimeters at GPS frequencies.

4.1.1 Atomic Clock Errors and Frequency Stability

A clock is a device which counts the cycles of a periodic phenomenon and among the most stable clocks in use are the atomic clocks which form the basis for atomic time scales such as International Atomic Time (TAI). Atomic time is used primarily as a measure of time interval and is based on the electromagnetic oscillations produced by quantum transitions within the atom. An excellent reference on time and frequency is edited by Blair [1974].

Global Positioning System satellites will incorporate rubidium frequency standards to provide short-term frequency stability for the navigator, and ground tracking receivers for geodetic utilization will be assumed to incorporate cesium frequency standards to insure good long-term stability. The precise definition of stability is found in Blair [1974]. Basically it is a measure, usually given statistically, of the random fluctuations in frequency which can occur in a clock's oscillator over specified periods of time. For a given time interval a particular oscillator is considered best if the expected level of frequency fluctuation is a minimum in terms of the Allan variance defined below.

This paragraph deals with the characterization of typical errors associated with atomic clock time scales and statistical measures of frequency stability. This information provides the general background

required for the discussion related to the development of observation statistics and their use in geodetic positioning studies.

4.1.1.1 Characterization of Atomic Clock Errors

Let C_I represent an ideal clock whose oscillator frequency f_I is constant. The period of this oscillator is by definition

$$T_I = 1/f_I \ . \tag{4.1.1}$$

In $(t - t_o)$ seconds of ideal time N_I cycles are counted and the time registered by the clock is

$$N_I T_I = N_I/f_I \tag{4.1.2}$$

where N_I is given by the integral

$$N_I = \int_{t_o}^{t} f_I d\tau = f_I(t - t_o) \ . \tag{4.1.3}$$

Thus the time elapsed from t_o is

$$N_I T_I = f_I(t - t_o)T_I = t - t_o \ . \tag{4.1.4}$$

Consider now a typical atomic clock C_i whose frequency is subject to error. From t_o this clock has a frequency represented by the model

$$f_i(t) = f_I + \Delta f + \dot{f}(t - t_o) + \tilde{f}(t) \tag{4.1.5}$$

where Δf is a frequency bias, $\dot{f}$ is a drift in frequency, and $\tilde{f}(t)$ are random fluctuations in frequency. The clock C_i records N_i cycles in the

time interval $[t_o, t]$ where

$$N_i = \int_{t_o}^{t} f_i(\tau)\,d\tau$$

$$= f_I(t - t_o) + \Delta f(t - t_o) + \frac{\dot{f}(t - t_o)^2}{2} + \int_{t_o}^{t} \tilde{f}(\tau)\,d\tau \ . \tag{4.1.6}$$

In addition the clocks C_i and C_I may not be synchronized at t_o introducing a time or phase error at t_o represented as $\Delta N_o T_I$. Each count N_i is incorrectly assigned the period T_I giving at t ideal the time t_i as

$$t_i = N_i T_I + \Delta N_o T_I = (t - t_o) + \frac{\Delta f}{f_I}(t - t_o)$$

$$+ \frac{\dot{f}(t - t_o)^2}{2f_I} + \frac{1}{f_I}\int_{t_o}^{t} \tilde{f}(\tau)\,d\tau + \Delta N_o T_I \ . \tag{4.1.7}$$

From a comparison of equations (4.1.4) and (4.1.7) the time error at t is

$$T_i(t) = t_i - t = \frac{\Delta f}{f_I}(t - t_o) + \frac{\dot{f}(t - t_o)^2}{2f_I} + \Delta N_o T_I + \frac{1}{f_I}\int_{t_o}^{t} \tilde{f}(\tau)\,d\tau \tag{4.1.8}$$

or, rearranging terms and introducing new notation,

$$T_i(t) = \frac{1}{2} D_i(t - t_o)^2 + R_i(t - t_o) + T_i(t_o) + \tilde{x}(t) \ . \tag{4.1.9}$$

The quantity $\tilde{x}(t)$ is the random time error at t defined by

$$\tilde{x}(t) = \frac{1}{f_I}\int_{t_o}^{t} \tilde{f}(\tau)\,d\tau = \int_{t_o}^{t} y(\tau)\,d\tau \tag{4.1.10}$$

where y(t) is the random <u>fractional frequency</u> error of oscillator i.

Consider the quantity $T_i(t)$ written as

$$T_i(t) = T_i(t_o) + R_i(t - t_o) + \frac{D_i}{2}(t - t_o)^2 + \int_{t_o}^{t} y(\tau)d\tau \ . \qquad (4.1.11)$$

Suppose an estimate of $T_i(t)$ was made at t_s as shown in Figure 4.1.1 based on available data taken prior to t_s. If a clock correction based on this estimate was applied to the time scale, then at t_o the error $T_i(t_o)$ is due to the error in the prior estimate $\hat{T}_i(t_s)$ which was applied to the time scale, the effect of fractional frequency errors over the interval $[t_s, t_o]$

$$\tilde{x}(t_o) = \int_{t_s}^{t_o} y(\tau)d\tau \qquad (4.1.12)$$

and, systematic contributions to the time error in the form of a time drift and ageing, the quadratic term in equation (4.1.11). The error $T_i(t_o)$ with no clock correction at t_s is approximately given by

$$T_i(t_o) \approx \hat{T}_i(t_s) + R_i(t_o - t_s) + \frac{D_i}{2}(t_o - t_s)^2 + \int_{t_s}^{t_o} y(\tau)d\tau \qquad (4.1.13)$$

since $\hat{T}_t(t_s)$ is an estimated quantity. If the time scale is corrected at t_o then $\hat{T}_i(t_o)$ would be an estimated offset independent of the current oscillator random error $y(t)$ for t greater than t_o.

The error equation (4.1.9) is the model used to describe the types of error present in atomic time scales. The deterministic errors consist of bias, drift, and ageing terms modeled as a quadratic polynominal in time. The ageing term is usually not observable for clocks

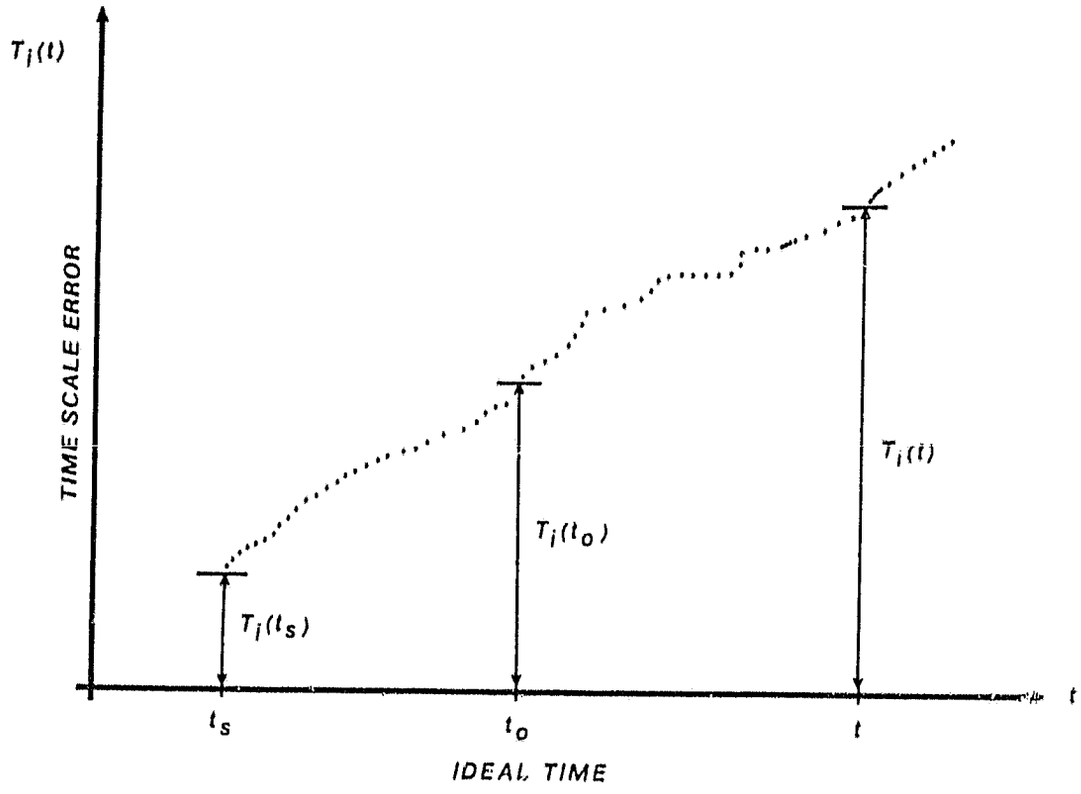

Figure 4.1.1. Time Scale Error

whose long-term stability is good such as cesium. The additional term in equation (4.1.9) represents the random time error due to the integration of random fluctuations in frequency. The magnitude of this term depends on the interval of time which has passed since the scale was reset or calibrated and on the stability of the clock. Table 4.1.1 lists the error terms associated with atomic clock time scales.

TABLE 4.1.1. ATOMIC TIME SCALE ERROR TERMS

DETERMINISTIC	*NOTATION*
TIME BIAS	$T_l\ (t_o)$
TIME DRIFT	R_l
AGEING TERM	D_l
RANDOM	
$\tilde{X}(t)$ *INTEGRATED FRACTIONAL FREQUENCY*	

4.1.1.2 Frequency Stability Measurement and Characterization

Hellwig [1977] points out that "the characterization of the stability of a frequency standard is usually the most important information to the user especially to those interested in scientific measurements and in the evaluation and intercomparison of the most advanced devices (clocks)." Since the frequency stability of a standard depends on a variety of physical and electronic influences both internal and external to the standard, measurement and characterization of frequency stability are always given subject to constraints or environmental and operating conditions. In addition frequency stability depends on the exact measurement procedure used to determine stability.

Frequency stability characterization is done in both the frequency and time domain. In the time domain a frequently used measure of stability is the Allan variance or its square root. In the frequency domain it is the power spectral density.

4.1.1.2.1 The Allan Variance. The Allan variance as a time domain measure of frequency stability is found especially useful in practice since it is obtainable directly from experimental measurements of fractional frequency error y(t) and because it contains all information on the second moments of the statistical distribution of fractional frequency error. The Allan variance is defined as follows: let $y_o, y_1, y_2, \ldots, y_k, y_{k+1}, y_{k+2}, \ldots$ be observed fractional frequency errors separated by a repetition interval of T seconds. For each integer N greater than or equal to two calculate $\overline{y}_m$, from

$$\overline{y}_m = \frac{1}{N} \sum_{k=mN}^{(m+1)N-1} y_k \qquad m = 0,1,2,\ldots M \; . \tag{4.1.14}$$

This is an average over N consecutive values of y_k. The Allan variance, $\sigma_y^2(N)$, is then obtained from the averages $\overline{y}_m$ by

$$\sigma_y^2(N) = \frac{1}{2M} \sum_{m=0}^{M-1} (\overline{y}_{m+1} - \overline{y}_m)^2 \; . \tag{4.1.15}$$

An examination of this equation reveals that the Allan variance for a particular sampling interval NT is the average two-sample variance of the $\overline{y}_m(N)$.

For frequency standards the square root of the Allan variance is usually given in graphical form on a log-log scale. For individual classes of frequency standards models for the Allan variance are used which portray general frequency stability characteristics. Hellwig [1975] gives examples of such models for many oscillator types. Figure 4.1.2 shows the typical form. In this form, $\sigma_y(\tau)$ is the square root of the Allan variance for the sample interval τ. The quantity σ_f is called the flicker floor and τ_1, τ_2, τ_3 are the break points of the plot. The constants associated with this figure are usually specified for each type of frequency standard. A comparison of such information can facilitate the selection of a frequency standard for a specific application.

The stability characteristics shown in the three regions of Figure 4.1.2 are typically present in many Allan variance plots of specified oscillator performance. The first part, region I, reflects the fundamental noise properties of the standard. This behavior continues with increased sampling time until a floor is reached corresponding to region II. After τ_2 the performance deteriorates with increased sampling time. Hellwig [1977] outlines the error sources corresponding to each portion of the graph. The magnitude and slope of each segment will depend on the particular category of standard.

Figure 4.1.3 details the performance specifications for the Allan variance for the GPS satellite rubidium oscillator and for the cesium oscillator used in tracking receivers supporting orbit determination. This latter oscillator is an example of the type which will be used in range and Doppler geodetic receivers.

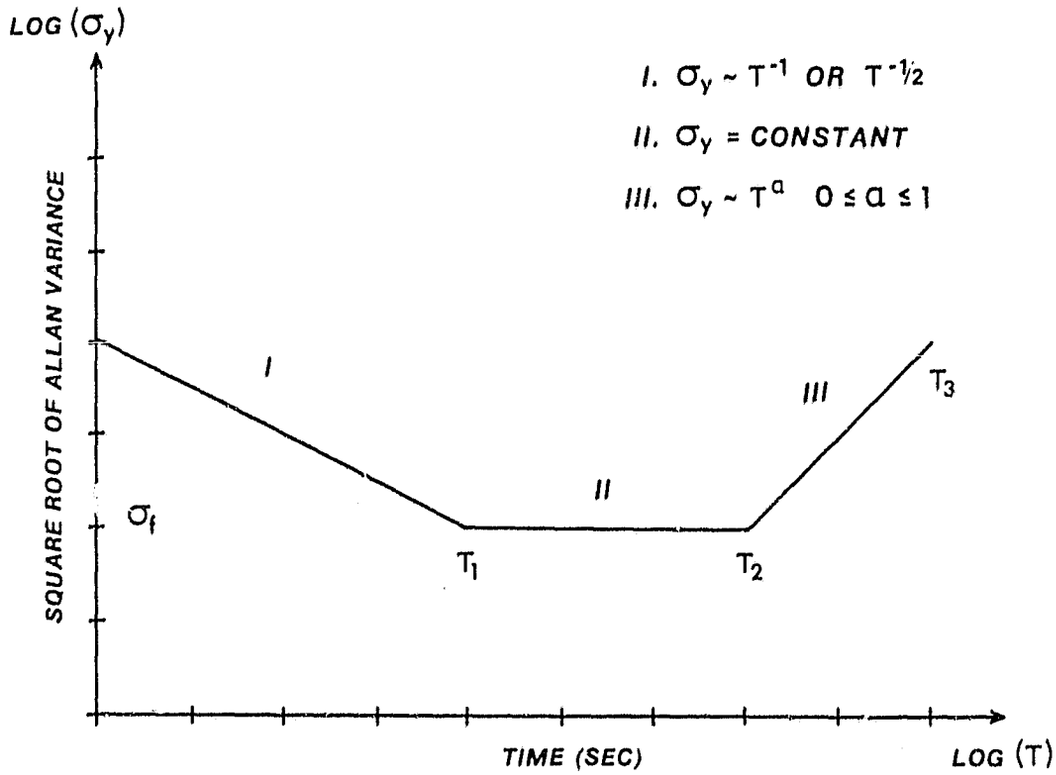

Figure 4.1.2. General Frequency Stability Characteristics

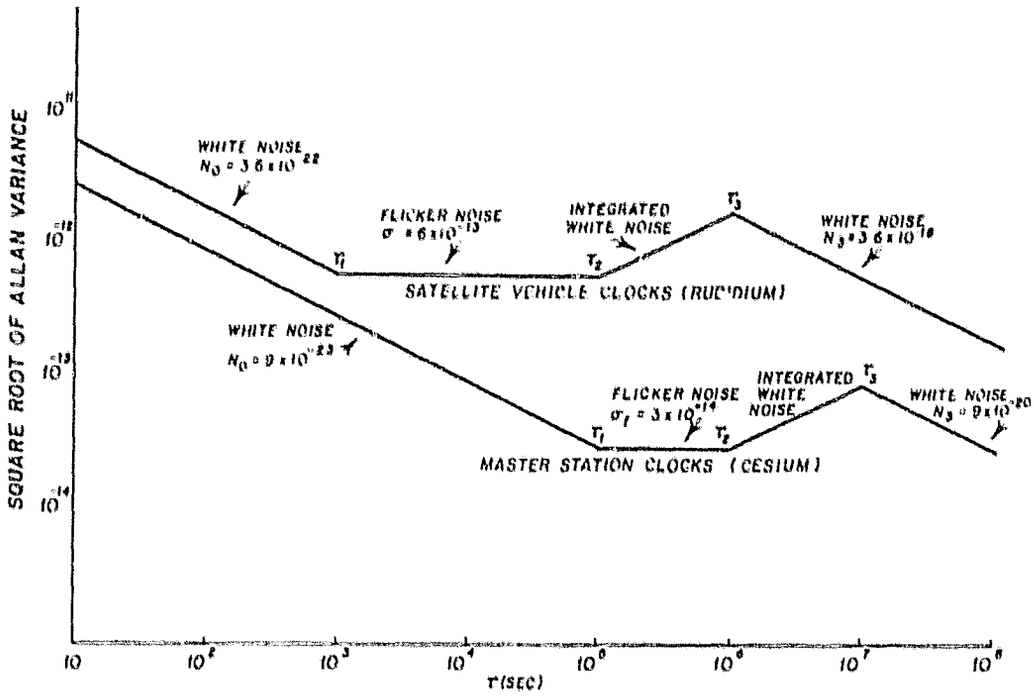

Figure 4.1.3. Allan Variance for Satellite and Station Oscillators

4.1.1.2.2 Power Spectral Density. An alternative procedure for specifying the stability of a frequency standard, in the frequency domain, is the use of the power spectral density (PSD) of instantaneous fractional frequency fluctuations y(t). Allan et al. [1974] have given a useful model to represent the PSD for various categories of frequency standards. This model is in the form of a power law spectral density having the form

$$S_{yy}(\omega) = \begin{cases} h_\alpha \left(\frac{\omega}{2\pi}\right)^\alpha & 0 \le \omega \le \omega_h \\ 0 & \omega > \omega_h \end{cases} \qquad (4.1.16)$$

where α takes on the integer powers between -2 and 2 inclusive depending on how the interval $[0,\omega_h]$ is to be divided into subintervals, one for

each α to be used. The quantity h_α is a scaling constant and the PSD is assumed to be negligible beyond the frequency range $[0,\omega_h]$.

Barnes et al. [1971] and Meditch [1975] give the transformations between the time domain measures of frequency stability in the form of the Allan variance and the power law spectral densities. Table 4.1.2 taken from Meditch gives these conversions for three types of fractional frequency error sources.

4.1.1.3 Range and Doppler Observation Errors Due to Random Atomic Clock Error

As previously discussed an atomic clock's time scale can be expected to differ from ideal time due to both deterministic and random errors. The random component is due to integration of fractional frequency errors. A range observation determined by correlating the PRN signal broadcast by the satellite with a similar signal generated in the receiver is subject to the random errors of both atomic frequency standards. The effective range error at time t due to the timing error in one of the time scales t_i is

$$\delta R_i(t) = cT_i(t) \tag{4.1.17}$$

with the random component being the random walk

$$\eta_i(t) = c \int_{t_s}^{t} y(\tau)d\tau \tag{4.1.18}$$

where c is the velocity of light. The random component is due to the accumulated effect of fractional frequency error since the clock's start or reset at t_s.

The random error $\eta_j(t)$ is correlated in time. Consider two measurements of range $R(t_j)$ and $R(t_k)$ based on the use of the oscillator in the satellite, and assume momentarily that the receiver's oscillator is free from random error. The covariance between these measured ranges due to correlated fractional frequency error in the satellite oscillator is

$$\begin{aligned} E[R(t_j)R(t_k)] &= E[\eta(t_j)\eta(t_k)] \\ &= c^2 E\left[\int_{t_s}^{t_j} y(\tau)d\tau \int_{t_s}^{t_k} y(\tau')d\tau'\right] \\ &= c^2 \int_{t_s}^{t_j}\int_{t_s}^{t_k} E[y(\tau)y(\tau')]d\tau d\tau' \\ &= c^2 \int_{t_s}^{t_j}\int_{t_s}^{t_k} \Phi_{yy}(\tau-\tau')d\tau d\tau' \end{aligned} \tag{4.1.19}$$

where $\Phi_{yy}(\tau-\tau')$ is the autocorrelation function for fractional frequency error $y(t)$ defined by

$$\begin{aligned} \Phi_{yy}(\tau-\tau') &= E[y(\tau)y(\tau')] \\ &= \int_{-\infty}^{\infty}\int_{-\infty}^{\infty} yy' f(y,y',\tau,\tau')dy\,dy' . \end{aligned} \tag{4.1.20}$$

The function $f(y,y',\tau,\tau')$ is the joint probability density function for fractional frequency error. Here it is assumed that $y(t)$ is a mean zero stationary random process. The function $\Phi_{yy}(\tau-\tau')$ can be obtained by

the inverse Fourier transform of the given power spectral density $S_{yy}(\omega)$:

$$\Phi_{yy}(t) = \frac{1}{2\pi} \int_{-\infty}^{\infty} S_{yy}(\omega) e^{i\omega t} d\omega \qquad (4.1.21)$$

where

$$t = \tau - \tau' \ . \qquad (4.1.22)$$

A procedure for obtaining the autocorrelation function $\Phi_{yy}(t)$ from the Allan variance is given in Section 4.4.

The variance of a range observation is obtained from equation (4.1.19) by taking t_j equal to t_k

$$\sigma^2_{R_j} = c^2 \int_{t_s}^{t_j} \int_{t_s}^{t_j} \Phi_{yy}(\tau - \tau') d\tau d\tau' \ . \qquad (4.1.23)$$

Allowing random frequency error in the receiver oscillator introduces additional, but similar, terms into equations (4.1.19) and (4.1.23) which must be considered when assessing the range uncertainty due to all random clock errors effecting the measurement.

For integrated Doppler or range difference observations the random measurement error associated with system clocks is the integral of fractional frequency error over the Doppler integration interval. The random error in range difference due to one oscillator is

$$\eta_{ij} = \eta(t_j) - \eta(t_k)$$
$$= c \int_{t_i}^{t_j} y(\tau)d\tau \ . \tag{4.1.24}$$

Notice in equation (4.1.24) that the random error η_{ij} is a function of t_i, t_j, and $y(t)$. The error does not depend on t_s. Range difference measurements have the following correlation from each oscillator

$$E[\Delta R_{ij}\Delta R_{k\ell}] = E[\eta_{ij}\eta_{k\ell}]$$
$$= c^2 \int_{t_i}^{t_j}\int_{t_k}^{t_\ell} \Phi_{yy}(\tau - \tau')d\tau d\tau' \tag{4.1.25}$$

with the variance

$$\sigma^2_{\Delta R_{ij}} = c^2 \int_{t_i}^{t_j}\int_{t_i}^{t_j} \Phi_{yy}(\tau - \tau')d\tau d\tau' \ . \tag{4.1.26}$$

Observe that the random range difference errors, whose statistics are given by equations (4.1.25) and (4.1.26), are stationary; however, random range errors, whose statistics are given by equations (4.1.19) and (4.1.23), are not. A stationary random process is one whose statistics are invariant in time.

For the oscillator performance specifications shown in Figure 4.1.3 examples of the contribution to the range error are given for both oscillators in Figures 4.1.4 and 4.1.5 over a five-day span. The clocks are assumed to be perfect initially. Also included is the standard error for the random walk $\eta(t)$ obtained using equation (4.1.23). The

procedure used in simulating the random range error is discussed in [Meditch, 1975].

TABLE 4.1.2. ALLAN VARIANCE AND POWER SPECTRAL DENSITY FOR COMMON ERROR SOURCES

ERROR SOURCE $y(t)$	*ALLAN VARIANCE* $\sigma_y^2(\tau)$	*TWO SIDED SPECTRAL DENSITY* $S_{yy}(\omega)$
WHITE NOISE	$\frac{N_0}{\tau}$	N_0
FLICKER NOISE	$\frac{2N_1 \ln 2}{\pi}$	$\frac{N_1}{\lvert\omega\rvert}$
INTEGRAL OF WHITE NOISE (RANDOM WALK)	$\frac{N_2 \tau}{3}$	$\frac{N_2}{\omega^2}$

4.1.2 Ephemeris Error

The ultimate accuracy of Global Positioning System satellite ephemerides and satellite clock solutions is difficult to predict since many factors influencing the final error budget have to be resolved. Among these are the number and location of tracking sites to support orbit determination, the exact estimation algorithm to be used including force modeling, and the final geometry of the satellite constellation. At present, errors in computed ephemerides significantly exceed accuracy design goals, especially in the prediction region used in navigation as reported by Schaibly [1979].

In order to establish bounds on expected ephemeris and satellite clock errors simulations of orbit determination were performed assuming expected levels of model error for gravity, solar radiation pressure,

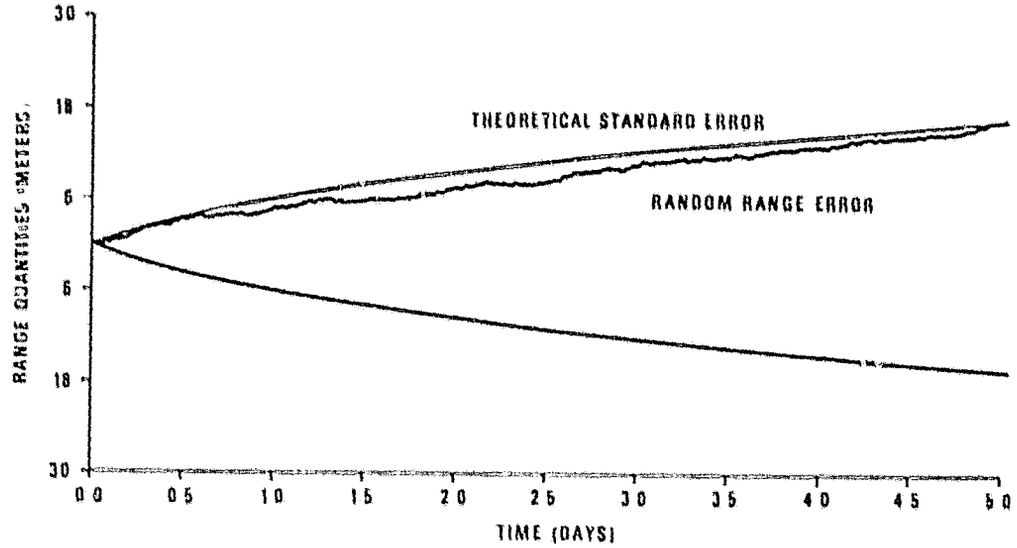

Figure 4.1.4. Standard Error and Random Range Error Based on Station Cesium Specifications

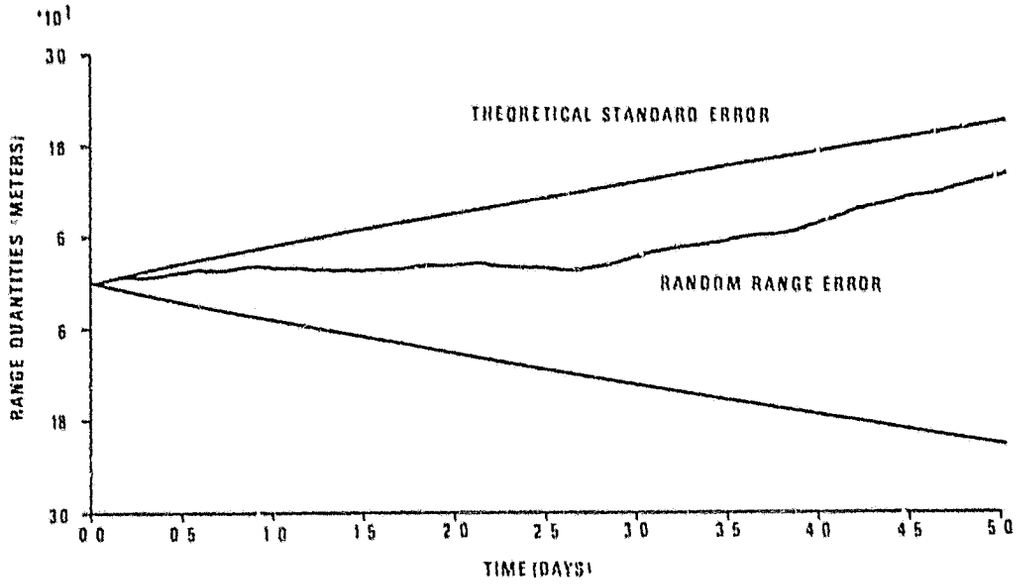

Figure 4.1.5. Standard Error and Random Range Error Based on Satellite Rubidium Specifications

pole position, tracking site coordinates, and system clock errors. The results of these studies reported by Schaibly [1976] indicate the following:

(i) the radial component of position error is a twelve-hour periodic function whose amplitude ranges form one to three meters;

(ii) the along-track component of position error has two components. The first is a twelve-hour periodic function whose amplitude ranges from two to five meters. The second component is a quadratic function in time introducing maximum errors of up to twenty meters. In most cases this error appears to average five meters;

(iii) the cross-track component of orbit error is a twelve-hour periodic function whose amplitude ranges from seven to twenty meters. This error and the periodic radial orbit error appear to have zero mean;

(iv) satellite clock solution errors have systematic components which may be modeled as a bias and drift;

(v) ephemeris and satellite clock errors will be correlated in the sense that the net effect of all error sources on an observation residual will be smaller than the sum of the individual error sources.

This analysis of expected orbital accuracy will be used as a basis for developing error models and a priori statistics for ephemeris state vector components and satellite clock parameters in simulation studies designed to predict accuracies for dynamic point positioning.

4.1.2.1 Ephemeris Error Model

Using the results of the simulations described above, models for ephemeris error can be developed for use in positioning studies. These models will consist of variations in the osculating orbital elements for each satellite which will produce radial, along-track, and cross-track orbit errors comparable with the simulation results. The magnitudes of these variations can be approximated by noting the errors introduced by changes in Keplerian orbital elements. For instance, radial orbit error is primarily a function of errors in the semimajor axis a and eccentricity e of the orbit. The model for radial orbit error will be developed as follows:

Taking

$$\Delta a = \delta a \cos(M+\omega+\beta_a) \tag{4.1.27}$$

and

$$\Delta e = \delta e \ , \tag{4.1.28}$$

where δa and δe are errors in a and e respectively and β_a is the phase of the error signal Δa, and differentiating the equation for the radius of a Keplerian orbit

$$r = a[1 - e \cos(E)] \tag{4.1.29}$$

with respect to a

$$\frac{dr}{da} = 1 - e \cos(E) \simeq 1 (e \simeq 0) \tag{4.1.30}$$

one arrives at the error introduced into r by Δa

$$\Delta r \simeq \Delta a \ . \tag{4.1.31}$$

Choosing Δa as in equation (4.1.27) gives periodic radial orbit error of amplitude δa and phase β_a. The period of the error is orbit period. Differentiating equation (4.1.29) with respect to e gives

$$\frac{dr}{de} = -a \cos(E) \tag{4.1.32}$$

or

$$\begin{aligned} \Delta r &= -a\Delta e \cos(E) \\ &\simeq -a\Delta e \cos(M+\omega) \end{aligned} \tag{4.1.33}$$

for e and ω approximately zero. Introducing a phase error and using equation (4.1.33) yields

$$\Delta r \simeq -a\delta e \cos(M+\omega+\beta_e) \ . \tag{4.1.34}$$

Thus an error in orbit eccentricity δe introduces a periodic radial orbit error whose amplitude is $a\delta e$ and whose phase is β_e.

Along-track orbit error can be produced by variations in mean anomaly M and argument of perigee ω as well as eccentricity Considering $M + \omega$ as a single element the following model will be adopted

$$\Delta(M+\omega) = \delta(M+\omega)\cos(M+\omega+\beta_{M+\omega}) \ . \tag{4.1.35}$$

For nearly circular orbits

$$r = a[1 - e \cos(E)] \simeq a \tag{4.1.36}$$

and the along-track error due to equation (4.1.35) is approximately

$$\begin{aligned} \Delta s &= a\Delta(M+\omega) \\ &= a\delta(M+\omega)\cos(M+\omega+\beta_{M+\omega}) \ . \end{aligned} \tag{4.1.37}$$

This orbit period error has an amplitude of $a\delta(M+\omega)$ and phase $\beta_{M+\omega}$.

An error in eccentricity will also introduce a periodic error in the along-track satellite position. This error will have the form

$$\Delta s = 2a\delta e \sin(M+\omega+\beta_e) \ , \tag{4.1.38}$$

Notice that the along-track error due to δe has twice the amplitude of induced radial error due to δe.

An error in the ascending node Ω of the orbit plane produces an along-track bias

$$\Delta s = a\delta\Omega\cos(i) \tag{4.1.39}$$

independent of the in-plane satellite position.

In addition a quadratic along-track error polynomial will be introduced to produce the quadratic error to fit found in the orbit accuracy simulation studies. This error is developed through an error in mean anomaly M of the form

$$\Delta M = (A+BM+CM^2)/a \tag{4.1.40}$$

where A is an epoch error given in meters and B and C are determined to allow the quadratic error to be symmetric over a seven-day span:

$$\begin{aligned} B &= -5040\,C \\ C &= 2A/6350400 \ . \end{aligned} \tag{4.1.41}$$

The cross-track or out-of-plane orbit error is due to error in inclination i and ascending node Ω. The cross-track error due to an error in orbital inclination has the form

$$\Delta(r \times v) = a \Delta i \sin (M+\omega+\beta_i) \qquad (4.1.42)$$

for a circular orbit. The error model chosen for inclination is

$$\Delta i = \delta i \ . \qquad (4.1.43)$$

The cross-track error due to a change in ascending node is

$$\Delta(r \times v) = -a\Delta\Omega\sin(i)\cos(M+\omega+\beta_\Omega) \qquad (4.1.44)$$

where $\Delta\Omega$ is given by

$$\Delta\Omega = \delta\Omega \ . \qquad (4.1.45)$$

This error has orbit period and amplitude $a\delta\Omega\sin(i)$.

Notice that the two radial error signals are 180 degrees out of phase when β_a and β_e are zero. Therefore let

$$\beta_a = \beta_e + 180^\circ \qquad (4.1.46)$$

in order that the total radial error have the functional form found in the orbit simulation results.

Since no along-track bias was present in the simulation results no error will be introduced into the ascending node in positioning simulations. As a result all cross-track error will be attributed to an error in inclination.

In addition the phase $\beta_{M+\omega}$ will be adjusted by 90 degrees to allow the along-track error due to inclination and mean anomaly plus argument of perigee to be in phase.

4.1.3 Refraction Errors

4.1.3.1 Tropospheric Refraction Error

The nonionized portion of the atmosphere slows the passage of electromagnetic signals introducing an error into electromagnetic measurements such as range, Doppler and interferometric phase. Computations of receiver positions for geodetic control utilizing such measurements must incorporate either refraction error modeling of sufficient accuracy to eliminate these atmospheric effects or incorporate corrections based on radiometry measurements as suggested by MacDoran [1979].

Currently, the Hopfield model [Hopfield, 1969] is used extensively to correct for tropospheric refraction present in satellite observations of range and Doppler. This model requires a knowledge of surface weather conditions at receiver sites to ensure proper scale. These weather observations are of surface pressure, temperature, and humidity. The error in this model is generally assumed to be less than five percent of the total refraction.

Alternatively, a water vapor radiometer may be used to measure the tropospheric refraction (wet component) in the slant range direction to the satellite at the time of observation. MacDoran [1979] has

indicated that such an approach may have an accuracy of 2 cm to a few millimeters, virtually eliminating this error source.

4.1.3.1.1 Refraction Modeling Approach. The tropospheric refraction model adopted in this analysis is a modified version of the Hopfield model [Anderle, 1974] involving a change in the form of the quartic polynomial to allow more rapid calculation.

The theoretical form of the first-order tropospheric refraction correction for range measurements is given by

$$\delta R = \int_{r_s}^{r_{sat}} (n-1) r (r^2 - k^2)^{-1/2} \, dr \qquad (4.1.47)$$

where

$$k = r_s \sin z \qquad (4.1.48)$$

and

$$\cos z = \hat{u}_s \cdot \hat{\rho} \, . \qquad (4.1.49)$$

The vectors $\bar{r}_s$ and $\bar{r}_{sat}$ represent the position vectors for the observing station and satellite, respectively. The zenith angle z is measured from the ellipsoidal normal $\bar{\mu}_s$ through the station (see Figure 4.1.6)

The index of refraction n is computed using surface weather measurements. Given the centigrade temperature T, the surface pressure P in millibars, and the relative himidity H, the index n is computed using the equations

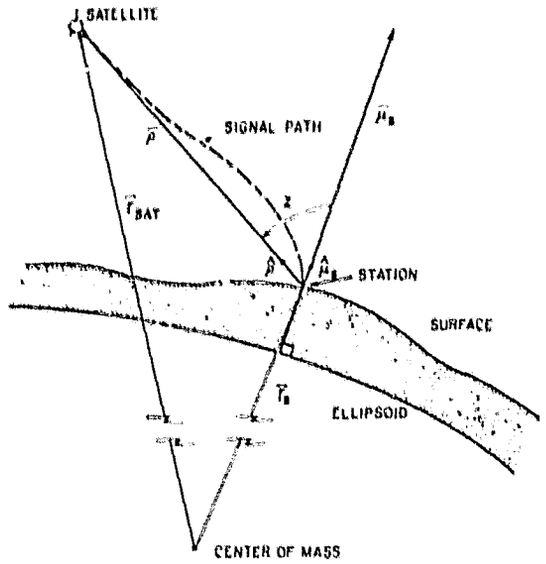

Figure 4.1.6. Geometry of Tropospheric Refraction

$$n - 1 = M_1 + M_2 \tag{4.1.50}$$

$$M_i = \begin{cases} N_i \left[\dfrac{r^2 - r_i^2}{r_s^2 - r_i^2} \right]^4 & \text{if } r_s \le r \le r_i \\ 0 \text{ otherwise} \end{cases} \tag{4.1.51}$$

where the surface refractivities N_i and radii r_i for the dry and wet components are given respectively by

$$N_1 = (.776 \times 10^{-4}) P / T_K \tag{4.1.52}$$

$$N_2 = (.373) E / T_K^2 \tag{4.1.53}$$

$$r_1 = r_s + 40.1 + .149T \text{ (km)} \tag{4.1.54}$$

$$r_2 = r_s + 12.0 \text{ (km)} \tag{4.1.55}$$

The quantity T_K represents the Kelvin equivalent of the Centigrade temperature T. The quantity E is the water vapor pressure given by

$$E = (H/100)\exp\{-37.2465 + .213166T_K - .000256908T_K^2\} \quad . \quad (4.1.56)$$

For radio frequencies up to 15 GHz tropospheric refraction is not a function of frequency.

For integrated Doppler the refraction correction is taken as the difference in equation (4.1.47) applied at the end times of the integration interval. The magnitude of tropospheric refraction on range observations is given in Figure 4.1.7 as a function of zenith angle. This error grows rapidly when the elevation angle of the satellite falls below ten degrees.

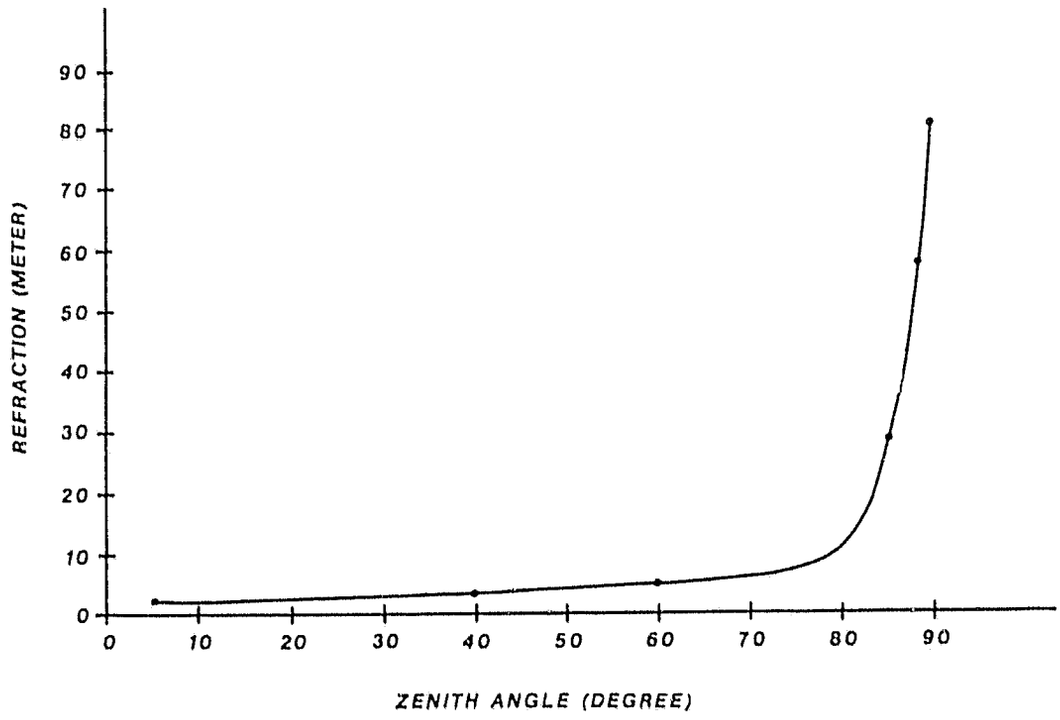

Figure 4.1.7. Tropospheric Refraction Profile for Range Observations

The tropospheric refraction model described above attempts to predict the refraction error as a function of surface weather conditions. How adequately this is done in practice is difficult to determine especially for non-vertical measurements. Hopfield [1972] has compared this model to values of tropospheric refraction computed using meterological balloon data and found good agreement for zenith measurements with the contribution due to the wet component suffering the largest error. However the dry component is predicted accurately from surface pressure alone.

An adopted technique in utilizing this model is to include in the mathematical model for the observation equation a scaling parameter C_R as an unknown to be determined in the adjustment procedure with an a priori uncertainty. For range observations the mathematical model equation (2.2.6) becomes

$$R = [(u_s - u)^2 + (v_s - v)^2 + (w_s - w)^2]^{1/2} + c\Delta\tau + (1 + C_R)\delta R \ . \quad (4.1.57)$$

Fell [1975] used such an approach for orbit determination using Doppler observations from Transit satellites. Although this procedure tends to weaken the normal equations it reduces the level of unmodeled error and improves the accuracy of the estimated quantities.

4.1.3.2 Ionospheric Refraction Error

The ionosophere, the charged portion of the atmosphere which extends above 100 kilometers, has a variable index of refraction which is a function of both the frequency of the passing electromagnetic signal and the altitude along the signal path since the electron density

varies with location. The electron density distribution which determines the refractive index at a particular frequency is quite variable with a dominate diurnal variation due to earth rotation and with long term variations with the solar cycle.

Clynch [1979] reviews the second order expansion of the refraction index n as a function of frequency

$$n \simeq 1 - \frac{A_1 N(h)}{f} - \frac{A_2 N^2(h)}{f^2} \qquad (4.1.58)$$

where the A_i are constants and N is the electron density, a function of height along the signal path.

The total ionospheric refraction for range observations is the difference between the integral of the refractive index along the optical path and the geometric range:

$$\delta R = \int_o n ds - \int_g ds \ . \qquad (4.1.59)$$

Using equation (4.1.58) in equation (4.1.59) gives to second order the ionospheric refraction as

$$\delta R = -\frac{B_1}{f^2} - \frac{B_2}{f^4} \qquad (4.1.60)$$

where

$$B_i = A_i \int_o N^i(h) ds \ . \qquad (4.1.61)$$

If two known frequencies are transmitted from a satellite, f_1 and f_2,

then each signal is refracted according to equation (4.1.60). These two equations may be combined to eliminate the first order effect:

$$R' = \left[(R+\delta R_1) - \left(\frac{f_1}{f_2}\right)^2 (R+\delta R_2) \right] : \left[1 - \left(\frac{f_1}{f_2}\right)^2 \right] \qquad (4.1.62)$$

where $(R+\delta R_1)$ represents the range observed using frequency f_1. This two frequency technique leaves a residual range error εR of

$$\varepsilon R = \frac{B_2}{f_1^2 f_2^2} . \qquad (4.1.63)$$

Clynch [1979] gives examples of two frequency corrected residual range errors for simulated Navy Navigation Satellite passes. These ionospheric errors were computed by ray tracing through an ionospheric model with a range of sunspot numbers considered. For elevation angles above ten degrees the upper bound on the residual range errors is five meters. Using equation (4.1.63) with εR equal to five meters and the 150 MHz and 400 MHz frequencies of the Transit system, an upper bound on B_2 is obtained. Computing εR using the Global Positioning System satellite frequencies of 1227 MHz and 1575 MHz gives an upper bound of 4.8 millimeters for the residual range error. For observations above twenty degrees this residual error has an upper bound of 1.9 millimeters. Since this error is small, residual ionospheric error was not included in the positioning studies conducted in Section 4.5.

4.1.4 Instrumental Error Sources

Tracking receivers designed to measure range and integrated Doppler from GPS satellites introduce random measurement error in

addition to the random clock error discussed in Section 4.1.1. The reasons for this error are jitter in the carrier tracking loops and in the code correlation process and electronic thermal noise. Specifications of the statistical properties of this noise are usually given for each receiver type; and in practice estimates of these properties are usually obtained through examination of observation residuals. Unfortunately it may be difficult to completely separate these receiver noise effects from clock noise since oscillator errors are manifest in the residuals.

Jorgensen [1978] attempts to predict the short-term quality of range observations by fitting a ninth degree polynomial to 70 minutes of six-second high quality range observations taken at the Hawaii and Vandenberg tracking stations from two satellites. In this procedure it is assumed that the polynomial models all systematic trends in the observations. The residuals from this least squares fit appear as white noise. Jorgensen concludes from this investigation that two frequency corrected range observations of high quality are subject to 60 centimeters of white noise. An extrapolation of Table 4.4.5 indicates that these residuals are due almost entirely to receiver noise since the expected level of residual clock error is much less than this magnitude.

For 60 second dual frequency Doppler observations the Stanford Telecommunications [1978] specifications for Model 5007 NGR receiver indicate that the error due to jitter in the carrier tracking loops should not exceed 0.9 centimeters. Thermal noise may increase this level to at least one centimeter.

Based on these results Table 4.1.3 gives bounds on the range of receiver noise which can be expected from present receiver technology. These levels will be used in Section 4.5.

TABLE 4.1.3. MAGNITUDE OF RECEIVER WHITE NOISE

DATA TYPE	NOMINAL LEVEL	OPTIMAL LEVEL
RANGE (6 sec)	1 m	60 cm
INTEGRATED DOPPLER (60 sec)	3 cm	1 cm

4.2 Simulation of Observations

4.2.1 Range and Doppler

Range and Doppler observations were simulated for the tracking stations of Table 4.2.1 over time intervals ranging from two to five days. The locations of the three station groups utilized are shown in Figures 4.2.1 through 4.2.3. Observations of topocentric range and range difference were based on satellite positions obtained from the numerical integration of the satellite's equations of motion using a force model consisting of the WGS72 [Seppelin, 1974] geopotential coefficients to degree and order eight, solar radiation pressure, and luni-solar gravitational perturbations. The initial conditions for the orbit integrations were obtained from Table 3.2.1 for each of the twenty-four GPS satellites. The observation sets consisted of range and Doppler range differences generated every five minutes. Satellites were tracked sequentially and selected on the basis of criteria discussed below. The duration of the satellite tracking interval varied from

TABLE 4.2.1. GEODETIC COORDINATES OF TRACKING STATIONS

STATION NO.	GEODETIC COORDINATES						
	LATITUDE			LONGITUDE			HEIGHT (m)
1001	30°	0'	0.00"	45°	0'	0.00"	0.0
1002	30	54	7.56	45	0	0.00	0.0
1003	30	0	0.00	43	57	48.96	0.0
1004	30	0	0.00	46	2	11.04	0.0
1005	30	0	0.00	43	26	43.44	0.0
1006	30	0	0.00	46	33	16.56	0.0
1007	30	0	0.00	46	24	32.25	0.0
1008	30	0	0.00	47	35	27.75	0.0
1009	90	0	0.00	0	0	0.00	0.0
1010	89	6	55.18	0	0	0.00	0.0
1011	0	0	0.00	0	0	0.00	0.0
1012	0	0	0.00	0	53	53.93	0.0
1013	0	53	53.93	0	0	0.00	0.0
1014	30	38	6.69	45	38	6.69	0.0
1015	23	39	39.70	38	37	18.74	0.0
1016	36	20	20.30	51	22	41.26	0.0

one to three hours as a function of the adopted clock error modeling procedure.

To the geometrically derived observations of range and range difference, equations (3.1.1) and (3.1.2), systematic and random error sources were added as required in accordance with Table 4.2.2. White noise consistent with that expected from six-second ranges smoothed over 300 seconds or one-minute integrated Doppler range differences aggregated over the same interval was added based on the adopted levels in Table 4.2.2 as described in Section 4.1.4. Random rubidium and cesium clock noise were simulated using the algorithm of Meditch [1975], based on the selected Allan variance models for the satellite and geodetic receiver oscillators. Random receiver cesium clock noise was added to the observations along with a time bias and drift as given in Table 4.2.2.

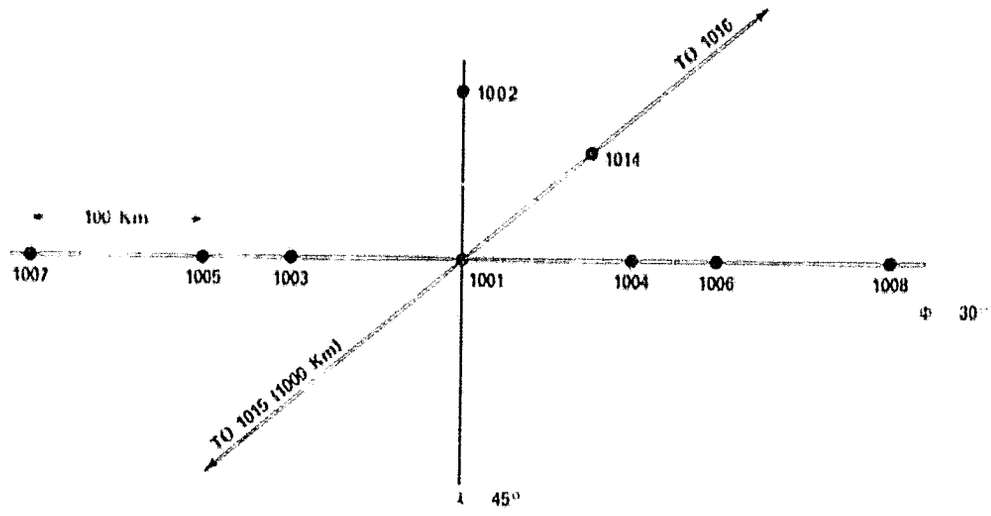

Figure 4.2.1. Station Locations - Mid-Latitude Group

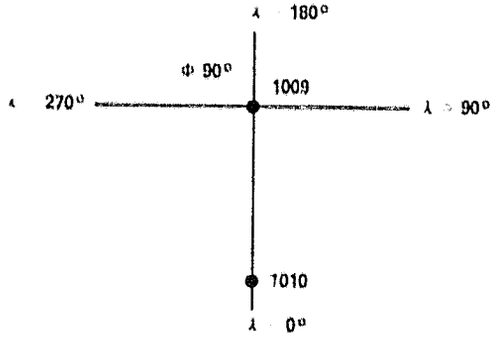

Figure 4.2.2. Polar Group

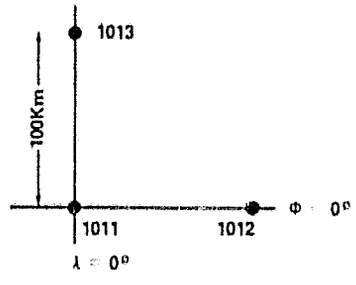

Figure 4.2.3. Equatorial Group

TABLE 4.2.2. SIMULATION ERROR SOURCES

ORBITAL ELEMENT	PERIODIC ERRORS (RMS)		
	RADIAL	ALONG TRACK	CROSS TRACK
a	2 m		
e	2.6 m	5.3 m	
i			12 m
$M + \omega$		6.4 m*	
Ω			

* PLUS 5 m QUADRATIC ERROR

TROPOSPHERIC REFRACTION — 5% OF HOPFIELD MODEL PREDICTION

CLOCK ERRORS

1. STATION
   - BIAS: 30 TO −10 nsec
   - DRIFT: .000083 TO −.00004 nsec/sec
   - RANDOM: CESIUM SPECIFICATIONS

2. SATELLITE
   - RMS BIAS: 5 nsec
   - RMS DRIFT: .0002 nsec/sec
   - RANDOM: RESIDUAL NOISE BASED ON RUBIDIUM MODEL FOR GPS SATELLITES

WHITE NOISE
- RANGE: 100 - 60 cm (6 sec)
- DOPPLER: 3 - 1 cm (60 sec)

For each satellite the total time error converted to distance is given by equation (4.1.11) as

$$cT_i(t) = cT_i(t_o) + cR_i(t - t_o) + \frac{cD_i}{2}(t - t_o)^2 + \eta_i(t) \qquad (4.2.1)$$

where

$$\eta_i(t) = c \int_{t_o}^{t} y_i(\tau')d\tau \ . \qquad (4.2.2)$$

Assuming the ageing to be negligible over the satellite tracking interval, equation (4.2.1) can be written as

$$cT_i(t) = a + b(t - t') + \xi_i(t) \qquad (4.2.3)$$

where

$$a = cT_i(t_o) + cR_i(t' - t_o) + \frac{cD_i}{2}(t - t_o)^2 + \eta_i(t') \qquad (4.2.4)$$

$$b = cR_i \qquad (4.2.5)$$

$$\xi_i(t) = \eta_i(t) - \eta_i(t') \ . \qquad (4.2.6)$$

Letting $c\hat{T}_i(t)$ be the best prior linear estimate of $cT_i(t)$ over the satellite tracking interval, the residual range error is defined as

$$c[T_i(t) - \hat{T}_i(t)] = (a - \hat{a}) + (b - \hat{b})(t - t') + r_i(t) \ . \qquad (4.2.7)$$

The expected standard errors of the residual random bias $(a-\hat{a})$ and drift $(b-\hat{b})$ of the satellite clocks were taken to be consistent with the ephemeris simulation results described in Section 4.1.2 and are given in Table 4.2.2. The residual random range error $r_i(t)$ is obtained from $\eta_i(t)$ by linear least squares approximation. These quantities are

added to the geometrically derived range and range differences accordingly, assuming the random bias and drift are normally distributed although constant within a particular tracking interval.

A residual tropospheric refraction error in the form of five percent of the Hopfield model prediction was applied to the observations in certain cases to represent a difference between actual and modeled refraction. In these cases the adjustment model (Section 4.3) included tropospheric scaling parameters as indicated in equation (4.1.57).

The resulting quantities are the observed range and range difference observations given by

$$\begin{aligned} R_b(t) = R(t) + \nu_R/\sqrt{n} + a + b(t - t') + \eta(t) \\ + (a_i - \hat{a}_i) + (b_i - \hat{b}_i)(t - t'') + r_i(t) + \beta\delta R(t) \end{aligned} \tag{4.2.8}$$

and

$$\begin{aligned} \Delta R_b(t) = R(t) - R(t - \Delta t) + \sqrt{m}\,\nu_{\Delta R} + b\Delta t + \eta(t) \\ - \eta(t - \Delta t) + (b_i - \hat{b}_i)\Delta t + r_i(t) - r_i(t - \Delta t) \\ + \beta[\delta R(t) - \delta R(t - \Delta t)] \end{aligned} \tag{4.2.9}$$

where n is the number of six-second ranges assumed smoothed, ν_R are independent zero mean Gaussian random numbers having a standard deviation equal to that of the six-second ranges, β is 0.05, $\delta R(t)$ is the tropospheric refraction error, m is the number of aggregated Doppler, observations, $\nu_{\Delta R}$ are independent zero mean Gaussian random numbers having a standard deviation equal to that of the Doppler measurements, t' and t'' are clock model epochs, and Δt is five minutes.

The white noise level applied to range differences according to equation (4.2.9) corresponds to the summation of m independent one minute Doppler counts. For continuous count integrated Doppler the total noise of the aggregated count may be less and possibly independent of the count interval; thus the coefficient of $\nu_{\Delta R}$ in equation (4.2.9) may be as small as one. The consequence of this will be examined in Section 4.5.

In the least squares adjustment of range or Doppler observations actual measurements are differenced from estimates of the measurements. The estimated observation value is obtained from the geometrically derived range or range difference by a linear adjustment of this quantity which introduces the assumed level of orbit error. For range observations this linear adjustment has the form

$$R_o(t) = R(t) + \sum_{k=1}^{6} \frac{\delta R(t)}{\delta e_k(t_c)} \Delta e_k(t_c) \qquad (4.2.10)$$

where the $\Delta e_k(t_c)$ represent errors in the orbital elements of the tracked satellite at the midpoint of the satellite tracking interval. These errors are assumed to be normally distributed varying with each satellite of the constellation. The expected ephemeris error is given in Table 4.2.2. The required partial derivatives in equation (4.2.10) are developed in Section 4.3.2 and approximated in Section 4.3.3. For range difference observations an equation analogous to equation (4.2.10) was utilized.

Notice that the error in the satellite clock was introduced into the observed quantity along with the estimates $\hat{a}$ and $\hat{b}$. Strictly speaking these error estimates should be introduced into the estimated

observation but the net effect on the difference of estimated and observed quantities in either case is identical. The same argument holds for the tropospheric refraction error.

4.2.2 Optimal Design for Dynamic Point Positioning

A Global Positioning System is designed so that six to nine satellites are usually available for observation from any geographic location. Since options in the tracking geometry are available, it is reasonable to design a data acquisition schedule which produces the best results for the adjusted station coordinates derived from dynamic point positioning. Some factors to be considered in such a design are the length of the tracking interval for each observed satellite, possible criteria for minimizing the coordinate covariance, the period of site occupation and the type of receiver operation anticipated, sequential tracking or the use of multiple channel receivers. With these factors defined a sequence of satellites can be selected whose observations give the best geometrical strength of solution according to the criterion adopted.

Various procedures for selecting the satellites to be tracked can be defined. These include the simplest approach of random selection from those visible to approaches based on choices for covariance minimization. For dynamic positioning performed using a sequential single satellite receiver two criteria will be discussed:

(i) the selection of satellites whose observations minimize the square root of the trace of the accumulated covariance matrix, and

(ii) the selection of satellites whose observations minimize the norm of the vector of correlation coefficients of the accumulated covariance matrix.

The first procedure is also known as the evaluation of the geometric dilution of precision. This second procedure allows a more statistically independent determination of individual parameters. In evaluating these criteria observations are assumed subject only to Gaussian white noise. No correlated random errors are introduced. However in addition to the station coordinates a receiver clock error model was incorporated in some cases.

Using globally distributed stations a geometric analysis of point positioning for range and Doppler tracking was made examining the two criteria. The use of various station locations insured that numerous samplings of satellite pass geometry were utilized such as those shown in Figures 4.2.4(a) and 4.2.4(b). For one particular station Figures 4.2.5(b) through 4.2.5(e) give the square root of the trace of the covariance matrix and standard error in latitude, longitude, and height as a function of the number of one-hour satellite tracking intervals of range observations having a one meter standard error. Range observations were assumed every five minutes and no clock error model was included in this case. Figure 4.2.5(a) gives the azimuth and elevation angles for the epoch of each tracking interval for selection based on minimizing the trace of the covariance matrix. Figure 4.2.6 gives analogous information for the second criterion. Observations below ten degrees elevation were excluded from the results.

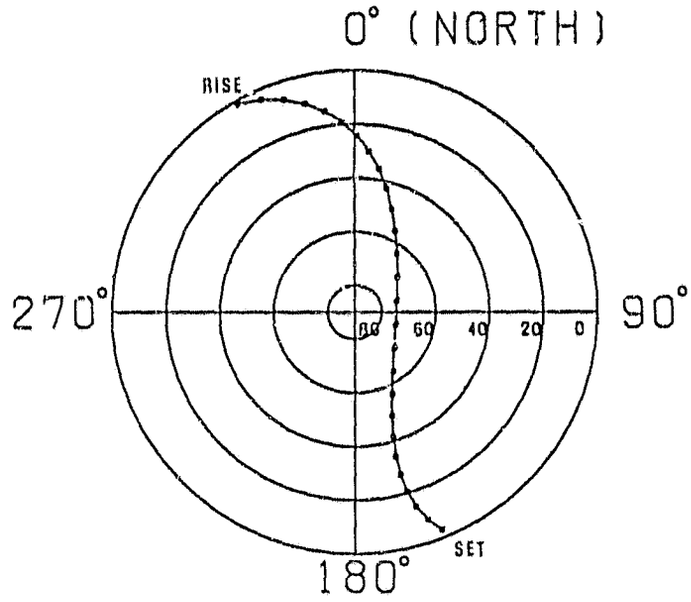

(a) Short Pass

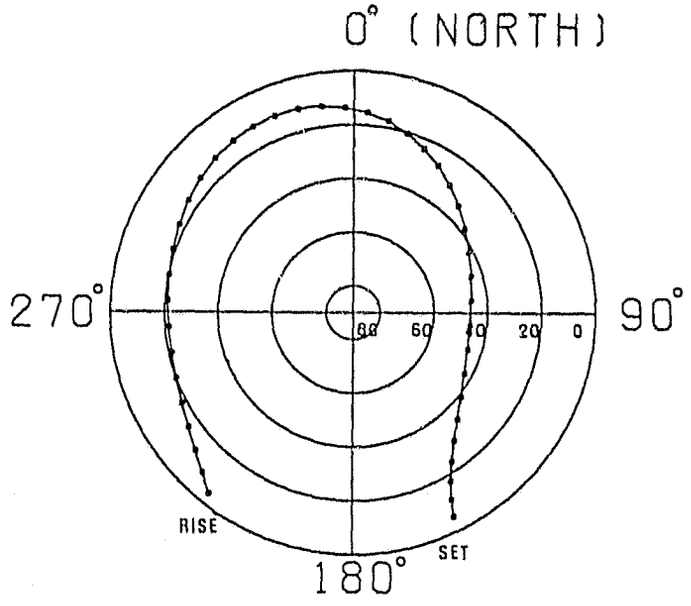

(b) Long Pass

Figure 4.2.4. Examples of Satellite Pass Geometry for an Equatorial Station

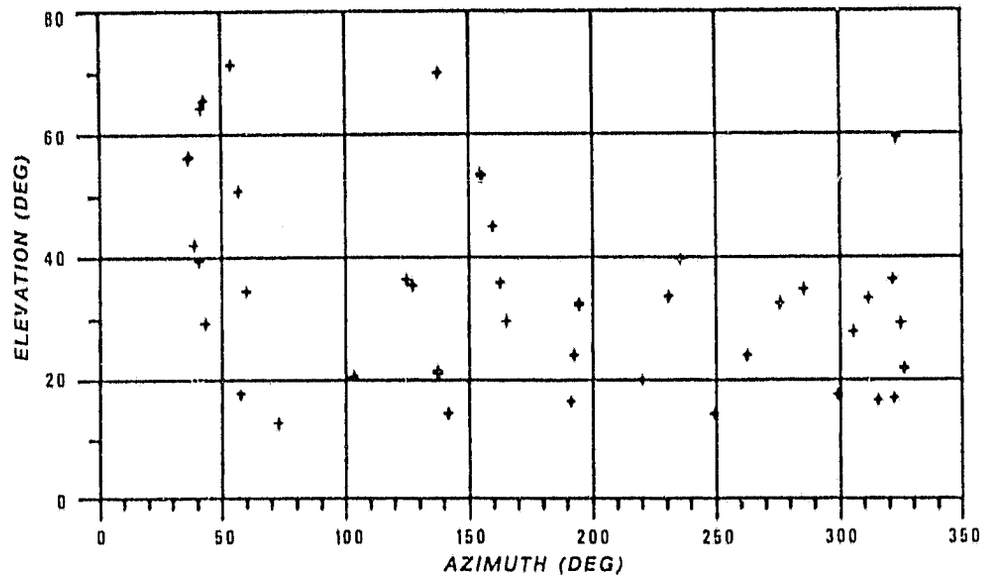

(a) Azimuth and Elevation of Selected Satellites

Figure 4.2.5. Satellite Selection Based on Minimum Trace Criterion ($\phi = 40°$, $\lambda = 45°$)

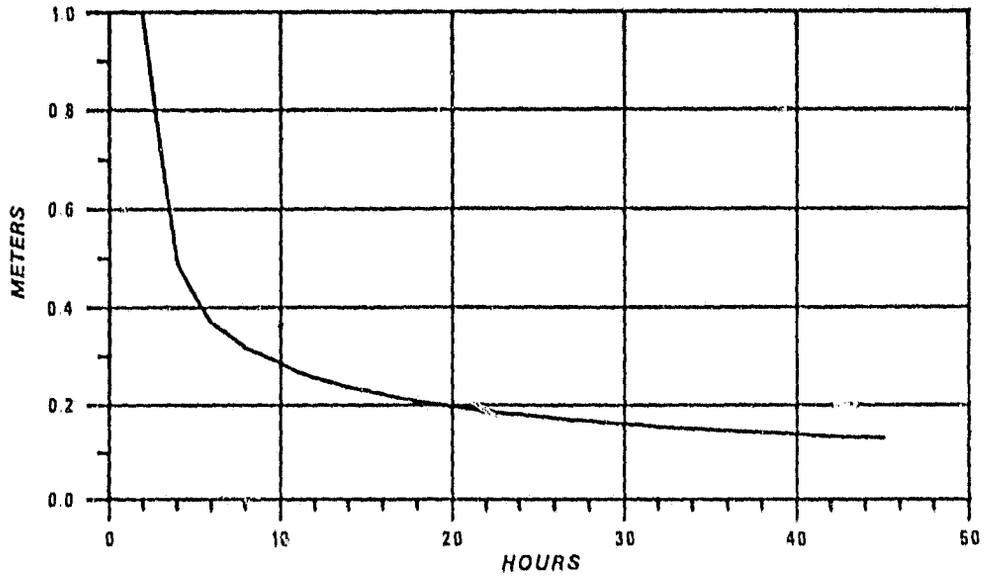

(b) Square Root of Trace of Parameter Covariance Matrix

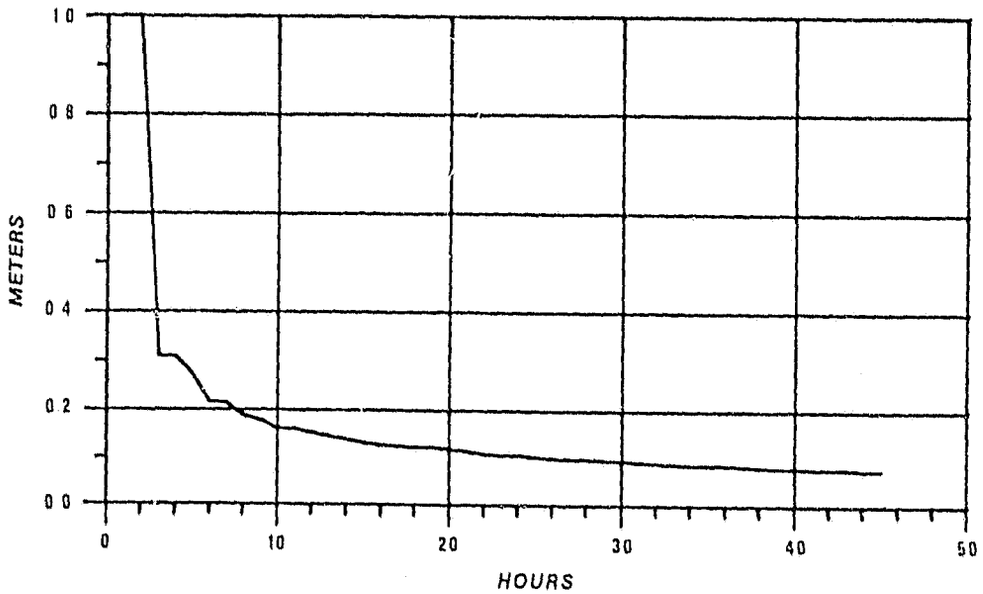

(c) Standard Error in Latitude

Figure 4.2.5 (continued)

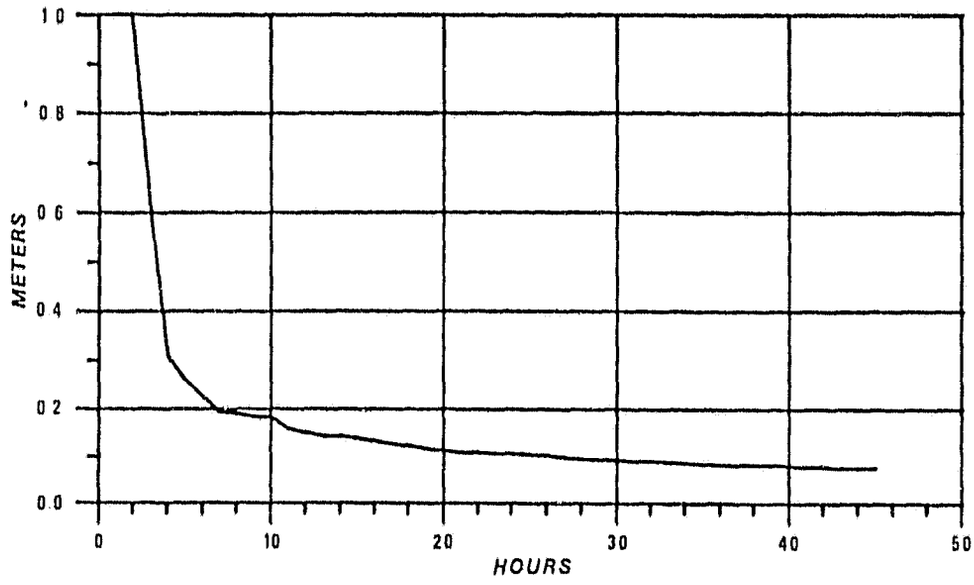

(d) Standard Error in Longitude

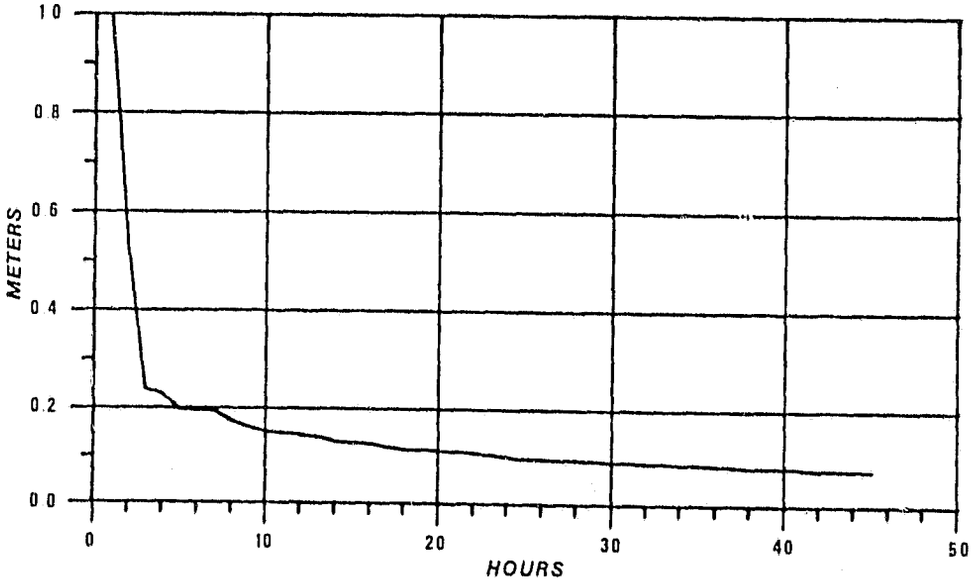

(e) Standard Error in Height

Figure 4.2.5 (continued)

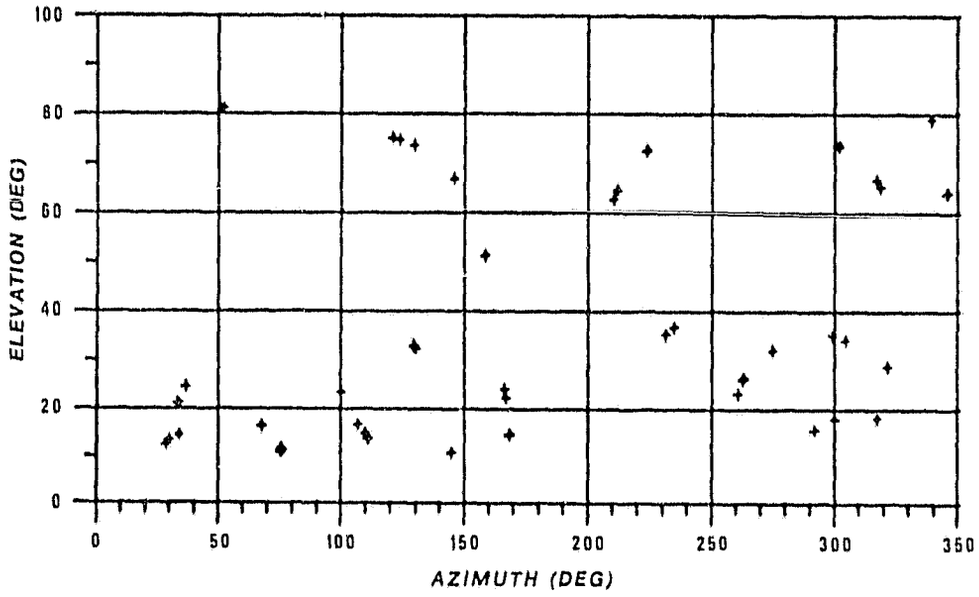

(a) Azimuth and Elevation of Selected Satellites

Figure 4.2.6. Satellite Selection Based on Minimum Correlation Criterion ($\phi = 40°$, $\lambda = 45°$)

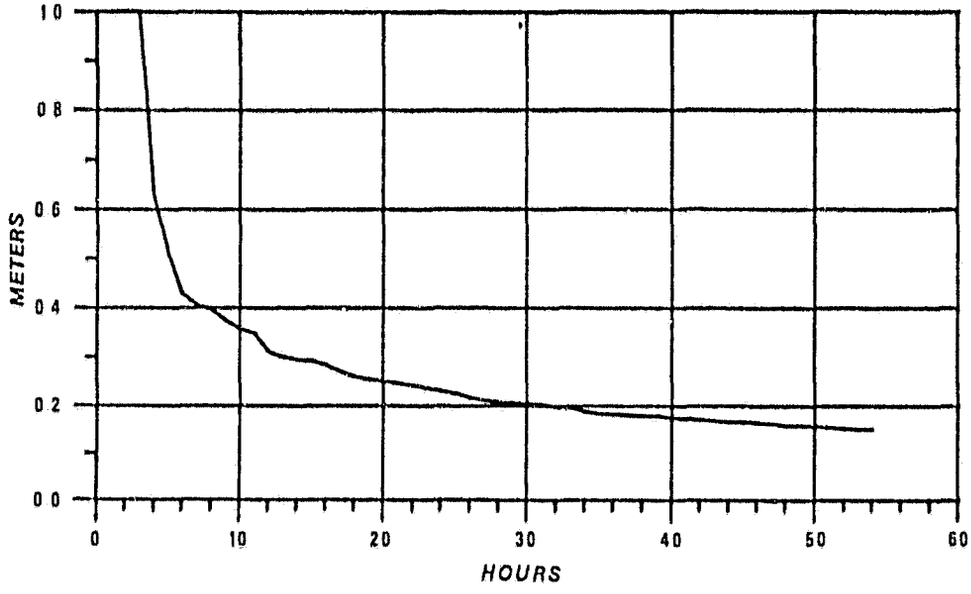

(b) Square Root of Trace of Parameter Covariance Matrix

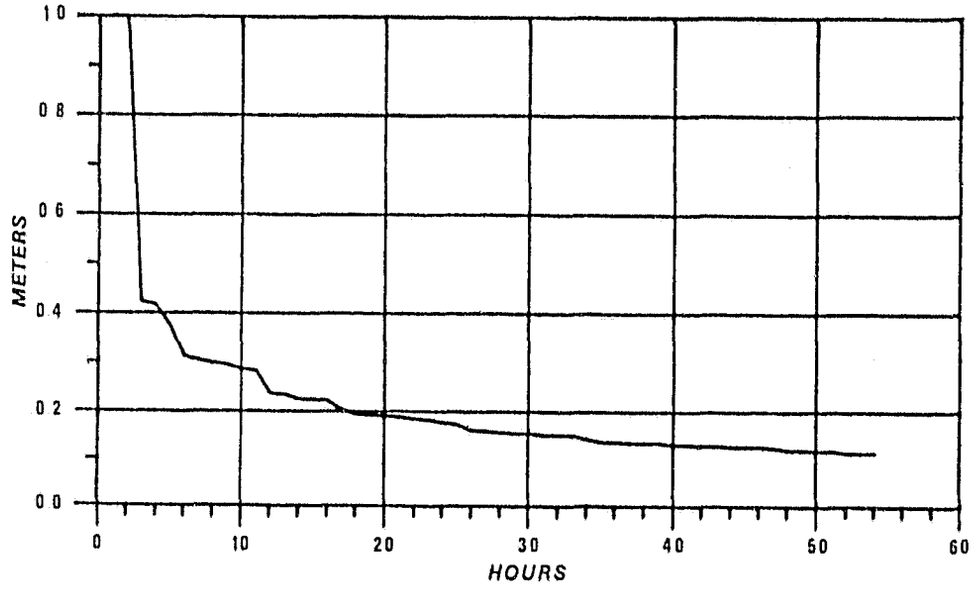

(c) Standard Error in Latitude

Figure 4.2.6 (continued)

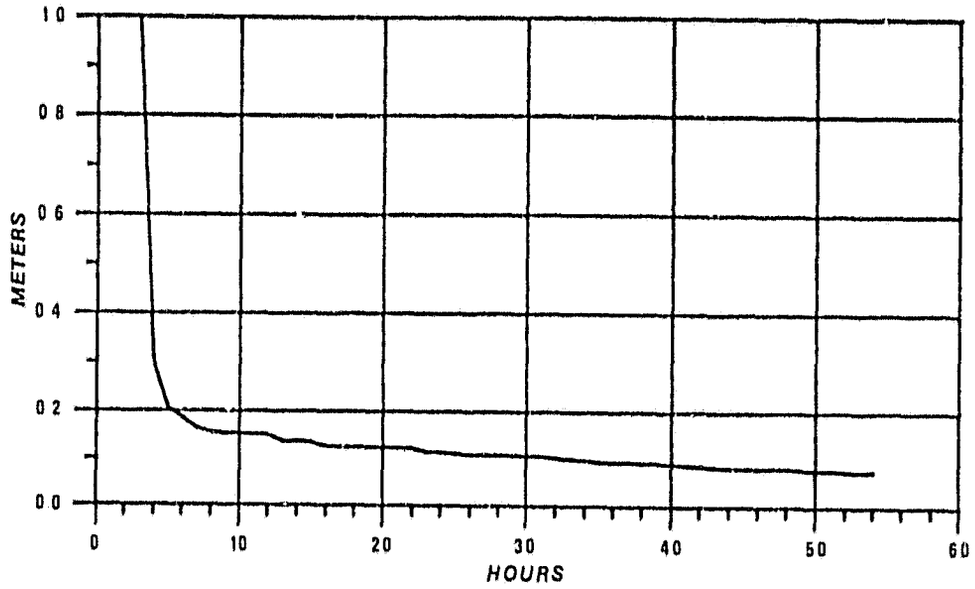

(d) Standard Error in Longitude

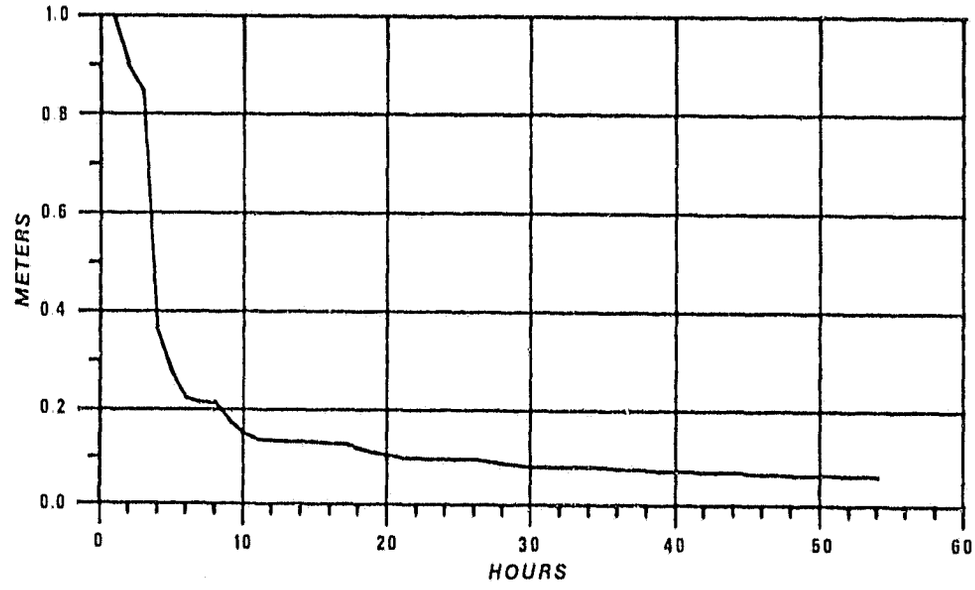

(e) Standard Error in Height

Figure 4.2.6 (continued)

Using these criteria the next satellite to be tracked is that whose observations over the upcoming interval, when combined with all previous observations, produces the optimum coordinate covariance with respect to the selection criterion. Notice in these examples that the standard error of each position component drops rapidly within the first day then shows only gradual improvement with additional data. An examination of the results using the second criterion shows some reduction in the parameter correlations but yields an increase in the expected standard error as evidenced in Figures 4.2.6(b) through 4.2.6(e).

Based on a number of similar determinations the following general conclusions can be drawn for the optimal selection of GPS satellites for both range and Doppler. First, it is readily apparent that the second technique results in somewhat lower parameter correlations but at the cost of increased parameter variances with respect to the first criterion. However, the technique adopted is a matter of choice since each is independent. For the positioning studies of Section 4.5 the first criterion was utilized to establish the observation schedules in all cases. Secondly, from the results it is noted that initially the variance of the estimated parameters increases rapidly as the interval of tracking each satellite is increased. For a fixed number of observations the results obtained are quite varied when the total observation time is less than six hours. With increased observation time allowing more sampling of pass geometries the results become virtually equivalent after twelve hours. Thirdly, with range observations the introduction of a receiver time bias significantly weakens the variance of station height as evidenced by comparing Figure 4.2.5(e) with Figure 4.2.7.

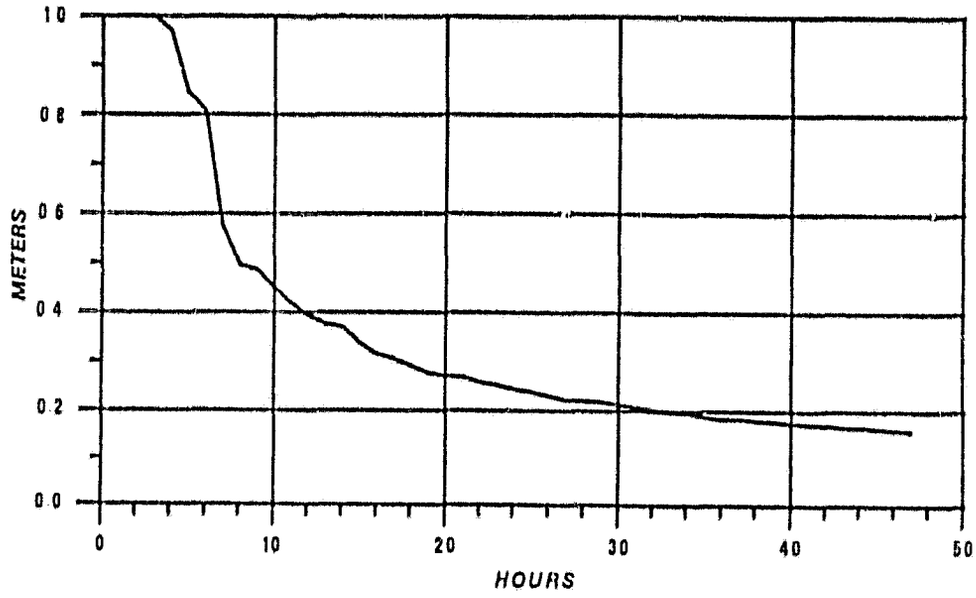

Figure 4.2.7. Standard Error in Height when Adjustment includes Time Bias (Selection Criterion Minimum Trace)

The variance of station latitude and longitude also increase but not as significantly. The reason for this increase in height uncertainty can be explained by noting that a time or range bias error in a given observation is equivalent to a linear combination of a vertical and horizontal position error of the station. The horizontal error lies along the projection of the slant range vector onto the horizon plane. Successive observations taken as a function of azimuth would yield horizontal error components whose sum would tend to cancel. However the vertical error component can only be separated from an actual station height error by using observations of low elevation. At ten degrees elevation the vertical component of range bias is approximately seventeen percent of the total bias. Therefore with the restriction of observations to elevation angles greater than ten degrees a weakening of the actual station

height uncertainty can be expected since a station height error will tend to be masked by the vertical component of range bias.

Finally, the satellite orbits have repeating ground tracks yielding a tracking geometry with a diurnal period. For the first selection criterion this tends to result in a clustering of the initial satellite azimuth of each tracking interval into a series of three bands separated by 50 to 150 degrees with a sampling of different elevations in each band. This is most obvious in cases where the tracking interval is short. This property is not a fixed rule but a general trend as demonstrated somewhat in Figure 4.2.5(a). For the second criterion the distribution of azimuth is less consistent, although in some cases considered the distribution may fall almost entirely within a single band of 150 degrees width.

For the determination of baseline components and chord length only the first criterion was examined and the results were discussed in Chapter 3.

4.3 Adjustment Procedure

The adjustment of range and Doppler observations using the method of observation equations may be developed in a mathematical form which accommodates the introduction of new observations and new parameters. Uotila [1967] discusses this sequential approach and it is emphasized that such a technique is valuable in assessing the effect of additional observations on current parameter estimates. This approach may be adopted for the analysis of GPS observations taken in a sequential fashion as discussed in Section 4.2. The estimation equations for this procedure are now developed.

4.3.1 Sequential Adjustment of Parameters

Given N statistically independent sets of observations L_{b_i} where

$$\begin{aligned} L_1 &= F(x,y_1) \\ &\vdots \\ L_N &= F(x,y_N) \end{aligned} \tag{4.3.1}$$

equations are developed for the least squares minimum variance estimate of the primary parameters x and secondary parameters y_i using all N observation sets. The primary parameters of interest are the earth-fixed station coordinates or coordinate differences. The secondary parameters consist of orbital elements, satellite clock model parameters, refraction bias parameters, and tracking receiver clock parameters. Formulas giving the parameter covariance matrices Σ_x and Σ_{y_i} and the weighted sum square of residuals after adjustment, $V^T PV$, are developed. The sequential forms of these equations are given as required. In sequential form the estimated quantity $\hat{z}_{N+1}$ based on N + 1 sets of observations is written as

$$\hat{z}_{N+1} = \hat{z}_N + \Delta z_{N+1} \tag{4.3.2}$$

where Δz_{N+1} is the correction to the prior estimate $\hat{z}_N$ due to the inclusion of observations $L_{b_{N+1}}$.

4.3.1.1 Estimation of Primary Parameters

The least squares minimum variance estimate for the parameters of primary interest x from any one set of observations L_{b_i} from equations (4.3.1) is given by

$$\hat{x}_i = -[N_{xx} - N_{xy}N_{yy}^{-1}N_{yx}]_i^{-1} \quad [U_x - N_{xy}N_{yy}^{-1}U_y]_i$$
$$= -\Sigma_{x_i} R_i = \hat{x}_I \tag{4.3.3}$$

where

$$N_i = \begin{bmatrix} N_{xx} & N_{xy_i} \\ N_{y_i x} & N_{y_i y_i} \end{bmatrix} = A_i^T P_i A_i \tag{4.3.4}$$

$$U_i = \begin{bmatrix} U_x \\ U_{y_i} \end{bmatrix} = A_i^T W_i L_i \tag{4.3.5}$$

$$A_i = \begin{bmatrix} A_x & A_{y_i} \end{bmatrix}_i \tag{4.3.6}$$

$$P_i = \Sigma_{L_{b_i}}^{-1} \tag{4.3.7}$$

$$L_i = L_{o_i} - L_{b_i} \tag{4.3.8}$$

$$L_{o_i} = F_i(x_o, y_{i_o}) \tag{4.3.9}$$

with the a priori variance of unit weight σ_0^2 equal to one. Equation (4.3.3) is the solution for x based on observations L_{b_i} which results after algebraic elimination of the secondary parameter set y_i.

With the addition of a second observation set L_{b_j} the estimate for x becomes

$$\hat{x}_{II} = -\left[\Sigma_{x_i}^{-1} + \Sigma_{x_j}^{-1}\right]^{-1} \left[R_i + R_j\right]. \tag{4.3.10}$$

Denoting the covariance matrix Σ_{x_i} as Σ_{x_I}, equation (4.3.10) may be written using matrix identities as

$$\hat{x}_{II} = -[\Sigma_{x_I} - \Sigma_{x_I}(\Sigma_{x_I} + \Sigma_{x_j})^{-1}\Sigma_{x_I}][R_i + R_j]$$
$$= \hat{x}_I - \Sigma_{x_I}(\Sigma_{x_I} + \Sigma_{x_j})^{-1}\hat{x}_I - (\Sigma_{x_I}^{-1} + \Sigma_{x_j}^{-1})^{-1}R_j \tag{4.3.11}$$

or

$$\hat{x}_{II} = \hat{x}_I + \Delta x_{II} \ . \tag{4.3.12}$$

The covariance matrix $\Sigma_{x_{II}}$ based on a pair of data sets, assumed uncorrelated set-wise, becomes

$$\Sigma_{x_{II}} = \left[\Sigma_{x_I}^{-1} + \Sigma_{x_j}^{-1}\right]^{-1} \ . \tag{4.3.13}$$

In general given $\hat{x}_N$ and Σ_{x_N} based on N sets of observations, the estimate based on the inclusion of an additional observation set is given by

$$\hat{x}_{N+1} = \hat{x}_N + \Delta x_{N+1} \tag{4.3.14}$$

where

$$\Delta x_{N+1} = -\Sigma_{x_N}[\Sigma_{x_N} + \Sigma_{x_{n+1}}]^{-1}\hat{x}_N$$
$$- [\Sigma_{x_N}^{-1} + \Sigma_{x_{n+1}}^{-1}]^{-1}R_{n+1} \tag{4.3.15}$$

and the covariance is

$$\Sigma_{x_{N+1}} = [\Sigma_{x_N}^{-1} + \Sigma_{x_{n+1}}^{-1}]^{-1}$$
$$= \Sigma_{x_N} - \Sigma_{x_N}[\Sigma_{x_N} + \Sigma_{x_{n+1}}]^{-1}\Sigma_{x_N} \tag{4.3.16}$$

or

$$\Sigma_{x_{N+1}} = \Sigma_{x_N} + \Delta\Sigma_{x_{N+1}} \tag{4.3.17}$$

where

$$\Delta\Sigma_{x_{N+1}} = -\Sigma_{x_N}\left[\Sigma_{x_N} + \Sigma_{x_{n+1}}\right]^{-1}\Sigma_{x_N} \quad . \tag{4.3.18}$$

Equations (4.3.15) and (4.3.18), although not necessarily computationally efficient, give a measure of the expected change to the primary parameter set estimates and their uncertainties if a new observation set is added. It is assumed here that:

(i) new normal equations are formed using the same initial parameter estimates x_o, y_{i_o} as used previously; and

(ii) the new data block $L_{b_{N+1}}$ is uncorrelated with all previously used observations.

4.3.1.2 Estimation of Secondary Parameters

Consider the least squares normal equations for the observation set L_{b_j}:

$$\begin{bmatrix} N_{xx} & N_{xy_j} \\ N_{y_j x} & N_{y_j y_j} \end{bmatrix} \begin{bmatrix} x \\ y_j \end{bmatrix} + \begin{bmatrix} U_x \\ U_{y_j} \end{bmatrix} = 0 \tag{4.3.19}$$

or

$$\begin{aligned} N_{xx}x + N_{xy_j}y_j + U_x &= 0 \\ N_{y_j x}x + N_{y_j y_j}y_j + U_{y_j} &= 0 \quad . \end{aligned} \tag{4.3.20}$$

The solution for y_j is given by

$$\hat{y}_j = -N_{y_j y_j}^{-1}\left[U_{y_j} + N_{y_j x}\hat{x}\right] \tag{4.3.21}$$

where $\hat{x}$ is based on all N observation sets:

$$\hat{x} = -\Sigma_x \left[\sum_{i=1}^{N} (U_x - N_{xy_i} N_{y_i y_i}^{-1} U_{y_i})_i \right] . \qquad (4.3.22)$$

Substituting equation (4.3.22) into (4.3.21) yields

$$\begin{aligned} \hat{y}_j &= -N_{y_j y_j}^{-1} A_{y_j}^T P_j L_j + N_{y_j y_j}^{-1} N_{y_j x} \Sigma_x \left[\sum_i (U_x - N_{xy_i} N_{y_i y_i}^{-1} U_{y_i})_i \right] \\ &= -N_{y_j y_j}^{-1} A_{y_j}^T P_j L_j + N_{y_j y_j}^{-1} N_{y_j x} \Sigma_x \left[\sum_i (A_x^T P_i L_i - N_{xy_i} N_{y_i y_i}^{-1} A_{y_i}^T P_i L_i)_i \right] . \end{aligned} \qquad (4.3.23)$$

Equation (4.3.23) can be written as

$$\hat{y}_j = -N_{y_i y_i}^{-1} A_{y_j}^T P_j L_j + N_{y_j y_j}^{-1} N_{y_j x} \Sigma_x \left\{ \left[A_x^T P_j L_j - N_{xy_j} N_{y_j y_j}^{-1} A_{y_j}^T P_j L_j \right]_j + Q \right\} \qquad (4.2.24)$$

where Q is a function of all data sets except L_{b_j}. The covariance matrix Σ_{y_j} is obtained from equation (4.3.23). Since all data sets are assumed statistically independent the covariance Σ_{y_j} is given by

$$\Sigma_{y_j} = \sum_{k=1}^{N} \left[\frac{dy_j}{dL_k} \right] P_k^{-1} \left[\frac{dy_j}{dL_k} \right]^T . \qquad (4.3.25)$$

Differentiating equation (4.3.23)

$$\left[\frac{dy_j}{dL_k} \right]^T = \begin{cases} -N_{y_j y_j}^{-1} A_{y_j}^T P_j + N_{y_j y_j}^{-1} N_{y_j x} \Sigma_x \left[A_x^T P_j - N_{xy_j} N_{y_j y_j}^{-1} A_{y_j}^T P_j \right]_k & k = j \\ N_{y_j y_j}^{-1} N_{y_j x} \Sigma_x \left[A_x^T P_k - N_{xy_k} N_{y_k y_k}^{-1} A_{y_k}^T P_k \right]_k . & k \neq j \end{cases} \qquad (4.3.26)$$

Substituting equation (4.3.26) into equation (4.3.25) and summing over k yields the final result

$$\Sigma_{y_j} = N_{y_j y_j}^{-1} + N_{y_j y_j}^{-1} N_{y_j x} \Sigma_x N_{xy_j} N_{y_j y_j}^{-1} . \qquad (4.3.27)$$

The residuals of fit after adjustment are given by the linearized form of equation (4.3.1)

$$V_i = \begin{bmatrix} A_x & A_{y_i} \end{bmatrix}_i \begin{bmatrix} \hat{x} \\ \hat{y}_i \end{bmatrix} + L_i \tag{4.3.28}$$

or

$$V_i = A_i \hat{X}_i + L_i \ . \tag{4.3.29}$$

In terms of N data sets equation (4.3.28) has the form

$$\begin{bmatrix} V_1 \\ V_2 \\ \vdots \\ V_N \end{bmatrix} = \begin{bmatrix} A_x^1 & A_{y_1} & 0 & \cdots & 0 \\ A_x^2 & 0 & A_{y_2} & \cdots & 0 \\ & & \vdots & & \\ A_x^N & 0 & 0 & \cdots & A_{y_N} \end{bmatrix} \begin{bmatrix} \hat{x} \\ \hat{y}_1 \\ \vdots \\ \hat{y}_N \end{bmatrix} + \begin{bmatrix} L_1 \\ \vdots \\ L_N \end{bmatrix} \ . \tag{4.3.30}$$

Since the observation blocks are uncorrelated

$$\begin{aligned} V^T P V &= \sum_{i=1}^{N} \left[L_i^T P_i L_i + \begin{bmatrix} \hat{x}^T & y_i^T \end{bmatrix} \begin{bmatrix} A_x & A_{y_i} \end{bmatrix}_i^T P_i L_i \right] \\ &= \sum_{i=1}^{N} \left[L_i^T P_i L_i + \hat{X}_i^T A_i^T P_i L_i \right] \\ &= \sum_{i=1}^{N} \left[L_i^T P_i L_i + \hat{X}_i^T U_i \right] \ . \end{aligned} \tag{4.3.31}$$

The a posteriori variance of unit weight is

$$\hat{\sigma}_o^2 = \frac{V^T P V}{d} \tag{4.3.32}$$

where d is the number of degrees of freedom in the total adjustment problem.

The equations developed here were utilized in the adjustment of simulated GPS range and Doppler observations. It is an illustrative approach for determining how the uncertainty and error in station positioning vary in time as a function of such variables as the number of observations, method of satellite selection, tracking interval, and others.

4.3.2 Model Parameters and Partial Derivatives

In the adjustment of range and Doppler observations the number of secondary parameters y_i for each data set of equation (4.3.1) is subject to variation depending on the tracking schedule and the choice of specific clock error models and additional bias parameters. The secondary parameter set includes six orbital elements for each satellite tracking interval, a polynomial clock model for receiver clocks over the time span of each observation set, a polynomial clock model for each satellite clock over the interval each is tracked, and may include tropospheric refraction scaling parameters for every satellite-station combination within an observation set. The primary parameter set x consists of the geodetic coordinates of the tracking stations in the adopted earth-fixed frame of reference.

The design matrix A introduced in Section 3.1.2 is developed from the first partials of the data function with respect to the model parameters. The partial derivatives of the range observation model, equation (4.1.57), with respect to the Cartesian earth-fixed coordinates of the tracking station are

$$\frac{\partial R(t)}{\partial u} = \frac{u_s(t) - u}{R(t)} \qquad u \rightarrow v,w \tag{4.3.33}$$

where u_s, v_s, w_s are the coordinates of the satellite at time t in the same frame. The partials for geodetic coordinates are obtained using equation (4.3.33) and the chain rule

$$\frac{\partial R(t)}{\partial \phi} = \frac{\partial R(t)}{\partial u}\frac{\partial u}{\partial \phi} + \frac{\partial R(t)}{\partial v}\frac{\partial v}{\partial \phi} + \frac{\partial R(t)}{\partial w}\frac{\partial w}{\partial \phi} \qquad \phi \rightarrow \lambda, h \tag{4.3.34}$$

where the partials of Cartesian coordinates with respect to geodetic coordinates are given in Rapp [1976] as the coefficients of the differential equations

$$\begin{aligned} du &= -(M+h)\sin\phi\cos\lambda d\phi - (N+h)\cos\phi\sin\lambda d\lambda + \cos\phi\cos\lambda dh \\ dv &= -(M+h)\sin\phi\sin\lambda d\phi + (N+h)\cos\phi\cos\lambda d\lambda + \cos\phi\sin\lambda dh \\ dw &= (M+h)\cos\phi d\phi + \sin\phi dh \end{aligned} \tag{4.3.35}$$

where M and N are the ellipsoid radii of curvature in the meridian and prime vertical.

The satellite coordinates are obtained in a mean inertial system by numerical integration of the equations of motion whose forces include the geopotential to degree and order eight, solar radiation pressure, and luni-solar gravitational perturbations and are rotated into the earth-fixed frame. The initial conditions for the integration are obtained from Table 3.2.1.

For range difference observations the partials for station coordinates are given by the difference

$$\frac{\partial \Delta R(t)}{\partial u} = \frac{u_s(t) - u}{R(t)} - \frac{u_s(t-\Delta t) - u}{R(t-\Delta t)} \qquad u \rightarrow v,w \tag{4.3.36}$$

where Δt is the Doppler integration interval. For geodetic coordinates a similar expression holds

$$\frac{\partial \Delta R(t)}{\partial \phi} = \frac{\partial R(t)}{\partial \phi} - \frac{\partial R(t-\Delta t)}{\partial \phi} \qquad \phi \rightarrow \lambda,h \tag{4.3.37}$$

Each interval a satellite is tracked six orbital elements are introduced to model ephemeris error. The elements are represented as the orbital semi-major axis a, the eccentricity multiplied by the cosine and sine of the argument of perigee, $e\cos\omega$ and $e\sin\omega$, the inclination i, the sum of mean anomaly M and argument of perigee ω, and the ascending node Ω. Letting t_c represent the midpoint of the satellite tracking interval and t_o the epoch associated with the initial orbital elements, the partial derivatives of range with respect to the elements at t_c are given by

$$\frac{\partial R(t)}{\partial e^*_{t_c}} = \frac{\partial R(t)}{\partial X^*_s(t)} \psi_o(t)\psi_o^{-1}(t_c)T(t_c) \tag{4.3.38}$$

where

$$\frac{\partial R(t)}{\partial X^*_s(t)} = \left[\frac{\partial R(t)}{\partial X_s(t)} \frac{\partial R(t)}{\partial Y_s(t)} \frac{\partial R(t)}{\partial Z_s(t)} \; 0 \; 0 \; 0\right] \tag{4.3.39}$$

and

$$\frac{\partial R(t)}{\partial X_s(t)} = \frac{X_s(t) - X(t)}{R(t)} \qquad X \rightarrow Y,Z \tag{4.3.40}$$

where X_s, Y_s, Z_s are the satellite Cartesian coordinates in the mean inertial system. The quantities X,Y,Z are the station coordinates in the same frame. The matrix $\psi_0(t)$ is the state transition whose elements are

obtained from the homogeneous solution of the satellite's variational equations [Baker, 1967].

$$\psi_o(t) = \begin{bmatrix} \frac{\partial X_s(t)}{\partial a(t_o)} & \cdots & \frac{\partial X_s(t)}{\partial \Omega(t_o)} \\ \vdots & & \vdots \\ \frac{\partial \dot{Z}_s(t)}{\partial a(t_o)} & \cdots & \frac{\partial \dot{Z}_s(t)}{\partial \Omega(t_o)} \end{bmatrix} \tag{4.3.41}$$

and T is the Jacobian matrix

$$T(t_c) = \begin{bmatrix} \frac{\partial X_s(t_c)}{\partial a(t_c)} & \cdots & \frac{\partial X_s(t_c)}{\partial \Omega(t_c)} \\ \vdots & & \vdots \\ \frac{\partial \dot{Z}_s(t)}{\partial a(t_c)} & \cdots & \frac{\partial \dot{Z}_s(t_c)}{\partial \Omega(t_c)} \end{bmatrix}. \tag{4.3.42}$$

For range difference observations equation (4.3.38) is modified using

$$\frac{\partial \Delta R(t)}{\partial X_s^*(t)} = \begin{bmatrix} \frac{\partial \Delta R(t)}{\partial X_s(t)} & \frac{\partial \Delta R(t)}{\partial Y_s(t)} & \frac{\partial \Delta R(t)}{\partial Z_s(t)} & 0 & 0 & 0 \end{bmatrix} \tag{4.3.43}$$

where

$$\frac{\partial \Delta R(t)}{\partial X_s(t)} = \frac{X_s(t) - X(t)}{R(t)} - \frac{X_s(t - \Delta t) - X(t - \Delta t)}{R(t - \Delta t)}. \tag{4.3.44}$$

For polynomial clock models of the form

$$P_n(t) = a_o + a_1(t - t') + \ldots + a_n(t - t')^n \tag{4.3.45}$$

the partials of range with respect to the model parameters $a_o, \ldots, a_n$ are just the parameter coefficients

$$\frac{\partial R(t)}{\partial a_i} = (t - t')^i \qquad i = o,\ldots,n \tag{4.3.46}$$

where t' is an arbitrary epoch for each model. The constant term in equation (4.3.46) represents the time (range) bias or phase error at t' associated with the modeled clock. The second parameter a_1 is proportional to the oscillator frequency bias Δf_i

$$a_1 = \frac{c}{f} \Delta f \tag{4.3.47}$$

and a_2 is proportional to the frequency drift $\dot{f}$

$$a_2 = \frac{c}{2f} \dot{f} \ . \tag{4.3.48}$$

For range difference observations derived from integrated Doppler over the interval $[t_k, t_\ell]$ the partials are

$$\frac{\partial \Delta R(t)}{\partial a_o} = 0 \tag{4.3.49}$$

$$\frac{\partial \Delta R(t)}{\partial a_1} = t_\ell - t_k \tag{4.3.50}$$

and

$$\frac{\partial \Delta R(t)}{\partial a_2} = (t_\ell - t')^2 - (t_k - t_\ell)^2 \ . \tag{4.3.51}$$

In terms of frequency bias and drift the partials are

$$\frac{\partial \Delta R(t)}{\partial \Delta f} = \frac{c}{f} (t_\ell - t_k) \tag{4.3.52}$$

and

$$\frac{\partial \Delta R(t)}{\partial \dot{f}} = \frac{c}{2f} [(t_\ell - t')^2 - (t_k - t')^2] \tag{4.3.53}$$

according to equation (4.1.7).

For the tropospheric refraction scaling parameter the partials of range and range difference are given by

$$\frac{\partial R(t)}{\partial C_R} = \delta R(t) \tag{4.3.54}$$

and

$$\frac{\partial \Delta R(t)}{\partial C_R} = \delta R(t_\ell) - \delta R(t_k) \tag{4.3.55}$$

using equation (4.1.57).

4.3.3 Use of Keplerian Partial Derivatives in the Adjustment Model

Numerical integration of the variational equations [O'Toole, 1976]

$$\frac{d\ddot{r}}{dr_o} = \frac{dF(r,\dot{r},p)}{dr_o} \quad r_o \rightarrow \dot{r}_o \tag{4.3.56}$$

gives the variation in a satellite's inertial position and velocity at time t with respect to changes in the initial state at time t_0. These partial derivatives are used in forming the observational partial derivatives of the design matrix A when the satellite state vector at t_0 is included in the adjustment. For satellites at extreme altitudes an approximation may be introduced. This approximation consists of replacing the numerically integrated solutions of the variational equations with Keplerian two body partial derivatives. This approximation is both economical and valid at GPS altitudes if observation times are within a few hours of the time at which the satellite state vector is to be improved. Keplerian partials are analytic expressions derived from the basic equations of two-body motion [Mueller, 1964].

The orbital elements at time t are obtained from the elements at time t_0 by the transformation

$$\begin{bmatrix} a \\ e \\ i \\ M \\ \omega \\ \Omega \end{bmatrix}_t = \begin{bmatrix} 1 & 0 & 0 & 0 & 0 & 0 \\ 0 & 1 & 0 & 0 & 0 & 0 \\ 0 & 0 & 1 & 0 & 0 & 0 \\ \alpha & 0 & 0 & 1 & 0 & 0 \\ 0 & 0 & 0 & 0 & 1 & 0 \\ 0 & 0 & 0 & 0 & 0 & 1 \end{bmatrix} \begin{bmatrix} a \\ e \\ i \\ M \\ \omega \\ \Omega \end{bmatrix}_{t_o} \tag{4.3.57}$$

where α is a time dependent quantity derived from Kepler's third law

$$\alpha = \sqrt{\frac{GM}{a}}\,(t - t_o) \ . \tag{4.3.58}$$

For Keplerian motion the only time varying element in equation (4.3.57) is the mean anomaly

$$M(t) = M(t_o) + n(t - t_o) \tag{4.3.59}$$

where n is the mean motion of the satellite. Differentiating equation (4.3.59) with respect to the orbital semi-major axis a at t_0 gives the rate of change of mean anomaly given a change in a at t_0:

$$\frac{\partial M(t)}{\partial a(t_o)} = -\frac{3}{2}\,\frac{n}{a(t_o)}\,(t - t_o) \ . \tag{4.3.60}$$

All other element variations are of the form

$$\frac{\partial e_i(t)}{\partial e_j(t_o)} = \begin{cases} 1 & i = j \\ 0 & i \neq j \end{cases} \ . \tag{4.3.61}$$

At observation time t let $\{u_s(t), v_s(t), w_s(t)\}$ be the coordinates of satellite position in the earth-fixed system. Let $\{u,v,w\}$ be the earth-fixed Cartesian coordinates of the tracking station. For range observations

$$\frac{\partial R(t)}{\partial u_s(t)} = \frac{u_s(t) - u}{R(t)} \qquad u \to v,w$$
$$\frac{\partial R(t)}{\partial \dot{u}_s(t)} = 0 \quad . \tag{4.3.62}$$

For orbital element estimation at time t' the partials of R(t) with respect to orbital elements are given by the matrix equation

$$\left[\frac{\partial R(t)}{\partial e^*(t')}\right]_{(6\times 1)} = G H \left[\frac{\partial R(t)}{\partial u_s^*(t)}\right]_{(3\times 1)} \tag{4.3.63}$$

where the matrix G is obtained from equations (4.3.60) and (4.3.61)

$$G = [G_{ij}] = \left[\frac{\partial e_j(t)}{\partial e_i(t')}\right] = \begin{cases} 1 & i = j \\ 0 & i \neq j \text{ except } i=1,\ j=4 \\ -\frac{3}{2}\frac{n}{a}(t-t') & i=1,\ j=4 \end{cases} \quad . \tag{4.3.64}$$

The last factor in equation (4.3.63) has row dimension three since the velocity partials of range are zero. The matrix H has the form

$$H = [H_{ij}] = \begin{bmatrix} \frac{\partial u_s(t)}{\partial a(t)} & \cdots & \frac{\partial w_s(t)}{\partial a(t)} \\ \vdots & & \vdots \\ \frac{\partial u_s(t)}{\partial \Omega(t)} & \cdots & \frac{\partial w_s(t)}{\partial \Omega(t)} \end{bmatrix} . \tag{4.3.65}$$

The development of the elements of H follows. The transformation from the mean inertial (I) system of epoch t_0 to the earth-fixed (EF) system at time t is given by

$$\begin{bmatrix} u_s(t) \\ v_s(t) \\ w_s(t) \end{bmatrix}_{EF} = R_2(-x_p)R_1(-y_p)R_3(GAST)NP \begin{bmatrix} X(t) \\ Y(t) \\ Z(t) \end{bmatrix}_I \tag{4.3.66}$$

$$= R \begin{bmatrix} X(t) \\ Y(t) \\ Z(t) \end{bmatrix}_I$$

where the coordinates in the mean inertial system are given by

$$\begin{bmatrix} X(t) \\ Y(t) \\ Z(t) \end{bmatrix} = R_3(-\Omega)R_1(-i)R_3(-\omega) \begin{bmatrix} x(t) \\ y(t) \\ z(t) \end{bmatrix} \tag{4.3.67}$$

and $\{x,y,z\}$ are the coordinates of the satellite in an in-plane coordinate system as defined in Mueller [1964]

$$\begin{aligned} x(t) &= a(\cos E - e) \\ y(t) &= a(1 - e^2)^{1/2} \sin E \\ z(t) &= o \ . \end{aligned} \tag{4.3.68}$$

The quantity E is the eccentric anomaly related to the mean anomaly by Kepler's equation

$$M = E - e \sin E \tag{4.3.69}$$

and x_p and y_p are the coordinates of the instantaneous rotation axis of

the earth [Mueller, 1969]. The rotation matrices P and N account for precession and nutation and GAST is the Greenwich apparent sidereal time. In terms of direction cosines equation (4.3.67) has the form

$$\begin{bmatrix} X(t) \\ Y(t) \\ Z(t) \end{bmatrix}_I = \begin{bmatrix} x\cos(xX) + y\cos(yX) \\ x\cos(xY) + y\cos(yY) \\ x\cos(xZ) + y\cos(yZ) \end{bmatrix}. \tag{4.3.70}$$

Equation (4.3.66) may be differentiated with respect to the orbital elements

$$\left[\frac{\partial u_s(t)}{\partial e(t)}\right]_{EF} = R\left[\frac{\partial X(t)}{\partial e(t)}\right]_I . \tag{4.3.71}$$

Using equation (4.3.70) and assuming a nearly circular orbit these partials derivatives are

$$\frac{\partial u_s(t)}{\partial a} = \frac{u_s(t)}{a} \tag{4.3.72}$$

$$\frac{\partial v_s(t)}{\partial a} = \frac{v_s(t)}{a} \tag{4.3.73}$$

$$\frac{\partial w_s(t)}{\partial a} = \frac{w_s(t)}{a} \tag{4.3.74}$$

$$\frac{\partial u_s(t)}{\partial e} = -a[R_{11}\cos(xX) + R_{12}\cos(xY) + R_{12}\cos(xZ)] \tag{4.3.75}$$
$$-\frac{ae\sin E}{\sqrt{1-e^2}}[R_{11}\cos(yX) + R_{12}\cos(yY) + R_{13}\cos(yZ)]$$

$$\frac{\partial v_s(t)}{\partial e} = -a[R_{21}\cos(xX) + R_{22}\cos(xY) + R_{23}\cos(xZ)] - \frac{a\,e\,\sin E}{\sqrt{1-e^2}}[R_{21}\cos(yX) + R_{22}\cos(yY) + R_{23}\cos(yZ)] \tag{4.3.76}$$

$$\frac{\partial w_s(t)}{\partial e} = -a[R_{31}\cos(xX) + R_{32}\cos(xY) + R_{33}\cos(xZ) - \frac{a\,e\,\sin E}{\sqrt{1-e^2}}[R_{31}\cos(yX) + R_{32}\cos(yY) + R_{33}\cos(yZ)] \tag{4.3.77}$$

$$\frac{\partial u_s(t)}{\partial M(t)} = -a\sin E[R_{11}\cos(xX) + R_{12}\cos(xY) + R_{13}\cos(xZ)] + a\sqrt{1-e^2}\cos E[R_{11}\cos(yX) + R_{12}\cos(yY) + R_{13}\cos(yZ)] \tag{4.3.78}$$

$$\frac{\partial v_s(t)}{\partial M(t)} = -a\sin E[R_{21}\cos(xX) + R_{22}\cos(xY) + R_{23}\cos(xZ) + a\sqrt{1-e^2}\cos E[R_{21}\cos(yX) + R_{22}\cos(yY) + R_{23}\cos(yZ)] \tag{4.3.79}$$

$$\frac{\partial w_s(t)}{\partial M(t)} = -a\sin E[R_{31}\cos(xX) + R_{32}\cos(xY) + R_{33}\cos(xZ)] + a\sqrt{1-e^2}\cos E[R_{31}\cos(yX) + R_{32}\cos(yY) + R_{33}\cos(yZ)] \tag{4.3.80}$$

$$\frac{\partial u_s(t)}{\partial i} = x[R_{11}\sin i\sin\omega\sin\Omega - R_{12}\sin i\sin\omega\cos\Omega + R_{13}\cos i\sin\omega] + y[R_{11}\sin i\cos\omega\sin\Omega - R_{12}\sin i\cos\omega\cos\Omega + R_{13}\cos i\cos\omega] \tag{4.3.81}$$

$$\frac{\partial v_s(t)}{\partial i} = x[R_{21}\sin i\sin\omega\sin\Omega - R_{22}\sin i\sin\omega\cos\Omega + R_{23}\cos i\sin\omega] + y[R_{21}\sin i\cos\omega\sin\Omega - R_{22}\sin i\cos\omega\cos\Omega + R_{23}\cos i\cos\omega] \tag{4.3.82}$$

$$\frac{\partial w_s(t)}{\partial i} = x[R_{31}\sin i \sin\omega\sin\Omega - R_{32}\sin i \sin\omega\cos\Omega + R_{33}\cos i \sin\omega]$$
$$+ y[R_{31}\sin i \cos\omega\sin\Omega - R_{32}\sin i \cos\omega\cos\Omega + R_{33}\cos i \cos\omega] \quad (4.3.83)$$

$$\frac{\partial u_s(t)}{\partial \omega} = x[R_{11}\cos(yX) + R_{12}\cos(yY) + R_{13}\cos(yZ)]$$
$$- y[R_{11}\cos(xX) + R_{12}\cos(xY) + R_{13}\cos(xZ)] \quad (4.3.84)$$

$$\frac{\partial v_s(t)}{\partial \omega} = x[R_{21}\cos(yX) + R_{22}\cos(yY) + R_{23}\cos(yZ)]$$
$$- y[R_{21}\cos(xX) + R_{22}\cos(xY) + R_{23}\cos(xZ)] \quad (4.3.85)$$

$$\frac{\partial w_s(t)}{\partial \omega} = x[R_{31}\cos(yX) + R_{32}\cos(yY) + R_{33}\cos(yZ)]$$
$$- y[R_{31}\cos(xX) + R_{32}\cos(xY) + R_{33}\cos(xZ)] \quad (4.3.86)$$

$$\frac{\partial u_s(t)}{\partial \Omega} = x[-R_{11}\cos(xY) + R_{12}\cos(xX)]$$
$$+ y[-R_{11}\cos(yY) + R_{12}\cos(yX)] \quad (4.3.87)$$

$$\frac{\partial v_s(t)}{\partial \Omega} = x[-R_{21}\cos(xY) + R_{22}\cos(xX)]$$
$$+ y[-R_{21}\cos(yY) + R_{22}\cos(yX)] \quad (4.3.88)$$

$$\frac{\partial w_s(t)}{\partial \Omega} = x[-R_{31}\cos(xY) + R_{32}\cos(xX)]$$
$$+ y[-R_{31}\cos(yY) + R_{32}\cos(yX)] \quad (4.3.89)$$

Partial derivatives for integrated Doppler measurements are obtained by differencing range observation partials formed at the end times of the Doppler integration interval.

The difference in positioning introduced through this approximation was determined from simulation results of absolute and relative positioning using range observations from two stations 100 kilometers apart. Results were obtained using two days of simulated observations with one hour of observation each time a satellite was acquired. Initial positioning adjustments were made in which orbital elements were included as parameters with a priori weights for each hour of tracking. Variational equations based on the WGS72 potential model [Seppelin, 1974] truncated to degree and order eight were numerically integrated and used in forming observational partial derivatives. Then the adjustments were repeated using the Keplerian two body partials. Except for this modification the adjustments were identical. A comparison of the covariance matrices obtained in each case was made. For absolute positioning the standard error of the station coordinates obtained using the Keplerian partial derivatives averaged 2.9 percent more optimistic. In the determination of coordinate differences the solutions using Keplerian partials had standard errors averaging 2.4 percent more optimistic.

As a result of this experiment it was decided that Keplerian two body partial derivatives could be adequately used in the adjustment of station coordinates when orbital elements were taken as parameters in the adjustment.

4.4 Development of Adjustment Weight Matrices

The minimum variance estimate of receiver earth-fixed coordinates obtained from range or Doppler observations by least squares adjustment requires that the weighting matrix be developed using the second order statistics of the random observation errors as outlined in [Liebelt, 1967]. In the application of Global Positioning System satellite observations of range and Doppler to geodetic positioning the adjustment weighting must include the observation error statistics for correlated atomic clock errors in both the satellite and receiver clocks and for noise from the tracking receiver. In this chapter the observation error statistics for atomic clock fractional frequency error are developed from the Allan variance for each system oscillator by an analytic procedure which transforms the Allan variance into the autocorrelation function for random frequency error. The integral of this function provides the statistics for range or range difference observations based on the two oscillators used to derive the measurement. Statistics of the residuals to selected polynomial clock models are obtained by an additional transformation of the range or Doppler error statistics. These residual statistics are incorporated with the instrumental white noise statistics into the adjustment weighting. The correlations between residuals to successive polynomial clock models are shown to be negligible allowing the adjustment to be performed sequentially.

4.4.1 Range and Doppler Observation Error Statistics

4.4.1.1 Fractional Frequency Autocorrelation from the Allan Variance

In section 4.1.1 the equations giving the second order statistics of random range and integrated Doppler observation errors due to random fractional frequency errors were presented. Those equations require that the fractional frequency autocorrelation function be known. In this section discussion of a procedure for obtaining an analytic approximation to this function from the Allan variance is given. This method avoids numerical difficulties that may arise when the inverse Fourier transform of the power spectral density is evaluated and yields simple analytic autocorrelation function.

The Allen variance models shown in Figure 4.1.3 for the satellite rubidium and receiver cesium oscillators are a function of the sampling time τ having the form

$$\sigma_y^2(\tau) = \begin{cases} \dfrac{N_o}{\tau} & \tau_\ell \leq \tau \leq \tau_1 \\ \sigma_f^2 & \tau_1 \leq \tau \leq \tau_2 \\ \dfrac{N_2\tau}{3} & \tau_2 \leq \tau \leq \tau_3 \\ \dfrac{N_3}{\tau} & \tau_3 \leq \tau \leq \infty \end{cases} \quad . \tag{4.4.1}$$

Using the transformations in Table 4.1.2 the power spectral density for fractional frequency may be developed from equation (4.4.1):

$$S_{yy}(\omega) = \begin{cases} N_3 & 0 \leq \omega \leq \omega_o \\ \dfrac{N_2}{\omega^2} & \omega_o \leq \omega \leq \omega_1 \\ \dfrac{N_1}{\omega} & \omega_1 \leq \omega \leq \omega_2 \\ N_o & \omega_2 \leq \omega \leq \omega_h \end{cases} . \qquad (4.4.2)$$

The square root of the power spectral density, or transfer function, corresponding to the Allan variance specifications of Figure 4.1.3 is given in Figure 4.4.1. The constants associated with the two functions and formulas for computing the constants associated with the power spectral density function based on the Allan variance are given in Table 4.4.1. These formulas are developed from the transformations of Table 4.1.2.

The autocorrelation function $\Phi_{yy}(t)$ can be obtained from the power spectral density using equation (4.1.21)

$$\Phi_{yy}(t) = \frac{1}{2\pi} \int_{-\infty}^{\infty} S_{yy}(\omega) e^{i\omega t} d\omega . \qquad (4.4.3)$$

With $S_{yy}(\omega)$ an even function equation (4.4.3) reduces

$$\begin{aligned} \Phi_{yy}(t) &= \frac{1}{2\pi} \int_{-\infty}^{\infty} S_{yy}(\omega) \cos \omega t \, d\omega \\ &= \frac{1}{\pi} \int_{o}^{\infty} S_{yy}(\omega) \cos \omega t \, d\omega . \end{aligned} \qquad (4.4.4)$$

Using the power spectral density model, equation (4.4.2), in

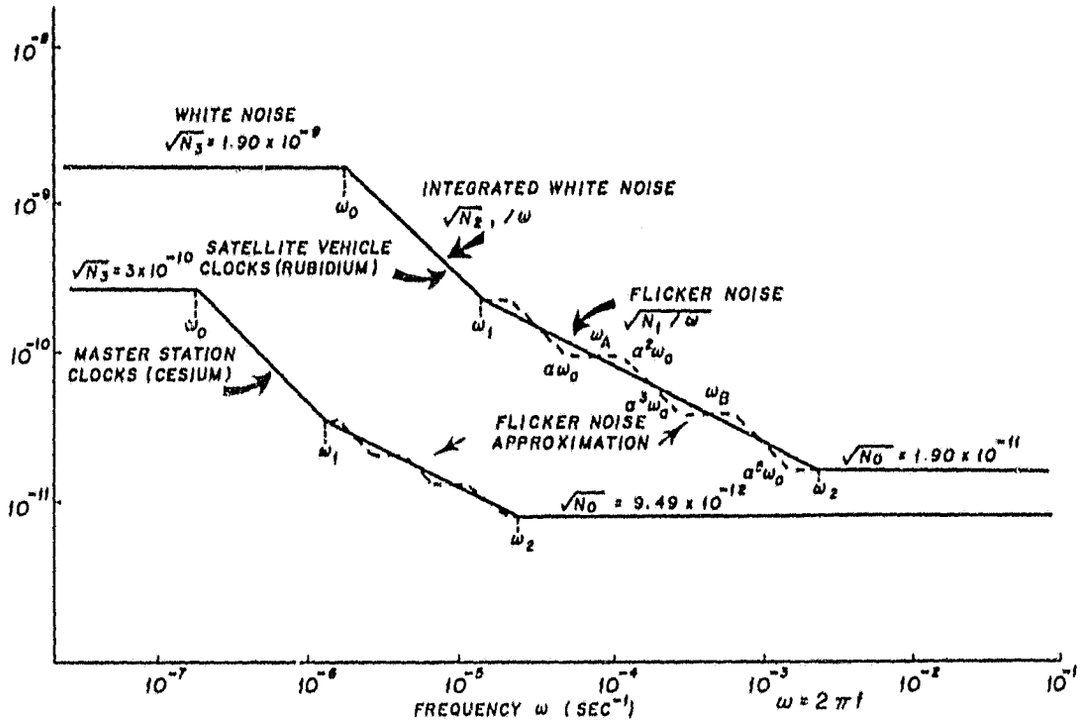

Figure 4.4.1. Oscillator Transfer Functions

TABLE 4.4.1. OSCILLATOR PARAMETERS

QUANTITY	UNITS	FORMULA	SATELLITE CLOCKS (RUBIDIUM)	STATION CLOCKS (CESIUM)
τ_1	sec		1.00×10^{3}	1.00×10^{5}
τ_2	sec		1.00×10^{5}	1.00×10^{6}
τ_3	sec		1.00×10^{6}	1.00×10^{7}
ω_0	sec^{-1}	$\sqrt{3}/\tau_3$	1.73×10^{-6}	1.73×10^{-7}
ω_1	sec^{-1}	$6\ln2/(\pi\tau_2)$	1.32×10^{-5}	1.32×10^{-6}
ω_2	sec^{-1}	$\pi/(2\tau_1\ln2)$	2.27×10^{-3}	2.27×10^{-5}
σ_1			6.00×10^{-13}	3.00×10^{-14}
N_0	sec	$\tau_1\sigma_1^2$	3.60×10^{-22}	9.00×10^{-23}
N_1		$\pi\sigma_1^2/2\ln2$	8.16×10^{-25}	2.04×10^{-27}
N_2	sec^{-1}	$3\sigma_1^2/\tau_2$	1.08×10^{-29}	2.70×10^{-33}
N_3	sec	$\sigma_1^2\tau_3^2/\tau_2$	3.60×10^{-18}	9.00×10^{-20}
a		$(\omega_2/\omega_1)^{1/6}$	2.36×10^{0}	1.61×10^{0}
ω_B	sec^{-1}	$\omega_1\sqrt{a}$	2.03×10^{-5}	1.67×10^{-6}

equation (4.4.4) gives the autocorrelation function for fractional frequency as

$$\Phi_{yy}(t) = \frac{1}{\pi}\int_{0}^{\omega_o} N_3\cos(\omega t)\,d\omega + \frac{1}{\pi}\int_{\omega_o}^{\omega_1} \frac{N_2\cos(\omega t)}{\omega^2}\,d\omega$$

$$+ \frac{1}{\pi}\int_{\omega_1}^{\omega_2} \frac{N_1\cos(\omega t)}{\omega}\,d\omega + \frac{1}{\pi}\int_{\omega_2}^{10^{-1}} N_o\cos(\omega t)\,d\omega$$

$$= \frac{N_3}{\pi}\frac{\sin(\omega_o t)}{t}$$

$$- \frac{N_2 t}{\pi}\left[\omega_1 t - \frac{(\omega_1 t)^3}{3\cdot 3!} + \frac{(\omega_1 t)^5}{5\cdot 5!} - \cdots\right.$$

$$+ \frac{N_2 t}{\pi}\left[\omega_o t - \frac{(\omega_o t)^3}{3\cdot 3!} + \frac{(\omega_o t)^5}{5\cdot 5!} - \cdots\right. \qquad (4.4.5)$$

$$- \frac{N_2\cos(\omega_1 t)}{\pi\omega_1} \quad \frac{N_2\cos(\omega_o t)}{\pi\omega_o}$$

$$+ \frac{N_1}{\pi}\left[\log(\omega_2 t) - \frac{(\omega_2 t)^2}{2\cdot 2!} + \frac{(\omega_2 t)^4}{4\cdot 4!} - \cdots\right.$$

$$- \frac{N_1}{\pi}\left[\log(\omega_1 t) - \frac{(\omega_1 t)^2}{2\cdot 2!} + \frac{(\omega_1 t)^4}{4\cdot 4!} - \cdots\right.$$

$$+ \frac{N_o\sin(10^{-1}t)}{\pi t} - \frac{N_o\sin(\omega_2 t)}{\pi t} \quad .$$

However this form for the autocorrelation function has an oscillatory behavior for small t as shown in Figure 4.4.2 as a result of transforming the band limited white noise portion of the spectrum. This is an artificiality of the model.

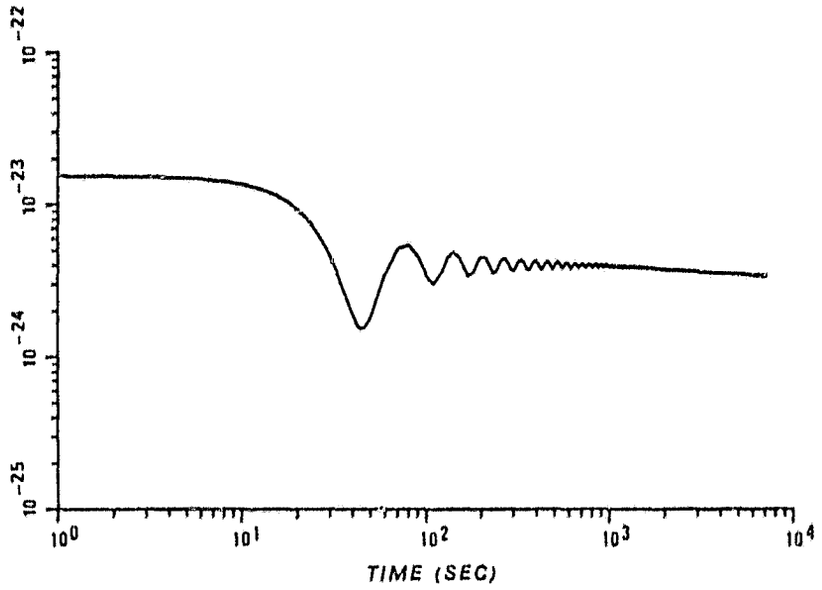

Figure 4.4.2. Satellite Rubidium Standard Fractional Frequency Autocorrelation from Inverse Fourier Transform

An alternate approach for obtaining an autocorrelation function is to approximate the power spectral density model with a smooth function whose autocorrelation is expressible in simple analytic form. The first step in this development is to approximate the flicker noise segment of the spectrum with a series of cascading functions whose value alternates between being constant and being inversely proportional to the square of the frequency. This type of procedure is described by Meditch [1975] in constructing a linear system which simulates flicker noise using a white noise input. Figure 4.4.3 shows the transfer function for flicker noise. A three stage cascading transfer function is superimposed consisting of the functions F_A, F_B, and F_C which are defined in Table 4.4.2. These functions are defined to have the

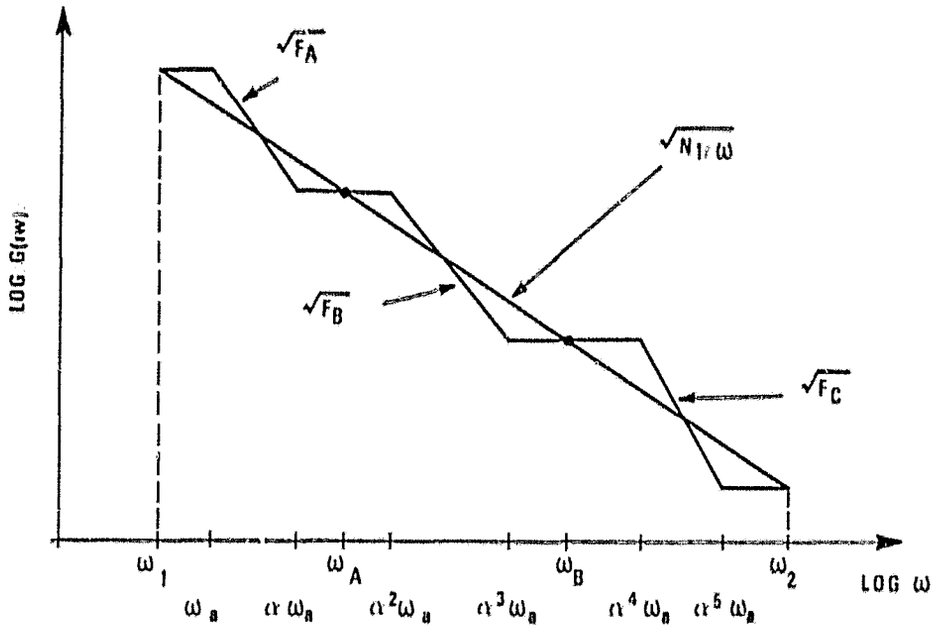

Figure 4.4.3. Three Stage Transfer Function Approximation of Flicker Noise Spectrum

TABLE 4.4.2. DEFINITION OF THREE STAGE TRANSFER FUNCTION APPROXIMATION

FUNCTION	INTERVAL	DEFINITION (PSD)
	$\omega_1 \leq \omega \leq \omega_a$	N_1/ω_1
F_A	$\omega_a \leq \omega \leq \alpha\omega_a$	N_A/ω^2
	$\alpha\omega_a \leq \omega \leq \omega_A$	$N_A/\alpha^2\omega_a^2$
	$\omega_A \leq \omega \leq \alpha^2\omega_a$	$N_A/\alpha^2\omega_a^2$
F_B	$\alpha^2\omega_a \leq \omega \leq \alpha^3\omega_a$	N_B/ω^2
	$\alpha^3\omega_a \leq \omega \leq \omega_B$	$N_B/\alpha^6\omega_a^2$
	$\omega_B \leq \omega \leq \alpha^4\omega_a$	$N_B/\alpha^6\omega_a^2$
F_C	$\alpha^4\omega \leq \omega \leq \alpha^5\omega_a$	N_C/ω^2
	$\alpha^5\omega \leq \omega \leq \omega_2$	N_o

WHERE

$N_A = \alpha\omega_1 N_1$ $\qquad$ $\alpha = \left(\frac{\omega_2}{\omega_1}\right)^{\frac{1}{2n}}$

$N_B = \alpha^3\omega_1 N_1$ $\qquad$ $\omega_a = \omega_1\sqrt{\alpha}$

$N_C = \alpha^5\omega_1 N_1$ $\qquad$ $n = 3$

required properties and give a continuous although not smooth approximation to the flicker noise power spectral density.

The constants of this approximation are now derived over frequency intervals as given in Meditch [1975]. The general form of the function F_A is

$$F_A(\omega) = \frac{N_A}{\omega^2} \tag{4.4.6}$$

between the frequencies ω_a and $\alpha\omega_a$. At frequency ω_a, defined in Table 4.4.1, the function F_A takes on the value

$$F_A(\omega_a) = \frac{N_A}{\omega_a^2} = \frac{N_1}{\omega_1} \tag{4.4.7}$$

since the flicker noise power spectral density has the same function value at frequency ω_1. Solving equation (4.4.7) gives

$$N_A = \frac{N_1\omega_a^2}{\omega_1} = \alpha\omega_1 N_1 \ . \tag{4.4.8}$$

A similar analysis gives the constant N_B. The function F_B has the form

$$F_B(\omega) = \frac{N_B}{\omega^2} \ . \tag{4.4.9}$$

At frequency $\alpha^2\omega_a$, F_B has the function value

$$F_B(\alpha^2\omega_a) = \frac{N_B}{\alpha^4\omega_a^2} = \frac{N_A}{\alpha^2\omega_a^2} \tag{4.4.10}$$

since at $\alpha^2\omega_a$ the function F_B has the same value as function F_A at frequency $\alpha\omega_a$ (see Figure 4.4.3). Solving equation (4.4.10) gives

$$N_B = \alpha^2 N_A = \alpha^3 \omega_1 N_1 \tag{4.4.11}$$

using equation (4.4.8). For the function F_C,

$$F_C(\omega) = \frac{N_C}{\omega^2} \tag{4.4.12}$$

its function value at frequency $\alpha^4\omega_a$ equals the value of F_B at frequency $\alpha^3\omega_a$ giving

$$F_C(\alpha^4\omega_a) = \frac{N_C}{\alpha^8\omega_a^2} = \frac{N_B}{\alpha^6\omega_a^2} \tag{4.4.13}$$

resulting in the solution

$$N_C = \alpha^2 N_B = \alpha^5 \omega_1 N_1 \tag{4.4.14}$$

using equation (4.4.11). Numerical values for α and ω_a are given in Table 4.4.1. The power spectral density consisting of the three cascading functions and the remainder of the original function will be denoted as the second power spectral density model for each oscillator.

The next step in the development of an analytic autocorrelation function is to approximate various segments of this second model with a first order Markov process power spectral density function, a function of the form

$$S(\omega) = \frac{2\sigma^2\beta}{\omega^2 + \beta^2} \qquad (4.4.15)$$

where β is the inverse of the correlation time (see [Gelb, 1974]). The autocorrelation function for a first order Markov process is

$$\Phi(t) = \sigma^2 e^{-\beta|t|} \qquad (4.4.16)$$

Graphs of these functions are given in Figure 4.4.4. Notice in equation (4.4.15) that the power spectral density decreases as the inverse of the square of the frequency which is the type of functional behavior seen in the interior of the cascading functions F_A through F_C. It is also the behavior of the original power spectral density in the interval $[\omega_0,\omega_1]$. In addition the power spectral density of the Markov process remains virtually flat until the frequency reaches a point when the function decreases rapidly. These properties make this function an excellent choice for approximating the second power spectral density model piecewise.

The second model is then divided into five segments defined in Table 4.4.3. The high frequency cut off ω_h, shown as 10^{-1} in Figure 4.4.1, will be increased so that that band limited white noise component of the power spectral density may be approximated better by the first order Markov power spectral density.

The approximation consists then of fitting a function in the form of equation (4.4.15) to each subdivision of the second model $S'_{yy}(\omega)$ given in Table 4.4.3. There are two parameters α and β to be determined for each segment giving a total of ten parameters.

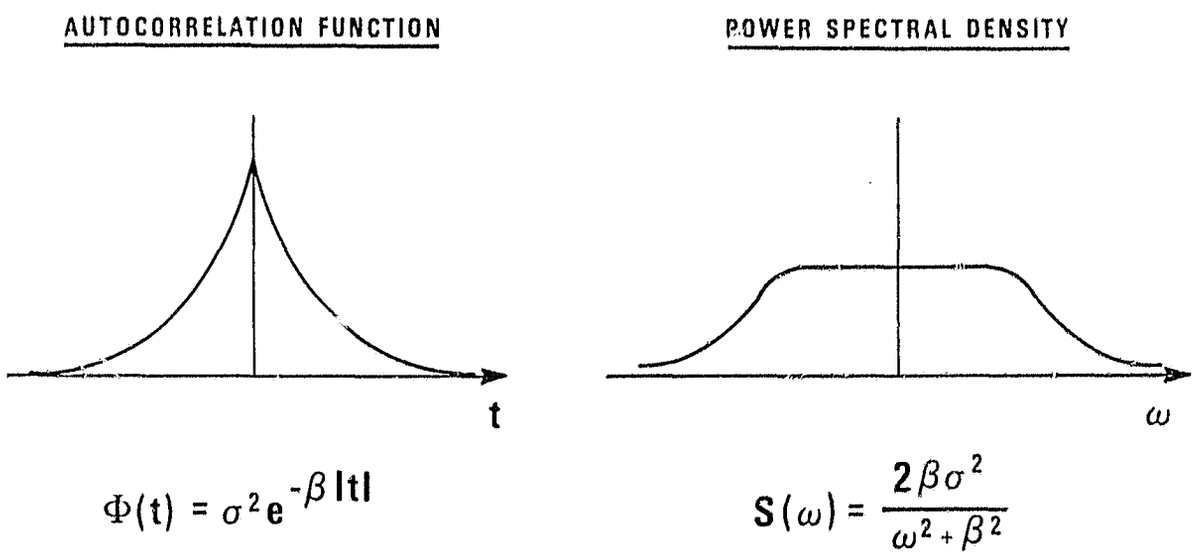

Figure 4.4.4. Markov Process (First Order)

Two procedures for this approximation were examined. The first was a least squares fit of the function $S(\omega)$ to each segment of $S'_{yy}(\omega)$. The second, which was adopted for use, was an assymptotic approximation whereby two constraints were imposed on the Markov power spectral density function giving α and β directly. The second procedure was implimented because of simplicity and because the results compared favorably with the least squares approach as seen by comparing Figures 4.4.6 and 4.4.7. The assymptotic approach develops an approximation on the interval I_j,

$$I_j \sim [\omega_k, \omega_\ell] \qquad (4.4.17)$$

using the following constraints:

(i) at zero frequency the approximating Markov power spectral density equals the second model at frequency ω_k:

$$S_j(o) = S'_{yy}(\omega_k) \tag{4.4.18}$$

(ii) in the limit as ω increases the value of the function $S_j(\omega)$ converges to the following function

$$\lim_{\omega \to \infty} S_j(\omega) = \frac{2\sigma^2\beta}{\omega^2} \tag{4.4.19}$$

and at ω_ℓ this limiting value is set equal to the value of $S'_{yy}(\omega)$:

$$\frac{2\sigma^2\beta}{\omega_\ell^2} = S'_{yy}(\omega_\ell) \ . \tag{4.4.20}$$

Equations (4.4.18) and (4.4.20) are a system of two equations in two unknowns. Their solution yields the parameters α_j and β_j for the approximating Markov power spectral density function $S_j(\omega)$. The nature of the second constraint, equation (4.4.20) is to force the function $S_j(\omega)$ to assymptotically approach $S'_{yy}(\omega)$ at ω_ℓ. The first constraint is necessary to approximate the white noise or flat component of $S'_{yy}(\omega)$ at the beginning of each subinterval.

Finally a comment concerning the approximation in the last subdivision I_5 is necessary. In order to obtain a good approximation to $S'_{yy}(\omega)$ in that interval it is necessary to choose ω_h large enough to allow the flat portion of the Markov process spectral density to fit the white noise component which dominates this interval as seen in

TABLE 4.4.3. DIVISION OF SECOND PSD MODEL FOR MARKOV PROCESS APPROXIMATION

NOTATION	INTERVAL
I_1	$[0, \omega_1]$
I_2	$[\omega_1, \alpha\omega_a]$
I_3	$[\alpha\omega_a, \alpha^3\omega_a]$
I_4	$[\alpha^3\omega_a, \alpha^5\omega_a]$
I_5	$[\alpha^5\omega_a, \omega_h]$

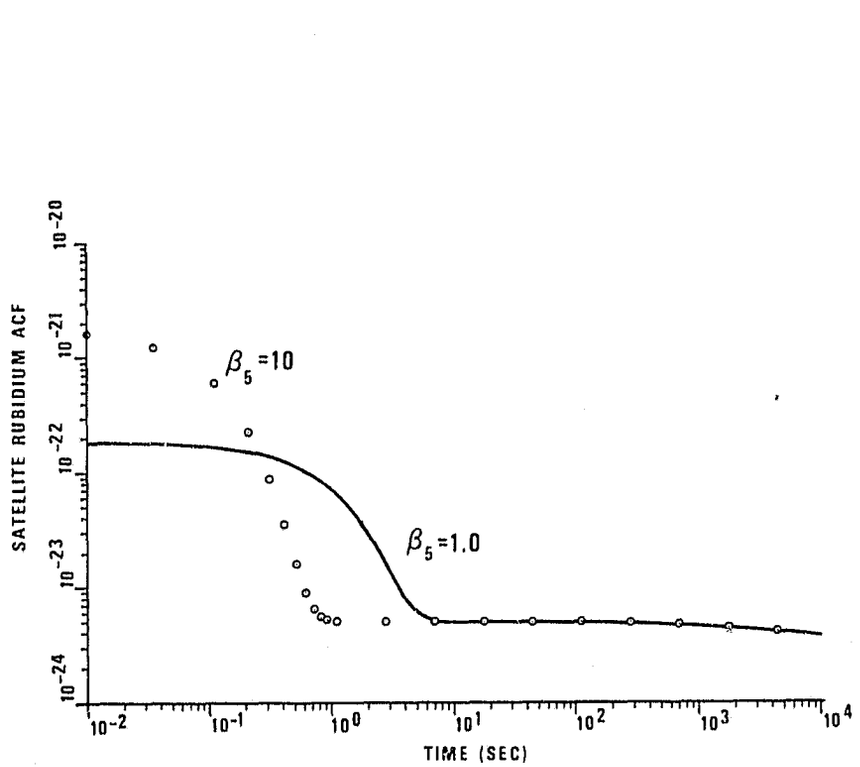

Figure 4.4.5. Assymptotic Fractional Frequency Autocorrelation Functions Based on Markov Process Approximations

Figure 4.4.1. Choosing ω_h three or four orders of magnitude larger than 0.1 and $S'_{yy}(\omega_h)$ two to three orders of magnitude smaller than N_0 enables a good approximation to be made but adds power at these higher frequencies. The result is an autocorrelation function whose variance will increase as ω_h is chosen larger (see Figure 4.4.5) and tends to a delta function as ω_h goes to infinity. However, this will have negligible effect on range and range difference statistics. This point will be examined in more detail after the development of additional equations based on the first order Markov approximations.

The smooth fractional frequency autocorrelation function $\Phi_{yy}(\tau)$ is given by the inverse Fourier transform of the five Markov process power spectral densities $S_j(\omega)$. The result of each transformation is an analytic function whose form is given by equation (4.4.16). The final result is the sum of these functions

$$\Phi_{yy}(\tau) = \sum_{j=1}^{5} \sigma_j^2 e^{-\beta_j|\tau|} \quad . \qquad (4.4.21)$$

For range and integrated Doppler observations the statistical contribution due to random oscillator error is obtained using equation (4.4.21) in equation (4.1.19) through (4.1.26). Figure 4.4.9 illustrates the steps discussed in the development of these statistics from the Allan variance model.

Figures 4.4.6 and 4.4.7 show the original transfer function for the satellite rubidium oscillator with the smooth least squares and assymptotic approximations. The least squares fit to each subinterval of the second model $S'_{yy}(\omega)$ was based on two hundred equally spaced

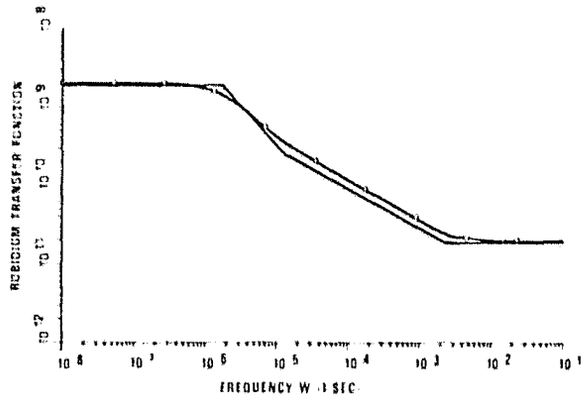

Figure 4.4.6. Satellite Oscillator Transfer Function and Sum of Least Squares Approximations

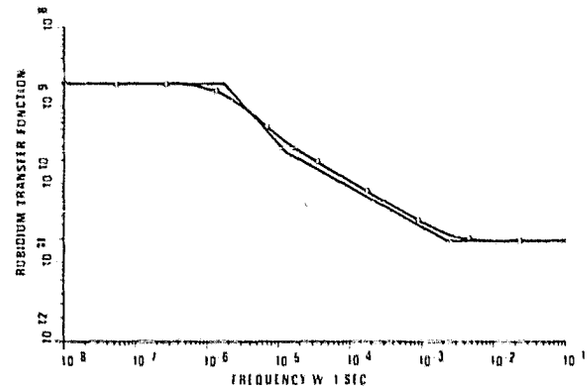

Figure 4.4.7. Satellite Oscillator Transfer Function and Sum of Assymptotic Approximations

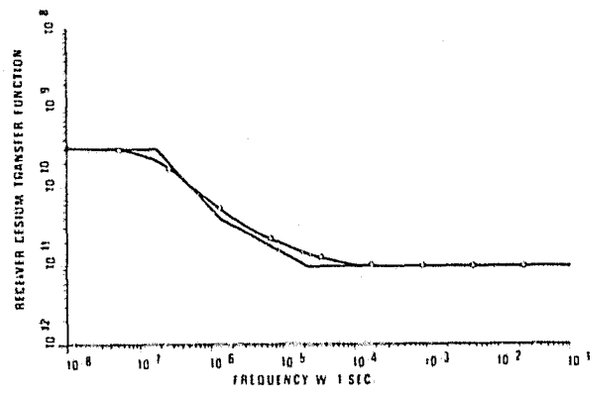

Figure 4.4.8. Receiver Cesium Transfer Function and Sum of Assymptotic Approximations

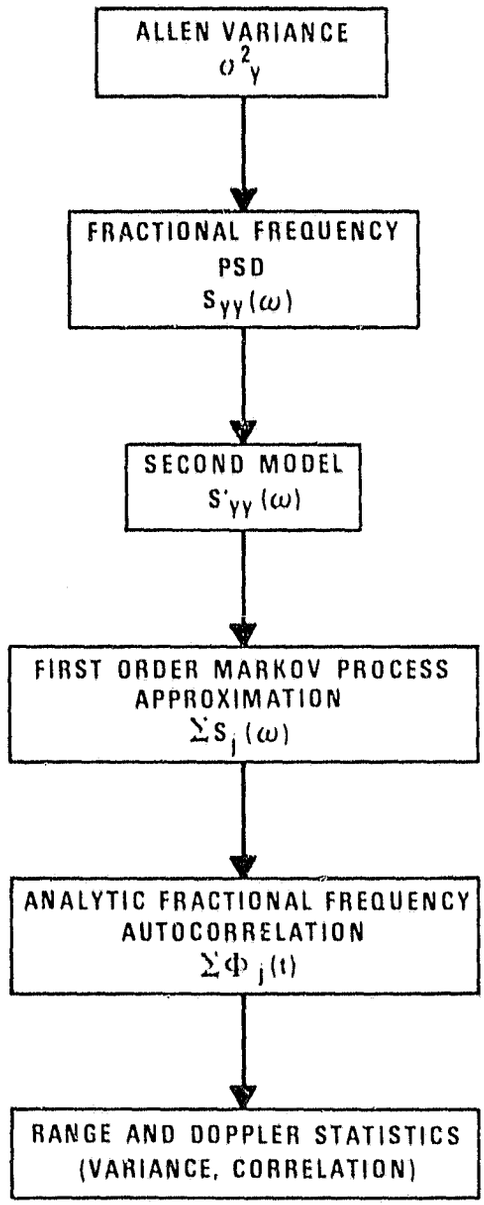

Figure 4.4.9. Development of Range and Doppler Statistics

TABLE 4.4.4. FRACTIONAL FREQUENCY AUTOCORRELATION FUNCTION PARAMETERS FOR MARKOV PROCESS APPROXIMATIONS

		ASSYMPTOTIC		LEAST SQUARES	
OSCILLATOR TYPE	INTERVAL	(ALPHA)^2	BETA	(ALPHA)^2	BETA
RUBIDIUM (SPEC)	I_1	3.1177×10^{24}	1.732×10^{6}	3.3719×10^{24}	1.661×10^{6}
	I_2	6.2625×10^{25}	2.032×10^{5}	7.6238×10^{25}	2.255×10^{5}
	I_3	6.2625×10^{25}	1.128×10^{4}	7.6245×10^{25}	1.252×10^{4}
	I_4	6.2625×10^{25}	6.262×10^{4}	7.6245×10^{25}	6.947×10^{4}
	I_6	1.8000×10^{19}	$1.000\times10^{3*}$	1.9343×10^{19}	$9.631\times10^{2*}$
CESIUM (SPEC)	I_1	7.7942×10^{27}	1.732×10^{7}		
	I_2	1.2922×10^{27}	1.677×10^{6}		
	I_3	1.2922×10^{27}	4.321×10^{5}		
	I_4	1.2922×10^{27}	1.113×10^{5}		
	I_6	4.5000×10^{20}	$1.000\times10^{3*}$		

*$\omega_h = 1.0\times10^{4}$ $\quad S'yy(\omega_h) = N_0/1.0\times10^{2}$

samples of the function within the subinterval. The parameters obtained using each approximation procedure are given in Table 4.4.4 for this rubidium oscillator. Since the assymptotic procedure produced results comparing favorably with the least squares procedure this method was adopted for use. Hence no least squares parameters appear in Table 4.4.4 for the cesium oscillator. The assymptotic transfer function for the cesium oscillator fractional frequency error and the original power spectral density are shown in Figure 4.4.8.

4.4.1.2 Observation Error Statistics Based on Markov Process Approximations

The first order Markov autocorrelation function, equation (4.4.21) and equations (4.1.19) through (4.1.26) give the second order

statistics for random range and integrated Doppler observation errors due to each oscillator used in the measurement process. These integrals may be evaluated giving analytical expressions for the variance and covariance of range and Doppler observations.

4.4.1.2.1 Range Observation Statistics. Let $R(t_i)$ and $R(t_k)$ be range observations subject to random clock error only. The covariance between the observations is given by equation (4.1.19). Using the first order Markov approximations, the integration of equation (4.1.19) gives the covariance as

$$E[R(t_i)R(t_k)] = E[\eta(t_i)\eta(t_k)]$$

$$= c^2 \sum_{j=1}^{5} \frac{\sigma_j^2}{\beta_j}\left[2(t_i - t_s) + \frac{1}{\beta_j}\left(e^{-\beta_j(t_j - t_s)}\right.\right. \quad (4.4.22)$$

$$\left.\left. + e^{-\beta_j(t_k - t_s)} - e^{-\beta_j(t_k - t_i)} - 1\right)\right]$$

for t_k greater than t_i where t_s is the start or reset time of the clock. The variance of the random range error is obtained by setting t_k equal to t_i in equation (4.4.22)

$$E[R(t_i)R(t_i)] = E[\eta(t_i)\eta(t_i)] \quad (4.4.23)$$

$$= c^2 \sum_{j=1}^{5} \frac{2\sigma_j^2}{\beta_j}\left[(t_i - t_s) + \frac{1}{\beta_j}\left(e^{-\beta_j(t_i - t_s)} - 1\right)\right]$$

The range error $\eta(t)$ resulting from the integration of fractional frequency error $y(t)$ is a statistically non-stationary process. An examination of equation (4.4.22) and (4.4.23) reveals terms in these expressions which are functions of t_i or t_k minus t_s. Thus the

variance, for instance, increases with time. This is illustrated in Figure 4.4.10 for the rubidium clock. The standard error of a range measurement based on the use of this clock is given for twenty range observations spaced at fifteen minute intervals starting five minutes, one hour, and five hours after the start of the clock. The increase in variance is almost linear. An examination of the autocorrelation function shows that this function, dominately flat, is similar to a random bias having a constant autocorrelation and whose integral is a random ramp which increases exactly linearly. Hence a linear growth in variance is expected as seen in Figure 4.4.10. The correlation coefficients ρ_{1i} between the first range observation and the i'th in each of these sequences are given in Figure 4.4.11. As the starting time of the sequence from t_s increases so does the correlation among the random errors which again is expected since the variance increases with time and the errors are correlated.

Figure 4.4.12 gives the autocorrelation function for the cesium clock based on the Markov process approximation and Figures 4.4.13 and 4.4.14 give the standard error and correlations of range errors based on this clock. A comparison of Figures 4.4.10 and 4.4.13 reveals the greater stability of the cesium clock. After ten hours of operation the standard error of the cesium clock output is approximately 3.5 nanoseconds compared to 63 nanoseconds for the rubidium standard. In addition the correlations among the cesium clock errors decreases more rapidly than the rubidium clock.

Considering both random clock error sources the total variance and correlation of range observations $R_k(t_i)$ and $R_k(t_j)$ measured by

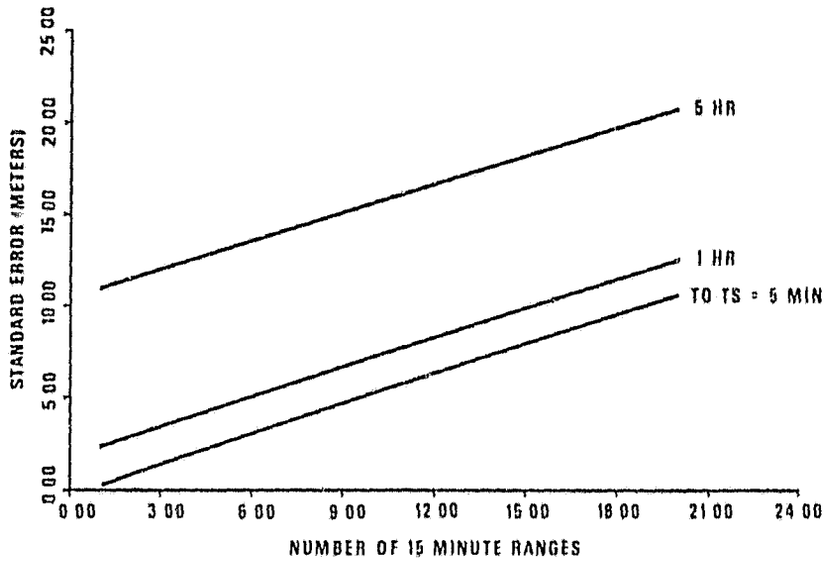

Figure 4.4.10. Standard Error of Range Observations Based on Satellite Rubidium Oscillator

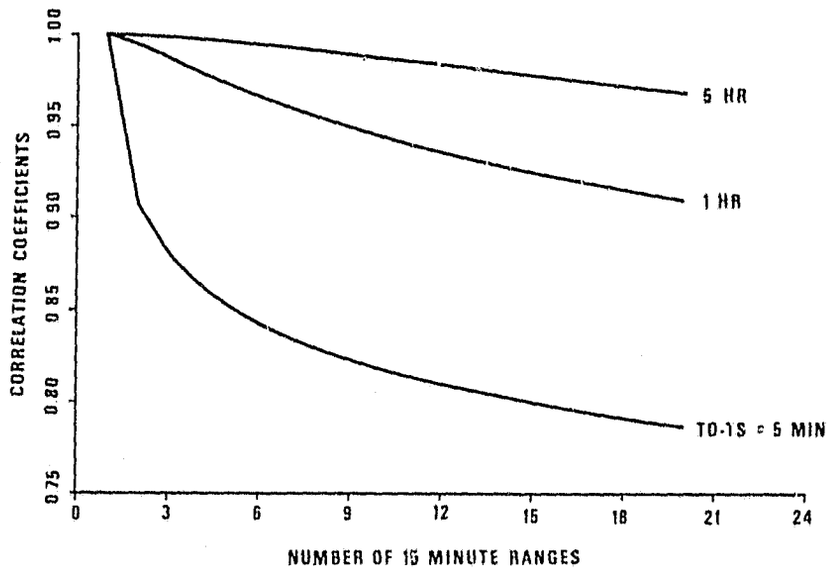

Figure 4.4.11. Correlation Coefficients between Range 1 and Range i (Rubidium Clock)

receiver k are given by the equations

$$E[R_k(t_i)R_k(t_i)] = E[\eta_s(t_i)\eta_s(t_i)] + E[\eta_k(t_i)\eta_k(t_i)] \qquad (4.4.24)$$

$$E[R_k(t_i)R_k(t_j)] = E[\eta_s(t_i)\eta_s(t_j)] + E[\eta_k(t_i)\eta_k(t_j)] \qquad (4.4.25)$$

where the variances and correlations of the random error η are given by equations (4.4.22) and (4.4.23). The subscript "s" refers to the satellite rubidium clock.

For simultaneous observations of range by two receivers the covariance of the observations $R_k(t_i)$ and $R_\ell(t_j)$ is given by

$$E[R_k(t_i)R_\ell(t_j)] = E[\eta_s(t_i)\eta_s(t_j)] \; . \qquad (4.4.26)$$

In the above equations the random errors η have zero-mean which is a consequence of fractional frequency error being zero mean.

4.4.1.2.2 Integrated Doppler Observation Statistics. Let $\Delta R(t_n)$ be an integrated Doppler or range difference measurement over the interval $[t_i, t_n]$ and $\Delta R(t_\ell)$ a similar measurement from the same receiver over the interval $[t_k, t_\ell]$. The covariance of the observations is

$$\begin{aligned} E[\Delta R(t_n), \Delta R(t_\ell)] &= E[\eta(t_n) - \eta(t_i), \eta(t_\ell) - \eta(t_k)] \\ &= E[\eta(t_n)\,\eta(t_\ell)] - E[\eta(t_n)\,\eta(t_k)] - E[\eta(t_i)\,\eta(t_\ell)] \\ &\quad + E[\eta(t_i)\,\eta(t_k)] \\ &= c^2 \sum_{j=1}^{5} \frac{\sigma_j^2}{\beta_j^2} \Big[e^{-\beta_j(t_\ell - t_n)} - e^{-\beta_j(t_k - t_n)} \\ &\qquad - e^{-\beta_j(t_\ell - t_i)} + e^{-\beta_j(t_k - t_i)} \Big] \; . \end{aligned} \qquad (4.4.27)$$

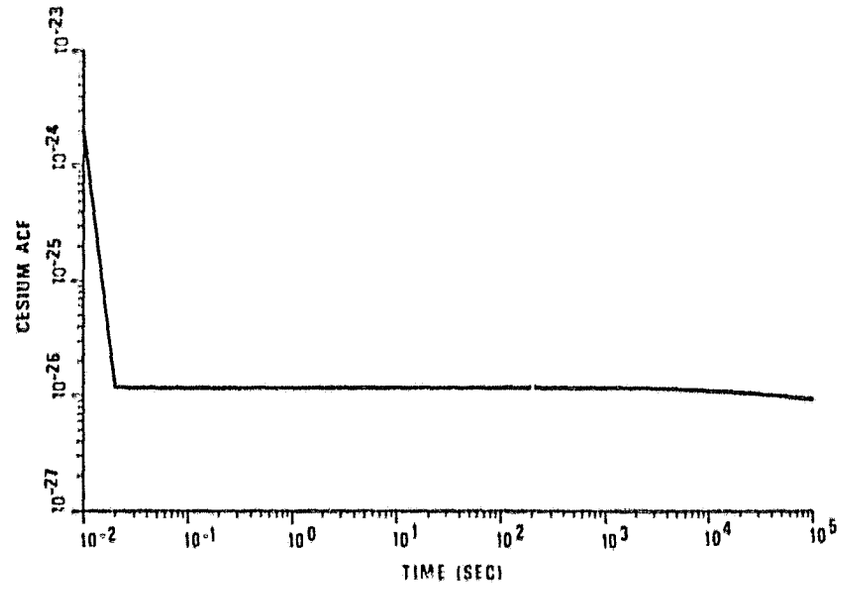

Figure 4.4.12. Assymptotic Fractional Frequency Autocorrelation Function for Cesium Standard

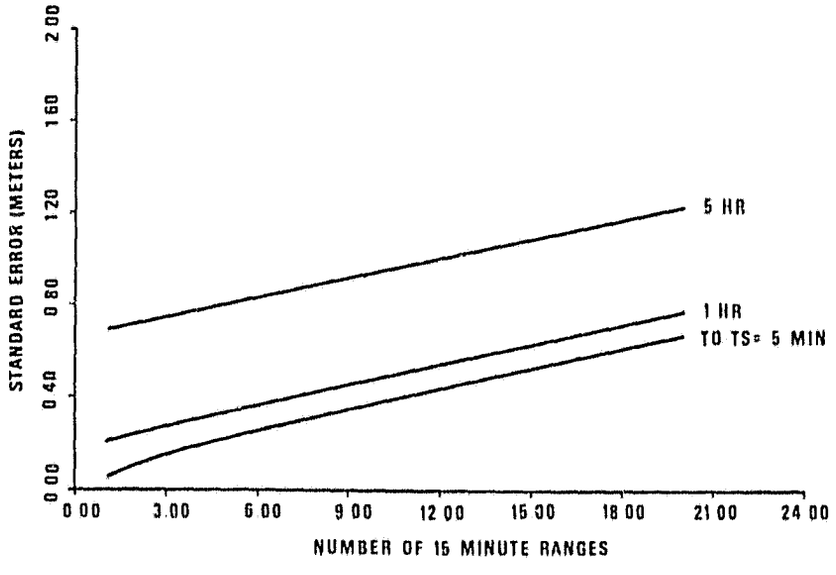

Figure 4.4.13. Standard Error of Range Observations Based on Cesium Oscillator

The variance of a range difference observation is given by

$$E[\Delta R(t_n)\Delta R(t_n)] = c^2 \sum_{j=1}^{5} \frac{2\sigma_j^2}{\beta_j}\left[(t_n - t_1) + \frac{1}{\beta_j}\left(e^{-\beta_j(t_n - t_1)} - 1\right)\right] . \quad (4.4.28)$$

Equations (4.4.27) and (4.4.28) are independent of the clock epoch t_0. The statistics of the range difference error depend only on the Doppler integration interval or the time difference between observations. Thus the random range difference error is stationary. Expressions analogous to equations (4.4.24) through (4.4.26) express the complete statistics of range difference observation errors for individual or simultaneous observations due to clock error.

4.4.2 Statistics of Residuals to Polynomial Clock Models

The statistical characteristics of fractional frequency error and its integrated effect on range and Doppler observations have been discussed in detail. For range observations the total random error is due to three sources, two of which are correlated noise processes. The total random range error is expressible as

$$\eta(t) = \eta_s(t) + \eta_k(t) + \xi(t) \quad (4.4.29)$$

where η_s and η_k are the correlated random range errors due to satellite and receiver random clock errors respectively. The quantity ξ represents receiver white noise as discussed in Section 4.1.4. The total integrated Doppler random error over the integration interval $[t_j, t_\ell]$ is

$$\Delta\eta(t_\ell) = \eta_s(t_\ell) - \eta_s(t_j) + \eta_k(t_\ell) - \eta_k(t_j) + \zeta_\ell \quad (4.4.30)$$

where ζ_ℓ is the white noise associated with the Doppler measurement procedure.

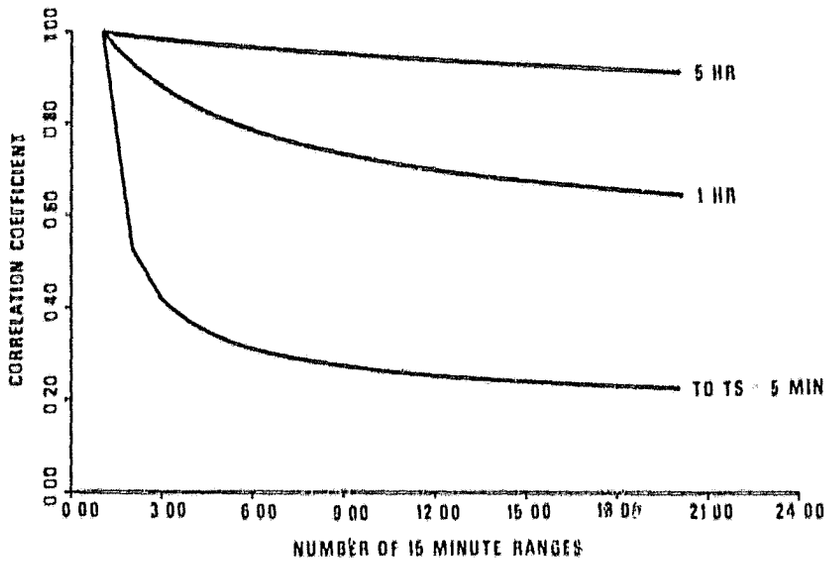

Figure 4.4.14. Correlation Coefficients between Range 1 and Range i (Cesium Clock)

Depending on the stability of the clock the random range or Doppler error components, $\eta_s(t)$ and $\eta_k(t)$, may appear quite systematic over fixed time intervals and may be represented by polynomial models of varying degree. For short time spans the models for the clocks considered in this analysis were taken to be a bias and drift for range observations or a frequency bias for Doppler observations. However these models and even higher order polynomial models are not sufficient to entirely represent this correlated error. Thus knowledge of the statistical properties of the deviations of the error from such a model becomes important since these residuals represent an unmodeled part of the observation equation after the inclusion of the polynomial model.

Proceeding, equation (4.4.29) is expressed as follows

$$\eta(t) = P_{ms}(t) + P_{nk}(t) + r_s(t) + r_k(t) + \xi(t) \qquad (4.4.31)$$

where $P_{ms}(t)$ is an m'th degree polynomial chosen to model the correlated random error $\eta_s(t)$ and $P_{nk}(t)$ is an n'th degree polynomial modeling the random process $\eta_k(t)$. The statistics of the residuals r(t) may be developed from the covariance of the random clock errors developed in Section 4.4.1 using the procedure derived in Appendix A which develops the mathematics for polynomial approximation to random walk segments. Using equation (A.1.9) the second order statistics of the range residuals r(t) to a polynomial model are obtained as

$$E[r(t)r^T(t)] = GE[R(t)R^T(t)]G^T \qquad (4.4.32)$$

where

$$G = [I - A(A^TA)^{-1}A^T] \qquad (4.4.33)$$

and A is the design matrix for the polynomial model selected. The $E[R(t)R^T(t)]$ is the covariance matrix of the random clock error being modeled. This covariance is given by equations (4.4.22) and (4.4.23).

For integrated Doppler observations the statistics of the residuals to a given degree polynomial model are similarly obtained from equations (4.4.32) and (4.4.33) with the use of the covariance matrix for integrated Doppler random error due to each system clock, equations (4.4.27) and (4.4.28). The equation may be written as

$$E[\Delta r(t)\Delta r^T(t)] = HE[\Delta R(t)\Delta R^T(t)]H^T \qquad (4.4.34)$$

where the matrix H is similar to the matrix G of equation (4.4.33)

with changes due to the choice of the model adopted for clock induced random Doppler errors

$$H = [I - A'(A'^{T}A')^{-1}A'^{T}] \quad . \tag{4.4.35}$$

Equation (4.4.30) has the form

$$\Delta\eta(t_\ell) = P_{is}(t_\ell) + P_{jk}(t_\ell) + \Delta r_s(t_\ell) + \Delta r_k(t_\ell) + \zeta_\ell \tag{4.4.36}$$

after the selection of the polynomial models.

If the statistics of these residuals were ignored in dynamic point positioning adjustments the resulting coordinate covariance matrix would be optimistic. An increase in the degrees of the polynomial clock models would offset this optimism to some extent since the level of unmodeled error would be decreased. However if a rigorous adjustment is to be performed then these residual statistics must be included in the least squares adjustment weight matrix to account for the unmodeled error r(t) or Δr(t) in a statistical rather than parametric fashion. The adjustment should then produce a valid coordinate covariance matrix regardless of the order of the polynomial models used provided numerical problems are not encountered and the parameters are independent and well observed.

The question of adequacy of a particular polynomial for a given data span needs to be addressed.

4.4.2.1 Comments on the Choice of Polynomial Error Models

To determine what degree polynomial model would be best to represent random clock error various factors have to be considered.

First among these are the length of the data span being modeled and the number of additional parameters which need to be introduced into the geodetic positioning adjustment. Use of a higher order polynomial will reduce the variance of the clock model residuals but may tend to numerically weaken the adjustment normal equations.

To determine how well a given order polynomial model represents correlated clock error over a fixed time interval a series of first and second order polynomial fits were made using simulated random clock error. The algorithm of Meditch [1975] was used to generate sequences of clock error which were then converted to range error. The polynomial fits were equal weighted least squares approximations to the range errors. A sampling rate of one minute was used. From the residuals of fit r(t) autocorrelation functions were numerically obtained for each approximation using

$$\Phi_j(\tau) = \frac{1}{n} \sum_{i=1}^{n} r(t_i) r(t_i + \tau) \qquad (4.4.37)$$

where n depends on τ and the total number of samples. The variance of the residuals from each case were averaged to determine an overall variance for the residuals of fit for both the linear and quadratic polynomials. For the rubidium clock three time intervals were considered with a linear polynomial fit. The root mean square errors are given in Table 4.4.5. For the cesium clock the results indicate that the longer the interval the better the second order polynomial performs, as expected. Howeve this increase in goodness of fit is less significant as the length of the interval decreases.

TABLE 4.4.5. RANGE RESIDUAL STANDARD ERRORS BASED ON POLYNOMIAL FITS TO SIMULATED CLOCK ERROR

CLOCK TYPE	POLYNOMIAL MODEL	NO. CASES	RMS ERROR OF FIT (cm)			
			4 hr	8 hr	16 hr	24 hr
CESIUM	LINEAR	10	8.7	11.8	18.7	25.6
	QUADRATIC	10	7.0	9.3	15.1	17.4
			2 hr		4 hr	8 hr
RUBIDIUM	LINEAR	30	18.1		36.5	66.3

It is obvious that a tradeoff exists between the level of model error remaining and the number of model parameter required. For instance two linear models over 16 hours leaves an 11.8-centimeter sample standard error for the residuals, while a single quadratic fit over the same interval leaves 15.1 centimeters of expected error. An increase in one parameter produces a 22-percent decrease in the expected error. For the rubidium clock the expected level of residual error is higher due to the poorer short term stability of this clock (see Figure 4.1.3) and is comparable only to the cesium if the fit interval is about one-eighth the length. Figures 4.4.15 and 4.4.16 give examples of the residuals of fit for each clock for a linear fit over 8 hours. In Table 4.4.5 the length of the rubidium clock cases was limited to 8 hours since one clock model for each satellite pass was anticipated for the positioning studies to be conducted.

Finally, the theoretical standard errors for range residuals to a linear fit were determined using equation (4.4.32) for these clocks

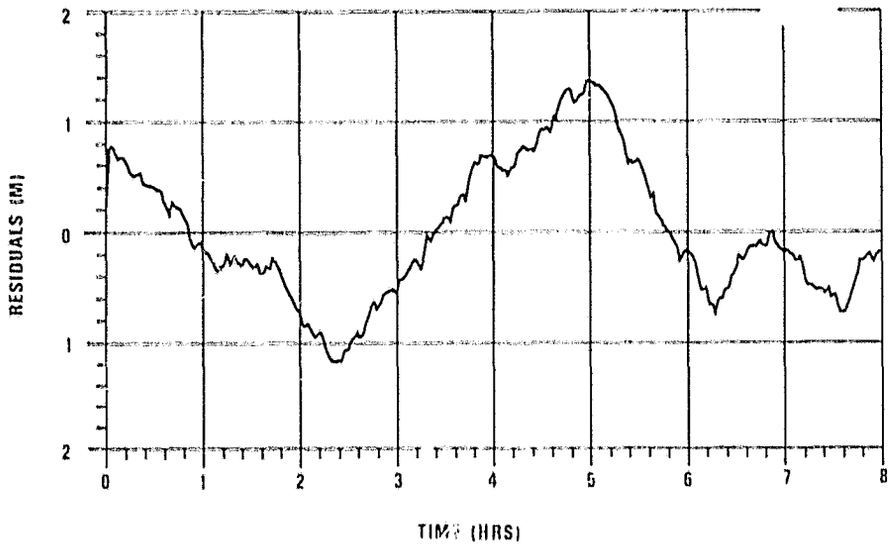

Figure 4.4.15. Residuals from a Linear Fit to Rubidium Clock Error

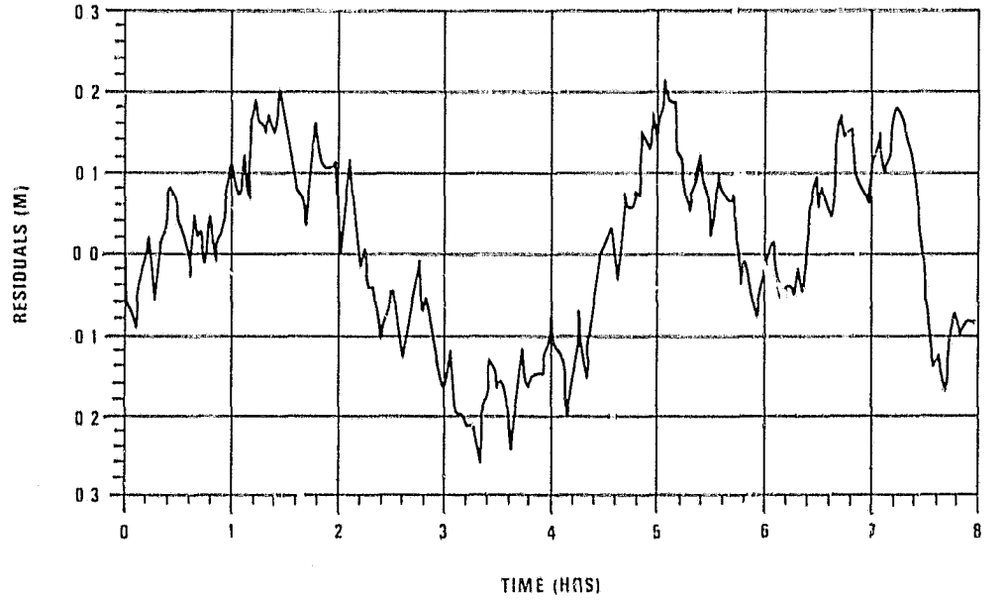

Figure 4.4.16. Residuals from a Linear Fit to Cesium Clock Error

for the same intervals with the exception of the 4-hour case for the cesium clock. The results are given in Figures 4.4.17 and 4.4.18. These figures support the conclusions drawn above, and in addition, graphically demonstrate that the statistics of the residuals to the clock modeling polynomial are not stationary. The variance of a residual depends on the order of the polynomial, the interval length and the location within the sample. The correlation coefficient matrix, contoured in Figure 4.4.19 for an 8-hour linear fit for the cesium clock, does not have the constant diagonals except for equally spaced samples of a stationary statistical process. However, by Theorem A.1 of Appendix A, the statistics of the residuals will be constant from interval to interval of the same length provided the sampling is performed equivalently and the same order polynomial is used.

4.4.2.2 Correlation Between Sets of Residuals

An examination of equations (4.4.22), (4.4.23), (4.4.27) and (4.4.28) shows that the random errors due to oscillator instability are correlated over all time. That this is the case is a consequence of the error being a random walk or the difference in elements of a random walk where the underlying process is fractional frequency error. Since correlation between range or Doppler observations is due entirely to clock error, it becomes interesting to examine the correlation between the residuals of two successive polynomial fits to random clock error. If the cross correlations are relatively small, the assumption that successive observation sets can be taken as statistically independent is justified when polynomial clock models are adopted.

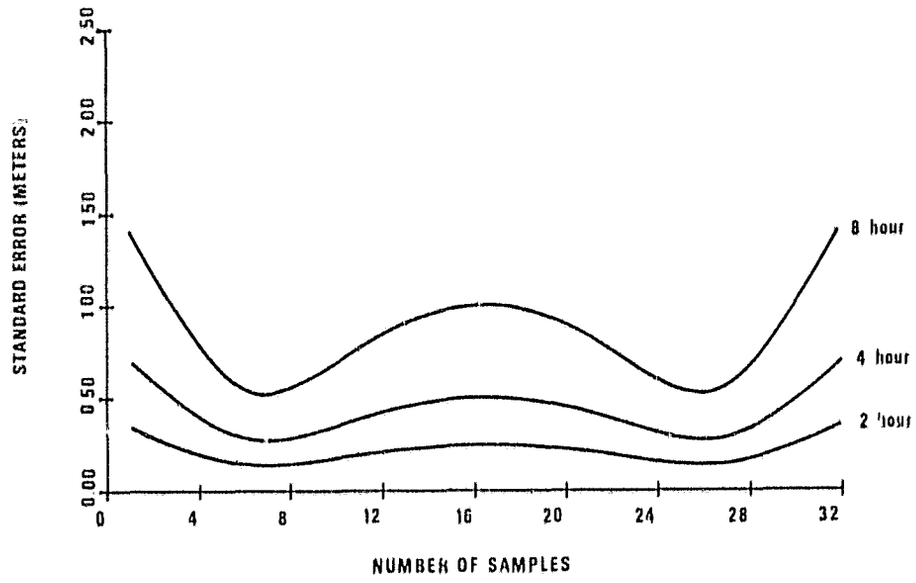

Figure 4.4.17. Standard Error of Satellite Rubidium Clock Residuals Based on a Linear Fit

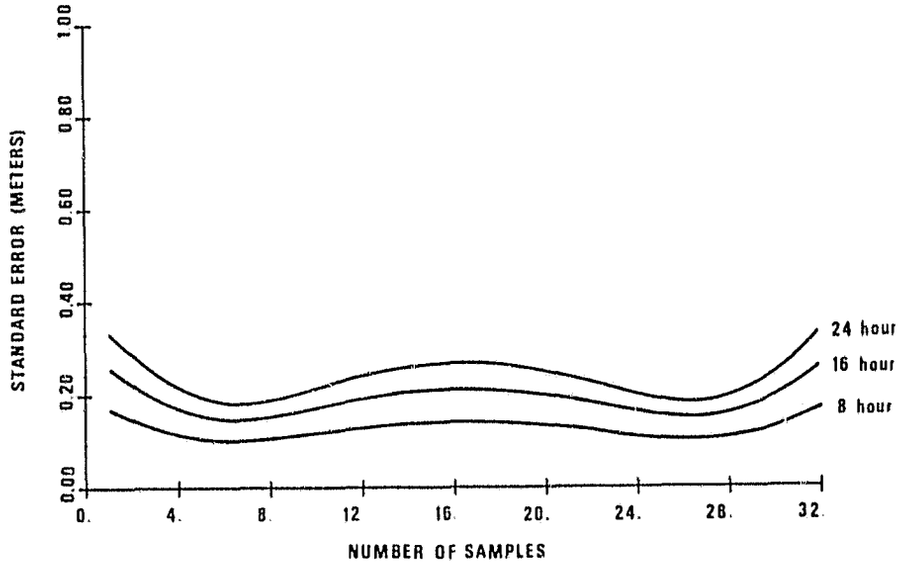

Figure 4.4.18. Standard Error of Cesium Clock Residuals Based on a Linear Fit

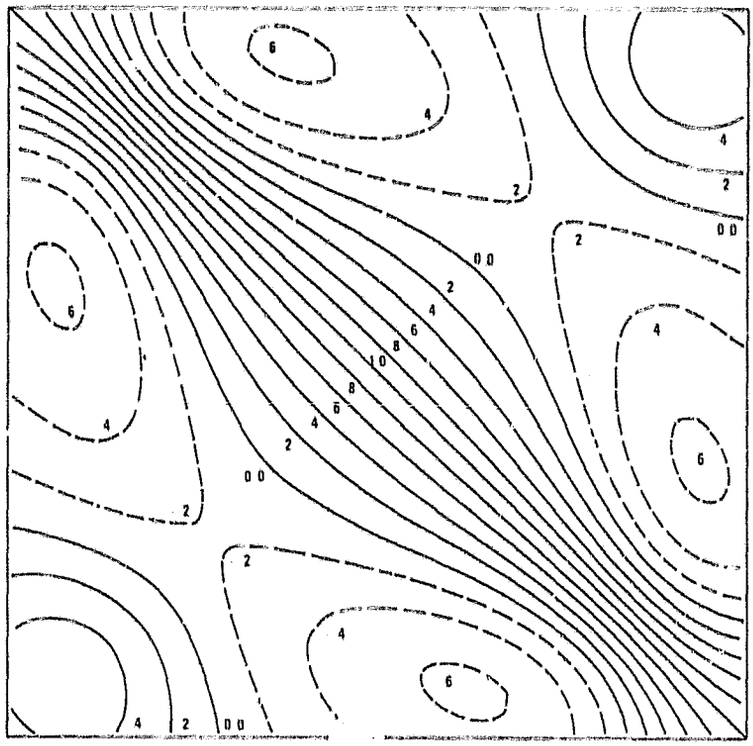

Figure 4.4.19. Contoured Correlation Coefficient Matrix for Residuals from an Eight Hour Linear Fit to Cesium Clock Error

This assumption would then permit sets of correlated observations to be introduced into a geodetic positioning adjustment as independent blocks in a sequential least squares approach. Computationally this implies that the dimension of the observation covariance matrix to be inverted to form the least squares weight matrix is reasonable.

To test that assumption the residual covariance matrix was computed using equation (A.2.5) of Appendix A for two linear fits to successive clock error segments for both the cesium and rubidium clocks:

$$\begin{bmatrix} E[\bar{r}_1\bar{r}_1^T] & E[\bar{r}_1\bar{r}_2^T] \\ E[\bar{r}_2\bar{r}_1^T] & E[\bar{r}_2\bar{r}_2^T] \end{bmatrix} = G \begin{bmatrix} E[\bar{R}_1\bar{R}_1^T] & E[\bar{R}_1\bar{R}_2^T] \\ E[\bar{R}_2\bar{R}_1^T] & E[\bar{R}_2\bar{R}_2^T] \end{bmatrix} G^T \qquad (4.4.38)$$

where

$$G = [I - A(A^TA)^{-1}A^T] \qquad (4.4.39)$$

and

$$A = \begin{bmatrix} A_1 & 0 \\ 0 & A_2 \end{bmatrix} . \qquad (4.4.40)$$

The correlation coefficient matrix for the residuals was computed and the coefficients from the off-diagonal block, $E[\bar{r}_1\bar{r}_2^T]$ were compared to the correlation coefficients from the diagonal blocks, $E[\bar{r}_1\bar{r}_1^T]$ and $E[\bar{r}_2\bar{r}_2^T]$. The results indicated in all cases that the correlation coefficients between residuals from two different fits were at least two orders of magnitude smaller than the correlation coefficients for residuals from the same polynomial fit. These results support the

assumption that successive blocks could be treated as independent although each block itself would be internally correlated.

4.4.3 Weight Matrix

The introduction of polynomial clock models tends to statistically decouple the residuals from successive polynomial fits; thus, GPS range and Doppler observation sets, which are correlated in time by random clock error, may be treated as independent when polynomials are adopted to model these random components. Each set is itself fully correlated and the statistics of the residuals to the adopted polynomial models must be included in forming the least squares adjustment weight matrix as shown in Figure 4.4.20. The size of each correlated data set will depend on the time interval over which the models are applied which, along with the degree of polynomial, determines the variance of the remaining residuals. Since the receiver cesium clock has better stability than the satellite rubidium clock the time interval over which a single receiver polynomial clock model is adopted may span multiple intervals of satellite tracking data each with its own clock model. This will of course depend not only on clock stability, but also on the geometric strength of the observations taken. Figure 4.4.21 illustrates this concept in which observations within block K are assumed statistically independent of observations within block L, each of which includes range observations from four satellites taken in this case simultaneously from two stations.

The weight matrix, taken as the inverse of the covariance matrix of random observation errors, is assumed to be block diagonal wherein

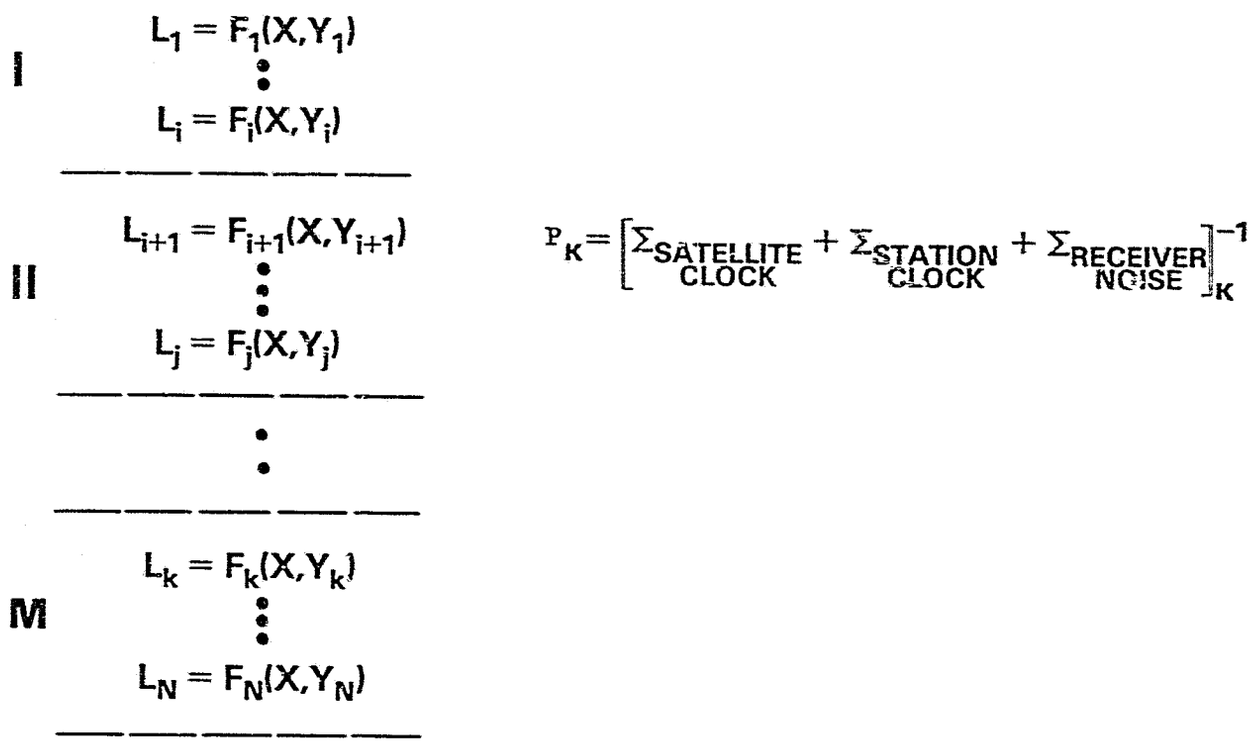

Figure 4.4.20. Division of Observation Set for Sequential Adjustment

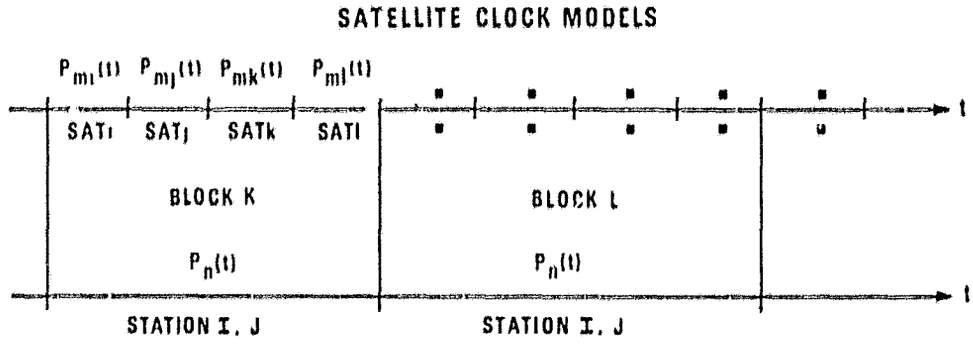

Figure 4.4.21. Clock Modeling Procedure (Simultaneous Observation)

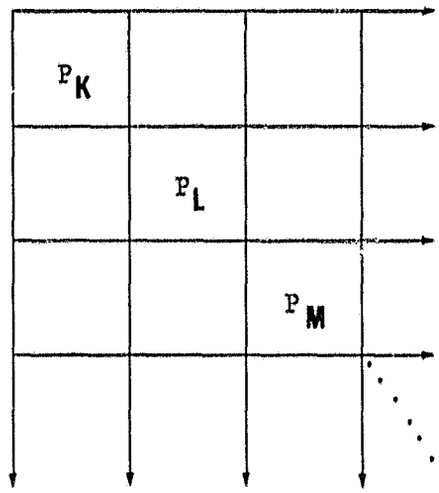

Figure 4.4.22. Assumed Block Diagonal Form for Weight Matrix

each block contains the second order statistics of the residuals to the selected polynomial clock models and of the white noise due to the receiver. The weight matrix corresponding to the observation schedule of Figure 4.4.21 is shown in Figure 4.4.24. Each diagonal block is the inverse of the sum of three covariance matrices. For relative positioning using range observations from two stations observing simultaneous the form of the diagonal block is given by equation (4.4.41) where the covariance matrices $E[rr^T]$ are based on equation (4.4.32). The form of the matrix is identical for Doppler observations using the covariance $E[\Delta r \Delta r^T]$ given in equation (4.4.34).

4.5 Results of Dynamic Positioning Studies

The simulated range and integrated Doppler observations developed in Section 4.2.1 according to equations (4.2.8) through (4.2.10) were used in the sequential least squares adjustment algorithm developed in Section 4.3.1 to obtain minimum variance estimates of geodetic station coordinates and baseline components using a dynamic positioning approach. Observations from three separate station groupings were considered in this analysis. The geodetic coordinates of these stations are found in Table 4.2.1. The GPS orbital elements adopted in this study are given in Table 3.2.1 referred to the mean equator and equinox of 1950.0.

Solutions were obtained for the geodetic coordinates of individual tracking stations then for baseline components and chord lengths from simultaneous observations from pairs of stations. Solutions were developed using either range or integrated Doppler observations separately. No solutions based on both observation types were considered

$$P_K^{-1} = \begin{bmatrix} \ddots & & & & & & & \\ & E[\bar{r}_i \bar{r}_i^T] & & & & & & \\ & & \ddots & & & & & \\ & & & E[\bar{r}_j \bar{r}_j^T] & & & & \\ & & & & \ddots & & & \\ & & & & & E[\bar{r}_k \bar{r}_k^T] & & \\ & & & & & & \ddots & \\ & & & & & & & E[\bar{r}_l \bar{r}_l^T] \end{bmatrix} + \begin{bmatrix} E[\bar{r}_i \bar{r}_i^T] & \\ & E[\bar{r}_j \bar{r}_j^T] \end{bmatrix} + \begin{bmatrix} \sigma^2 I & \\ & \sigma^2 I \end{bmatrix}$$

EQUATION (4.4.41)

although this possibility may be available with two frequency Doppler receivers having a two frequency ranging capability. For each positioning problem the effects of the random and systematic error sources of Section 4.1 were addressed and the adjustment weighting procedure developed in Section 4.4.3 was utilized as a function of the random error sources considered and the error models chosen to represent atomic clock error.

Integrated Doppler observations were assumed to be independent sixty-second measurements aggregated every five minutes, not correlated range differences, as in Chapter 3. This latter type of treatment would add additional strength to the least squares normal equations enhancing the Doppler results presented below. The type of correlations considered in this analysis however are those due to the correlated random atomic clock error present in both the receiver and satellite clocks.

Range observations were considered subject to time errors and the normal equations included timing parameters in accordance with the tracking scenario under consideration. The inclusion of such parameters weakens the normal equations as considered in Chapter 3. However in actual applications these parameters are necessary since tracking receiver clocks will be subject to timing offsets and drifts with respect to an adopted time system such as GPS system time.

The solutions presented were based on two basic tracking procedures each with the adaptation of similar modeling for atomic clock errors. The first data acquisition procedure consisted of tracking satellites over three hour intervals and performing the least squares

adjustment for station coordinates every nine hours. In this case a linear model was used to approximate the error in each separate clock. Thus the satellite rubidium clocks were modeled by a linear function of time over three hour intervals and the tracking station's cesium clock error was modeled by the same type of function over the nine hour interval. Solutions were performed sequentially approximately every nine hours with some variation if a tracked satellite's period of observability is less than three hours. Observations were utilized only if the topocentric elevation angle of the satellite exceeded ten degrees. The second tracking scenario reduces the satellite tracking interval to one hour with a sequential adjustment of parameters occurring after four hours of observation. A similar clock modeling procedure was adopted but over the shorter intervals. This latter tracking procedure allows a more rapid sampling of the satellite pass geometries and a better approximation of the random clock error; however, this procedure introduces a larger number of parameters of solution over a fixed period of site occupation.

In all cases considered parameters representing the satellite orbital elements were introduced into the adjustment with a priori weighting consistent with the amplitude of the ephemeris error introduced, as described in Section 4.1.2. Orbital elements were introduced for each satellite tracking interval and corrections to these elements at the midpoint of the interval were estimated as described in Section 4.3.2. The inclusion of these parameters in the adjustment is consistent with the approach of Brown [1976] although the modeling procedure for ephemeris error is different.

As a final introductory comment it must be noted that the transformations between the mean Celestial System of 1950.0 and the earth-fixed coordinate system are assumed known. This implies that no errors in precession, nutation, earth rotation, or polar motion are introduced into the results. The consequence of errors in these variables is of great importance in geodesy but are not addressed in this study. Therefore in the following it is assumed that an error free transformation into the earth-fixed coordinate system exists.

4.5.1 Dynamic Point Positioning

4.5.1.1 Range Solutions Based on Three-Hour Tracking Intervals

A limited set of simulations based on two frequency compensated range observations were made using observations from Stations 1001 and 1002 with each selected satellite of the GPS constellation tracked for three hours. A sequential adjustment of the earth-fixed Cartesian station coordinates was performed every nine hours over a five day period. The complete parameter set included a linear clock model for each satellite rubidium clock for every three-hour interval of tracking, a linear model for the receiver cesium clock for every nine-hour interval, ephemeris parameter corrections for every three hours of tracking, and the earth-fixed Cartesian coordinates of the station. In addition a tropospheric scaling parameter, as described in Section 4.1.3, was included for every three hours of observation when tropospheric refraction errors were introduced into the observations.

To evaluate the effects of random and systematic error sources on station positioning, simulations were made in which individual error sources were introduced into the range observations and only a limited number of parameters were adjusted. First, the effect of random cesium clock error on station positioning was examined. Simulated random cesium clock errors were developed for the cesium clock specifications given in Figure 4.1.3 using the algorithm of Meditch [1975]. This random cesium clock error was added to the geometric ranges to GPS satellite positions according to equation (4.2.8). The satellites were selected using the criterion of minimizing the trace of the station covariance matrix as described in Section 4.2.2. To these ranges an optimistic ten centimeters of Gaussian white noise was introduced. The adjustment parameters included the Cartesian coordinates of the station and a first degree polynomial in time to represent the cesium clock error every nine hours. The adjustment weighting was based solely on the white noise statistics and the station coordinates were in error initially by 100 meters in latitude. Figure 4.5.1 gives the error in estimated position of station 1001 as a function of time with a sequential adjustment in station position performed every nine hours. With a random white noise level of ten centimeters the range observations would predict standard errors of 0.17, 0.21, and 0.15 centimeters for the u, v, and w components of station position in this example. According to Figure 4.4.18 adopting a linear model to .epresent random cesium clock error over nine-hour intervals would leave an unmodeled random residual error with approximately a 12 to 16 centimeters standard error. The thirteen sets of this random residual error introduced the

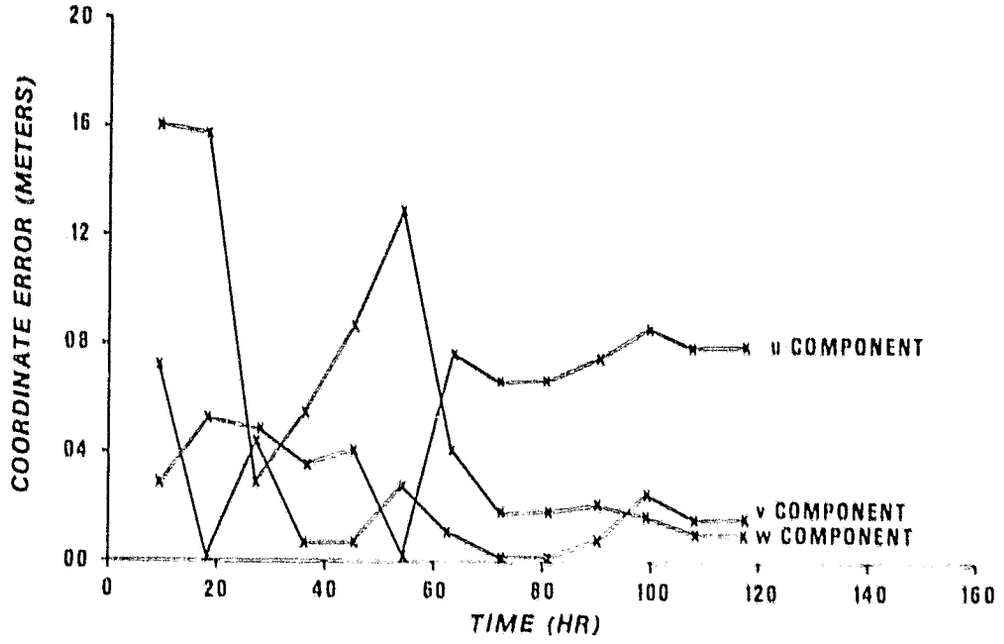

Figure 4.5.1. Effect of Random Cesium Clock Error on Positioning Using Range Observations (Station 1001)

station position errors in Figure 4.5.1. The residual random clock errors represented by the difference between the random clock error and the best fitting linear model are correlated as shown in Figure 4.4.19. The errors introduced into station positioning by these random clock errors, modeled as a linear function, will not average as those introduced by Gaussian white noise of a similar magnitude as evidenced by the station position errors shown in Figure 4.5.1. A comparison of these errors with the standard errors expected by 10 centimeter Gaussian white observation noise, given above, indicates the level of error expected from unmodeled cesium clock noise. Errors of similar magnitude although different in their distribution were present in the results from station 1002. The magnitude of this error plays a more critical role for the determination of baseline components and is discussed in Section 4.5.2.

The effect of atomic clock error on station positioning also includes the effect of unmodeled random satellite rubidium clock error. For the dynamic positioning approach under examination in this analysis it is assumed that estimates of each satellite's clock error are provided with the ephemerides. For the current study this implies that these estimates will take the form of the best linear fit and will provide an estimate of the systematic rubidium clock error over the interval of satellite tracking utilized in geodetic positioning. In the current examples that represents a three-hour interval of time. Assuming for the moment that over this interval the bias and drift of the satellite clock are known, then the question raised is what effect will the unmodeled random residual satellite clock error produce in station positioning? To obtain an estimate of this error station positioning simulations were made introducing this residual rubidium clock error into the same geometric ranges used in the previous examples. This random residual error was computed by differencing simulated random rubidium clock noise with the best linear least squares fit to the noise over the tracking interval. The residuals from such a fit have an average standard error of approximately 30 centimeters as seen from Figure 4.4.17. The rubidium clock noise simulated was consistent with the rubidium oscillator Allan variance given in Figure 4.1.3. Ten centimeter Gaussian white noise was also introduced into the observations representing an unrealistiely optimistic level of random receiver noise. The adjustment parameters included the station's earth-fixed Cartesian coordinates. Figure 4.5.2 gives the position errors for station 1001 as a function of time. The error represents the magnitude

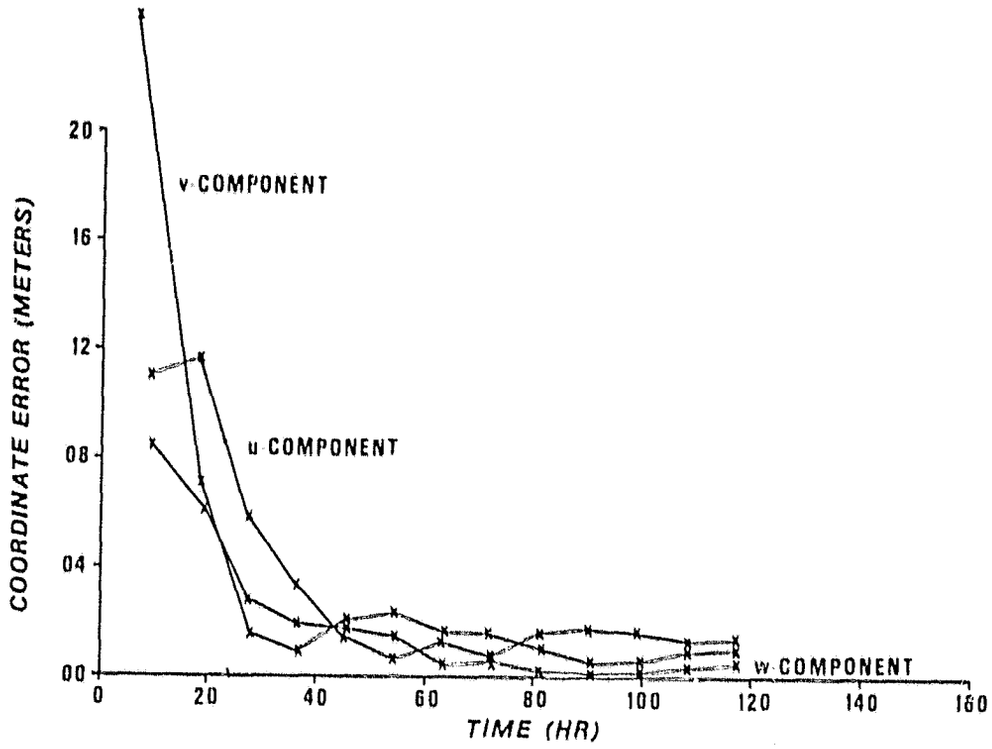

Figure 4.5.2. Effect of Residual Random Rubidium Clock Error on Positioning Using Range Observations (Station 1001)

of the difference between actual and estimated station coordinates after each nine hour update. The observations were weighted using only the white noise statistics. Based on a ten centimeter standard error of observation the full set of range observations would predict an uncertainty in station position of 0.11, 0.12, and 0.09 centimeters for the u, v, and w coordinates. The final errors in the station coordinates were 1.3, 0.8, and 0.6 centimeters after 117 hours of observation. Again, scaling the predicted standard errors by 3.0, the error introduced into station coordinates by the sequences of correlated residual rubidium clock error averages although not as rapidly as errors introduced by white observation noise of an equivalent variance. In this example the residual rubidium clock error even though of higher

variance than the residual cesium clock noise produces a smaller positioning error. The rate at which the errors in station positioning average will depend on the variance and correlation of the residual noise process, the number of noise segments introduced, and the correlations among station position coordinates and the clock modeling parameters introduced into the adjustment. However, as in the previous example, the effect of unmodeled residual rubidium clock error on the determination of station coordinates is negligible.

To further refine the estimate of station position error introduced by atomic clock error sources, an adjustment of station coordinates and linear clock error models was made in which random cesium clock error, residual rubidium clock error and ten centimeters of Gaussian white receiver noise were introduced into the geometric ranges. Adjustment weighting was based on the statistical modeling developed in Section 4.4 including the fully correlated weighting due to unmodeled atomic clock errors. The results of this adjustment are given in Figure 4.5.3(a) through 4.5.3(c) for each Cartesian coordinate of station 1001. The atomic clock errors introduced into the range observations were simulated as previously described for the cesium and rubidium clocks under consideration. Remembering the results of the previous two examples where the resulting standard errors of station positioning based only on Gaussian white noise were extremely small, it can be seen that the standard error in station position components due to correlated atomic clock error sources ranges from 8 to 11 centimeters after one day of observation and from 4 to 5 centimeters after

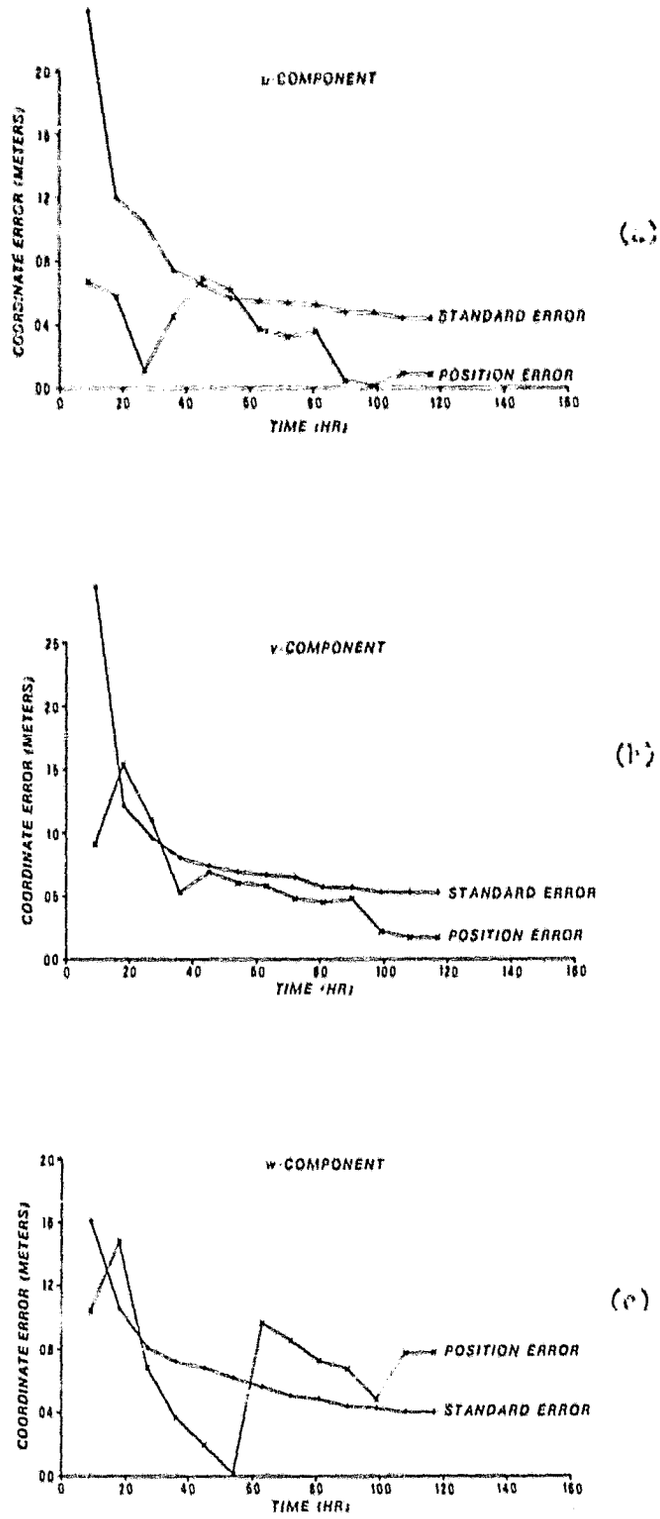

Figure 4.5.3. Effect of Atomic Clock Error Sources on Positioning Derived from Range Observations (Station 1001)

five days. The magnitude of this error will be of importance in the determination of baseline components discussed in Section 4.5.2.

To obtain an estimate of the effect of the ephemeris error described in Section 4.1.2 orbit error was introduced into station positioning simulations using equation (4.2.10). The nominal level of ephemeris error utilized throughout this study is given in Table 4.2.2 and the assumptions regarding its distribution are discussed in Section 4.2.1. Adjustment results for the Cartesian coordinates of Station 1001 are given in Figure 4.5.4 where the absolute value of the coordinate errors are given. Parameters in the adjustment included only station coordinates, ephemeris error modeling being momentarily ignored. Ten centimeters of Gaussian white noise were again applied to the observations and formed the basis for the adjustment weighting. The results indicate that the level of orbit error addressed in this analysis may introduce errors into station position of greater than one meter in each component even after five days of continuous observation. Modeling of the ephemeris error tends to reduce this error. These results are similar to those obtained for Station 1002. The errors introduced into positioning by each error source are dominated by the effect of errors in the satellite ephemerides. This error will be the limiting factor in the overall accuracy to which geodetic station positions may be obtained using GPS ranging.

To define an upper bound on the effect of unmodeled tropospheric refraction error on station positioning a five percent error was assumed in the predicted tropospheric refraction correction based on the

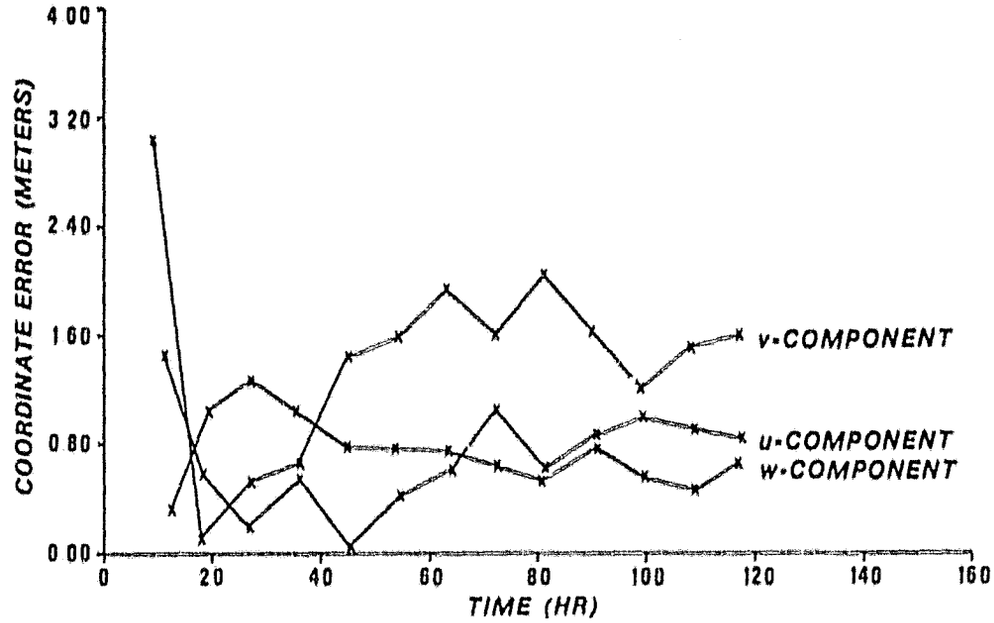

Figure 4.5.4. Effect of Uncompensated Systematic Orbit Error on Positioning Using Range Observations (Station 1001)

Hopfield model discussed in Section 4.1.3. This error was taken with a constant sign. Observations below ten degrees elevation angle were excluded. The results of a positioning simulation for Station 1001 are given in Figure 4.5.5 where the adjustment included only the Cartesian coordinates of the station. Ten centimeter Gaussian white noise was included as before. Refraction scaling parameters discussed in Section 4.1.3 were not included in the adjustment. The results demonstrate that a constant percentage model error in tropospheric refraction of five percent can introduce errors in station position varying between 8 and 12 centimeters. If the actual modeling error had taken the form of a constant percentage for each observation but with a random sign variation for each tracking interval, the error in station positioning would be considerably less since the sign of the station position errors from each interval of tracking would have variations resulting in better

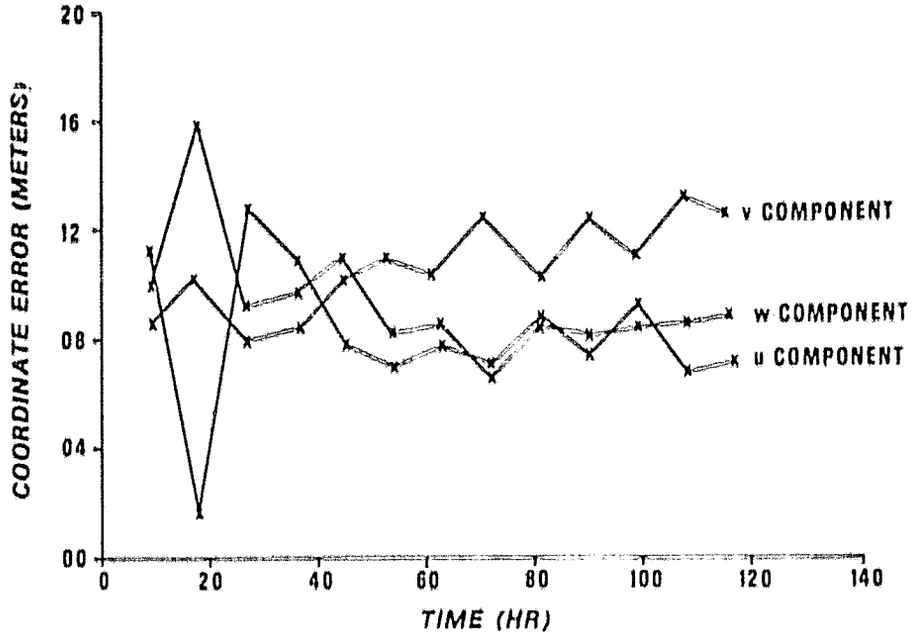

Figure 4.5.5. Effect of Uncompensated Systematic Error in Tropospheric Refraction (5%) on Positioning Using Range Observations (Station 1001)

averaging. Subtracting the mean of each component of station position error from the results in Figure 4.5.5 gives an estimate of 4 to 6 centimeters of variation at 1 day and 1-2 at 5 days which could be expected in such a case. Again the magnitude of this error, even considering a worst case as in this example, is small in comparison to the effect of ephemeris error.

Finally, the effect of a realistic level of receiver white noise is assessed in Figure 4.5.6 in which the standard error of the Cartesian station coordinates are given as a function of time. After twenty-four hours of continuous observation the standard error of the solution for each coordinate is approximately 2 centimeters and reduces exponentially to approximately 1 centimeter after five days of observation. A comparison of Figures 4.5.6 and 4.5.3 reveals that, in the absence of

systematic errors such as satellite position and tropospheric refraction, improvement in the receiver range measurement noise will not improve the quality of station positioning since the effect of random atomic clock error will dominate.

Table 4.5.1 summarizes the approximate levels of error introduced into station positioning from the error sources discussed above when the satellite tracking interval is three hours.

For Stations 1001 and 1002 complete simulations of dynamic point positioning were made using range observations from three hour tracking intervals. The error sources introduced into the observations consisted of ephemeris error, satellite rubidium clock error, receiver cesium clock error, tropospheric refraction error, and one meter of Gaussian receiver white noise in accordance with Table 4.2.2. Various independent sequences of random atomic clock error were utilized in the analysis of station positioning for both stations. Figure 4.5.7 gives the standard errors and actual position errors for Station 1001 for one case. The parameters of the adjustment consisted of the full set described above weighted according to the level of error introduced into the observations. This set included station coordinates, ephemeris parameters for each three hour interval, a linear error model for the receiver clock over every nine-hour interval, a linear error model for each satellite clock for every three-hour tracking interval, and a tropospheric refraction scaling parameter every three hours. The least squares adjustment algorithm incorporated the fully correlated adjustment weighting based on random atomic clock error and the Gaussian white receiver noise. Initially the station's position was in error by 100

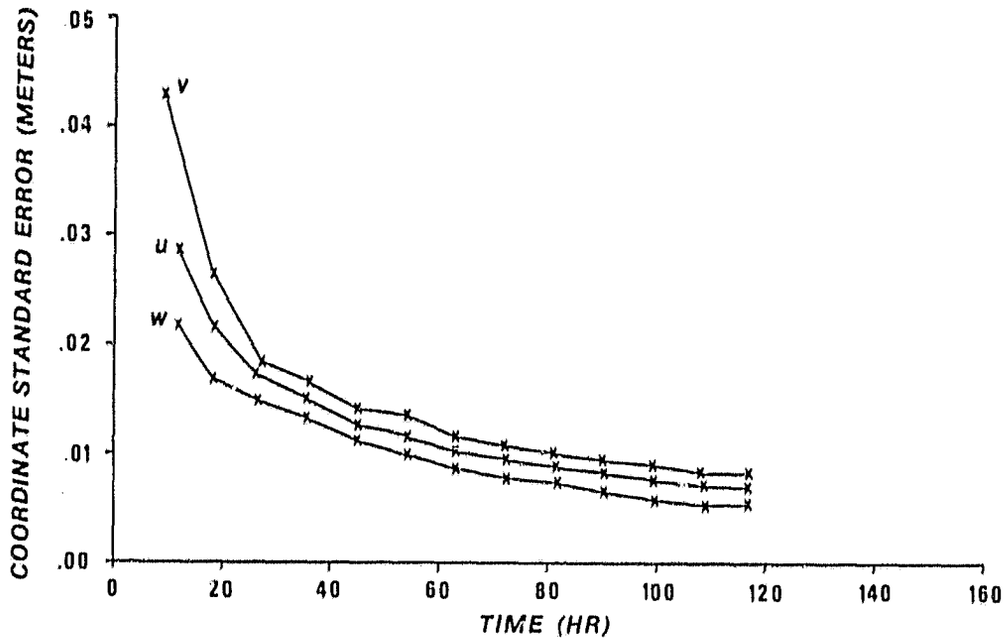

Figure 4.5.6. Standard Error of Station 1001 Coordinates Obtained from Range Observations Subject to One Meter Gaussian White Noise

TABLE 4.5.1. EFFECT OF ERROR SOURCES ON POSITIONING DERIVED FROM RANGE OBSERVATIONS USING A THREE-HOUR TRACKING INTERVAL

ERROR SOURCE	APPROXIMATE COORDINATE ERROR (cm)	
	1 DAY	5 DAYS
TROPOSPHERIC REFRACTION (± 5%)	8-12	4-6*
EPHEMERIS	150-200	80-120
RESIDUAL SATELLITE RUBIDIUM CLOCK ERROR	6	2
RANDOM RECEIVER CESIUM CLOCK ERROR	8	4
RECEIVER WHITE NOISE (1m)	1.5-2.0	.7-.9

*ASSUMING AN AVERAGING DUE TO SIGN VARIATIONS

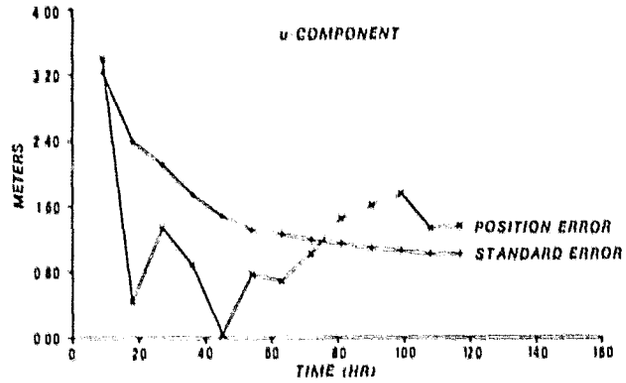

(a)

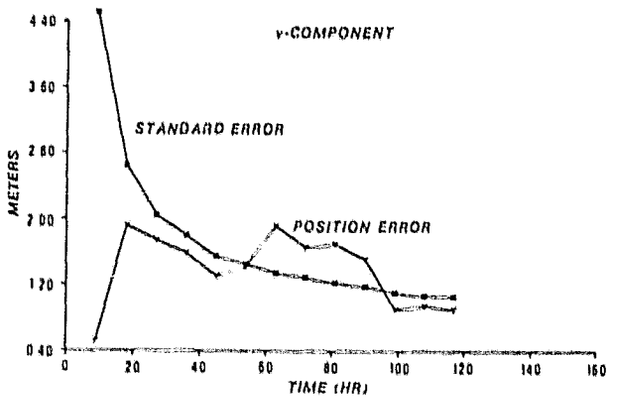

(b)

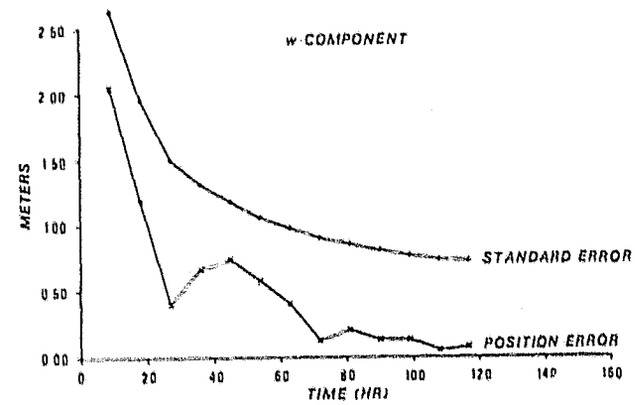

(c)

Figure 4.5.7. Complete Simulation of Station 1001 Positioning Using Range Observations over Three-Hour Tracking Intervals

meters in latitude. An examination of the solution with all error sources included indicates that each component of station position can be determined with an accuracy of from 1.5 to 2.3 meters after one day of observation and from 0.8 to 1.2 meters after five days.

The station positioning analysis based on a three-hour tracking interval was not immediately extended to include the other stations in Table 4.2.1. Instead consideration was given to improving the current results.

4.5.1.2 Range Solutions Based on One-Hour Tracking Intervals

Taking into account the results obtained in Section 4.2.2 for the optimal selection of satellites for point positioning, improvement in the geometric strength of the solution could be obtained by decreasing the tracking interval and sampling the satellite constellation geometry more rapidly. Thus a second scenario was investigated consisting of tracking each selected satellite for one hour and estimating station position every four hours. For a fixed interval of site occupation this approach introduces additional modeling parameters but allows a better sampling of satellite-station geometry. Using this approach ephemeris parameters are included for each hour of observation along with a linear satellite clock error model. A linear receiver clock error model is introduced every four hours. Since the clock modeling intervals are reduced the linear models are a better approximation to the random noise processes and the residual error statistics are reduced. However the inclusion of additional modeling parameters will have the opposite effect of weakening the least squares normal equations.

To determine if an improvement in the prior station positioning results was achievable a series of solutions were made for Stations 1001 and 1002 adopting this new approach. These positioning simulations were based on one hour tracking intervals with a total site occupation ranging from two to five days and were designed to measure the effect of random and systematic errors on positioning based on this tracking scenario. Table 4.5.2 gives estimates of the effects of these error sources in a form comparable with Table 4.5.1. The magnitude of the errors introduced are again taken from Table 4.2.2.

TABLE 4.5.2. EFFECT OF ERROR SOURCES ON POSITIONING DERIVED FROM RANGE OBSERVATIONS USING A ONE-HOUR TRACKING INTERVAL

ERROR SOURCE	APPROXIMATE COORDINATE ERROR (cm)	
	1 DAY	5 DAYS
TROPOSPHERIC REFRACTION (±5%)	8-12	4-6*
EPHEMERIS	50-80	25-40
RESIDUAL SATELLITE RUBIDIUM CLOCK ERROR	4	1
RANDOM RECEIVER CESIUM CLOCK ERROR	5	2
RECEIVER WHITE NOISE (1m)	1.5-2.0	.7-.9

*ASSUMING AN AVERAGING DUE TO SIGN VARIATIONS

An examination of Tables 4.5.1 and 4.5.2 reveals that this change in the observation and modeling procedure reduces the effect of two primary error sources, ephemeris error and random atomic clock error. The effect on positioning due to residual tropospheric refraction and receiver white noise remain virtually the same. These latter effects will be discussed first.

Simulations of station positioning were made in which Gaussian white noise with a standard error of one meter was introduced into the geometrical ranges to GPS satellites selected using the criterion which produces the smallest trace of the station coordinate covariance developed sequentially. The adjustment results for Station 1001 are given in Figure 4.5.8 where the standard error and magnitude of the station position error are given for each component. The results are similar to those given in Figure 4.5.6 for the three-hour tracking interval demonstrating that the effect of receiver instrumental noise on positioning averages equivalently for each observation procedure. The results indicate that the error in each component of position due to receiver noise is approximately 1.5 to 2.0 centimeters after one day and 0.7 to 0.9 centimeters after five days of continuous observation.

For tropospheric refraction the results based on a five percent bias in the predicted refraction corrections show station position component errors ranging from 5 to 20 centimeters. With the sign of the modeling error taken as constant the error in the station coordinates appears as a bias in the range of values just given with variations generally on the order of five centimeters. Thus the overall effect of residual tropospheric refraction error remains at a level similar to that from the prior tracking approach. However with the introduction of refraction bias parameters this error is substantially reduced. Figure 4.5.9 gives the results of an adjustment with range observations subject to a systematic tropospheric refraction error of five percent and random instrumental noise with a one meter standard error. In addition to the Cartesian station coordinates refraction scaling parameters, as

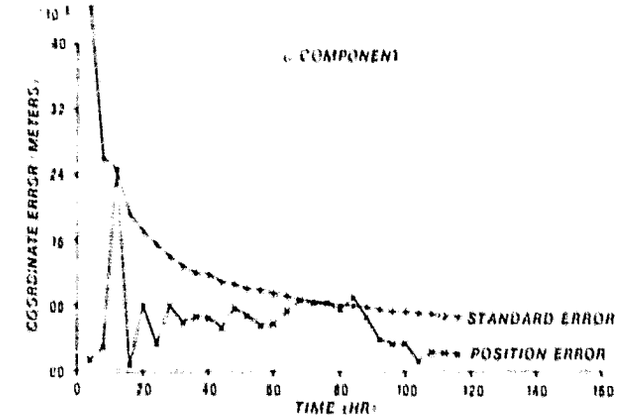

(a)

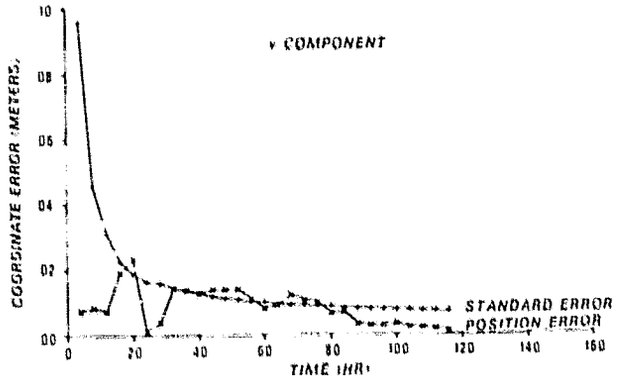

(b)

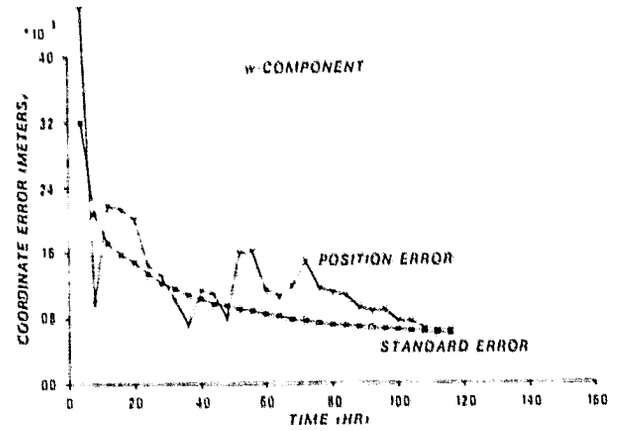

(c)

Figure 4.5.8. Position Error for Station 1001 Due to One Meter Gaussian White Noise (Range Observations/One-Hour Tracking Interval)

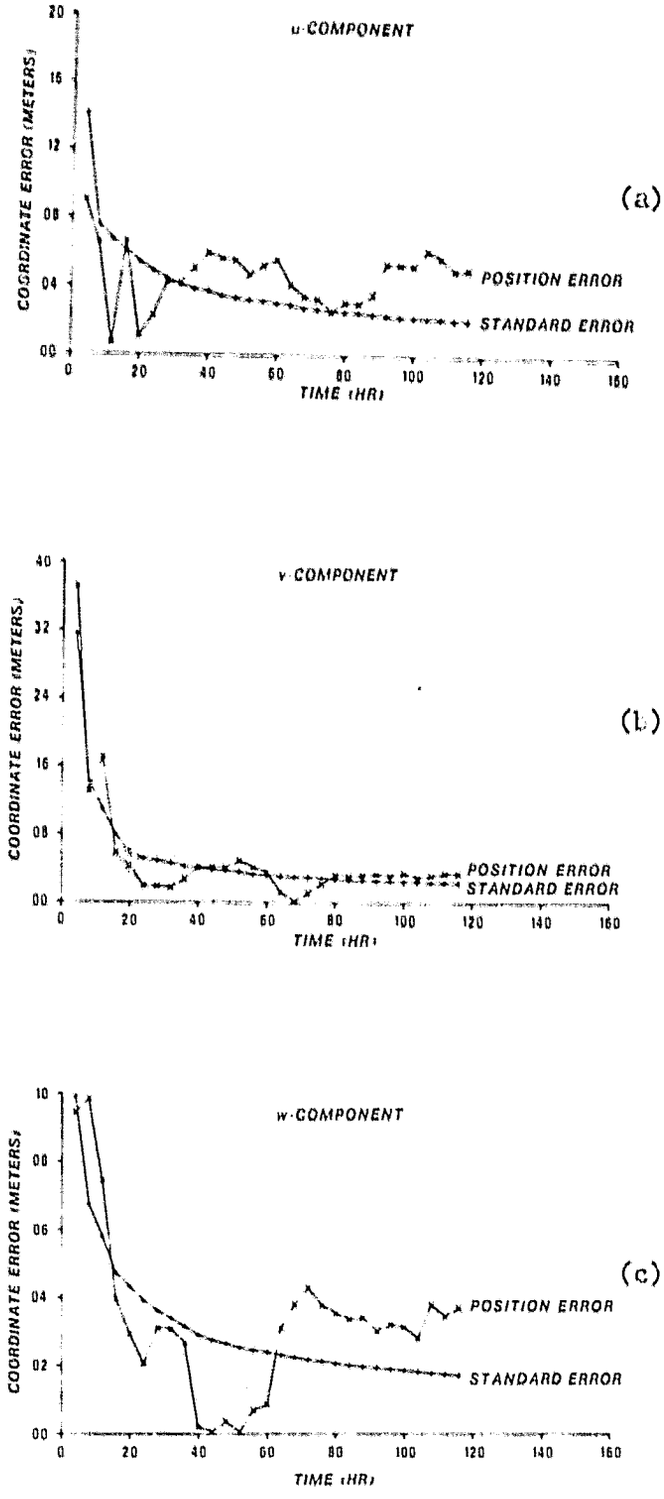

Figure 4.5.9. Position Error for Station 1001 Due to a Five Percent Systematic Tropospheric Refraction Error. Adjustment Includes Tropospheric Scaling Parameters (Range Observations/One-Hour Tracking Interval)

given in equation (4.1.57), were included, one for each hour of tracking. The errors in positioning due to refraction were reduced to a level of approximately 4 to 6 centimeters after one day and 2 to 4 centimeters after five days of observation. Thus refraction errors will not play a critical role in the determination of earth-fixed coordinates from GPS range observations.

The adoption of a one hour satellite tracking interval with linear modeling of random clock error over shorter time intervals decreases the effective error in station positioning as mentioned earlier. After a linear approximation of random cesium clock error over a four hour interval the unmodeled correlated residual errors remaining have standard errors of approximately 9 centimeters compared to the 12 to 16 centimeter standard error after an eight hour linear approximation. Similarly residual rubidium clock noise over a one hour interval has a standard error of approximately 12 centimeters compared to approximately 30 centimeters for a three hour fit interval. Thus the expected magnitude of the unmodeled clock error will decrease with this alternate tracking approach. However the number of model parameters required in the adjustment will increase tending to weaken the normal equations for station position. Figure 4.5.10 gives an example of the errors in station position when random cesium clock error and instrumental receiver noise with a standard error of one meter are present in the observations. The adjustment parameters included station position and a linear receiver clock model for each four-hour interval. The adjustment weighting was developed using the statistics of the two random error sources. Taking into account the results given in Figure 4.5.8,

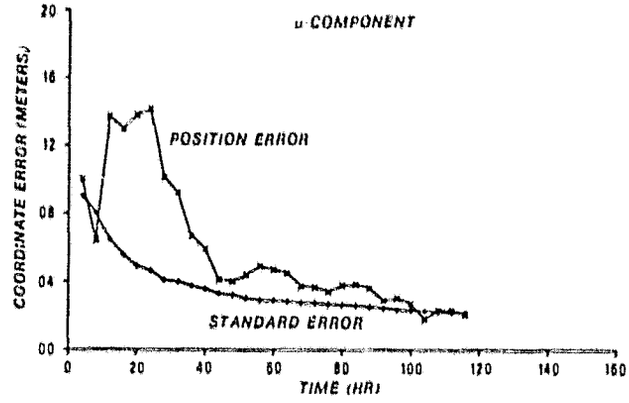

(a)

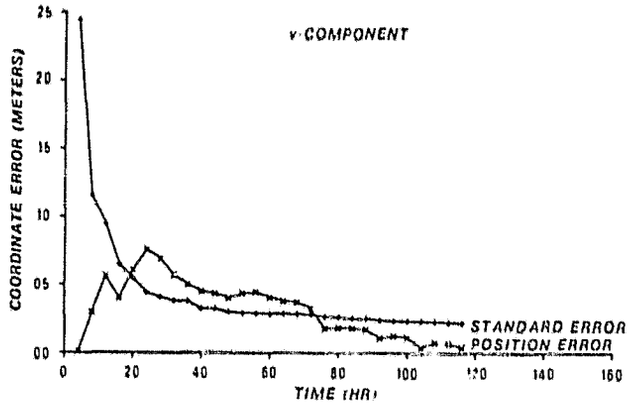

(b)

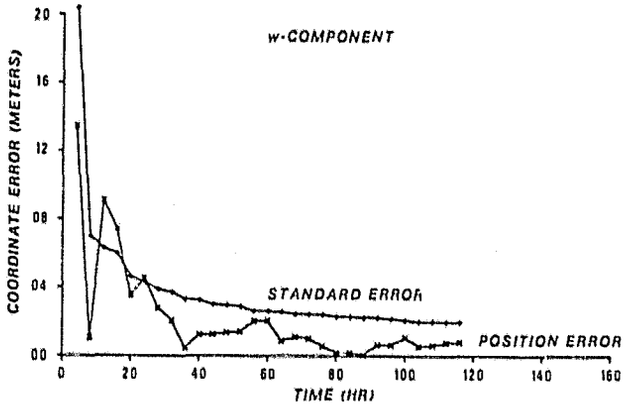

(c)

Figure 4.5.10. Position Error for Station 1001 Due to Random Cesium Clock Error (Range Observations/One-Hour Tracking Interval)

Figure 4.5.10 indicates that random cesium clock errors, consistent with the stability specifications adopted for the receiver oscillator, introduce approximately 5 centimeters of error in each component of station position after one day of observation and 2 centimeters after five days.

The random rubidium clock error modeled as a linear function of time over one-hour intervals was also considered. This error source introduces errors of approximately 4 and 1 centimeters after one and five days of continuous observation respectively. With both atomic clock random error sources and random instrumental noise included in the adjustment, using the complete statistical weighting, the standard errors of station position were reduced to approximately 60 percent of the error present in the three-hour tracking procedure.

With the selection of a satellite occurring each hour the effects of ephemeris error, whose distribution is discussed in Section 4.2.1, averages to a greater extent than in the three-hour tracking scheme. Figure 4.5.11 gives an example of the errors in positioning expected from range observations subject to one meter random instrumental error when ephemeris errors are present. Adjustment parameters include station position and six orbital elements for each one-hour interval. A priori weighting consistent with the amplitude of ephemeris error introduced was included for the orbital elements. The expected error in position due to the level of ephemeris error outlined in Table 4.2.2 is given in Table 4.5.2 to be 50 to 80 centimeters after one day and 25 to 40 centimeters after five days of observation.

Finally in Figure 4.5.12 results are given for Station 1001 for a complete simulation of station positioning in which all error sources

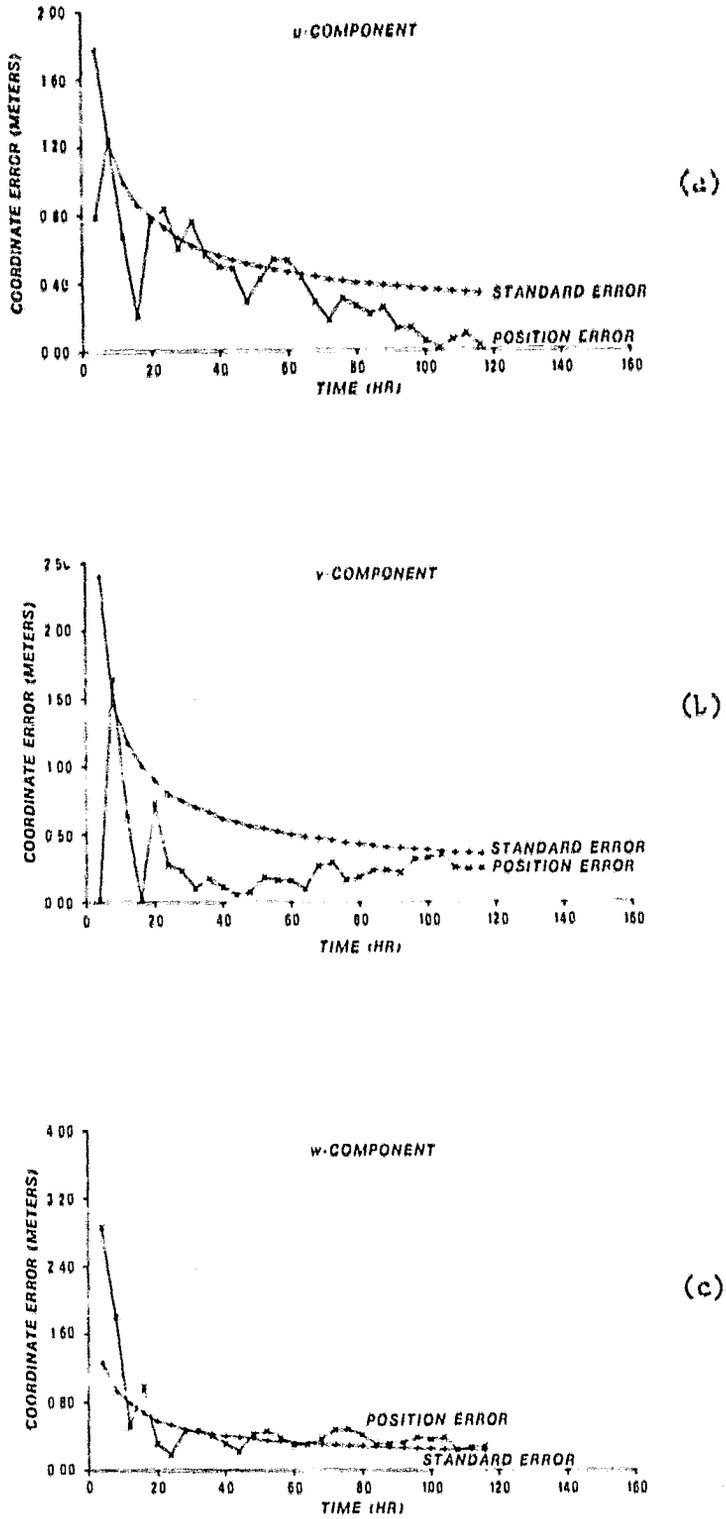

Figure 4.5.11. Position Error of Station 1001 Due to Ephemeris Error (Range Observations/One-Hour Tracking Interval)

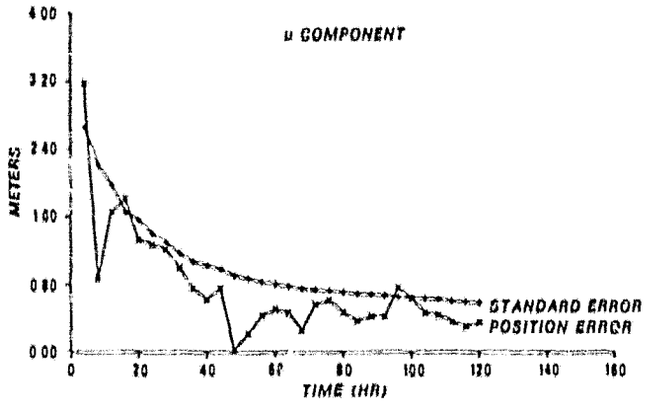

(a)

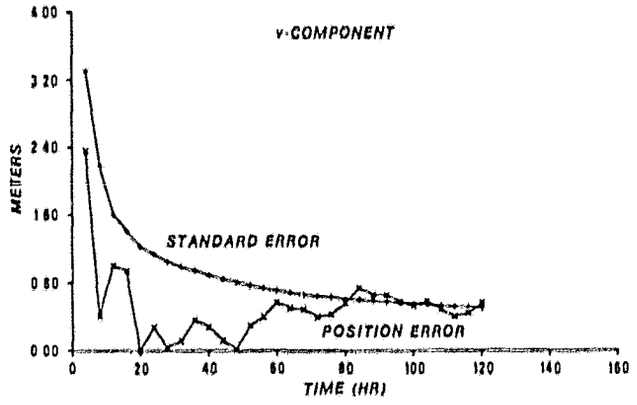

(b)

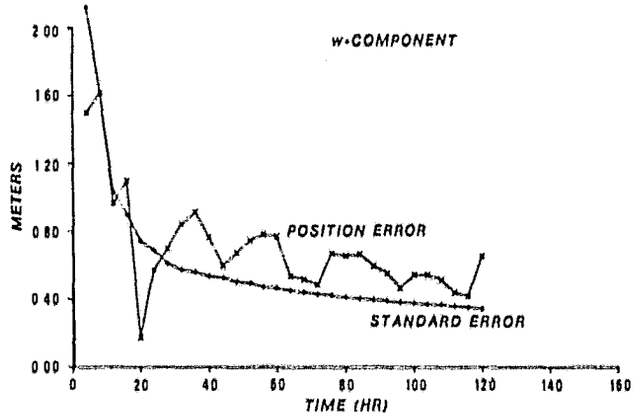

(c)

Figure 4.5.12. Range Positioning Results for Station 1001 for Complete Simulation (One-Hour Tracking Interval)

from Table 4.2.2 were included. All modeling parameters were included in the adjustment and the full weight matrix based on all unmodeled random error sources was utilized. These results indicate that the expected error in the components of station position range from 70 to 140 centimeters after one day of observation and from 35 to 60 centimeters after five days. A comparison of Figures 4.5.7 and 4.5.12 gives the improvement obtained using the shorter tracking interval. The improvements in the accuracy of the recovered station coordinates for Station 1001 were approximately 125, 90, and 30 centimeters for the u, v, and w coordinates respectively after one day of observation and 65, 55, and 20 centimeters respectively after five days of continuous observation. Similar gains in accuracy were achieved for Station 1002.

Since the adoption of the shorter tracking interval produced a significant increase in the accuracy of the recovered station position, simulations of dynamic point positioning were made for all stations in Table 4.2.1. These simulations incorporated all error sources from Table 4.2.2, the full set of modeling parameters with a priori weights consistent with the level of error introduced, and the weighting procedure developed in Section 4.4.3 for single station tracking. Table 4.5.4 presents the uncertainties in the geodetic coordinates for all stations under investigation obtained from dynamic point positioning using range observations. Table 4.5.3 is provided as a key for tables presenting simulation results. For the adopted levels of systematic and random errors utilized these results indicate that the geodetic coordinates may be recovered to the 100 to 150 centimeter level or better after one day of continuous GPS range observations. After five

TABLE 4.5.3. KEY TO ADJUSTMENT ERROR SOURCES, PARAMETERS AND WEIGHTING FOR SIMULATION RESULTS

ERROR SOURCES	
EPHEMERIS	1 — TABLE 4.2.2 VALUES UTILIZED 2 — 50% OF TABLE 4.2.2 VALUES
TROPOSPHERIC REFRACTION	0 — NO ERROR 1 — 5% OF MODEL PREDICTION
SATELLITE CLOCKS	1 — RESIDUAL BIAS AND DRIFT 2 — RESIDUAL RANDOM ERROR BASED ON ADOPTED RUBIDIUM CLOCK
STATION CLOCK	1 — BIAS AND DRIFT 2 — RANDOM CESIUM CLOCK ERROR
ADJUSTMENT PARAMETERS	1 — COMPLETE PARAMETER SET 2 — TROPOSPHERIC SCALING PARAMETERS DELETED
ADJUSTMENT WEIGHTING	1 — INCLUDES WHITE NOISE AND RANDOM CLOCK ERROR STATISTICS

TABLE 4.5.4. LATITUDE, LONGITUDE, AND HEIGHT UNCERTAINTIES BASED ON GPS RANGE OBSERVATIONS USING A ONE-HOUR TRACKING INTERVAL

STATION NO.	SYSTEMATIC AND RANDOM ERROR SOURCES					PARAMETER SET	WEIGHT MATRIX	ADJUSTMENT RESULTS (cm)								
	EPHEMERIS	TROPOSPHERIC REFRACTION	SATELLITE CLOCK	STATION CLOCK	WHITE NOISE (cm)			1 DAY			2 DAYS			5 DAYS		
								σ_ϕ	σ_λ	σ_h	σ_ϕ	σ_λ	σ_h	σ_ϕ	σ_λ	σ_h
1001	1	1	1, 2	1, 2	100	1	1	87.8	118.4	125.1	59.7	81.2	84.6	36.7	52.3	55.6
1002	1	1	1, 2	1, 2	100	1	1	88.9	115.7	123.7	60.1	83.9	86.4	36.4	54.4	57.9
1003	1	1	1, 2	1, 2	100	1	1	82.4	126.6	113.8	58.5	86.4	83.3	37.5	53.7	55.4
1004	1	1	1, 2	1, 2	100	1	1	86.5	117.8	119.5	57.8	83.7	84.0	37.1	53.9	56.3
1005	1	1	1, 2	1, 2	100	1	1	81.9	125.8	113.5	57.5	83.3	83.2	36.7	52.5	54.5
1006	1	1	1, 2	1, 2	100	1	1	86.2	115.1	124.6	58.8	82.0	83.5	37.3	54.6	53.6
1007	1	1	1, 2	1, 2	100	1	1	82.2	127.0	113.3	57.0	83.6	83.0	36.6	52.6	54.3
1008	1	1	1, 2	1, 2	100	1	1	86.5	114.5	125.1	58.8	81.3	83.7	37.4	54.2	54.0
1009	1	1	1, 2	1, 2	100	1	1	112.4	105.3	107.0	77.6	74.1	75.3	47.5	47.8	45.9
1010	1	1	1, 2	1, 2	100	1	1	111.6	104.1	106.7	78.1	73.5	75.0	47.9	47.7	45.8
1011	1	1	1, 2	1, 2	100	1	1	71.0	104.5	145.3	49.9	75.9	110.3	31.0	51.1	69.0
1012	1	1	1, 2	1, 2	100	1	1	72.6	102.3	150.6	55.3	77.8	115.2	32.8	48.9	70.9
1013	1	1	1, 2	1, 2	100	1	1	70.5	107.5	147.9	49.6	75.1	107.6	30.8	51.0	69.2
1014	1	1	1, 2	1, 2	100	1	1	88.5	119.6	126.1	60.2	81.3	84.6	36.9	52.4	55.9
1015	1	1	1, 2	1, 2	100	1	1	77.8	127.9	105.4	55.6	89.6	85.1	32.7	52.2	53.7
1016	1	1	1, 2	1, 2	100	1	1	84.9	132.4	98.6	59.6	91.3	80.0	36.1	53.2	51.8

days the accuracy of the recovered coordinates is between 30 to 70 centimeters. The dominant error source in these results is the satellite ephemeris.

Some variations in the results are evident. For instance, the solutions for the polar Stations 1009 and 1010 have a larger standard error for latitude and a smaller uncertainty in longitude and height than the results obtained in the mid-latitude station group solutions. This difference can be explained by examining the change in station-satellite geometry. For high latitude stations the maximum elevation angle is considerable less. Up to a latitude of 63 degrees satellite crossings of the zenith are possible. However for higher latitudes the maximum elevation angle decreases to approximately 54.5 degrees meaning that a larger percentage of the observations will be at lower elevation angles. As noted in Section 4.2.2 increasing the number of lower elevation observations increases the strength of the height solution in the presence of timing errors. With lower elevation angle observations the strength of the latitude and longitude components will depend on the distribution of observing azimuths. The equitorial stations show a larger uncertainty in height and a lower uncertainty in latitude and longitude, again due to the distribution of observing elevations and azimuths. The increased frequency of higher elevation observations is reflected in the increased height uncertainty. Figure 4.5.13 gives the positioning results for Station 1011.

For these adjustment solutions the a posteriori variance of unit weight was computed from equation (4.3.32). The square root of this quantity, $\hat{\sigma}_0$, for the solutions given in Table 4.5.4 ranged from 0.879

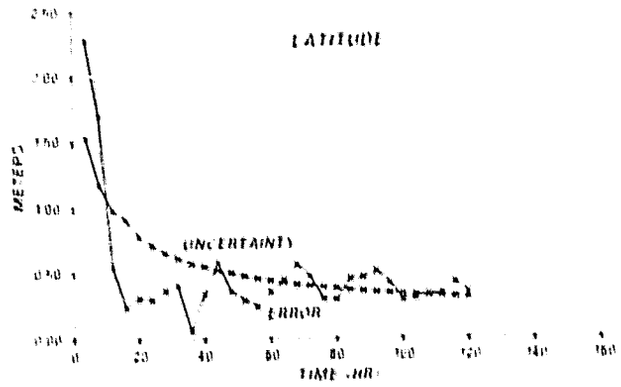

(a)

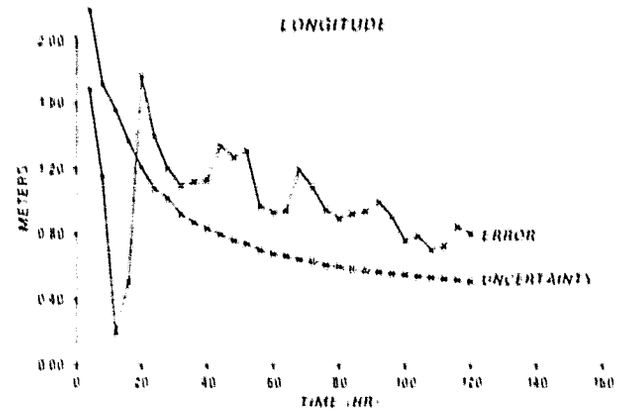

(b)

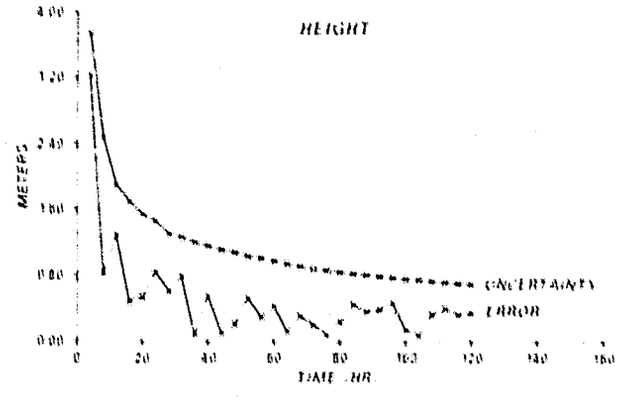

(c)

Figure 4.5.13. Range Positioning Results for Station 1011 for Complete Simulation (One-Hour Tracking Interval)

to 0.914. For a least squares adjustment in which the mathematical model for the observation equation is exact and the second order statistics of the random processes are modeled correctly in the weighting, the theoretical value of the a posteriori variance is unity. Deviation from unity is primarily due to error in the above assumptions. The range adjustment results given in Table 4.5.4 are not scaled by this quantity.

Some specific reasons for the range adjustment a posteriori variance not being unity are the following. First, the Markov process transfer functions given in Figures 4.4.7 and 4.4.8 both assign more power to certain frequencies than the specified transfer functions given in the same figures. For the satellite rubidium oscillator this additional power is at frequencies whose wavelength is greater than 100 seconds. The actual clock noise sequences simulated using the Meditch [1975] algorithm do not contain the same power at these frequencies. Thus the second order range statistics will predict observation uncertainties in excess of their value based on the exact use of the specified transfer function. This tends to decrease the a posteriori variance. Secondly, the errors introduced into the ephemeris using the equations of Section 4.1.2 are periodic in mean anomaly but modeled by a constant amplitude correction at the midpoint of each tracking interval. This modeling difference affects the a posteriori variance since the level of error introduced into the observations was smaller than the a priori orbital element uncertainty. And finally with a small number of degrees of freedom for each tracking interval white and correlated noise sequences will tend to be fit better than expected causing

a decrease in the a posteriori variance. The interpretation of the results should take these factors into consideration.

Finally Table 4.5.5 gives the decrease in the standard error of geodetic coordinates obtained in two previous examples when the variance of the instrumental white noise is decreased and the tropospheric refraction is compensated completely. The first case shows that no significant increase in the accuracy of the adjusted station coordinates can be expected by decreasing this instrumental random error component. Decreasing the standard error of this component from 100 to 60 centimeters produces a decrease of only 1.1 centimeters or less as opposed to an expected decrease of 40 percent based on range measurements subject to white measurement noise only. In this case however, with the inclusion of the fully correlated statistics for unmodeled atomic clock error, the resulting decrease is marginal.

In the second case assuming that tropospheric refraction effects can be compensated the refraction scaling parameters are excluded from the adjustment. The decrease in the standard error of the geodetic coordinates ranges from 1.1 to 3.0 centimeters after one day of observation and from 0.8 to 1.6 centimeters after five days. The largest decrease is in the height uncertainty; although, the net effect on the determination of earth-fixed coordinates is minor.

4.5.1.3 Integrated Doppler Solutions

Solutions based on integrated Doppler or range difference observations were examined subsequently. Range differences over five-minute intervals were formed by aggregating independent one minute integrated Doppler observations with an instrumental measurement uncertainty of

TABLE 4.5.5. VARIATION IN RESULTS FROM TABLE 4.5.4 DUE TO DECREASE IN INSTRUMENTAL WHITE NOISE AND ACCURATE PREDICTION OF TROPOSPHERIC REFRACTION (RANGE OBSERVATIONS, ONE-HOUR TRACKING INTERVAL)

STATION NO.	SYSTEMATIC AND RANDOM ERROR SOURCES					PARAMETER SET	WEIGHT MATRIX	VARIATION IN ADJUSTMENT RESULTS (cm)								
	EPHEMERIS	TROPOSPHERIC REFRACTION	SATELLITE CLOCK	STATION CLOCK	WHITE NOISE (cm)			1 DAY			2 DAYS			5 DAYS		
								σ_ϕ	σ_λ	σ_h	σ_ϕ	σ_λ	σ_h	σ_ϕ	σ_λ	σ_h
1001	1	1	1, 2	1, 7	60	1	1	0.5	0.6	1.1	0.4	0.4	1.0	0.2	0.4	0.7
1003	1	0	1, 2	1, 2	100	2	1	1.1	1.7	3.0	1.0	1.1	2.3	0.9	0.2	1.6

three centimeters. The parameters of the adjustment were equivalent to the range solution set with the exception of the clock models. For integrated Doppler observations the linear clock error models were each replaced with a single parameter representing time drift or frequency bias. Ephemeris elements, tropospheric refraction corrections, and the geodetic station coordinates were retained.

An initial solution was made for Station 1001 using range difference observations over three-hour tracking intervals. Observations were simulated using equation (4.2.9) and ephemeris error was introduced into the adjustment using an equation analogous to equation (4.2.10). Error sources were taken from Table 4.2.2. Adjustment weighting included both the instrumental white noise statistics and the random clock error statistics developed in Section 4.4.2. The receiver clock was modeled over a nine-hour interval as in the range solutions based on the same interval of tracking. Table 4.5.6 gives the results for this adjustment. These results indicate that after one day of observation the geodetic coordinate errors can be expected to range from 125 to 215 centimeters and reduce to from 60 to 100 centimeters after five days.

For this station a simulation based on a one-hour tracking interval was next tried to determine if better results could be obtained as in the range case with a receiver clock model adopted every four hours. The results from this solution are given at the beginning of Table 4.5.7. A comparison of the three and one-hour tracking interval results shows that significant improvement is obtained with the shorter tracking interval. This latter tracking procedure allows a better

TABLE 4.5.6. UNCERTAINTY IN GEODETIC COORDINATES OF STATION 1001 BASED ON GPS INTEGRATED DOPPLER OBSERVATIONS USING A THREE-HOUR INTERVAL

STATION NO.	SYSTEMATIC AND RANDOM ERROR SOURCES					PARAMETER SET	WEIGHT MATRIX	ADJUSTMENT RESULTS (cm)								
	EPHEMERIS	TROPOSPHERIC REFRACTION	SATELLITE CLOCK	STATION CLOCK	WHITE NOISE (cm)			1 DAY			2 DAYS			5 DAYS		
								σ_ϕ	σ_λ	σ_h	σ_ϕ	σ_λ	σ_h	σ_ϕ	σ_λ	σ_h
1001	1	1	1, 2	1, 2	3	1	1	124.5	215.6	176.1	95.0	165.2	140.2	58.5	99.1	82.5

TABLE 4.5.7. LATITUDE, LONGITUDE, AND HEIGHT UNCERTAINTIES BASED ON GPS INTEGRATED DOPPLER OBSERVATIONS USING A ONE-HOUR TRACKING INTERVAL

STATION NO.	SYSTEMATIC AND RANDOM ERROR SOURCES					PARAMETER SET	WEIGHT MATRIX	ADJUSTMENT RESULTS (cm)								
	EPHEMERIS	TROPOSPHERIC REFRACTION	SATELLITE CLOCK	STATION CLOCK	WHITE NOISE (cm)			1 DAY			2 DAYS			5 DAYS		
								σ_ϕ	σ_λ	σ_h	σ_ϕ	σ_λ	σ_h	σ_ϕ	σ_λ	σ_h
1001	1	1	1, 2	1, 2	3	1	1	102.7	145.2	139.2	71.8	100.4	97.0	46.9	63.2	53.5
1002	1	1	1, 2	1, 2	3	1	1	100.3	147.0	141.7	68.8	99.0	96.9	45.4	62.2	56.2
1003	1	1	1, 2	1, 2	3	1	1	103.0	150.8	140.7	72.4	99.5	93.6	46.1	62.0	54.5
1004	1	1	1, 2	1, 2	3	1	1	104.6	149.7	141.5	70.3	97.5	98.0	45.8	62.1	55.6
1007	1	1	1, 2	1, 2	3	1	1	103.2	151.0	139.9	72.5	99.4	95.5	45.7	61.9	54.8
1008	1	1	1, 2	1, 2	3	1	1	102.4	149.4	142.1	71.2	98.3	96.3	46.3	62.8	54.4
1009	1	1	1, 2	1, 2	3	1	1	145.1	193.2	96.2	106.8	127.1	66.9	70.9	76.4	43.3
1010	1	1	1, 2	1, 2	3	1	1	143.3	190.6	95.7	107.5	127.7	66.1	71.3	75.9	42.7
1011	1	1	1, 2	1, 2	3	1	1	91.3	131.3	127.9	63.6	93.5	93.0	43.5	58.9	60.2
1012	1	1	1, 2	1, 2	3	1	1	96.2	130.9	126.1	65.8	96.8	92.7	43.7	60.7	55.9
1013	1	1	1, 2	1, 2	3	1	1	87.7	131.8	128.0	61.4	90.9	92.1	43.3	57.1	56.0
1015	1	1	1, 2	1, 2	3	1	1	97.7	139.7	136.3	67.2	93.8	90.3	42.7	59.4	55.0
1016	1	1	1, 2	1, 2	3	1	1	107.8	153.1	127.2	74.8	102.3	84.9	47.0	64.3	51.2

representation of random clock error with the same model, permits better sampling of satellite geometry, and produces a more rapid averaging of the effects due to systematic and random error sources. The result is an uncertainty in station position coordinates in the range of 100 to 150 centimeters after one day and 45 to 65 centimeters after five days of observation.

Since this shorter tracking interval yielded such improvement in the results, station positioning adjustments were made for most of the stations in Table 4.2.1. These results are given in Table 4.5.7. Again the height uncertainties for the polar Stations 1009 and 1010 are significantly less than for all other stations since the higher occurrence of lower elevation observations allows a better separation of height and timing errors. However for these stations the latitude and longitude solutions are weaker. The results for the mid-latitude stations show less variation than the range solution results. In general the results indicate that range difference observations yield position component accuracies of from 85 to 200 centimeters after one day of observation and from 40 to 80 centimeters after five days of continuous tracking. Variations in the results with location are to be expected with the weakest solution for latitude and longitude occurring toward the poles. Figure 4.5.14 gives the positioning results for Station 1013.

The a posteriori variance of unit weight was computed using equation (4.3.32) for each adjustment of Table 4.5.7. The square root of this quantity varied from 0.967 to 0.998 indicating more consistency in the adjustment modeling and weighting than in the range observation simulations.

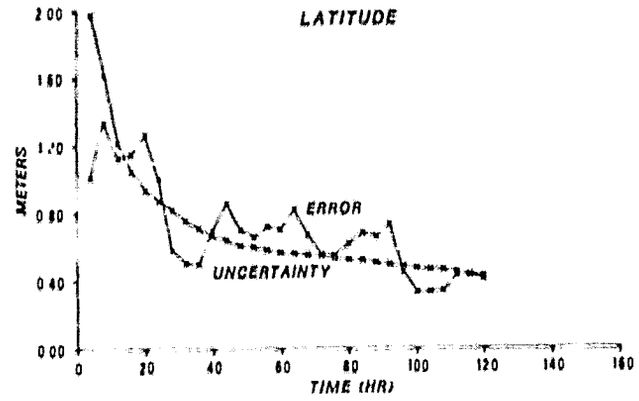

(a)

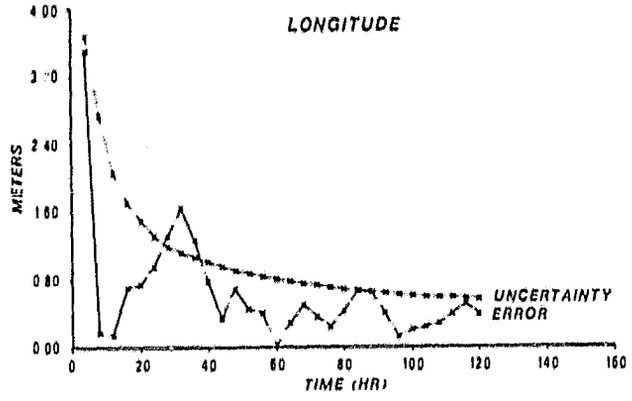

(b)

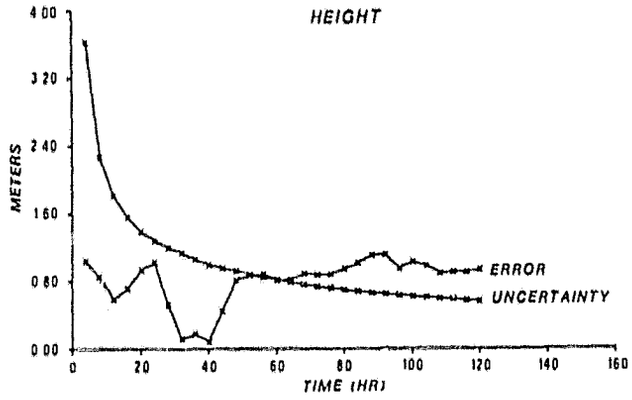

(c)

Figure 4.5.14. Doppler Positioning Results for Station 1013 for Complete Simulation (One-Hour Tracking Interval)

Table 4.5.8 summarizes the effects of various error sources on positioning based on integrated Doppler observations using a one-hour tracking interval. Again the ephemeris error dominates the effects of all other error sources. Because of the geometric weakness of the integrated Doppler observations the effect produced by three centimeter instrumental white noise is much larger than that due to a one meter standard error in range.

TABLE 4.5.8. EFFECT OF ERROR SOURCES ON POSITIONING DERIVED FROM DOPPLER OBSERVATIONS USING A ONE-HOUR TRACKING INTERVAL

ERROR SOURCE	APPROXIMATE COORDINATE ERROR (cm)	
	1 DAY	5 DAYS
TROPOSPHERIC REFRACTION (5%)	20	10*
EPHEMERIS	60-150	30-70
RESIDUAL RANDOM RUBIDIUM CLOCK ERROR	5	2
RANDOM RECEIVER CESIUM CLOCK ERROR	7	3
RECEIVER WHITE NOISE	16-18	6-8

*ASSUMING AN AVERAGING DUE TO SIGN VARIATIONS. TROPOSPHERIC REFRACTION SCALING PARAMETERS WOULD REDUCE THIS ERROR TO APPROXIMATELY 5 CENTIMETERS.

And finally Table 4.5.9 gives the reduction in the geodetic coordinate uncertainties with modifications to the assumed error levels introduced into the adjustment for Station 1007. Assuming that tropospheric refraction can be accounted for completely either through measurement or modeling and that the scaling parameters are deleted from

TABLE 4.5.9. VARIATION IN RESULTS FOR STATION 1007 DUE TO MODIFICATION OF ERROR MAGNITUDES AND ADJUSTMENT PARAMETERS (DOPPLER OBSERVATIONS, ONE-HOUR TRACKING INTERVAL)

STATION NO.	SYSTEMATIC AND RANDOM ERROR SOURCES					PARAMETER SET	WEIGHT MATRIX	VARIATION IN ADJUSTMENT RESULTS (cm)								
	EPHEMERIS	TROPOSPHERIC REFRACTION	SATELLITE CLOCK	STATION CLOCK	WHITE NOISE (cm)			1 DAY			2 DAYS			5 DAYS		
								σ_ϕ	σ_λ	σ_h	σ_ϕ	σ_λ	σ_h	σ_ϕ	σ_λ	σ_h
1007	1	0	1, 2	1, 2	3	2	1	0.2	0.1	1.9	0.3	1.0	1.6	0.1	0.4	0.8
1007	1	1	1, 2	1, 2	1	1	1	1.6	2.4	2.7	1.3	1.5	1.6	0.7	0.8	0.9
1007	1	1	1, 2	1, 2	0.2	1	1	1.8	2.7	3.1	1.4	1.7	1.8	0.8	0.9	1.0
1007	2	1	1, 2	1, 2	3	1	1	46.3	68.4	60.3	32.0	45.8	41.5	20.0	29.1	24.6

the set of adjustment parameters, the resulting decrease in position uncertainty is negligible as shown in the table. Also a decrease in the instrumental noise level from three centimeters to 0.2 centimeters produces only a minimal reduction in the coordinate uncertainty. Minor decreases are realized in these cases because the ephemeris error totally dominates these error sources. Thus for absolute positioning, additional refinements in the refraction prediction or improvements in the noise level of the receiver will not provide any real improvement unless the ephemeris error is greatly reduced. As a final example the level of ephemeris error adopted in Table 4.2.2 was halfed and as expected a significant level of improvement in position uncertainty was achieved. The uncertainty in the results improved by approximately 45 percent.

A comment concerning continuous count integrated Doppler is in order. In the above analysis one-minute integrated Doppler counts, assumed statistically independent, were aggregated to form five minute range differences. The instrumental noise thus increased by $\sqrt{5}$. For a continuous count integrated Doppler system this is not true. The five minute Doppler counts in that case would still be subject to approximately the same white noise level as one minute observations. The results presented here consider one-minute observation noise levels of from 0.2 to 3 centimeters or 0.45 to 6.7 centimeters for five minute aggregated range differences. For continuous count integrated Doppler this latter interval would be approximately 0.2 to 3 centimeters, a more optimistic but partially overlapping interval. From the results in Tables 4.5.7 and 4.5.9 the accuracy of continuous count Doppler utilized as independent range differences can be established.

4.5.2 Determination of Baseline Components

In this section results are presented for the determination of baseline components and chord length from simultaneous range and integrated Doppler observations from two stations. The least squares normal equations now include the earth-fixed coordinates of each tracking station. After each sequential solution the resulting station coordinate covariance matrix is linearly transformed into coordinate differences and chord length using equations (3.1.22) and (3.1.25) or analogous equations when the coordinates are expressed as geodetic latitude, longitude, and height. Satellites are selected using the criterion discussed in Chapter 3 and the simulations described in this section include Table 4.2.2 error sources.

4.5.2.1 Range Solutions

As in Section 4.5.1 initial results were based on the three-hour tracking interval. Simultaneous range observations were simulated for five days for Station 1001 and 1002. These stations lie on the same meridian separated by approximately 100 kilometers as shown in Figure 4.2.1. Simultaneous observations were excluded from the adjustment if the elevation angle from either station was below ten degrees.

The effect of individual error sources on baseline components was investigated for these stations by introducing each into the adjustment. For this 100 kilometer north-south baseline the results are given in Table 4.5.10. A comparison of these results with Table 4.5.1 demonstrates that the sensitivity of the baseline components to these error sources is quite different than for the determination of geodetic coordinates from range. Since the baseline distance is small relative

TABLE 4.5.10. EFFECT OF ERROR SOURCES ON BASELINE COMPONENTS DERIVED FROM RANGE OBSERVATIONS USING A THREE-HOUR TRACKING INTERVAL (100 km BASELINE)

ERROR SOURCES	APPROXIMATE COMPONENT ERROR (cm)	
	1 DAY	5 DAYS
TROPOSPHERIC REFRACTION (5%)	6-8	2-3
EPHEMERIS	1-3	0.5-1.5
RESIDUAL RANDOM SATELLITE RUBIDIUM CLOCK ERROR	0.2	0.1
RANDOM RECEIVER CESIUM CLOCK ERROR	12	6
RECEIVER WHITE NOISE (1 m)	2-3	1-1.5

to the distance to the satellites the effects of errors in the satellite ephemeris and clock project almost identically into the coordinates of each station. The transformation into coordinate differences removes the majority of the effect. Thus although satellite position errors can contribute 150 to 200 centimeters of uncertainty in station position after one day of observation, this same error has only an effect of from 1 to 3 centimeters on the coordinate differences. This fact precludes a requirement for a precise ephemeris in this application. Figure 4.5.13 demonstrates the error in the Cartesian baseline components due to ephemeris error. After five days this error can be expected to range from 0.5 to 1.5 centimeters. The effect of the satellite clock error is likewise minor.

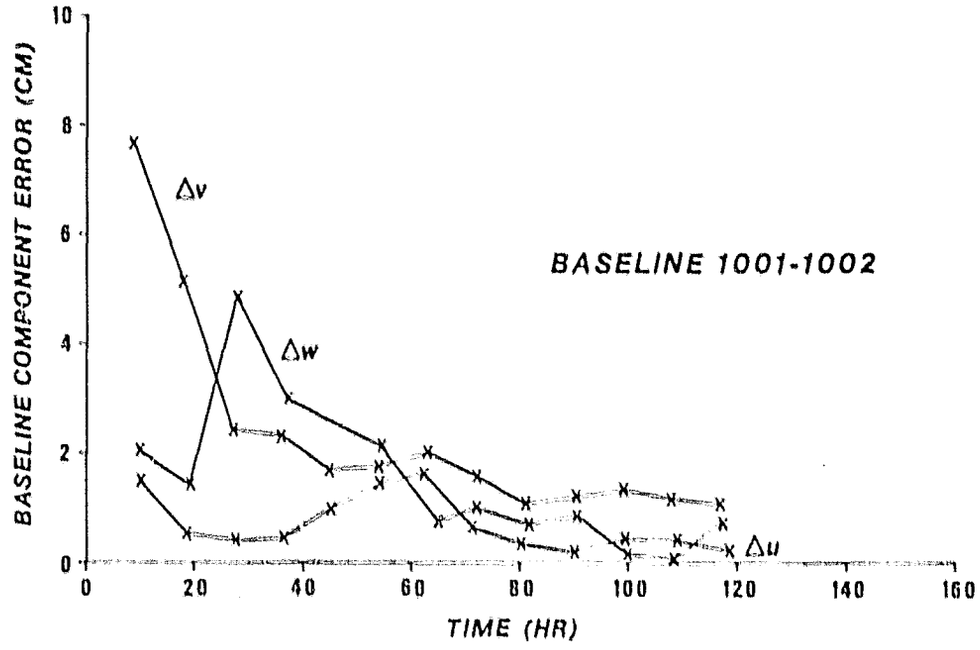

Figure 4.5.15. Effect of Uncompensated Systematic Orbit Error on Baseline Components Using Range Observations (Three-Hour Tracking Interval)

The effect of tropospheric refraction error will also be reduced if the signature of the error is almost equivalent at both sites. In the cases considered here a common five percent error was introduced. For sites separated by up to a few hundred kilometers the difference in tropospheric refraction will be primarily a function of elevation angle difference and the difference in weather conditions. Assuming the difference is a function of the former, a constant percentage error will produce approximately the same error at each site and the effect on baseline components will be small. In actual applications where a more complicated prediction of tropospheric refraction exists the baseline component errors may increase to a value greater than that given in Table 4.5.10.

The dominant error source in this application is the instability of the tracking receiver clock. For the cesium oscillator considered in this study the error introduced into baseline components can be expected to range from 12 to 6 centimeters after one and five days of observation respectively. Figure 4.5.16 presents the Cartesian baseline component errors as a function of time. These errors tend to average with time but at a rate which depends on the stability of the clock. For the dynamic determination of baseline components a significant decrease in this error can only be achieved by increasing the stability of the receiver oscillator if the tracking interval is held fixed.

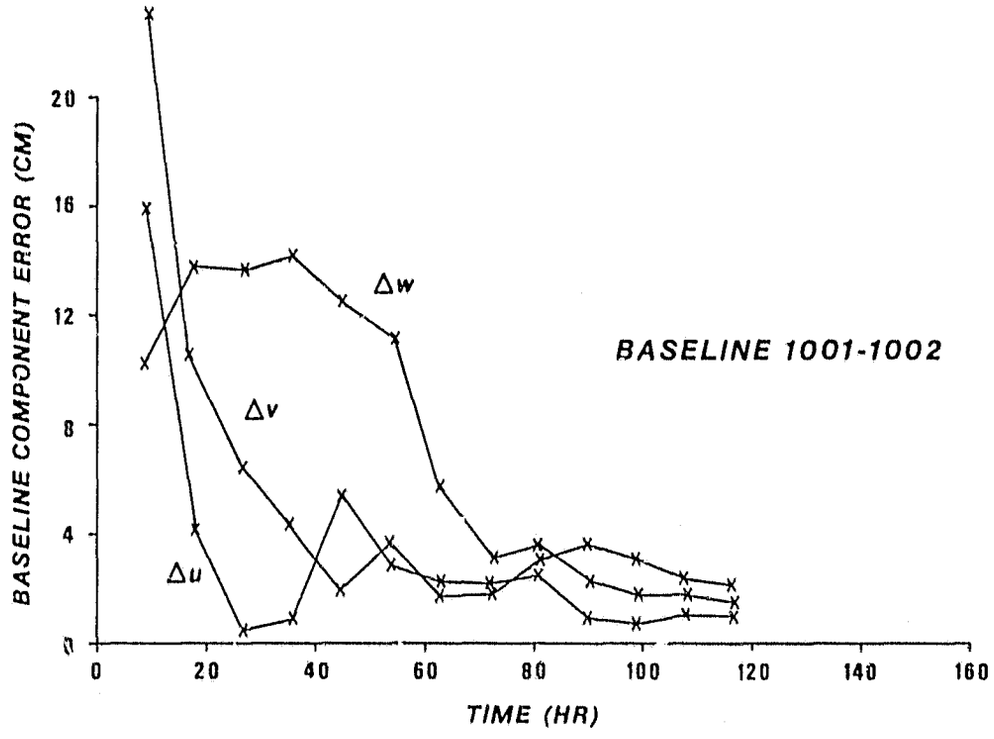

Figure 4.5.16. Effect of Random Cesium Clock Error on Baseline Components derived from Range Observations (Three-Hour Tracking Interval)

For a complete simulation of relative positioning five days of range observations were adjusted sequentially. The parameters of the adjustment included two pairs of station coordinates, ephemeris parameters, a linear satellite clock model every three hours and a linear model for each tracking station clock every nine hours. Two tropospheric refraction scaling parameters were introduced for every three hours of tracking. The adjustment weighting was based on all random errors added to the observations. The weight matrix used every nine hours had the form of equation (4.4.41). Errors were introduced into the range observations according to Table 4.2.2 with the instrumental white noise uncertainty taken as one meter. The result of the adjustment was Cartesian baseline coordinate uncertainties of 23, 21, and 18 centimeters after one day of observation and 10, 11, and 8 centimeters after five days.

The simulation for Stations 1001 and 1002 was repeated using a one-hour tracking interval. The uncertainties in the Cartesian baseline components after one day of observation were 28, 15, and 12 centimeters. After five days of continuous observation the resulting standard errors were 12, 7, and 6 centimeters for the Δu, Δv, Δw components. A comparison of the trace of the covariance matrix with that from the previous three-hour interval simulation shows that the shorter tracking interval produces marginally better results. This is consistent with the marginal increase in geometric strength for range observations demonstrated in Chapter 3.

For the one-hour tracking procedure the effects of error sources on baseline components are given in Table 4.5.11 for the 100

kilometer baseline. The major difference between Tables 4.5.11 and 4.5.10 is the decrease in the effect of random receiver clock noise.

TABLE 4.5.11. EFFECT OF ERROR SOURCES ON BASELINE COMPONENTS DERIVED FROM RANGE OBSERVATIONS USING A ONE-HOUR TRACKING INTERVAL (100 km BASELINE)

ERROR SOURCE	APPROXIMATE COMPONENT ERROR (cm)	
	1 DAY	5 DAYS
TROPOSPHERIC REFRACTION (5%)	6-8	2-3
EPHEMERIS	1-3	0.5-1.5
RESIDUAL RANDOM SATELLITE RUBIDIUM CLOCK ERROR	0.2	0.1
RANDOM RECEIVER CLOCK ERROR	8	3
RECEIVER WHITE NOISE (1 m)	2-3	1.0-1.5

Using the one-hour tracking scenario simulations were performed to assess the accuracy to which baseline components and chord lengths might be determined using simultaneous GPS range observations from two sites. The complete parameter set and weighting based on all random error sources were included in the adjustment. The resulting uncertainties in the baseline parameters are given in Table 4.5.12. The uncertainty in the chord length d is also expressed in parts per million (ppm). For baselines less than 300 kilometers in length these results indicate that the uncertainty in the latitude component of the baseline ranges from between 10.1 and 12.7 centimeters after one day of observation and from 4.4 to 5.8 centimeters after five days. The longitude component uncertainties are slightly weaker ranging from 10.6 to

TABLE 4.5.12. BASELINE COMPONENT AND CHORD LENGTH UNCERTAINTIES BASED ON SIMULTANEOUS RANGING (SATELLITE TRACKING INTERVAL ONE HOUR)

BASELINE CONFIGURATION	APPROXIMATE CHORD LENGTH (km)	SYSTEMATIC AND RANDOM ERROR SOURCES					PARAMETER SET	WEIGHT MATRIX	ADJUSTMENT RESULTS (cm)														
		EPHEMERIS	TROPOSPHERIC REFRACTION	SATELLITE CLOCK	STATION CLOCKS	WHITE NOISE (cm)			1 DAY					2 DAYS					5 DAYS				
									σ_x	σ_y	σ_z	σ_d	$\frac{d\sigma}{d}$ (ppm)	σ_x	σ_y	σ_z	σ_d	$\frac{d\sigma}{d}$ (ppm)	σ_x	σ_y	σ_z	σ_d	$\frac{d\sigma}{d}$ (ppm)
1001-1002	100	1	1	1 2	1 2	100	1	1	111	147	270	110	11	84	98	198	83	08	58	60	150	57	06
1001-1003	100	1	1	1 2	1 2	100	1	1	135	153	252	157	15	78	101	182	100	10	49	60	121	59	06
1001-1014	80	1	1	1 2	1 2	100	1	1	111	150	276	138	18	81	100	191	96	12	54	63	140	63	08
1003-1004	200	1	1	1 2	1 2	100	1	1	120	162	260	155	08	85	95	186	89	04	51	64	122	60	03
1005-1006	300	1	1	1 2	1 2	100	1	1	127	174	272	160	05	89	105	193	92	03	54	70	127	62	02
1007-1008	500	1	1	1 2	1 2	100	1	1	140	192	356	143	03	98	131	227	98	02	64	87	144	68	01
1015-1016	1860	1	1	1 2	1 2	100	1	1	340	420	472	185	01	243	293	367	122	007	160	189	229	83	004
1009-1013	100	1	1	1 2	1 2	100	1	1	101	106	275	99	10	73	67	195	72	07	44	43	126	43	04
1011-1012	100	1	1	1 2	1 2	100	1	1	118	146	277	145	15	92	115	206	114	11	56	70	125	69	07
1011-1013	100	1	1	1 2	1 2	100	1	1	129	149	257	126	13	90	105	190	88	09	57	75	120	56	06

17.4 centimeters after one day and from 4.3 to 7.5 centimeters after five days of simultaneous observation. The height difference between the stations has the largest uncertainty due to the correlation of height error with receiver timing error and refraction. For baselines under 300 kilometers the height difference uncertainty ranges from 25.2 to 27.7 centimeters for one day of observation and from 12.0 to 15.0 centimeters after five days. For these baselines the uncertainty in chord length ranges from 9.9 to 16.0 centimeters (0.5 to 1.8 ppm) after one day and from 4.3 to 6.9 centimeters (0.2 to 0.8 ppm) after five days. The chord length uncertainty increases with baseline distance as seen in the results for baselines 1007-1008 and 1015-1016. However the relative error in parts per million decreases. The increase in the uncertainty is due to an increasing projection of the ephemeris error onto the baseline components. Figure 4.5.17 gives the baseline component errors and uncertainties for baseline 1011-1012. The chord length between these stations is approximately 100 kilometers. The chord uncertainty as a function of time is given in Figure 4.5.17(d).

Two final examples are presented in Table 4.5.13 which show how the uncertainty in the results given in Table 4.5.12 are subject to change with variations in the simulation. Decreasing the instrumental white noise to 60 centimeters decreases the uncertainties of the baseline components from 1.5 to 2.4 centimeters after one day of observation and from 0.6 to 1.2 centimeters after five days for the 80 kilometer baseline 1001-1014. The decrease in the uncertainty of the

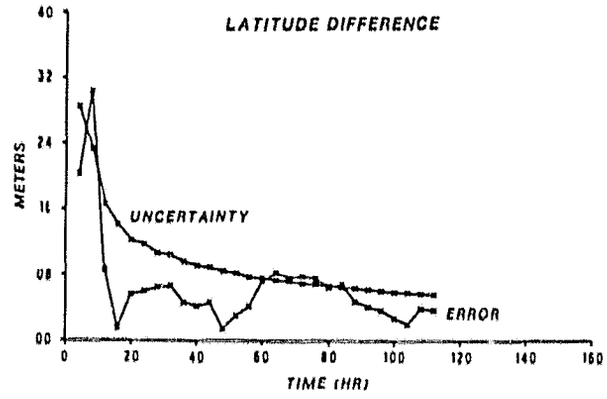

(a)

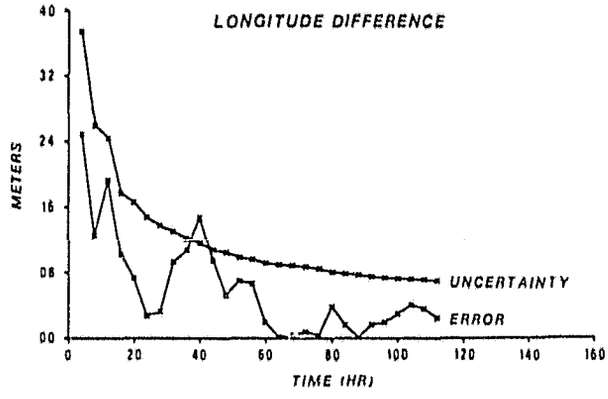

(b)

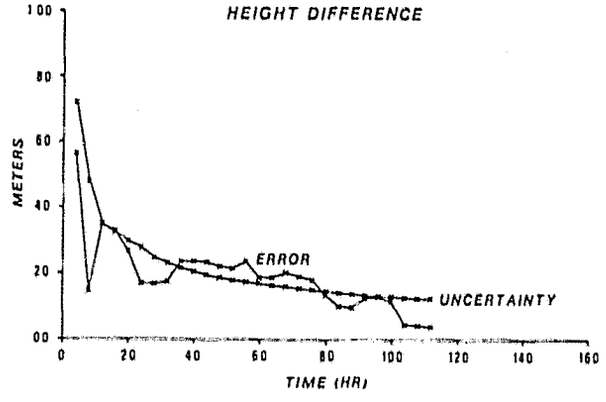

(c)

Figure 4.5.17. Baseline Parameter Error for Complete Simulation Using Range Observations from Stations 1011 and 1012 (One-Hour Tracking Interval)

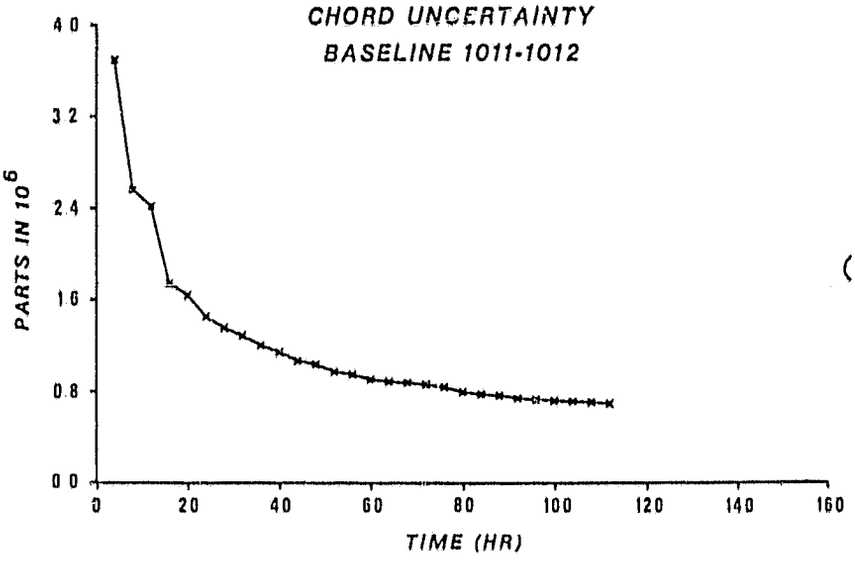

(d)

Figure 4.5.17 (continued)

TABLE 4.5.13. DECREASE IN BASELINE COMPONENT AND CHORD UNCERTAINTIES DUE TO MODIFICATIONS OF ERROR SOURCES (SIMULTANEOUS RANGING; ONE-HOUR TRACKING INTERVAL)

BASELINE CONFIGURATION	CHORD LENGTH (km)	SYSTEMATIC AND RANDOM ERROR SOURCES					PARAMETER SET	WEIGHT MATRIX	VARIATION IN ADJUSTMENT RESULTS (cm)													
		EPHEMERIS	TROPOSPHERIC REFRACTION	SATELLITE CLOCK	STATION CLOCKS	WHITE NOISE (cm)			1 DAY					2 DAYS					5 DAYS				
									$\sigma_{\Delta x}$	$\sigma_{\Delta y}$	$\sigma_{\Delta z}$	σ_d	$\sigma_{d/d}$ (ppm)	$\sigma_{\Delta x}$	$\sigma_{\Delta y}$	$\sigma_{\Delta z}$	σ_d	$\sigma_{d/d}$ (ppm)	$\sigma_{\Delta x}$	$\sigma_{\Delta y}$	$\sigma_{\Delta z}$	σ_d	$\sigma_{d/d}$ (ppm)
1001-1014	80	1	1	1.2	1.2	60	1	1	15	16	21	17	03	09	12	19	11	01	06	09	12	08	01
1003-1004	200	1	0	1.2	1.2	100	2	1	56	89	147	97	05	40	47	107	54	02	23	33	73	37	02

chord length ranges from 0.3 ppm to 0.1 ppm for the interval of site occupation in this case. Finally if tropospheric refraction error can be measured or predicted with high accuracy then the deletion of the tropospheric refraction scaling parameters will produce a significant decrease in the standard error of the baseline parameters since the removal of these parameters will strengthen the normal equations. The results for the 200 kilometer baseline 1003-1004 are given in Table 4.5.13 demonstrating that the measurement of tropospheric refraction with a water vapor radiometer may be required to obtain the best possible results using a dynamic approach.

4.5.2.2 Integrated Doppler Solutions

Simultaneous integrated Doppler observations from a pair of stations were analyzed to determine the accuracy to which baseline parameters can be determined. Adopting a one-hour tracking interval the effect of the systematic and random error sources given in Table 4.2.2 on the vector components of the baseline were evaluated for Stations 1001 and 1002. These results are given in Table 4.5.14. As with the use of range observations the stability of the tracking receiver clock will contribute significantly to the error in this positioning problem while satellite ephemeris and clock errors have no significance for such short baselines. As mentioned previously a five percent unmodeled error in tropospheric refraction having constant sign can introduce errors of up to 50 centimeters in position. However for short baselines a large portion of this error is in common at both sites and the resulting error in the coordinate differences ranges from 4 to 8

TABLE 4.5.14. EFFECT OF ERROR SOURCES ON BASELINE COMPONENTS DERIVED FROM DOPPLER OBSERVATIONS USING A ONE-HOUR TRACKING INTERVAL (100 km BASELINE)

ERROR SOURCE	APPROXIMATE COMPONENT ERROR (cm)	
	1 DAY	5 DAYS
TROPOSPHERIC REFRACTION	4-8	2-3
EPHEMERIS	.5	.1
RESIDUAL SATELLITE RUBIDIUM CLOCK ERROR	.2	.05
RANDOM RECEIVER CLOCK ERROR	10	4
RECEIVER WHITE NOISE (3 cm)	20-25	8-10

centimeters after one day to 2 to 3 centimeters after five days of observation. In actual applications the signature of this error may not be equivalent at each site and the resulting baseline component errors may be different. The receiver white noise plays the most important role. Because of the geometric weakness of range difference observations a 3 centimeter standard error for receiver noise will restrict baseline component uncertainties to be more than 20 to 25 centimeters after one day of observation and from 8 to 10 centimeters after five days. Furthermore it will be shown below that reducing the receiver noise level will have only limited success in reducing the baseline component uncertainties.

For the case just considered a complete simulation was made to determine the uncertainty in the baseline components and chord using

five days of continuous observation. The results are presented in Table 4.5.15. In terms of the geodetic coordinate differences the uncertainties are 27.7, 41.6, and 45.5 centimeters after one day and 13.0, 17.1, and 18.2 centimeters after five days for the latitude, longitude, and height differences. The uncertainty in the chord was 2.8 ppm and 1.3 ppm after one and five days respectively. Results for the same baseline were then obtained using a three hour-satellite tracking interval. These uncertainties are given in Table 4.5.16. Comparing the 24 hour results with those obtained using 27 hours of observation from three-hour tracking intervals demonstrates that each tracking procedure gives comparable results. After five days of observation it appears that using a longer tracking interval has some advantage for determining the chord.

Since the three-hour tracking procedure did not appear to produce a significant overall advantage results for other baselines were determined using the one-hour tracking interval and are also presented in Table 4.5.15. These results indicate for baselines less than 500 kilometers that the latitude difference uncertainty ranges from approximately 30 centimeters after one day to 13.5 centimeters after five days and is the best determine component of the baseline as in the case of range observation. This is due to the fact that the majority of the observations are from north or south going pass geometries as shown in Figures 4.2.4(a) and (b). The uncertainty of the longitude component of the baselines ranges from 37.3 to 44.8 centimeters after one day and from 14.5 to 19.1 centimeters after five days. Height difference uncertainty ranges from 35.1 to 44.8 centimeters after one day and from

TABLE 4.5.15. BASELINE COMPONENT AND CHORD LENGTH UNCERTAINTIES BASED ON SIMULTANEOUS DOPPLER OBSERVATIONS (SATELLITE TRACKING INTERVAL ONE HOUR)

BASELINE CONFIGURATION	CHORD LENGTH (km)	SYSTEMATIC AND RANDOM ERROR SOURCES					PARAMETER SET	WEIGHT MATRIX	ADJUSTMENT RESULTS (cm)														
		EPHEMERIS	TROPOSPHERIC REFRACTION	SATELLITE CLOCK	STATION CLOCKS	WHITE NOISE (cm)			1 DAY					2 DAYS					5 DAYS				
									σ_{Zs}	σ_{Zs}	σ_{Zh}	σ_d	$\sigma_{d/d}$ (ppm)	σ_{Zs}	σ_{Zs}	σ_{Zh}	σ_d	$\sigma_{d/d}$ (ppm)	σ_{Zs}	σ_{Zs}	σ_{Zh}	σ_d	$\sigma_{d/d}$ (ppm)
1001-1002	100	1	1	1, 2	1, 2	3	1	1	27.7	41.6	45.5	27.6	2.8	19.6	27.3	32.3	19.5	2.0	13.0	17.1	18.2	12.9	1.3
1001-1003	100	1	1	1, 2	1, 2	3	1	1	28.4	40.6	43.2	40.6	4.1	20.5	28.2	29.3	28.1	2.8	13.7	17.2	17.4	17.2	1.7
1003-1004	200	1	1	1, 2	1, 2	3	1	1	28.7	42.7	47.5	42.3	2.1	21.1	28.5	31.2	28.3	1.4	13.1	17.2	18.1	17.1	0.8
1007-1008	500	1	1	1, 2	1, 2	3	1	1	29.5	44.8	49.5	42.9	0.9	21.8	29.9	32.6	28.6	0.6	13.5	18.1	19.1	17.3	0.3
1015-1016	1860	1	1	1, 2	1, 2	3	1	1	52.4	69.2	59.7	46.4	0.3	36.2	45.9	41.1	31.1	0.2	29.9	28.5	25.0	19.5	0.1
1009-1010	100	1	1	1, 2	1, 2	3	1	1	28.9	37.3	35.1	28.8	2.9	21.7	23.3	24.2	21.7	2.2	13.9	14.5	15.8	13.9	1.4
1011-1012	100	1	1	1, 2	1, 2	3	1	1	28.6	44.3	37.2	44.2	4.4	20.3	31.5	27.8	31.5	3.2	13.3	19.1	18.5	19.1	1.9
1011-1013	100	1	1	1, 2	1, 2	3	1	1	28.3	44.6	37.6	28.2	2.8	19.9	31.4	27.6	19.9	2.0	14.0	18.4	17.2	14.0	1.4

TABLE 4.5.16. BASELINE PARAMETER UNCERTAINTIES FOR STATIONS 1001 AND 1002 BASED ON SIMULTANEOUS DOPPLER OBSERVATIONS USING A THREE-HOUR TRACKING INTERVAL

BASELINE CONFIGURATION	CHORD LENGTH (km)	SYSTEMATIC AND RANDOM ERROR SOURCES					PARAMETER SET	WEIGHT MATRIX	ADJUSTMENT RESULTS (cm)															
		EPHEMERIS	TROPOSPHERIC REFRACTION	SATELLITE CLOCK	STATION CLOCKS	WHITE NOISE (cm)			1 DAY					2 DAYS					5 DAYS				
1001-1002	100	1	1	1, 2	1, 2	3	1	1	23.4	42.5	43.3	23.2	2.3	16.6	33.3	33.5	16.4	1.6	10.6	20.6	20.3	10.6	1.1

15.8 to 19.1 centimeters after five days. The uncertainty in the chord is significantly smaller for north-south baselines for the same reason as the latitude component. This is also true for the range observation examples although the difference as a function of orientation is less pronounced after five days of observation. Finally, the uncertainty increases with station separation although the ratio of the uncertainty in the chord to its length decreases with the longer baselines given here. The increase in uncertainty is again due to the increased effect of ephemeris error. Figure 4.5.18 gives the results obtained for baseline 1015-1016. As is typical with the results from the other baselines considered the decrease in parameter variance appears as an exponential decay.

Finally, in Table 4.5.17 various cases are considered in which modifications are made to the error sources. Elimination of tropospheric refraction produces a decrease in the baseline component uncertainties ranging from 1.0 to 7.3 centimeters after one day of observation to 0.7 to 2.7 centimeters after 5 days. The height uncertainty is decreased to the greatest extent. The chord uncertainty decreases by 0.2 ppm after one day of observation and by 0.1 ppm after an additional four days of observation. Decreasing the ephemeris error by 50 percent produces only minor variations in the results as expected. And finally the last two cases of Table 4.5.17 show that reducing the random receiver noise to 1 centimeter produces a significant increase in accuracy but improvement beyond that level gives only limited success since the effect of random receiver clock error begins to dominate the resulting parameter uncertainties.

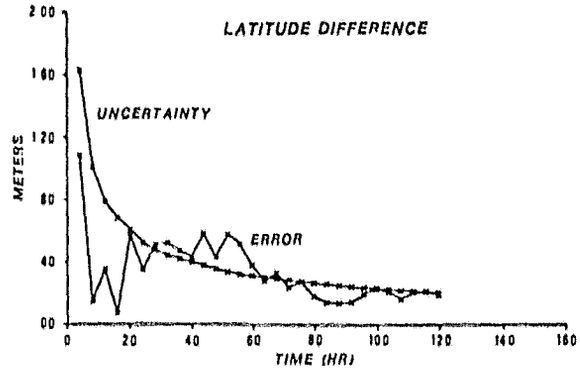

(a)

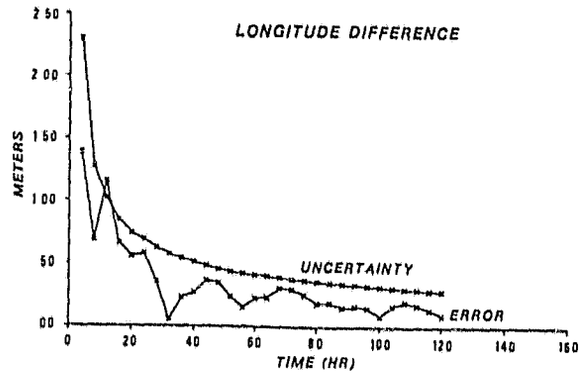

(b)

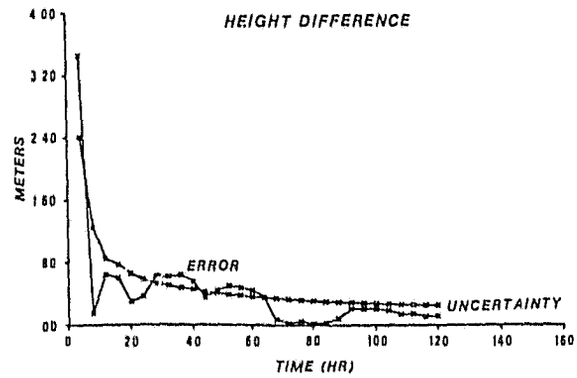

(c)

Figure 4.5.18. Baseline Parameter Error for Complete Simulation Using Integrated Doppler Observations from Stations 1015 and 1016

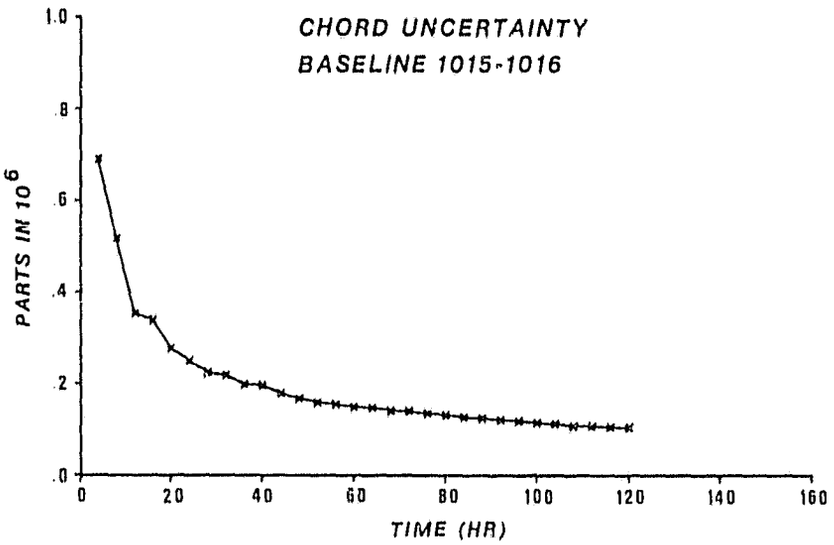

(d)

Figure 4.5.18 (continued)

TABLE 4.5.17. DECREASE IN BASELINE PARAMETER UNCERTAINTIES DUE TO MODIFICATION OF DOPPLER ERROR SOURCES (ONE-HOUR TRACKING INTERVAL)

BASELINE CONFIGURATION	CHORD LENGTH (km)	SYSTEMATIC AND RANDOM ERROR SOURCES					PARAMETER SET	WEIGHT MATRIX	VARIATION IN ADJUSTMENT RESULTS (cm)														
		EPHEMERIS	TROPOSPHERIC REFRACTION	SATELLITE CLOCK	STATION CLOCKS	WHITE NOISE (cm)			1 DAY					2 DAYS					5 DAYS				
									$\sigma_{\Delta\phi}$	$\sigma_{\Delta\lambda}$	$\sigma_{\Delta h}$	σ_{d}	$\sigma_{d/d}$ (ppm)	$\sigma_{\Delta\phi}$	$\sigma_{\Delta\lambda}$	$\sigma_{\Delta h}$	σ_{d}	$\sigma_{d/d}$ (ppm)	$\sigma_{\Delta\phi}$	$\sigma_{\Delta\lambda}$	$\sigma_{\Delta h}$	σ_{d}	$\sigma_{d/d}$ (ppm)
1003-1004	200	1	0	1, 2	1, 2	3	2	1	1.0	3.6	7.3	3.5	0.2	1.2	2.8	5.2	2.8	0.1	0.7	1.3	2.7	1.3	0.1
1007-1008	500	2	1	1, 2	1, 2	3	1	1	1.4	1.3	2.3	0.7	—	0.9	1.6	1.5	0.4	—	0.5	1.0	1.1	0.3	—
1007-1008	500	1	1	1, 2	1, 2	1	1	1	8.9	12.6	12.5	13.2	0.3	6.5	8.3	8.2	8.8	0.2	4.0	5.1	4.8	5.3	0.1
1007-1008	500	1	1	1, 2	1, 2	0.2	1	1	1.4	1.9	2.0	2.1	—	1.0	1.3	1.4	1.4	—	0.6	0.8	0.8	0.9	—

5. A PRELIMINARY EVALUATION OF SATELLITE INTERFEROMETRY FOR BASELINE DETERMINATION

5.1 Introduction

In the preceding chapter the accuracy of baseline determinations from range and Doppler observations was analyzed considering the effects of various error sources. It was found that the range results were predominantly influenced by tropospheric refraction modeling error and random receiver clock error while Doppler results were influenced most by the same and by random receiver noise. Tropospheric refraction errors may be reduced by the use of a water vapor radiometer [MacDoran, 1979] and Doppler receiver noise levels may actually be as low as one centimeter [Stanford Telecommunications, Inc., 1978], hence the baseline uncertainties obtained from range and Doppler may be enhanced as demonstrated in Tables 4.5.13 and 4.5.15. However the resulting baseline uncertainties would still be effected by random correlated clock errors and, in the case of Doppler, also by the weaker geometric strength of the observations themselves. Accuracies on the order of 1 ppm may be achieved using these methods if the period of site occupation is at least 2 days for range and 5 days for Doppler observation.

Since neither of these two observational approaches will support a rapid first-order determination of baselines, this chapter is included to address the utilization of interferometric phase measurements

for this application. Although the interferometric proposals discussed in Chapter 2 are currently under development, enough information is available to support a general estimate of the performance of an interferometric approach. The technique examined in this chapter is based on the double differencing of interferometric phase from two satellites made simultaneously at two sites. This approach has the advantage of eliminating most of the clock errors which required polynomial modeling in the range and Doppler approaches. The analysis presented here is of a preliminary nature intended to provide a general estimate of the accuracy of baseline determination using interferometry. A more detailed analysis of the proposed interferometric procedures of Chapter 2 should be performed as the specifics of these techniques are refined.

5.2 Double Differencing of Interferometric Phase

The approach which is introduced in this section assumes that interferometric phase observations are based on the reconstructed continuous wave GPS carrier frequencies. The following observational model is adopted for the phase measurement with station i observing satellite j:

$$\theta_{ij}(t) = \frac{2\pi}{\lambda_{ij}(t)} [R_{ij}(t) - m_{ij}(t)\lambda_{ij}(t) - c\delta t_i(t) + c\delta t_j(t) - \beta\delta R_{ij}(t) + \gamma_{ij}(t)] \quad (5.2.1)$$

In this equation λ_{ij} is the wavelength of the GPS carrier frequency, R_{ij} is the geometric distance between station i and satellite j, m_{ij} is the integer number of full wavelengths comprising R_{ij}, δR_{ij} is the

tropospheric refraction error modeled to within a percent β, and γ represents uncorrelated measurement error. The quantities $c\delta t_i$ and $c\delta t_j$ represent systematic and correlated random time or phase errors, converted into units of length, of the geodetic receiver and satellite atomic clocks respectively arising from the accumulation of fractional frequency error. The wavelength λ_{ij} is also a function of time due to the Doppler shift caused by the relative motion of the satellite with respect to the receiver. Hence,

$$\lambda_{ij}(t) = \frac{\lambda_j}{1 - \dot{\rho}/c} \tag{5.2.2}$$

where λ_j is the carrier frequency and $\dot{\rho}$ is the component of relative velocity along the topocentric range vector.

If satellite j is simultaneously observed at station ℓ then the difference in phase measured at the two sites is

$$\Delta\theta_j(t) = \theta_{ij}(t) - \theta_{\ell j}(t) \ . \tag{5.2.3}$$

Ignoring for the moment the Doppler shift in the carrier frequency and assuming the same level of refraction modeling error at both sites, equation (5.2.3) may be written as

$$\begin{aligned}\Delta\theta_j(t) = \frac{2\pi}{\lambda_j}\Big\{ & R_{ij}(t) - R_{\ell j}(t) - [m_{ij}(t) - m_{\ell j}(t)]\lambda_j \\ & - c[\delta t_i(t) - \delta t_\ell(t)] - \beta[\delta R_{ij}(t) - \delta R_{\ell j}(t)] - [\gamma_{ij}(t) - \gamma_{\ell j}(t)]\Big\}.\end{aligned} \tag{5.2.4}$$

Notice that the error in the satellite clock does not appear in equation (5.2.4) due to the differencing.

If in addition a second satellite k is simultaneously observed at both stations then the double difference is defined as

$$\begin{aligned}\Delta\theta_{ik}(t) &= \Delta\theta_j(t) - \Delta\theta_k(t) \\ &= \theta_{ij}(t) - \theta_{\ell j}(t) - \theta_{ik}(t) + \theta_{\ell k}(t) \ .\end{aligned} \tag{5.2.5}$$

Again ignoring the Doppler shift and assuming that the frequencies λ_j and λ_k are equal and that β is constant for all observations, equation (5.2.5) may be written as

$$\begin{aligned}\Delta\theta_{jk}(t) = \frac{2\pi}{\lambda_j}\Big\{&R_{ij}(t) - R_{\ell j}(t) - R_{ik}(t) + R_{\ell k}(t) + n_{jk}(t)\lambda_j \\ &- \beta\left[\delta R_{ij}(t) - \delta R_{\ell j}(t) - \delta R_{ik}(t) + \delta R_{\ell k}(t)\right] - \gamma_{i\ell jk}\Big\}\end{aligned} \tag{5.2.6}$$

where

$$n_{jk} = -m_{ij} + m_{\ell j} + m_{ik} - m_{\ell k} \tag{5.2.7}$$

and

$$\gamma_{i\ell jk} = \gamma_{ij} - \gamma_{\ell j} - \gamma_{ik} + \gamma_{\ell k} \ . \tag{5.2.8}$$

In equation (5.2.6) no atomic clock errors appear; thus, the double differencing approach appears to eliminate the timing errors which required modeling previously. The integer term $n_{jk}(t)$ represents the difference between a pair of "2π ambiguities" which exist in each single differencing of phase according to equation (5.2.4). This ambiguity represents the integer number of full wavelengths comprising the difference in the distances between the stations and the satellite.

If the Doppler shift in frequency is included, then the double difference equation (5.2.6) would be replaced by the substitution of the

appropriate equations (5.2.1) into equation (5.2.5) and a complete cancellation of clock error could not be expected. In the preliminary analysis presented in this chapter the carrier frequency $\lambda_j(t)$ will be assumed known and equation (5.2.6) will be adopted as the observation equation. Introduction of the Doppler shift will some cause additional uncertainty in the results depending on the a priori errors in station position and satellite position and velocity.

An additional assumption implied in equation (5.2.6) is that simultaneous observations of phase are to be differenced. The recognition of simultaneous events depends on accurate time tagging of the observations or knowledge of the relative time error between station clocks. The first of these is impossible to achieve and the latter requires either portable clock comparisons or the adoption of additional parameters in the estimation algorithm. If phase differences are formed from observations at two sites having a time of observation difference of Δt seconds, then the error introduced into the double difference is given approximately by

$$\delta\Delta\theta_{jk} = \frac{2\pi\Delta t}{\lambda_j}\left[\left(\frac{\partial R_{\ell k}}{\partial t} - \frac{\partial R_{\ell j}}{\partial t}\right) + \lambda_j\left(\frac{\partial m_{\ell i}}{\partial t} - \frac{\partial m_{\ell k}}{\partial t}\right) - c\left(\frac{\partial \delta t_j}{\partial t} - \frac{\partial \delta t_k}{\partial t}\right) + \beta\left(\frac{\partial \delta R_{\ell i}}{\partial t} - \frac{\partial \delta R_{\ell k}}{\partial t}\right)\right]. \tag{5.2.9}$$

This equation is obtained from a first order Taylor series expansion of equation (5.2.6) assuming that the observations selected from station ℓ for differencing are Δt seconds away from those from station i. An examination of equation (5.2.9) reveals that the time synchronization

error consists of a geometric term due to the position change of each satellite relative to station ℓ, a term which is a function of satellite clock frequency stability and a term due to the variation in tropospheric refraction over Δt. An evaluation of this equation for a synchronization error of 200 nanoseconds gives a bound on this error of 0.05 centimeters. Synchronization to much better than this level could be achieved by time tagging observations with the satellite time information encoded in the transmitted GPS signals.

Adjustment of baseline parameters using double differenced interferometric phase observations requires the differentiation of equation (5.2.6) with respect to the earth-fixed coordinates of the observing stations, the integer n_{jk} and the constant β, at a minimum. Satellite position also enters into equation (5.2.6) and represents an additional set of parameters which strictly should be included. In the results given below corrections to the satellite ephemerides are not incorporated but the effect of error in satellite position is discussed. The partial derivatives used to form the design matrix for the least squares adjustment are the following

$$\frac{\partial \Delta\theta_{jk}(t)}{\partial u_i} = \frac{2\pi}{\lambda_j}\left[\frac{u_j(t) - u_i}{R_{ij}(t)} - \frac{u_k(t) - u_i}{R_{ik}(t)}\right] \qquad (5.2.10)$$

$$u \rightarrow v, w$$

$$\frac{\partial \Delta\theta_{jk}(t)}{\partial u_\ell} = \frac{2\pi}{\lambda_j}\left[\frac{u_\ell - u_j(t)}{R_{\ell j}(t)} - \frac{u_\ell - u_k(t)}{R_{\ell k}(t)}\right] \qquad (5.2.11)$$

$$u \rightarrow v, w$$

$$\frac{\partial \Delta\theta_{jk}(t)}{\partial n_{jk}} = 2\pi \tag{5.2.12}$$

$$\frac{\partial \Delta\theta_{jk}(t)}{\partial \beta} = -\frac{2\pi}{\lambda_j}\left[\delta R_{ij}(t) - \delta R_{\ell j}(t) - \delta R_{ik}(t) + \delta R_{\ell k}(t)\right] . \tag{5.2.13}$$

The integer n_{jk} for an observed satellite pair is a function of time, changing at each observation time. If the receiver however maintains a count of accumulated phase change over the tracking interval, then the rate of change of n_{jk} is known and only a single integer unknown needs to be incorporated for each interval of tracking. An adjustment based on equations (5.2.10) through (5.2.13) will not produce integer solutions for the n_{jk}. Since no constraints are known which will produce an integer result directly, this initial adjustment will provide a set of estimates and variances for the n_{jk}. From these quantities various test sets of integers may be formed. The number of such sets will depend on the estimates of the n_{jk} and on the magnitude of their corresponding variances. For each test set a second least squares adjustment would be required utilizing these integers. This second adjustment would include a set of absolute constraints fixing the n_{jk}. From these adjustments the weighted sum of squares of residuals $V^T PV$ may be compared to determine which test set of integers produces a minimum. The covariance matrix of the station coordinates from this solution may be transformed using equations (3.1.24) or (3.1.25) into baseline component and chord length uncertainties.

5.3 Effect of Error Sources

The error sources influencing satellite interferometry measurements were mentioned in Chapter 2. For the double differencing approach the error sources will be the same except that it appears that most error due to frequency instability will be removed. The error sources considered in the results presented here are the satellite ephemerides, tropospheric refraction, and the random error associated with the measurement of phase. The magnitudes of the ephemeris and tropospheric refraction errors are equivalent to those used in the range and Doppler positioning studies as outlined in Table 4.2.2. The precision of a single phase measurement is assumed to be 3 centimeters which was the nominal precision adopted for integrated Doppler observations in Chapter 4. Counselman [1979] estimates the random phase error of the Miniature Interferometer Terminals to be less than 1 centimeter. Table 5.3.1 gives estimates of the effects these error sources have on baseline components and chord length for sites separated by 100 kilometers. These results are based on simulations using a total of six hours of observation, tracking individual satellites for a fixed one-hour interval.

TABLE 5.3.1. EFFECT OF ERROR SOURCES ON BASELINE PARAMETERS DERIVED FROM SIX HOURS OF DOUBLE DIFFERENCED INTERFEROMETRIC PHASE USING A ONE-HOUR TRACKING INTERVAL (100 km BASELINES)

ERROR SOURCE	COMPONENT ERROR (cm)	CHORD ERROR (cm)
TROPOSPHERIC REFRACTION (5%)	2-4	1-2
EPHEMERIS	1-5	2-3
RECEIVER WHITE NOISE (3 cm)	1-4	1

5.4 Baseline Determination Results

Double differenced interferometric phase observations were simulated every five minutes for the baselines previously considered in Chapter 4. These observations were developed using equation (5.2.6). Three initial adjustments were performed using observations from stations 1001 and 1002 simulated using a one-half, one, and two hour satellite tracking interval. Satellite position error and a five percent error in tropospheric refraction modeling were introduced into the adjustment. Parameters of the adjustment included the latitude, longitude, and height of each station, the integer n_{jk}, and the constant β for each tracking interval. The uncertainty of the latitude, longitude, and height components of the baseline and of the chord length obtained from these initial adjustments are given in Table 5.4.1 after six hours of observation. As the fixed interval for observing a pair of satellites is increased from one-half to two hours, there is a marked decrease in the parameter uncertainties except for the height component. However, with additional observations this trend is apparent for height also. After ten hours of observation the height component uncertainties are 7.8, 4.6, and 3.2 centimeters for the three intervals utilized. This trend is due to the decrease in the total number of parameters required in the adjustment as the tracking interval is lengthened resulting in a general strengthening of the normal equations.

TABLE 5.4.1. VARIATION IN BASELINE PARAMETER UNCERTAINTY WITH SATELLITE TRACKING INTERVAL (BASELINE 1001-1002, SIX HOUR RESULTS, INITIAL ADJUSTMENT)

TRACKING INTERVAL	$\sigma_{\Delta\varphi}$	$\sigma_{\Delta\lambda}$	$\sigma_{\Delta h}$	σ_d
0.5 hr	9.3 cm	12.2	11.4	5.6
1	5.3	8.1	7.5	3.1
2	2.5	4.6	9.0	1.8

For the solution based on a one-hour observing interval Table 5.4.2 gives the actual and estimated values for the integers n_{jk} and the uncertainty of their solution. It is typical in the shorter tracking interval cases for the uncertainty of the estimated n_{jk} to exceed 0.5. When this occurs, the number of test sets of integers required in subsequent adjustments may be large. For instance in Table 5.4.2 the solution for n_{jk} for the fourth hour of observation was -15.2. With the standard error of this solution 0.71 any of the following integer values, -13, -14, -15, -16, -17, could be expected as the correct solution for this interval. If all solutions lying within a 95 percent confidence interval are considered, the number of possible unique sets of integers to be used in subsequent adjustments may be extremely large.

TABLE 5.4.2. RESULTS OF ADJUSTMENT FOR INTEGERS n_{jk} BASED ON INTERFEROMETRIC PHASE MEASUREMENTS AT STATIONS 1001 AND 1002 USING ONE-HOUR TRACKING INTERVAL

TRACKING INTERVAL	INTEGER n_{jk}	ESTIMATE $\hat{n}_{jk}$	UNCERTAINTY $\sigma_{n_{jk}}$
1	7	7.2	.16
2	-6	-5.8	.15
3	1	0.5	.16
4	-16	-15.2	.71
5	-13	-13.0	.24
6	-11	-10.7	.54

Since initial adjustments using observations from two-hour tracking intervals produced the smallest uncertainty in both baseline components and more importantly in the integers n_{jk}, solutions were made for all baselines considered in Chapter 4 using observation schedules based on two-hour tracking intervals. Ephemeris, tropospheric refraction, and instrumental errors were added to the observations. The satellite pairs were selected for tracking to optimize the trace of the baseline parameter covariance matrix given by either equation (3.1.25) when the chord was estimated or by an equation analogous to equation (3.2.3) when latitude, longitude, and height components were estimated. After an initial adjustment the same observational data were utilized in a subsequent adjustment in which the correct integer values n_{jk} were included and fixed by absolute constraints. In actual practice many such solutions may be required. The results of the second adjustment are given in Table 5.4.3. The results after six hours of observation indicate that the uncertainty of the baseline components generally ranges from between 1.0 and 4.0 centimeters for baselines of 100 kilometers. These uncertainties increase with baseline length. For shorter baselines the height component has the largest uncertainty. The accuracy of the chord length exceeds 0.1 ppm in all cases considered with the relative accuracy improving with increasing station separation.

Although these results do not reflect the uncertainty due to ephemeris error, they include the uncertainty due to a five percent error in tropospheric refraction and a measurement uncertainty of 3 centimeters. The ephemeris error will increase the uncertainties of the estimated parameters as demonstrated by the error magnitudes given in

TABLE 5.4.3. BASELINE COMPONENT AND CHORD UNCERTAINTIES BASED ON SATELLITE INTERFEROMETRY (TWO-HOUR TRACKING INTERVAL)

BASELINE CONFIGURATION	APPROXIMATE CHORD LENGTH (km)	SYSTEMATIC AND RANDOM ERROR SOURCES			PARAMETER SET	ADJUSTMENT RESULTS (cm)														
		EPHEMERIS	TROPOSPHERIC REFRACTION	WHITE NOISE (cm)		2 HOURS					4 HOURS					6 HOURS				
						σ_ϕ	σ_λ	σ_h	σ_d	ppm	σ_ϕ	σ_λ	σ_h	σ_d	ppm	σ_ϕ	σ_λ	σ_h	σ_d	ppm
1001-1002	100	1	1	3	*	24.7	27.8	12.2	2.0	0.2	1.5	2.4	3.2	1.2	0.1	1.2	1.1	2.9	1.0	0.1
1001-1003	100	1	1	3	*	19.6	26.9	16.2	2.0	0.2	1.2	2.0	3.4	1.6	0.2	1.2	2.0	3.6	0.9	0.1
1011-1014	80	1	1	3	*	25.0	27.9	12.7	1.3	0.2	1.6	2.8	3.9	1.1	0.1	1.3	1.6	3.1	0.8	0.1
1003-1004	200	1	1	3	*	24.9	28.3	13.1	2.5	0.1	1.7	4.3	4.2	1.9	0.1	1.5	3.6	3.9	1.2	0.05
1005-1006	300	1	1	3	*	26.9	30.5	15.4	2.9	0.1	2.2	5.8	4.9	2.2	0.07	2.0	5.4	4.7	1.5	0.05
1007-1008	500	1	1	3	*	31.1	35.4	19.8	3.5	0.07	3.1	9.1	6.5	2.8	0.06	3.1	8.5	6.4	1.8	0.04
1015-1016	1860	1	1	3	*	39.6	43.3	27.5	8.5	0.05	6.8	13.6	9.7	6.3	0.03	6.2	12.8	9.1	4.8	0.03
1009-1010	100	1	1	3	*	31.3	28.7	133.1	4.7	0.5	3.7	1.5	8.0	1.2	0.1	2.3	1.5	6.6	0.8	0.1
1011-1012	100	1	1	3	*	13.4	23.9	8.3	3.6	0.4	1.1	2.0	3.3	1.5	0.2	1.0	1.9	2.2	0.9	0.1
1011-1013	100	1	1	3	*	15.8	29.1	9.9	2.7	0.3	1.8	1.4	3.5	1.7	0.2	1.7	1.0	2.4	1.0	0.1

*ADJUSTMENT PARAMETERS INCLUDE STATION COORDINATES AND TROPOSPHERIC REFRACTION CORRECTION. RESULTS ARE BASED ON SIMULTANEOUS OBSERVATIONS EVERY 5 MINUTES.

Table 5.3.1. However even with such increases the double differencing approach appears to be adequate for providing rapid first-order determination of baselines.

6. SUMMARY AND RECOMMENDATIONS

6.1 Precision Comparison

Some general conclusions were drawn in Chapter 3 from an examination of the results. For the observation types considered it was evident that ranging measurements provided the best geometric strength of solution. The two other derived observation types, correlated range difference and interferometry, were geometrically weaker although the results obtained from these latter procedures can be greatly improved upon by increasing the observational precision. Correlated range difference observations had best geometric strength when observed satellites were tracked over longer time intervals. With this type of tracking procedure both the baseline component and chord length uncertainties were minimized. For range and interferometric observations shorter satellite tracking intervals produced the least uncertainty in the baseline parameters. Lengthening the tracking interval for these observation types increased the resulting parameter uncertainties. However the rate of increase was smaller than the variation produced in the Doppler results by decreasing the satellite tracking interval. And finally the interferometry approach became geometrically weaker as the baseline length increased to become a more significant percentage of the distance to the satellite; although, the relative error in parts per million decreased for the baselines considered.

The analysis presented in Chapter 3 considered the relative geometric strength of three observation types, two derived from basic ranging. The results were based on the assumptions that satellite positions in space were known and that the basic ranging measurements were subject to uncorrelated stationary random noise.

6.2 Dynamic Point Positioning

The range observation results presented in Chapter 4 indicate that such observations from GPS satellites can provide geodetic coordinates to an accuracy of approximately 85 to 125 centimeters using twenty-four hours of continuous observation. Those results were based on the use of a one-hour tracking interval, selecting satellites which provide the best geometric strength for the solution. If a longer site occupation period is utilized, then the uncertainty in the geodetic coordinates can be reduced further to approximately 35 to 65 centimeters after five days of observation. Since the majority of satellite passes are north-south, the estimated latitude has a smaller standard error than longitude and height except for stations located toward the poles. For these latter stations height uncertainty tends to be smaller since a higher frequency of lower elevation observations provide a better separation of height and timing errors. If a longer tracking interval is utilized, larger uncertainties in estimated position are to be expected since the effects of systematic satellite position error will not average as rapidly. The dominant error source limiting the accuracy of geodetic coordinates is this error in satellite position. Thus improvement in the receiver noise level and in measurement or modeling

of tropospheric refraction will yield only minor increases in accuracy. Therefore the geodetic utilization of GPS range observations in a dynamic point positioning approach will require satellite ephemerides to be estimated as accurately as possible.

Integrated Doppler observations based on independent counts can be expected to yield geodetic coordinate uncertainties ranging from 95 to 150 centimeters after twenty-four hours of observation. The uncertainties will diminish to 45 to 65 centimeters after an additional four days of observation. These results are based on a one-hour tracking interval with an expected receiver noise level of 3 centimeters. An increase in the tracking interval to three hours produces a substantial increase in the geodetic coordinate uncertainties. Thus, as with ranging, the best procedure is to track satellites over short intervals to obtain stronger geometric strength of solution. Increasing the precision of the Doppler receiver or the accuracy of tropospheric refraction prediction will produce only a minor change in the results. Again the uncertainty introduced into station position by ephemeris error dominates the effects of all other error sources. Reduction of the ephemeris error by fifty percent produces a decrease in position uncertainty of approximately 45 percent. Therefore precise ephemeris computation will be required for accurate geodetic positioning using GPS Doppler observations.

The major conclusion which can be stated regarding dynamic point positioning using range and Doppler observations from a Global Positioning System of navigation satellites is that the accuracy of estimated geodetic coordinates will be comparable with the results

obtainable with Transit Doppler observations. No major increase in accuracy can be anticipated. Thus replacement of the Transit System with a Global Positioning System will not be detrimental to the geodetic community since with proper electronic receivers similar levels of performance can be expected. The GPS system does offer a distinct advantage. This system provides continuous observation thereby decreasing the interval of time required to obtain comparable results with the Transit System enabling satellite surveying to become a more efficient operation. Table 6.2.1 summarizes the effect of systematic and random error sources on dynamic point positioning.

TABLE 6.2.1. EFFECT OF SYSTEMATIC AND RANDOM ERROR SOURCES ON DYNAMIC POINT POSITIONING USING ONE-HOUR SATELLITE TRACKING INTERVALS

ERROR SOURCE	APPROXIMATE COORDINATE ERROR (cm)			
	RANGE		DOPPLER	
	1 DAY	5 DAYS	1 DAY	5 DAYS
TROPOSPHERIC REFRACTION	10	5	10	5
EPHEMERIS	50-80	25-40	60-150	30-70
RESIDUAL SATELLITE RUBIDIUM CLOCK ERROR	4	1	5	2
RECEIVER CESIUM CLOCK ERROR	5	2	7	3
RECEIVER WHITE NOISE (RANGE 1m, DOPPLER 3cm)	2	1	18	8

6.3 Baseline Determination

Simultaneous range observations from two stations were utilized to determine baseline components and chord length. Solutions based on a one-hour tracking interval, selecting satellites which provide the best geometry, indicated after one day of observation that the latitude and longitude components of the baseline have uncertainties

of from 10 to 17 centimeters for baselines under 300 kilometers. The latitude component was determined with greater accuracy because of the frequency of north and south going satellite passes. For baselines under 300 kilometers the uncertainty of the height component ranged from 25 to 28 centimeters. After five days of observation uncertainties in the latitude and longitude components were reduced to approximately 4 to 7 centimeters and the height component uncertainty to 12 to 15 centimeters. The uncertainty of these components increased with baseline distance reflecting an increasing projection of orbit uncertainty into the estimates. For shorter baselines the uncertainty in chord length ranged from 10 to 16 centimeters after one day of observation and from 4 to 7 centimeters after five days. The uncertainty was less for north-south baselines and increased with station separation. However for the baselines considered here the relative uncertainty or ratio of the uncertainty in the chord to its length decreased with increased baseline distance. The accuracy of 100 kilometer baselines was approximately 1 to 1.5 parts per million after one day of observation. An increase in the length of the satellite tracking interval slightly degraded these results.

The dominant error sources which will effect the accuracy of baseline determination using range observations are the stability of the receiver clock and error in refraction prediction. Increasing the modeling accuracy of tropospheric refraction will significantly increase the accuracy of the baseline parameters. Reducing the receiver noise level from 1 meter to 60 centimeters will produce a marginal increase in accuracy.

The stability of the receiver clock can be improved by using an atomic oscillator with better stability properties. However the oscillator model chosen for use in this study was typical of cesium oscillators having good stability; thus, it is anticipated that the baseline parameter uncertainties attributed to random receiver clock error in this study are typical of those expected for an operational survey system.

With Doppler observations from one-hour satellite tracking intervals the uncertainties in the baseline components ranged from 27 to 50 centimeters after one day and from 13 to 19 centimeters after five days of continuous observation. The chord length uncertainty ranged from 28 to 44 centimeters after one day and from 13 to 19 centimeters after five days. The latitude component of the baseline was determined with the least uncertainty and the chord lengths of north-south baselines were determined significantly better. These results are for baselines under 200 kilometers and are based on a 3 centimeter receiver white noise standard error. Increasing the tracking interval to three hours produced some increase in the accuracy of the chord but the results appeared mixed for the baseline component uncertainties.

The accuracy of the baseline parameters obtained by the geometrically weaker Doppler observations are improved significantly by decreasing the receiver noise level to 1 centimeter. Below that level the clock error statistics dominate and further increased precision will yield only marginal improvement. Enhanced modeling or measurement of tropospheric refraction would improve the Doppler results but not as significantly as for ranging.

Assuming an instrumental noise level of 1 centimeter, uncertainties in the baseline components would be reduced to approximately 9 to 14 centimeters after five days of observation. The uncertainty in the chord would also be approximately 9 to 14 centimeters after five days for baselines under 200 kilometers. The errors limiting the accuracy of baseline determination using GPS Doppler observations are receiver noise and the stability of the receiver oscillator.

Simultaneous interferometric phase observations from two sites, twice differenced to eliminate timing errors, were examined as an alternative procedure for the determination of baseline components. The use of continuous wave phase measurements requires the introduction of integer unknowns into the adjustment related to the ambiguity in recognizing the exact cycle on which phase measurements were made at the two sites. As a consequence initial and secondary adjustments of the baseline parameters are required.

Results obtained using a two-hour tracking interval with a phase measurement uncertainty of 3 centimeters revealed that baseline components may be recovered with an uncertainty of from 1.0 to 4.0 centimeters after six hours if sites are separated by up to a few hundred kilometers. The uncertainty in the recovered height difference between observing sites was larger than the uncertainties in the latitude and longitude differences for baselines under a few hundred kilometers. The accuracy of the chord length exceeded 0.1 ppm in all cases considered and improved with station separation. These results included uncertainty due to a five percent error in tropospheric refraction. Probable ephemeris error will increase the uncertainty of the baseline components

as indicated in Table 6.3.1; however, even with such increases this approach appears to be adequate for rapid first-order determination of baselines under 200 kilometers. Table 6.3.1 summarizes the effect of various systematic and random error sources on baseline component determination.

6.4 Recommendations

The results presented in Chapter 4 demonstrated that GPS range and integrated Doppler observations will provide sufficient accuracy for estimation of geodetic coordinates. These observations taken simultaneously at two sites can be utilized to determine baseline parameters to better than 15 centimeters after five days of observation. A limiting factor for both observational approaches is the stability of the receiver oscillator. For certain geodynamic applications such as earthquake prediction accuracies of 10 centimeters or better may be required within a short time interval. GPS range and Doppler observations might be capable of providing such accuracies in the future but the time interval required to obtain such results will preclude this application.

Satellite interferometry techniques can be developed which circumvent the requirements for high stability frequency standards. This lead to the examination of the double differencing of interferometric phase. Thus one limiting factor for the range and Doppler approaches is theoretically not a critical limitation for interferometry.

There are several interferometric approaches which have been proposed using GPS satellites as radio sources. These proposals

TABLE 6.3.1. EFFECT OF SYSTEMATIC AND RANDOM ERROR SOURCES ON BASELINE DETERMINATION USING ONE-HOUR SATELLITE TRACKING INTERVALS

ERROR SOURCE	APPROXIMATE COMPONENT ERROR (cm)				
	RANGE		DOPPLER		DOUBLE DIFFERENCED PHASE
	1 DAY	5 DAYS	1 DAY	5 DAYS	6 HOURS
TROPOSPHERIC REFRACTION	6-8	2-3	4-8	2-3	2-4
EPHEMERIS	1-3	0.5-1.5	.5	.1	1-5
RESIDUAL SATELLITE RUBIDIUM CLOCK ERROR	.2	.1	.2	.1	–
RECEIVER CESUIM CLOCK ERROR	8	3	10	4	–
RECEIVER WHITE NOISE (RANGE 1m, DOPPLER 3 cm, PHASE 3 cm)	2-3	1-1.5	20-25	8-10	1-4

have been described in this study and the error sources associated with satellite interferometry have been mentioned. It is recommended that a detailed error analysis of these interferometry proposals be made to determine their effectiveness for determining baseline components. The specific details of each need to be examined so that a fair comparison is realized. Further consideration should be given to the long-term cost effectiveness of these proposals including the range and Doppler instrumentation utilized in dynamic point positioning.

APPENDIX A

LEAST SQUARES POLYNOMIAL APPROXIMATION OF RANDOM WALK SEGMENTS

A.1 General Polynomial Approximation

Let $\{u_k\}$ be a discrete stationary zero-mean stochastic process and define $\{z_n\}$ to be its running sum with

$$z_\ell = \sum_{k=1}^{\ell} u_k \ . \qquad \text{(A.1.1)}$$

The quantity z_ℓ is one element in the discrete random walk sequence $\{z_n\}$. By stationary it is meant that the random process $\{u_k\}$ is one whose statistical properties are invariant in time. Further, assume that over selected time intervals the random walk $\{z_n\}$ appears to be dominated by systematic components enabling $\{z_n\}$ to be modeled by an m^{th} degree polynomial $P_m(t)$. The difference between z_ℓ and $P_m(t_\ell)$ will be called the residual r_ℓ:

$$r_\ell = z_\ell - P_m(t_\ell) \qquad \ell = 1,2,\ldots,N \qquad \text{(A.1.2)}$$

where the polynomial model is defined by

$$P_m(t) = \sum_{j=o}^{m} a_j (t - t_o)^j \ . \qquad \text{(A.1.3)}$$

The constant t_o in equation (A.1.3) is arbitrary. The coefficients of the approximating polynomial can be determined by a least squares fit of $P_m(t)$ to the random walk elements z_n sampled within a selected time interval. The least squares solution for this approximation is [Uotila, 1967]

$$\bar{a} = (A^T A)^{-1} A^T \bar{z} \tag{A.1.4}$$

where

$$\bar{a}^T = [a_o, a_1, \ldots, a_m]$$

$$\bar{z}^T = [z_1, z_2, \ldots, z_N] \ .$$

The design matrix A is given by

$$A = \begin{bmatrix} 1 & (t_1 - t_o) & \ldots\ldots & (t_1 - t_o)^m \\ 1 & (t_2 - t_o) & \ldots\ldots & (t_2 - t_o)^m \\ & & \vdots & \\ 1 & (t_N - t_o) & \ldots\ldots & (t_N - t_o)^m \end{bmatrix}. \tag{A.1.5}$$

The covariance for the polynomial coefficients $\bar{a}$ depends on the choice of t_o. In terms of the underlying process $\{u_k\}$, it is given by the following equations

$$\begin{aligned} E[\bar{a}] &= (A^T A)^{-1} A^T E[\bar{z}] = 0 \\ E[\bar{a}\bar{a}^T] &= (A^T A)^{-1} A^T E[\bar{z}\bar{z}^T] A (A^T A)^{-1} \end{aligned} \tag{A.1.6}$$

where the covariance $E[\bar{z}\bar{z}^T]$ is given by

$$E[\bar{z}\bar{z}^T] = [R \ S] E[\bar{u}\bar{u}^T] \begin{bmatrix} R^T \\ S^T \end{bmatrix} \tag{A.1.7}$$

and

$$\bar{u}^T = [u_1, u_2, \ldots, u_N] \ .$$

The matrices R and S are given below.

Notice that the fitting procedure, equation (A.1.4), is non-weighted least squares. The problem considered here is one of approximation, not linear estimation, since the a_i are based on samples from $\{z_n\}$ not subject to an observation or sampling error. Also the procedure is independent of how the z_n are selected within the time interval.

Using equations (A.1.2), (A.1.3), and (A.1.4), the residual vector $\bar{r}$ can be written as

$$\begin{aligned} \bar{r} &= \bar{z} - A(A^TA)^{-1}A^T\bar{z} \\ &= [I - A(A^TA)^{-1}A^T]\bar{z} \\ &= G\bar{z} \ . \end{aligned} \tag{A.1.8}$$

The residuals represent the discrepancy between the samples of the random walk and the approximating polynomial and may be interpreted as "noise" with respect to $P_m(t)$. The statistics of these residuals are obtained from the statistics of the random walk by the linear transformation

$$E[\bar{\bar{r}}\bar{\bar{r}}^T] = GE[\bar{\bar{z}}\bar{\bar{z}}^T]G^T \ . \tag{A.1.9}$$

This equation is derived using equation (A.1.8). For the residuals

$$E[\bar{r}] = E[G\bar{z}] = GE[\bar{z}] = 0 \tag{A.1.10}$$

since, using equation (A.1.1), each z_n has zero mean.

Thus,

$$E[\bar{\bar{r}}\bar{\bar{r}}^T] = E[G\bar{\bar{z}}\bar{\bar{z}}^T G^T] = GE[\bar{\bar{z}}\bar{\bar{z}}^T]G^T \ . \qquad \text{(A.1.11)}$$

Therefore given the statistics of $\{u_k\}$ and an m^{th} degree polynomial model $P_m(t)$ to approximate $\{z_n\}$ over a given interval of time, the statistics of the residuals to that model may be developed.

Theorem A.1: The covariance $E[\bar{\bar{r}}\bar{\bar{r}}^T]$ is (i) independent of the epoch of $\{u_k\}$ provided this underlying process is stationary, and is (ii) invariant provided the $\{z_n\}$ are sampled in an identical fashion in each of two intervals with comparable polynomial models being adopted.

The proof is as follows:

Let

$$\bar{z}_I^T = \{z_1, z_2, \ldots, z_N\}$$

and

$$\bar{z}_{II}^T = \{z_{N+1}, z_{N+2}, \ldots, z_{2N}\}$$

be two identically sampled sequences of the random walk $\{z_n\}$. Since

$$\begin{aligned} z_{N+1} &= z_N + u_{N+1} \\ &\vdots \\ z_{2N} &= z_N + u_{N+1} + \ldots + u_{2N} \end{aligned} \qquad \text{(A.1.12)}$$

where

$$z_N = \sum_{k=1}^{N} u_k \ ,$$

equation (A.1.12) can be written using

$$\bar{z}_I = S\bar{u}_I$$

as

$$\bar{z}_{II} = R\bar{u}_I + S\bar{u}_{II} \tag{A.1.13}$$

where R is an N × N matrix of all ones and S is an N × N lower-triangular matrix of ones. Equation (A.1.13) can be written as

$$\bar{z}_{II} = [R\ S]\begin{bmatrix}\bar{u}_I \\ \bar{u}_{II}\end{bmatrix} . \tag{A.1.14}$$

By a linear transformation, taking $\bar{u}^T = (\bar{u}_I^T, \bar{u}_{II}^T)$,

$$\begin{aligned} E[\bar{z}_{II}\bar{z}_{II}^T] &= [R\ S]E[\bar{u}\bar{u}^T]\begin{bmatrix}R^T \\ S^T\end{bmatrix} \\ &= RE[\bar{u}_I\bar{u}_I^T]R^T + SE[\bar{u}_{II}\bar{u}_I^T]R^T \\ &\quad + RE[\bar{u}_I\bar{u}_{II}^T]S^T + SE[\bar{u}_{II}\bar{u}_{II}^T]S^T . \end{aligned} \tag{A.1.15}$$

From equation (A.1.9)

$$\begin{aligned} E[\bar{r}_{II}\bar{r}_{II}^T] &= GE[\bar{z}_{II}\bar{z}_{II}^T]G^T \\ &= GRE[\bar{u}_I\bar{u}_I^T]R^TG^T + GSE[\bar{u}_{II}\bar{u}_I^T]R^TG^T \\ &\quad + GRE[\bar{u}_I\bar{u}_{II}^T]S^TG^T + GSE[\bar{u}_{II}\bar{u}_{II}^T]S^TG^T . \end{aligned} \tag{A.1.16}$$

However

$$GR = [I - A(A^TA)^{-1}A^T]R = [I - C]R$$

$$= \begin{bmatrix} 1 - \sum_{k=1}^{N} C_{1k} \\ \vdots \\ \sum_{k=1}^{N} C_{Nk} \end{bmatrix}. \qquad \text{(A.1.17)}$$

Since the coefficients $C_{\ell k}$, $\ell = 1,2,\ldots,N$, are based on the least squares approximation of $P_m(t)$ to the sampled $\{z_n\}$, it is true that (see lemma below)

$$\sum_{k=1}^{N} C_{\ell k} = 1 \qquad \text{(A.1.18)}$$

for every ℓ. Therefore

$$GR = 0 \qquad \text{(A.1.19)}$$

and equation (A.1.16) reduces to

$$E[\bar{r}_{II}\bar{r}_{II}^T] = GSE[\bar{u}_{II}\bar{u}_{II}^T]S^TG^T \ . \qquad \text{(A.1.20)}$$

Using the stationarity assumption on $\{u_k\}$ and the result that

$$E[\bar{z}_I\bar{z}_I^T] = SE[\bar{u}_I\bar{u}_I^T]S^T \ , \qquad \text{(A.1.21)}$$

equation (A.1.20) becomes

$$E[\bar{r}_{II}\bar{r}_{II}^T] = GE[\bar{z}_I\bar{z}_I^T]G^T = E[\bar{r}_I\bar{r}_I^T] \qquad \text{(A.1.22)}$$

since the matrix G in either case is identical. Thus the quantity $SE[\bar{u}_{II}\bar{u}_{II}^T]S^T$ is the only partial sum of the $\bar{z}_{II}$ statistics which is

mapped by G into the statistics of $\bar{r}_{II}$. The additional terms in equation (A.1.16) involving the R matrix are mapped into zero by G.

Lemma A.1: For least squares polynomial approximation

$$\sum_i C_{ij} = 1 \text{ and } \sum_i G_{ij} = 0 \tag{A.1.23}$$

where

$$G = I - C$$

$$C = A(A^TA)^{-1}A^T .$$

The proof is as follows:

The coefficients of the approximating polynomial

$$P_m(t) = \sum_{\ell=0}^{m} a_\ell (t - t_0)^\ell$$

are determined through a least squares procedure.

Thus

$$\bar{a} = (A^TA)^{-1}A^T\bar{z}$$

and

$$\bar{r} = \bar{z} - A\bar{a} = \bar{z} - A(A^TA)^{-1}A^T\bar{z}$$

$$= \bar{z} - C\bar{z} = G\bar{z} .$$

Consider the matrix product A^TG

$$A^TG = A^T(I - C) = A^T[I - A(A^TA)^{-1}A^T]$$

$$= A^T - A^T = 0 . \tag{A.1.24}$$

Since by definition the first row of A^T consists only of ones because the approximating function is a polynomial, it follows from equation (A.1.24) that

$$\sum_i G_{ij} = 0 (i = \text{row}, j = \text{column})$$

for all j. Since G is symmetric

$$\sum_j G_{ij} = 0$$

for all i. From equation (A.1.23)

$$\sum_i C_{ij} = 1 - \sum_i G_{ij} .$$

Therefore,

$$\sum_i C_{ij} = 1 .$$

The above theorem also holds for random walks in which the underlying process is continuous. For instance if equation (A.1.1) is replaced by the continuous random walk

$$z_N = z(t_N) = \int_{t_0}^{t_N} u(t)dt , \qquad (A.1.25)$$

then using equation (A.1.25), equation (A.1.13) can be expressed as

$$\bar{z}_{II} = \begin{bmatrix} \int_{t_0}^{t_N} u(t)dt \\ \vdots \\ \int_{t_N}^{t_N} u(t)dt \end{bmatrix} + \begin{bmatrix} \int_{t_N}^{t_{N+1}} u(t)dt \\ \vdots \\ \int_{t_N}^{t_{2N}} u(t)dt \end{bmatrix} \qquad (A.1.26)$$

$$= Q + T \ .$$

The residuals based on the m^{th} degree polynomial fit are

$$\begin{aligned} \bar{r}_{II} &= (I - C)\bar{z}_{II} \\ &= (I - C)(Q + T) \\ &= (I - C)Q + (I - C)T \ . \end{aligned} \qquad (A.1.27)$$

Since Q is a vector of equal constants and since equation (A.1.18) holds as before, it is obvious that

$$(I - C)Q = 0 \qquad (A.1.28)$$

and therefore

$$\begin{aligned} \bar{r}_{II} &= (I - C)T \\ &= GT \ . \end{aligned} \qquad (A.1.29)$$

The covariance for the second set of residuals is

$$E[\bar{r}_{II}\bar{r}_{II}^{T}] = GE[TT^{T}]G^{T} \qquad (A.1.30)$$

since

$$E[T] = 0 \ . \qquad (A.1.31)$$

Since $\{u_k\}$ is assumed stationary with autocorrelation function $R_u(t - t')$, the following integral equation is valid

$$\int_{t_N}^{t_{N+J}} \int_{t_N}^{t_{N+I}} R_u(t - t')dtdt' = \int_0^{t_{N+J} - t_N} \int_0^{t_{N+I} - t_N} R_u(t^* - t^{*\prime})dt^*dt^{*\prime}$$

$$= \int_0^{t_J} \int_0^{t_I} R_u(t^* - t^{*\prime})dt^*dt^{*\prime} \qquad \text{(A.1.32)}$$

where

$$t^* = t - t_N$$

$$t^{*\prime} = t' - t_N \ .$$

Applying equation (A.1.32) to each element of the covariance matrix $E[TT^T]$, it is seen that

$$E[TT^T] = E[\bar{z}_I \bar{z}_I^T] \qquad \text{(A.1.33)}$$

and thus equation (A.1.30) becomes

$$E[\bar{r}_{II} \bar{r}_{II}^T] = GE[\bar{z}_I \bar{z}_I^T]G^T$$

$$= E[\bar{r}_I \bar{r}_I^T] \ . \qquad \text{(A.1.34)}$$

Therefore the theorem is valid in the continuous case.

A.2 Correlation Between Residuals from Approximations to Successive Random Walk Segments

Consider two elements of the random walk sequence $\{z_n\}$

$$z_{N+1} = \sum_{k=1}^{N+1} u_k \tag{A.2.1}$$

and

$$z_N = \sum_{k=1}^{N} u_k \quad . \tag{A.2.2}$$

From the assumption that $\{u_k\}$ is a zero-mean process

$$E[z_{N+1}] = E[z_N] = 0 \quad . \tag{A.2.3}$$

The correlation between these elements is given by

$$\begin{aligned} E[z_{N+1}\ z_N] &= E[z_N\ z_N] + E[u_{N+1}\ z_N] + \ldots + E[u_{N+1}\ z_N] \\ &= \sigma^2_{z_N} + E[u_{N+1}\ z_N] + \ldots + E[u_{N+1}\ z_N] \quad . \end{aligned} \tag{A.2.4}$$

The correlations between z_N and the elements u_{N+j} depend on the correlations among the elements of the underlying process $\{u_k\}$.

Now consider the following question. If samples or a segment of $\{z_n\}$ are to be modeled by a polynomial of degree m, what correlations exist between the residuals from successively fitted segments? Consider for example the random quantities $z(t_n)$ where

$$z(t_n) = \sum_{k=1}^{n} u(t_k) \qquad n = 1,\ldots,\ell,\ldots,2\ell \quad .$$

Suppose the distribution of the z_n is as follows:

$$
\begin{matrix}
z(t_1) \\
\vdots \\
z(t_\ell)
\end{matrix}
\qquad \text{(Segment 1)}
$$

$$
\begin{matrix}
z(t_{\ell+1}) \\
\vdots \\
z(t_{2\ell})
\end{matrix}
\qquad \text{(Segment 2)} \quad .
$$

Let t' and t'' represent, without loss of generality, the midpoint of each segment. If a polynomial is chosen to model the z_n over each segment as

$$P_m(t) = \sum_{j=o}^{m} a_j (t - t')^j \qquad \text{(Segment 1)}$$

and

$$Q_m(t) = \sum_{j=o}^{m} b_j (t - t'')^j \qquad \text{(Segment 2)}$$

can it then be assumed that $\bar{r}_I$ and $\bar{r}_{II}$ are uncorrelated? To answer this question perform a least squares fit of $P_m(t)$ and $Q_m(t)$ simultaneously to the $\{z_n\}$ segments and then linearly transform the statistics of $\{z_n\}$ to obtain the residual statistics and compare the correlation coefficients between the two groups of residuals with those within each group. The equation for this transformation is

$$\begin{bmatrix} E[\bar{r}_I \bar{r}_I^T] & E[\bar{r}_I \bar{r}_{II}^T] \\ E[\bar{r}_{II} \bar{r}_I^T] & E[\bar{r}_{II} \bar{r}_{II}^T] \end{bmatrix} = G \begin{bmatrix} E[\bar{z}_I \bar{z}_I^T] & E[\bar{z}_I \bar{z}_{II}^T] \\ E[\bar{z}_{II} \bar{z}_I^T] & E[\bar{z}_{II} \bar{z}_{II}^T] \end{bmatrix} G^T \qquad \text{(A.2.5)}$$

where

$$G = [I - A(A^T A)^{-1} A^T] \tag{A.2.6}$$

and

$$A = \begin{bmatrix} A_1 & 0 \\ 0 & A_2 \end{bmatrix}. \tag{A.2.7}$$

A comparison of the correlation coefficients

$$\rho_{r_i r_j} = \frac{E[r_i r_j]}{\sqrt{E[r_i r_i]E[r_j r_j]}} \tag{A.2.8}$$

of the off-diagonal blocks, $E[\bar{r}_I \bar{r}_{II}^T]$ or $E[\bar{r}_{II} \bar{r}_I^T]$, with those of the diagonal blocks, $E[\bar{r}_I \bar{r}_I^T]$ and $E[\bar{r}_{II} \bar{r}_{II}^T]$, can be a basis for deciding if the sets of residuals may be assumed to be independent of not.

REFERENCES

Allan, D. W., J. H. Shoaf, and D. Halford, 1974. "Statistics of Time and Frequency Data Analysis", Time and Frequency: Theory and Fundamentals, National Bureau of Standards Monograph 140, Blair (Editor).

Anderle, R. J., 1974. "Transformation of Terrestrial Survey Data to Doppler Satellite Datum", Journal of Geophysical Research, Vol. 79, No. 35.

Anderle, R. J., 1975. "Error Model for Geodetic Positions Derived from Doppler Satellite Observations", Naval Surface Weapons Center Technical Report TR-3368, Dahlgren, Virginia.

Anderle, R. J., 1976. "Point Positioning Concept Using Precise Ephemeris", Proceedings of the First International Geodetic Symposium on Satellite Doppler Positioning, The Physical Science Laboratory, New Mexico State University, Las Cruses.

Anderle, R. J., 1978a. "Geodetic Applications of NAVSTAR Global Positioning System", Proceedings of the Second International Symposium on Problems Related to the Redefinition of North American Geodetic Networks, U. S. Government Printing Office, Washington, D.C.

Anderle, R. J., 1978b. "Application of Global Positioning System to Determination of Tectonic Plate Movements and Crustal Deformations", Proceedings of the Ninth Geodesy/Solid Earth and Ocean Physics (GEOP) Research Conference, Department of Geodetic Science Report No. 280, The Ohio State University, Columbus.

Anderle, R. J., 1978c. "Clock Performance as a Critical Parameter in Navigation Satellite Systems", Proceedings of the Tenth Annual Precise Time and Time Interval (PTTI) Applications and Planning Meeting, National Aeronautics and Space Administration Technical Memorandum 80250, Greenbelt, Maryland.

Anderle, R. J. and M. G. Tanenbaum, 1974. "Practical Realization of a System for Earth Dynamics by Satellite Methods", On Reference Coordinate Systems for Earth Dynamics, B. Kolaczek and G. Weiffenbach, eds., IAU Colloquium No. 26, Torun, Poland.

Arur, M. G., 1977. "Experiments for Improved Positioning by Means of Integrated Doppler Satellite Observations and the NNSS Broadcast Ephemeris", Department of Geodetic Science Report No. 258, The Ohio State University, Columbus.

Baker, R.M.L., 1967. Astrodynamics, Applications and Advanced Topics, Academic Press, New York.

Barnes, J. A. and S. Jarvis, 1971. "Efficient Numerical and Analog Modeling of Flicker Noise Processes", National Bureau of Standards Technical Note 604, Boulder, Colorado.

Barnes, J. A., A. R. Chi, L. S. Cutler, D. J. Healey, D. B. Leeson, T. E. McGunigal, J. A. Mullen, Jr., W. L. Smith, R. L. Sydnor, R.F.C. Vessot, and G.M.R. Winkler, 1971. "Characterization of Frequency Stability", IEEE Transactions on Instrument and Measurements, Vol 20, No. 2.

Bartholomew, C. A., 1978. "Satellite Frequency Standards", Navigation, Vol. 25, No. 2.

Blair, B. E. (Editor), 1974. Time and Frequency: Theory and Fundamentals, U. S. Department of Commerce/National Bureau of Standards Monograph 140, U. S. Government Printing Office, Washington, D.C.

Borel, M. J., D. J. Pinkos, J. N. Damoulakis, and T. D. Fuchser, 1978. "Phase 1 GPS User Equipment", Navigation, Vol. 25, No. 2.

Brown, D. C., 1976. "Doppler Positioning By the Short Arc Method", Proceedings of the First International Geodetic Symposium on Satellite Doppler Positioning, The Physical Science Laboratory, New Mexico State University, Las Cruses.

Butler, R. F., 1978. "Technical Feasibility of a Beacon-Aided Guidance System", Naval Surface Weapons Center Technical Report TR-3867, Dahlgren, Virginia.

Clynch, J. and R. Altenberg, 1979. "Ionospheric Residual Range Error Model", Applied Research Laboratory Technical Report 79-9, The University of Texas at Austin.

Colquitt, E. S., 1979. "Effect of Oscillator Performance on Doppler Geodesy", Proceedings of the Second International Geodetic Symposium on Satellite Doppler Positioning, Applied Research Laboratories, The University of Texas at Austin.

Counselman, C. C., 1978. "Miniature Interferometer Terminals for Earth Surveying", Proceedings of the Ninth Geodesy/Solid Earth and Ocean Physics (GEOP) Research Conference, Department of Geodetic Science Report No. 280, The Ohio State University, Columbus.

Counselman, C. C., and I. I. Shapiro, 1979. "Miniature Interferometer Terminals for Earth Surveying", Bulletin Geodésique, Vol. 53, No. 2.

Cox, D. B., 1978. "Integration of GPS with Inertial Navigation Systems", Navigation, Vol. 25, No. 2.

Denaro, R., V. G. Harvester, and R. L. Harrington, 1978. "GPS Phase 1 User Equipment Field Tests", Navigation, Vol. 25, No. 2.

Dermanis, A., 1977. "Design of Experiment For Earth Rotation and Baseline Parameter Determination from Very Long Baseline Interferometry", Department of Geodetic Science Report No. 245, The Ohio State University, Columbus.

Fell, P. J., 1975. "The Use of Standard Weather Values and Refraction Bias Parameters in Orbit Determination", The Canadian Surveyor, Vol. 29, No. 3.

Fell, P. J. and B. R. Hermann, 1979. "An Empirical Evaluation of the Effect of Oscillator Errors on Dynamic Point Positioning Based on the NAVSTAR GPS System", Proceedings of the Second International Geodetic Symposium on Satellite Doppler Positioning, Applied Research Laboratories, The University of Texas at Austin.

Gelb, A., (Editor), 1974. Applied Optimal Estimation, MIT Press, Cambridge, Massachusetts.

Hellwig, H. W., 1975. "Atomic Frequency Standards: A Survey", Proceedings of the IEEE, Vol. 63, No. 2.

Hellwig, H. W., 1977. "Frequency Standards and Clocks: A Tutorial Introduction", National Bureau of Standards Technical Note 616, U. S. Government Printing Office, Washington, D.C.

Hopfield, H. S., 1969. "Two-Quartic Tropospheric Refractivity Profile for Correcting Satellite Data", Journal of Geophysical Research, Vol. 74, No. 18.

Hopfield, H. S., 1970. "Tropospheric Effect on Electromagnetically Measured Range: Prediction from Surface Weather Data", Johns Hopkins University/Applied Physics Laboratory Report TG1119, Laurel, Maryland.

Hopfield, H. S., 1972. "Tropospheric Range Error Parameters: Further Studies", Johns Hopkins University/Applied Physics Laboratory Report CP015, Laurel, Maryland.

Jorgensen, P. S., 1978. "The Short-Term Quality of NAVSTAR Tracking Data", Aerospace Corporation Technical Report T04-0078 (3475-10), El Segundo, California.

Kruczynski, L. R., 1978. "Aircraft Navigation with the Limited Operational Phase of the NAVSTAR Global Positioning System", Navigation, Vol. 24, No. 4.

Kumar, M., "Monitoring of Crustal Movements in the San Andreas Fault Zone by a Satellite-Borne Ranging System", Department of Geodetic Science Report 243, The Ohio State University, Columbus.

Laurila, S. H., 1975. Electronic Surveying and Navigation, John Wiley and Sons, New York.

Liebelt, P. B., 1967. An Introduction to Optimal Estimation, Addison-Wesley, Reading, Massachusetts.

Lindsey, W. C. and M. K. Simon, 1973. Telecommunication Systems Engineering, Prentice-Hall, Inc., Englewood Cliffs, New Jersey.

MacDoran, P. F., 1979. "Satellite Emission Radio Interferometric Earth Surveying SERIES-GPS Geodetic System", Bulletin Geodesique, Vol. 53, No. 2.

MacDoran, P. F., A. E. Mill, K. M. Ong, G. M. Resch, D. D. Morabito, E. S. Claflin, and T. G. Lockhart, 1978. "Mobile Radio Interferometric Geodetic Systems", Proceedings of the Ninth Geodesy/Solid Earth and Ocean Physics (GEOP) Research Conference, Department of Geodetic Science Report No. 280, The Ohio State University, Columbus.

Meditch, J. S., 1969. Stochastic Optimal Linear Estimation and Control, McGraw-Hill, New York.

Meditch, J. S., 1975. "Clock Error Models for Simulation and Estimation", The Aerospace Corporation, Report No. TOR-0076 (6474-01)-2, El Segundo, California.

Mikhail, E. M., 1976. Observation and Least Squares, Dun-Donnelley Publisher, New York.

Miller, P. L., 1977. "Application of the NAVSTAR Global Positioning System to Ocean Navigation", Report on the 1976 Topical Conference on the Geodetic Measurements in the Ocean, by N. Saxena, Marine Technology Society Journal, Vol. II, No. 3.

Milliken, R. J., and C. J. Zoller, 1978. "Principle of Operation of NAVSTAR and System Characteristics", Navigation, Vol. 25, No. 2.

Mueller, I. I., 1964. Introduction to Satellite Geodesy, Frederick Ungar Publishing Company, New York.

Mueller, I. I., 1969. Spherical and Practical Astronomy as Applied to Geodesy, Frederick Ungar Publishing Company, New York.

O'Toole, J. W., 1976. "CELEST Computer Program for Computing Satellite Orbits", Naval Surface Weapons Center Technical Report TR-3565, Dahlgren, Virginia.

Pavlis, E. C., 1979. "Error Analysis for a Spaceborne Laser Ranging System", Department of Geodetic Science Report 290, The Ohio State University, Columbus.

Proceedings of the First International Geodetic Symposium on Satellite Doppler Positioning, 1976. The Physical Science Laboratory, New Mexico State University, Las Cruses.

Proceedings of the Second International Geodetic Symposium on Satellite Doppler Positioning, 1979. Applied Research Laboratories, The University of Texas at Austin.

Rapp, R. H., 1976. Geometric Geodesy Volume II (Advanced Techniques), Department of Geodetic Science, The Ohio State University, Columbus.

Russell, S. S. and J. H. Schaibly, 1978. "Control Segment and User Performance", Navigation, Vol. 25, No. 2.

Sims, T., 1972. "The NWL Precision Ephemeris", Naval Weapons Laboratory Technical Report TR-2872, Dahlgren, Virginia.

Schaibly, J. H., 1976. "Simulated and Projected Performance of the NAVSTAR GPS Control Segment", Presented at the AIAA Guidance and Control Conference, San Diego, Calif., August.

Schaibly, J. H. and M. D. Harkins, 1979. "The NAVSTAR Global Positioning System Control Segment Performance During 1978", Proceedings of the Second International Geodetic Symposium on Satellite Doppler Positioning, Applied Research Laboratories, The University of Texas at Austin.

Seppelin, T. O., 1974. "The Department of Defense World Geodetic System 1972", Canadian Surveyor, Vol. 28, No. 5.

Shoaf, J. H., 1971. "Specifications and Measurement of Frequency Stability", National Bureau of Standards Report 9794, Boulder, Colorado.

Smith, D. and W. Criss, 1976. "GPS NAVSTAR Positioning System", Astronautics and Aeronautics, Vol. 14, April.

Spilker, J. J., 1977. Digital Communications by Satellite, Prentice-Hall, New York.

Spilker, J. J., 1978. "GPS Signal Structure and Performance Characteristics", Navigation, Vol. 25, No. 2.

Stanford Telecommunications Incorporated, 1978. "Operating Manual STI Model 5007 NAVSTAR Geodetic System Receiver", Sunnyvale, California.

Stansell, T. A., 1978a. "The TRANSIT Navigation Satellite System", Publication R-5933, Magnavox Government and Industrial Electronics Company, Torrance, Calif.

Stansell, T. A., 1978b. "Civil Marine Applications of the Global Positioning System", Navigation, Vol. 25, No. 2.

Uotila, U. A., 1967. Introduction to Adjustment Computations With Matrices, Department of Geodetic Science, The Ohio State University, Columbus.

Van Gelder, B.H.W., 1978. "Estimability and Simple Dynamic Analysis of Range (Range-Rate and Range Difference) Observations to Artificial Satellites", Department of Geodetic Science Report 284, The Ohio State University, Columbus.